

EVALUATION OF POLY (2-ETHYL-2-OXAZOLINE) (PETOX)-BASED
MULTIFUNCTIONAL CARRIER SYSTEMS FOR BREAST CANCER TARGETED
THERAPY



by
Zeynep Būşra Bolat


Submitted to Graduate School of Natural and Applied Sciences
in Partial Fulfillment of the Requirements
for the Degree of Doctor of Philosophy in
Biotechnology

Yeditepe University
2019

EVALUATION OF POLY (2-ETHYL-2-OXAZOLINE) (PETOX)-BASED
MULTIFUNCTIONAL CARRIER SYSTEMS FOR BREAST CANCER TARGETED
THERAPY

APPROVED BY:

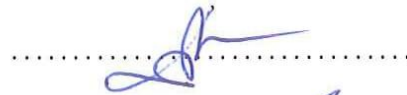
Prof. Dr. Fikretin Şahin
(Thesis Supervisor)
(Yeditepe University)



Prof. Dr. Dilek Telci
(Thesis Co-Supervisor)
(Yeditepe University)



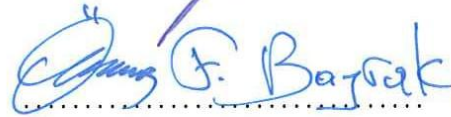
Prof. Dr. Elif Damla Arısan
(İstanbul Kültür University)



Assoc. Prof. Dr. Mustafa Güzel
(Medipol University)



Assoc. Prof. Dr. Ömer Faruk Bayrak
(Yeditepe University)



Assist. Prof. Dr. Hüseyin Çimen
(Yeditepe University)



DATE OF APPROVAL: / / 2019



*This thesis is dedicated to my beloved
parents Gülay, and Ahmet Bolat...*

ACKNOWLEDGEMENTS

First or foremost I would like to express my sincere gratitude to my thesis supervisor Prof. Dr. Fikretin Şahin for the continuous support, guidance and encouragement during my PhD study. I am deeply thankful to my co-advisor Prof. Dr. Dilek Telci for being there for me at all times. Her guidance helped me in all the time of research and writing of this thesis.

Besides my advisors, I would like to express thanks to my thesis committee: Assoc. Prof. Dr. Ömer Faruk Bayrak and Assist. Prof. Dr. Hüseyin Çimen for their insightful comments, but also for the challenging questions which incentivized me to widen my research from various perspectives.

I am thankful to Sevgi Gülyüz and Umut Uğur Özköse from TUBITAK-MAM for providing the copolymers; to Assoc. Prof. Dr. Burcu Devrim and Assist. Prof. Dr. Ongun M. Saka for constructing liposomes and to Dr. Umut Can Öz for formulating the polymersomes from Pharmaceutical Technology Department in Ankara University; to Dr. Aslı Kara and Naile Öztürk for micelle nanostructures from Hacettepe University that were used in this study: your cooperation has been most constructive.

It is my great pleasure to express appreciation to Assoc. Prof. Dr. İtir Ebru Zemheri for the histopathological examinations and Engin Sümer for his help during animal studies. Special thanks to Ayla Burçin Asutay and Melike Sarıçam for technical support in flow cytometry.

Furthermore, I would like to express my thankfulness for the financial support received from TUBITAK with the project number of 213M726 entitled as “Development of The Poly(2-ethyl-2-oxazoline) (PEtOx) Based Multifunctional Carrier Systems for Treatment and Diagnosis of The Prostate and The Breast Cancer”, during my thesis study.

My heartfelt gratitude to Ayca Ece Nezir for her support in this project, especially at endless in vivo experiments. I am indebted to my fellow labmates Halime İlhan Sığınç and Hazel Erkan for motivating me at the sleepless nights that we worked together before

deadlines. I would like to acknowledge my other lab members, Esra Aydemir oban, Polen Koak, Huseyin and Ezgi Abdik, Pakize Neslihan Taşlı, Oğuz Kaan Kırbaş, Ezgi Taşkan, Zeynep İşlek, Nurdan Sena Değirmenci, Eslem Essam, Bilun Demir, Ayşe Hande Nayman, İnci Kurt Celeb, Meltem Selen Önal and Kaan Öztürk for their friendship and support.

I am especially grateful to my dearest friends Betul Karadoğan, Neslihan Kayra, Merve Uslu, Bürge Ulukan, Mehtap Aydın and Esra Albayrak for their moral supports and friendships.

Last bu not least, my deepest heartfelt gratitude is to my parents; Gülay Bolat, Ahmet Bolat, my siblings; Abdullah, Betül, Hatice, Esmâ, my nephew; Halid and to my grandfathers; Ünal Okçu and Şevki Bolat, without their unconditional love and support it would have been impossible for me to finish my Ph.D.

ABSTRACT

EVALUATION OF POLY (2-ETHYL-2-OXAZOLINE) (PETOX)-BASED MULTIFUNCTIONAL CARRIER SYSTEMS FOR BREAST CANCER TARGETED THERAPY

Breast cancer is the major cause of death in females with the highest incidence rate worldwide. It is categorized as a public health problem with no current effective treatment, thus more target specific therapeutic methods are required. Tumor homing peptides show a high potential in targeting cancer, and Peptide 18 shows a high targeting specificity toward breast cancer. Thus, it was used in labeling three different nanocarrier constructs: PEtOx-DOPE liposome, PEtOx-*b*-PLA polymersome, and PEtOxPEIPCL micelles. These polymers have high biocompatibility, biodegradability and low toxicity characteristics. Toxicology studies showed that these nanocarrier formulations did not affect the cell survival of HUVEC, kidney HEK293, mesenchymal stem cell, and normal epithelial breast cells, characterizing these constructs with minimal toxicity. Target specificity and cellular uptake studies indicate that the Peptide 18-targeted nanocarriers possessed higher binding affinity to breast cancer AU565 line compared to the normal epithelial breast MCF10A cell line. These targeted nanocarriers were then used as carriers for the pro-apoptotic BikDD gene and doxorubicin. High effectiveness of the targeting nanocarriers in AU565 cells was determined with increase of mRNA expression levels of Bik leading to apoptosis. Furthermore, treatment of doxorubicin loaded peptide 18 labeled nanocarriers showed enhanced apoptotic activity in AU565 cells. Following *in vitro* studies, the delivery of pro-apoptotic BikDD gene and doxorubicin using nanocarriers were analyzed in CD-1 nude mice animal model. The animal study suggested that doxorubicin delivery by peptide 18 labeled nanocarriers significantly decreased tumor volume when compared to doxorubicin treatment alone. Although, there was a decrease in tumor volume of CD-1 female nude mice treated with BikDD gene loaded into peptide 18 labeled nanocarriers, it was not significant. Our results suggest that this breast cancer targeted therapy has the potential to become a substitute for current conventional approaches. This project is funded by TUBITAK (213M726).

ÖZET

MEME KANSERİ HEDEFLEME TEDAVİSİNDE KULLANILACAK POLİ(2-ETİL-2-OKSAZOLİN) (PETOX) ESASLI ÇOK İŞLEVSEL TAŞIYICI SİSTEMLERİN DEĞERLENDİRİLMESİ

Meme kanseri, dünyada kadınlar arasında görülen en yüksek insidans oranına sahiptir ve ana ölüm nedenleri arasında ilk sırada yer almaktadır. Halk sağlığı problemleri arasında önemli bir yeri olan meme kanserinin, günümüzde etkili tedavi yöntemi olmadığı için, hedefe yönelik spesifik tedavi yöntemlerine ihtiyaç duyulmaktadır. Tümör hedefleyici peptit olan Peptit 18 meme kanseri hücrelerinin hedeflenmesinde yüksek potansiyele sahip olduğu bilinmektedir. Peptit 18, kopolimerlerden oluşan PEtOx-DOPE lipozom, PEtOx-*b*-PLA polimerzom, ve PEtOxPEIPCL misel nanotaşıyıcı formülasyonlarını etiketlemek için kullanılmıştır. Bu kopolimerlerin yüksek biyoyumluluk, biyoparçalanabilirlik ve düşük toksisite karakterlerine sahiptir. Bu nanotaşıyıcılar ile yapılan toksikoloji çalışmaları sonucunda, mezenkimal kök hücre, endotel hücresi, sağlıklı böbrek ve meme epitel hücrelerinin yaşamına olumsuz bir etki görülmemiş ve bu nanotaşıyıcılar ile hücrelere düşük toksisite göstermiştir. Hedefleme spesifitesi ve hücre alım çalışmalarında ise, Peptit 18 bağlı nanotaşıyıcıların AU565 meme kanseri hücrelerinin sağlıklı MCF10A hücrelerine kıyasla daha yüksek bağlanma gözlemlenmiştir. Doksorubisin ilacı ve proapoptotik BikDD bu hedeflendirilmiş nanotaşıyıcılara yüklenmiştir. AU565 hücre hattında görülen, Bik mRNA ekspresyon seviyelerindeki artış, peptit 18-nanotaşıyıcıların yüksek verimliliğini göstermektedir. Doksorubisin ve BikDD peptit 18-nanotaşıyıcıları tarafından AU565 hücrelerine yüksek bir apoptotik aktivite görülmüştür. Sonrasında yapılan *in vitro* çalışmalarında ise, doksorubisin hedeflendirilmiş nanotaşıyıcılar ile gönderimi CD-1 fare hayvan modelleri kullanarak gerçekleştirilmiştir. Bu çalışmalar sonucunda, peptit 18-nanotaşıyıcılarının göndermiş olduğu doksorubisinin, sadece doksorubisin gönderimine kıyasla tümör hacmini düşürmüştür. Bu çalışma, meme kanserine yönelik hedeflendirilmiş tedavi yöntemleri içerisinde bilinen yaklaşımlara potansiyel sağlayarak alternatif sunmaktadır. BikDD yüklü peptit 18 bağlı nanotaşıyıcıları, CD-1 farelerin tümör hacimlerini küçültme gözlemlenmemiştir. Bu çalışma TÜBİTAK tarafından 213M726 numaralı proje ile desteklenmiştir.

TABLE OF CONTENTS

ACKNOWLEDGEMENTS.....	iv
ABSTRACT.....	vi
ÖZET	vii
LIST OF FIGURES	xiv
LIST OF TABLES.....	xx
LIST OF SYMBOLS/ABBREVIATIONS.....	xxii
1. INTRODUCTION.....	1
1.1. CANCER.....	1
1.2. BREAST CANCER	4
1.3. GRADING OF BREAST CANCER.....	6
1.4. CLASSIFICATION OF BREAST CANCER.....	7
1.4.1. Luminal A and B Breast Cancer	7
1.4.2. Triple-Negative Breast Cancer	8
1.4.3. HER-2 Positive Breast Cancer.....	8
1.5. THE MECHANISM OF BREAST CANCER METASTASIS	10
1.6. TREATMENT OF BREAST CANCER	11
1.6.1. Chemotherapeutic Drugs	11
1.6.2. Doxorubicin	14
1.7. BIK, A PROAPOPTOTIC MEMBER OF BCL-2 FAMILY PROTEINS	15
1.8. NANOCARRIERS.....	21
1.8.1. Copolymers in Design and Development of Nanocarriers	21
1.8.2. Liposomes	24
1.8.3. Micelles.....	26
1.8.4. Polymersomes	26
1.9. SMART TARGETING OF NANOPARTICLES	27
1.9.1. Tumor Targeting Peptides	29
1.10. AIM OF THE STUDY	32
2. MATERIALS	33

2.1.	INSTRUMENTS	33
2.2.	EQUIPMENT	33
2.3.	DRUGS	34
2.4.	PEPTIDES	34
2.5.	CHEMICALS	34
2.5.1.	Chemicals used for Cell Culture	34
2.5.2.	Chemicals used for Plasmid Isolation and Site-Directed Mutagenesis	35
2.5.3.	Chemicals used for Flow Cytometry and Confocal Microscopy	35
2.5.4.	Chemicals used for Cell Cycle and Cell Death	35
2.5.5.	Chemicals used for Real-time PCR	36
2.5.6.	Chemicals used for animal studies	36
2.6.	PLASMIDS	36
2.7.	CELL LINES	38
2.8.	MOUSE RACE	38
3.	METHODS	39
3.1.	CELL CULTURE	39
3.1.1.	Cell Thawing	39
3.1.2.	Cell Lines and Culturing Conditions	39
3.1.3.	Cell Subculturing	40
3.1.4.	Calculation of Cell Number	40
3.1.5.	Cryopreservation of Cells	40
3.2.	SYNTHESIS AND CHARACTERIZATION OF PROAPOPTOTIC BIK GENE	41
3.2.1.	Plasmid Isolation	41
3.2.2.	Bik Plasmid Cloning by Restriction Enzyme Digest	42
3.2.2.1.	Restriction Digestion	42
3.2.2.2.	Plasmid DNA Purification After Digestion	42
3.2.2.3.	Ligation	43
3.2.3.	Transformation	43
3.3.	SITE-DIRECTED MUTAGENESIS	44
3.4.	PREPARATION OF COPOLYMER AND NANOCARRIER FORMULATIONS	45

3.4.1. Copolymers.....	45
3.4.2. Liposome	45
3.4.3. Polymersome	46
3.4.4. Micelles.....	46
3.4.5. Stability Studies of Nanocarriers	46
3.5. DETERMINATION OF PEPTIDE AND FLUORESCHEIN LOADED CONSTRUCTS BINDING AFFINITY BY FLOW CYTOMETRY.....	46
3.5.1. Binding Affinity of Peptides.....	46
3.5.2. Binding Affinity of Fluorescein Loaded P18-Nanocarrier Formulations.....	47
3.6. DETERMINATION OF PEPTIDE AND FLUORESCHEIN LOADED CONSTRUCTS BINDING AFFINITY BY CONFOCAL MICROSCOPY	47
3.7. TRANSFECTION OF BIKDD GENE	48
3.8. CELL VIABILITY ASSAY.....	48
3.8.1. The Cytotoxicity of Copolymers and Nanocarrier Formulations on Normal Cell Lines.....	48
3.8.2. Determination of the Effect of Gene or Drug Loaded Nanocarrier Formulations on AU565 Cell Line	49
3.9. DETECTION OF GENE EXPRESSION LEVELS OF EGFR AND BIKDD IN AU565 CELL LINE.....	49
3.9.1. RNA isolation for EGFR Gene Analysis.....	49
3.9.2. RNA isolation for BikDD Gene Analysis.....	50
3.9.3. Reverse Transcriptase Polymerase Chain Reaction.....	50
3.9.4. Quantitative Polymerase Chain Reaction	50
3.10. CELL CYCLE ASSAY	51
3.11. DETERMINATION OF CELL DEATH BY ANNEXIN-V	52
3.12. <i>IN VIVO</i> STUDIES	52
3.12.1. Animals.....	52
3.12.2. Development of Orthotopic Breast Cancer Model in CD-1 Nude Female Mice and Drug Applications.....	53
3.12.3. Tumor Volume Measurements	53
3.12.4. Histopathological Analysis	53
3.13. STATISTICAL ANALYSIS.....	54
4. RESULTS.....	55

4.1. DETERMINATION OF THE MODEL HER2-POSITIVE BREAST CANCER CELL LINE FOR THE STUDY	55
4.1.1. Cell Proliferation Rate of AU565 and SKBR3 Cells.....	55
4.1.2. Gene Expression Level of EGFR in AU565 and SKBR3 Cells	56
4.2. BINDING AFFINITY OF PEPTIDE MC10, PEPTIDE 11 AND PEPTIDE 18 TO BREAST CANCER AND CONTROL CELL LINES DETERMINED BY FLOW CYTOMETRY.....	57
4.3. DETERMINATION OF BINDING AFFINITY OF PEPTIDES ON BREAST CANCER AND CONTROL CELL LINE BY CONFOCAL MICROSCOPY	60
4.4. DETERMINATION OF THE PROAPOPTOTIC PLASMID AND SITE-DIRECTED MUTAGENESIS OF BIK TO BIKDD GENE.....	64
4.4.1. Gene Expression Level of Bik in AU565 Cell Line	64
4.4.2. Chromatogram Analysis of Site-Directed Mutagenesis	65
4.5. GENE EXPRESSION LEVELS OF BIKDD IN AU565 CELL LINE	66
4.6. LIPOSOME DELIVERY OF BIKDD OR DOXORUBICIN TO AU565 CELLS	67
4.6.1. Analysis of Cellular Cytotoxicity for PEtOx-DOPE Copolymer and Liposomes.....	67
4.6.2. Binding Affinity of P18 Labeled PEtOx-DOPE Liposomes to the Breast Cancer and Control Cell Lines.....	73
4.6.3. Cellular Uptake of P18 Labeled PEtOx-DOPE Liposomes to the Breast Cancer and Control Cell Lines.....	73
4.6.4. Cell Viability of AU565 Cells Treated with BikDD or Doxorubicin Loaded to P18-Labeled PEtOx-DOPE Liposomes.....	74
4.6.5. Bik Levels in AU565 Cells Treated with BikDD Loaded P18-Labeled PEtOx-DOPE Liposome	79
4.6.6. Effect of Doxorubicin Loaded P18-PEtOx-DOPE Liposomes on Cell Cycle... ..	80
4.6.7. Effect of Doxorubicin Loaded P18-PEtOx-DOPE Liposomes on Cell Death	82
4.7. POLYMERSOME DELIVERY OF BIKDD OR DOXORUBICIN TO AU565 CELLS	85

4.7.1. Analysis of Cellular Cytotoxicity of PEtOx- <i>b</i> -PLA Copolymer and Polymersome	85
4.7.2. Binding Affinity of P18-Labeled PEtOx- <i>b</i> -PLA Polymersome to the Breast Cancer and Control Cell Lines.....	91
4.7.3. Cellular Uptake of P18-Labeled PEtOx- <i>b</i> -PLA Polymersome to the Breast Cancer and Control Cell Lines.....	92
4.7.4. Cell Viability of AU565 Cells Treated with BikDD or Doxorubicin Loaded P18-Labeled PEtOx- <i>b</i> -PLA Polymersome	93
4.7.5. Bik Levels in AU565 Cells Treated with BikDD Loaded P18-Labeled PEtOx- <i>b</i> -PLA Polymersomes	97
4.7.6. Effect of Doxorubicin Loaded P18-Labeled PEtOx- <i>b</i> -PLA Polymersome on Cell Cycle	98
4.7.7. Effect of Doxorubicin Loaded P18-Labeled PEtOx- <i>b</i> -PLA Polymersome on Cell Death	100
4.8. MICELLE DELIVERY OF BIKDD OR DOXORUBICIN TO AU565 CELLS	103
4.8.1. Analysis of Cellular Cytotoxicity for PetOx-PEI-PCL Copolymer and Micelles	103
4.8.2. Binding Affinity of P18-Labeled PEtOx-PEI-PCL Micelles to the Breast Cancer and Control Cell Lines.....	108
4.8.3. Cellular Uptake of P18-Labeled PEtOx-PEI-PCL Micelles to the Breast Cancer and Control Cell Lines.....	109
4.8.4. Cell Viability of AU565 Cells Treated with BikDD or Doxorubicin Loaded P18-Labeled PEtOx-PEI-PCL Micelle	110
4.8.5. Bik Levels in AU565 Cells Treated with BikDD Loaded P18-Labeled PEtOx-PEI-PCL Micelles	114
4.8.6. Effect of Doxorubicin Loaded P18-Labeled PEtOx-PEI-PCL Micelle on Cell Cycle	115
4.8.7. Effect of Doxorubicin Loaded to P18-PEtOx-PEI-PCL Micelles on Cell Death	117
4.9. THERAPEUTIC EFFECT OF TARGETED NANOCARRIERS ON AU565 TUMOR MODELS.....	120
4.9.1. Therapeutic effect of P18-PEtOx-DOPE-DOX Liposomes on AU565 Tumor Models	120

4.9.2. Therapeutic effect of P18-PEtOx-b-PLA-DOX Polymersomes on AU565 Tumor Models.....	126
4.9.3. Therapeutic effect of P18-PEtOx-PEI-PCL-DOX Micelles on AU565 Tumor Models	132
4.9.4. Therapeutic effect of P18-PEtOx-DOPE-BikDD Liposomes on AU565 Tumor Models.....	138
4.9.5. Therapeutic effect of P18-PEtOx-b-PLA-BikDD Polymersome on AU565 Tumor Models.....	144
4.9.6. Therapeutic effect of P18-PEtOx-PEI-PCL-BikDD Micelles on AU565 Tumor Models.....	150
5. DISCUSSION.....	156
6. CONCLUSION AND FUTURE PERSPECTIVE	164
REFERENCES	166
APPENDIX A.....	190

LIST OF FIGURES

Figure 1.1. Hallmarks of cancer.....	3
Figure 1.2. Breast tissue structure.....	4
Figure 1.3. Heat map showing cell growth of different cells treated with different compounds.....	13
Figure 1.4. Effect of doxorubicin on cell death.....	14
Figure 1.5. Bcl-2 family proteins affecting apoptotic pathway.....	17
Figure 1.6. Comparisons of domain structures for the proteins of Bcl-2-family.....	18
Figure 1.7. Components polymeric drug delivery systems.....	20
Figure 1.8. Biophysichemical properties of nanoparticles that have been explored as carriers for drug delivery in cancer therapy.....	21
Figure 1.9. Structure of polyethylenimines in receptor-targeted polycation complexes.....	23
Figure 1.10. Nanoparticles formed from amphiphilic block copolymers containing PLA and their general characteristics.....	24
Figure 1.11. Representation of a micelle, a liposome, and a lipid bilayer.....	25
Figure 1.12. Representation of liposome nanocarriers that takes place in active and passive targeting of drug.....	28
Figure 1.13. Schematic outline of peptide 18 binding specifically to breast cancer.	31
Figure 2.1. Map of pEGFP-Bik plasmid.....	36
Figure 2.2. Map of pCMV6-XL-Bik plasmid.....	37
Figure 2.3. Map of pCAG-GFPd2 plasmid.....	37
Figure 4.1. Determination of the cell proliferation rate of AU565 and SKBR3 cells.	56

Figure 4.2. The relative EGFR/18sRNA mRNA levels in SKBR3 and AU565 cells was evaluated using qPCR.....	57
Figure 4.3. The representative histograms showing binding affinity of MC10, P11, and P18 on AU565, SKBR3, MCF10A, MCF12A, and HUVEC cell lines.....	59
Figure 4.4. Peptide MC10, P11, and P18 binding affinity on AU565 cell line by confocal microscopy.....	61
Figure 4.5. Peptide MC10, P11, and P18 binding affinity on MCF10A cell line by confocal microscopy.....	62
Figure 4.6. Peptide MC10, P11, and P18 binding affinity on MCF12A cell line by confocal microscopy.....	63
Figure 4.7. Relative Bik/18sRNA mRNA expression using qPCR for non-transfected control and AU565 cell line transfected with pEGFP-C3-Bik, pCMV6-XL5-Bik, and pCAG-GFPd2-Bik plasmids.....	64
Figure 4.8. Chromatogram results of pEGFP-BikDD vector	65
Figure 4.9. Relative Bik/18sRNA mRNA expression using qPCR for non-transfected and AU565 cells transfected with pEGFP-C3-BikDD, and mock vector pEGFP-C3.....	66
Figure 4.10. Effect of PEtOx-DOPE copolymer and liposome on HUVEC cell line viability.....	69
Figure 4.11. Effect of PEtOx-DOPE copolymer and liposome on HEK293 cell line viability.....	70
Figure 4.12. Effect of PEtOx-DOPE copolymer and liposome on MSC line viability..	71
Figure 4.13. Effect of PEtOx-DOPE copolymer and liposome on MCF10A cell line viability.....	72
Figure 4.14. The representative histograms showing binding affinity of P18-PEtOx-DOPE liposome on MCF10A and AU565 cell lines.....	73

Figure 4.15. P18-PEtOx-DOPE liposome binding affinity on MCF10A and AU565 cell lines by confocal microscopy	74
Figure 4.16. Determination of the cytotoxic effect of P18-PEtOx-DOPE-BikDD on AU565 cells.....	76
Figure 4.17. Determination of the cytotoxic effect of P18-PEtOx-DOPE-DOX on AU565 cells.....	78
Figure 4.18. Relative Bik/18sRNA mRNA expression using qPCR for non-transfected and AU565 cells transfected with 4 and 8 μ g of P18-PEtOx-DOPE-BikDD.	79
Figure 4.19. Cell cycle profiles of AU565 cells examined by flow cytometry.. ..	81
Figure 4.20. Effect of P18-PEtOx-DOPE-DOX liposomes on AU565 cell death at 48 hours.....	83
Figure 4.21. Effect of P18-PEtOx-DOPE-DOX liposomes on AU565 cell death at 72 hours.....	84
Figure 4.22. Effect of PEtOx-b-PLA copolymer and polymersome on HUVEC cell line viability.....	87
Figure 4.23. Effect of PEtOx-b-PLA copolymer and polymersome on HEK293 cell line viability.....	88
Figure 4.24. Effect of PEtOx-b-PLA copolymer and polymersome on MSC cell line viability.....	89
Figure 4.25. Effect of PEtOx-b-PLA copolymer and polymersome on MCF10A cell line viability.....	90
Figure 4.26. The representative histograms showing the binding affinity of P18-PEtOx-b-PLA polymersome on MCF10A and AU565 cell line.	91
Figure 4.27. P18-PEtOx-b-PLA polymersome binding affinity on MCF10A and AU565 cell lines by confocal microscopy.....	92

Figure 4.28. Determination of the cytotoxic effect of P18-PEtOx-b-PLA-BikDD on AU565 cells.....	94
Figure 4.29. Determination of the cytotoxic effect of P18-PEtOx-b-PLA-DOX polymersome on AU565 cells.....	96
Figure 4.30. Relative Bik/18sRNA mRNA expression for non-transfected (Cnt) and AU565 cells transfected with P18-PEtOx-b-PLA-BikDD using qPCR.	97
Figure 4.31. Cell cycle profiles of AU565 cells examined by flow cytometry..	99
Figure 4.32. Effect of P18-PEtOx-b-PLA-DOX polymersome on AU565 cell death at 48 hours.....	101
Figure 4.33. Effect of P18-PEtOx-b-PLA-DOX polymersome on AU565 cell death at 72 hours.....	102
Figure 4.34. Cytotoxicity of PEtOx-PEI-PCL copolymer and micelles against HUVEC.	104
Figure 4.35. Cytotoxicity of PEtOx-PEI-PCL copolymer and micelles against HEK293 cells.	105
Figure 4.36. Cytotoxicity of PEtOx-PEI-PCL copolymer and micelles against MSC cell	106
Figure 4.37. Cytotoxicity of PEtOx-PEI-PCL copolymer and micelles against MCF10A cells.....	107
Figure 4.38. The representative histograms showing binding affinity of P18-PEtOx.PEI-PCL micelles on MCF10A and AU565 cells.....	108
Figure 4.39. P18-PEtOxPEIPCL micelles binding affinity on MCF10A and AU565 cell lines by confocal microscopy	109
Figure 4.40. Determination of the cytotoxic effect of P18-PEtOxPEIPCL-BikDD on AU565 cells	111
Figure 4.41. Determination of the cytotoxic effect of P18-PPP30-DOX micelle on AU565 cells.	113

Figure 4.42. Relative Bik/18sRNA mRNA expression using qPCR for non transfected and AU565 cells transfected 4 and 8 μ g of BikDD in P18PPP60 micelle/BikDD complex....	114
Figure 4.43. Cell cycle profiles of AU565 cells examined by flow cytometry.	116
Figure 4.44. Effect of P18-PPP30-DOX micelle on AU565 cell death at 48 hours.....	118
Figure 4.45. Effect of P18-PPP30-DOX micelle on AU565 cell death at 72 hours.....	119
Figure 4.46. Effect of P18-PEtOx-DOPE-DOX liposomes on tumor growth.....	121
Figure 4.47. Effect of P18-PEtOx-DOPE-DOX liposomes on the CD-1 nude mice body weight.....	122
Figure 4.48. Antitumor effect of P18-PEtOx-DOPE-DOX liposomes on CD-1 nude mice models.....	123
Figure 4.49. Histopathological analysis of the P18-PEtOx-DOPE-DOX liposomes tumor samples.....	124
Figure 4.50. Effect of P18-PEtOx-b-PLA-DOX polymersomes on tumor growth	127
Figure 4.51. Effect of P18-PEtOx-b-PLA-DOX polymersomes on the CD-1 nude mice body weight.....	128
Figure 4.52. Antitumor effect of P18-PEtOx-b-PLA-DOX polymersomes on CD-1 nude mice models	129
Figure 4.53. Histopathological analysis of the P18-PEtOx-b-PLA-DOX polymersomes tumor samples	130
Figure 4.54. Effect of P18-PEtOx-PEI-PCL-DOX micelles on tumor growth	133
Figure 4.55. Effect of P18-PEtOx-PEI-PCL-DOX micelles on the CD-1 nude mice body weight.....	134
Figure 4.56. Antitumor effect of P18-PEtOx-PEI-PCL -DOX micelles on CD-1 nude mice models.....	135

Figure 4.57. Histopathological analysis of the P18-PEtOx-PEI-PCL-DOX micelles tumor samples.....	136
Figure 4.58. Effect of P18-PEtOx-DOPE-BikDD liposomes on tumor growth.....	139
Figure 4.59. Effect of P18-PEtOx-DOPE-BikDD liposomes on the CD-1 nude mice body weight.....	140
Figure 4.60. Antitumor effect of P18-PEtOx-DOPE-BikDD liposomes on CD-1 nude mice models.....	141
Figure 4.61. Histopathological analysis of the tumor samples of P18-PEtOx-DOPE-BikDD liposomes.....	142
Figure 4.62. Effect of P18-PEtOx-b-PLA-BikDD polymersome on tumor growth.....	145
Figure 4.63. Effect of P18-PEtOxbPLA-BikDD polymersome on CD-1 nude mice body weight.....	146
Figure 4.64. Antitumor effect of P18-PEtOx-b-PLA-BikDD polymersome on CD-1 nude mice models.....	147
Figure 4.65. Histopathological analysis of the tumor samples of P18-PEtOx-b-PLA-BikDD polymersome.....	148
Figure 4.66. Effect of P18-PEtOx-PEI-PCL-BikDD micelles on tumor growth.....	151
Figure 4.67. Effect of P18-PEtOx-PEI-PCL-BikDD micelle on CD-1 nude mice body weight.....	152
Figure 4.68. Antitumor effect of P18-PEtOx-PEI-PCL-BikDD micelle on CD-1 nude mice models.....	153
Figure 4.69. Histopathological analysis of the tumor samples of P18-PEtOx-PEI-PCL-BikDD micelles.....	154

LIST OF TABLES

Table 1.1. Molecular classification of breast cancer subtypes	7
Table 1.2. Response of different breast cancer when treated with EGFR inhibitors and chemotherapy drugs.	12
Table 1.3. Short homing peptides used for targeted nanoparticle.	30
Table 3.1. Components for NotI restriction enzyme digest.	42
Table 3.2. Components for ligation	43
Table 3.3. Site-directed mutagenesis components.	44
Table 3.4. RT-PCR reaction master mix.....	50
Table 3.5. Quantitative PCR conditions	51
Table 4.1. Average percentage binding affinity of peptide MC10, peptide 11, and peptide 18 to AU565, SKBR3, MCF10A, MCF12A, and HUVEC cells.....	58
Table 4.2. Effect of P18-PEtOx-DOPE-DOX liposomes on tumor tissues of CD-1 nude mice used in the study.....	125
Table 4.3. Effect of P18-PEtOx-b-PLA-DOX polymersomes on tumor tissues of CD-1 nude mice used in the study.	131
Table 4.4. Effect of P18-PEtOx-PEI-PCL-DOX micelles on tumor tissues of CD-1 nude mice used in the study.....	137
Table 4.5. Effect of P18-PEtOx-DOPE-BikDD liposomes on tumor tissues of CD-1 nude mice used in the study.....	143
Table 4.6. Effect of P18-PEtOx-b-PLA-BikDD polymersomes on tumor tissues of CD-1 nude mice used in the study.	149

Table 4.7. Effect of P18-PEtOx-PEI-PCL-BikDD micelles on tumor tissues of CD-1 nude mice used in the study.....	155
---	-----



LIST OF SYMBOLS/ABBREVIATIONS

β -actin	beta actin
$^{\circ}\text{C}$	Degree centigrade
μg	Microgram
μL	Microlitre
μm	Micrometer
μM	Micro Molar
Asp (D)	Aspartic acid
ATCC	American Type Culture Collection
Bcl-2	B-cell lymphoma 2
Bik	Bcl-2-interacting killer
bp	Base pair
cDNA	Complementary
CO_2	Carbon dioxide
DAPI	Diamidino phenylindole
DDS	Drug delivered systems
DMEM	Dulbecco's modified eagle medium
DMSO	Dimethyl sulfoxide
DNA	Deoxyribonucleic acid
DOPE	Dioleoylphosphatidylethanolamine
DOX	Doxorubicin
ECL	Enhanced chemo luminescence
ECM	Extracellular matrix
<i>E. coli</i>	<i>Escherichia coli</i>
EGFR	Epidermal growth factor receptor
EGFP	Enhanced green fluorescein protein
EPR	Enhanced permeability and retention
ER	Estrogen receptor
FBS	Fetal bovine serum
FDA	U.S. Food and Drug Administration

g	Gram
HER2	Human epidermal growth factor receptor 2
HDF	Human dermal fibroblast
IC ₅₀	Inhibitory concentration for 50 percent
kDa	Kilo Dalton
LB	Luria-Bertani
MEGM	Mammary epithelial cell growth medium
mL	Millilitre
mm	Millimeter
mM	Milli Molar
mol/L	Mol/Liter
MSC	Mesenchymal Stem Cell
ng	Nanogram
NGR	Asparagine-Glycine-Arginine
nm	Nanometer
PBS	Phosphate buffer saline
PCL	Poly(ϵ -caprolactone)
PCR	Polymerase chain reaction
PEt(Ox)	Poly(2-ethyl-2-oxazoline)
PEI	Polyethylenimine
PI	Propidium iodide
PLA	Poly(lactic acid)
PR	Progesterone receptor
PS	Penicillin and streptomycin
qPCR	Quantitative polymerase chain reaction
RGD	Arginine-Glycine-Aspartic acid
SDS-PAGE	Sodium dodecyl-sulfate polyacrylamide gel electrophoresis
Ser (S)	Serine
TAMRA	Tetramethylrhodamine
Thr (T)	Threonine
TEMED	Tetramethylethylenediamine
U	Unit(s)
V	Volt

WST

Water soluble tetrazolium



1. INTRODUCTION

1.1. CANCER

Cancer, abnormal growth and division cells, is a major public health problem worldwide and is ranked as the leading cause of death in developed countries [1]. In order to understand the biology of cancer, the distinctive and complementary capabilities of tumor growth and metastatic dissemination are summarized under the ten hallmark of cancer [2]. The most fundamental trait of cancer cells is the ability of cancer cell to sustain chronic proliferation. Cancer cells deregulate growth promoting signals, thus become masters of their own destinies [3]. They either produce growth factor ligands themselves or send signals to stimulate normal cells in the tumor-associated stroma [4, 5]. Somatic mutations in certain tumors have been revealed with high-throughput DNA sequencing analyses of cancer cell genomes. Nearly 40 percent of melanomas have mutations affecting B-Raf protein structure, which results in constitutive signaling through Raf to MAP-kinase pathway [6], and mutation in PI3-kinase are detected in an array of tumors [7].

Excessive elevated signaling by ras, myc, and raf oncoproteins can induce cell senescence and apoptotic cell death [8, 9]. Cancer cells also evade growth suppressors and RB and TP53 proteins are the prototypical tumor suppressors that operate as central control nodes which govern the decision of cell proliferation, senescence, and apoptosis [2]. The upstream regulators and downstream effectors are components of apoptotic machinery. The regulators of apoptosis are divided as extrinsic and intrinsic apoptotic program and both culminate in activation of caspases. The pro- and anti-apoptotic members of Bcl-2 family proteins control the counterbalance the signals between regulators and effectors of apoptotic trigger [10]. In cellular stress like nutrient deficiency autophagy is a cellular physiological response which break down cellular organelles in cell [11]. Necrosis involves cells to become bloated, explode, and release content into local tissue microenvironment under genetic control [12].

Another distinctive characteristic of cancer cell is the replicative immortality. Telomeres, protect the end of chromosomes, involve in the capability of unlimited proliferation [13]. Telomerase is expressed in 90 percent of human cancer cells and function as to extend

telomeric DNA. In premalignant growths eroded telomeres and end-to-end chromosomal fusions have been reported [14]. Cancer cells require nutrients and oxygen along with evacuation of metabolic wastes and carbon dioxide like normal cells and this is fulfilled by inducing angiogenesis by producing blood vessels within tumors [3]. The epithelial-mesenchymal transition (EMT) pathway is involved in the invasion and metastasis of transformed epithelial cells [15, 16]. The physical dissemination of cancer cells from primary tumor and adapting these cells to foreign tissue are the major phases of metastasis. The primary tumor release systemic suppressor factors in some cancer types and render micrometastases in dormant state [17], whereas in melanoma and breast cancer macroscopic metastases may erupt after decades of surgical removal of primary tumor [2]. Tumor-associated inflammatory response is another hallmark of cancer and is contributed by supplying bioactive molecules to the tumor microenvironment. Inflammatory cells can release reactive oxygen species to nearby cells [18].

The ability to reprogram their energy metabolism is also another distinctive characteristic of cancer cell. In 1956, Otto Warburg observed that even in presence of oxygen cancer cells can reprogram their glucose metabolism, leading to aerobic glycolysis state [19]. This glycolytic fueling is associated with mutant tumor suppressors like TP53 and oncogenes such as ras and myc [20] and dependence on glycolysis can be emphasized under hypoxic conditions, where glucose transporters and multiple enzymes are upregulated [21, 22].

The immune systems role in resisting late-stage tumors is still an unsolved issue. Cells and tissues are constantly monitored by immune system thus, developing cancer cells are recognized and eliminated by immune system [2]. Immunoediting is the process of elimination of immunogenic cancer cell clones in the immunocompetent hosts. The immunogenic cancer cells are rejected when cells from nonedited tumors are transplanted into recipients [23]. Studies have shown that organ transplant recipients have developed donor-derived cancer [24]. Cancer cells have the ability to paralyze CD8⁺ cytotoxic T lymphocytes and natural killer cells by secreting immunosuppressive factors [25]. In the late 1990s, neoplastic tissue infiltration of immune systems promotes tumor progression. This had led to the chronic inflammation site associated with tumor formation and tumors could be portrayed as wounds that never heal [26]. In normal wound healing and fighting infection process the immune inflammatory cells appear briefly and then disappear.

However, at chronic inflammation, these cells presence is associated with angiogenesis, tissue pathologies and neoplasia [18]. Figure 1.1 summarizes the ten hallmarks of cancer.

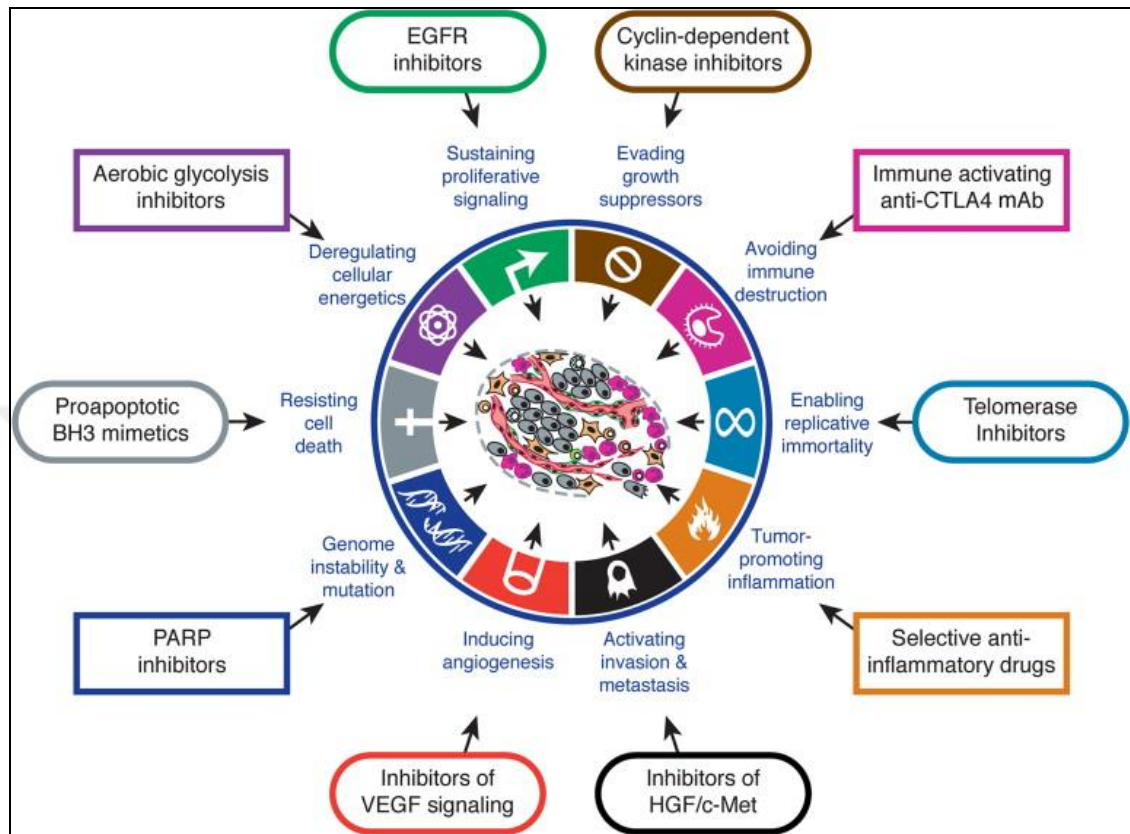


Figure 1.1. Hallmarks of cancer [2].

Early diagnosis of cancer is important for survival of patient and successful diseases prognosis [27]. One methods in identification of cancer is the tumor associated antigens which are used as biomarkers which could be detected from blood, urine and other body fluids [28]. Different cancer types have different diagnostic methods; PET, CT, and MR imaging procedure is followed in cancers such as; breast, colorectal, lung, brain and prostate cancers [29-33]. Keratins (K) are used extensively as diagnostic tumor markers in cancer. Epithelial cancers (adenocarcinomas) may arise in different organs and keratins are used as markers to differentiate the tissue origin of each adenocarcinoma. Most adenocarcinomas express K8, K18, and K19 whereas, K7 and K20 expression is variable [34]. K20 and K7 co-expression is reported in advanced colorectal cancers [35], whereas an important characteristic of ovarian, endometrial and lung carcinomas is the $K7^+/K20^-$ phenotype [36]. Keratin also play an important role in the evaluation of breast cancer and

studies show that K7, K8, K18, and K19 expression is observed in more than 90 percent of all breast cancers [37].

1.2. BREAST CANCER

The breast is an organ whose function is to produce milk. It consists of lactiferous ducts which later at puberty proliferate so their termination forms solid masses of cells making breast lobules [38]. Although, man and woman both have breasts, breast tissue is more in a woman compared to man. Breast starts from the collarbone to the armpit and covers a larger area across the breast bone. Connective, glandular, and fatty tissues are found in the breast. The anatomy of the breast comprises of lobules, alveolus, ducts, and nipples and their functions are to produce, store, carry, and secrete milk, respectively [39, 40]. Figure 1.2 shows the anatomy of the human mammary glands. Changes start to begin in the breast anatomy when a woman becomes pregnant or when lactation starts. At first trimester, rapid growth of ducts, lobules and alveolus takes place. Prior to the birth of the infant, prolactin hormone induces alveolus to secrete and then ducts starts to release milk [41]. After weaning, the mammary glands regresses through programmed cell death to a near pre-pregnancy state [42].

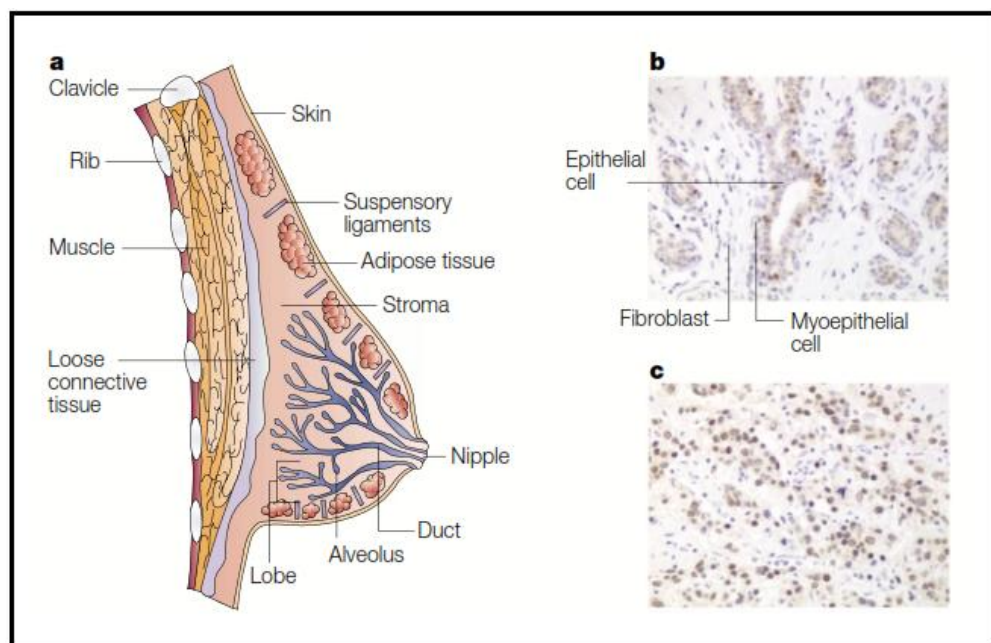


Figure 1.2. Breast tissue structure. Anatomy of the mammary gland (a), cells in a normal (b) and malignant breast tissue (c) [42].

Breast cancer is the most common diagnosed cancer seen worldwide, consisting of 24.2 percent incidence rate of all cancers. For the year 2018, there was an estimation of 2.1 million diagnosed breast cancer cases and this is equivalent to 1 in 4 cancer cases in seen in women. The mortality profile of breast cancer is estimated to be approximately 627,000, thus, it accounts for the highest cancer type seen in 103 countries [43]. Therefore, breast cancer is categorized as a major health problem and the main cause of death in females [44]. 60 percent of the deaths were seen in economically developing countries, while economically strong countries like those in Europe and North America, showed higher incidence rate than underdeveloped countries [44, 45]. Among United States women, 266,120 breast cancer incidence cases are expected for 2018, and 40,920 of deaths [46].

The most recent report on breast cancer among Turkish women shows that breast cancer has an incidence rate of 40.7 cases per 100,000 [47]. Developing countries like Turkey show an increase of cancer incidence and mortality rates each passing year. A major problem in Turkey is the bad registry system for patients with cancer, which is the main reason for the increase of incidence rate, as this makes it hard to collect past data about cancer incidence rates [48]. Although, many countries have mammographic screening programs, everyone does not show equal importance to these programs. Countries such as Turkey and Japan only have 20 percent participation rate while this rate is over 80 percent in United States and Netherlands. Breast cancer early stage detection by screening programs is very important as there is a strong link between stage of diagnosis and survival rate [49]. Worldwide epidemiological studies conducted on breast cancer demonstrated that, 89 percent of women diagnosed of breast cancer had an age of 40 and onwards [50].

Breast cancer is a heterogeneous disease; each breast cancer type can have differences within itself and is caused by different factors unrelated to one another [51]. Some of the risk factors that lead to increase of breast cancer were heavy menstrual history, recent usage of postmenopausal hormone therapy, giving birth at late age, high alcohol consumption, and having a family history of breast cancer [52-54]. Further factors include other reproductive factors, such as age at menopause and menarche [55]. Although, genetics is another risk factor which plays a very important role in the development of breast cancer, it accounts to 5 - 6 percent of cases in breast cancer. BRCA-1 and BRCA-2 were detected in nearly 80 percent of hereditary breast cancer. Germline mutations of TP53, PTEN, CDH1, and STK11 genes are also associated with high risks for developing

breast cancer [56]. Weight of a woman is also a cause of breast cancer, as fat tissues have the ability to produce hormones which are converted to estrogen. Hormonal history of a woman is another important factor, as it is associated with estrogen and progesterone hormones exposed to the breast [56]. The growth of the female breast at puberty is affected by estrogen hormone and paracrine factors within the tissues of breast, affect differentiation and cell division of breast [57]. Breast cancer shows high heterogeneous disease characteristics related to cell origin, histology, and mutations. Metastasis potential, disease progression, therapeutics response, and outcome of clinical data are also factors effecting heterogeneity of the disease [58, 59].

Thus, to be able to understand the disease better, it is important to have a correct classification of the breast cancer. Breast cancer related deaths can be connected to recurrence of breast cancer, which is a major clinical problem. Unfortunately, discomfort or pain in breast cancer patients is not seen frequently; one can have a malignant tumor with no pain at all. Depending on the stage of the breast cancer surgery can be an option for the breast cancer patients [60]. Usually, patients at an early stage get surgery and then mastectomy or radiation therapy. Improvements have been made in the current breast cancer treatment strategies including surgical resection, chemotherapy, and radiotherapy. However, major challenges still exist in survival rate of breast cancer [61].

1.3. GRADING OF BREAST CANCER

Grading system includes nuclear and histological grading in breast cancer. Van Nuys is a classification system includes comedo-type necrosis and nuclear grade, it is widely used in predicting the recurrence of the disease [62]. Grading breast carcinoma histologically provides important information to clinicians [63]. Miller and Payne grading system is routinely used for histological response to chemotherapy, where grades 1-4 are partial pathological responsive while, grade 5 is complete pathological responsive. Pathological examination of tumor stained in haematoxylin and eosin detectable macroscopically determine the grading of the tumor. Grade 1 shows no alteration in malignant tumor, whereas; Grade 2 shows up to 30 percent loss of tumor cells. Grade 3 has nearly 30 and 90 percent reduction in tumor cells. In Grade 4, more than 90 percent loss of tumor can be detected and Grade 5 shows no malignant cells but vascular fibroelastotic stroma [64].

1.4. CLASSIFICATION OF BREAST CANCER

1.4.1. Luminal A and B Breast Cancer

A comprehensive study by Perou *et al.* 2000 showed the gene expression profiling and molecular classification of breast cancer. Breast cancer is classified under four subtypes as; luminal A and B, triple negative/basal, and human epidermal growth factor receptor 2 (HER2) [65]. Clinically, estrogen receptor (ER), progesterone receptor (PR), and HER-2 gene expression levels are checked in breast cancer patients. This classification method helps patients to be grouped as positive for hormone receptor tumors or HER2 tumors, or as negative for all three (tumors that show no PR, ER and HER-2 expression) [66, 67]. Table 1.1 shows the subtype, prevalence, immunoprofile and other characteristics of breast cancer. Luminal A breast cancer, both hormone receptors are positive and often found to be responsive to chemotherapy. Subtype of luminal B breast cancer shows ER and PR positive along with HER2 expression. The prevalence of this cancer type is nearly 20 percent, where as luminal A shows a 40 percent prevalence rate.

Table 1.1. Molecular classification of breast cancer subtypes [66, 68].

Classification	Prevalence	Immunoprofile	Other Characteristics
Luminal A	40%	ER ⁺ , PR ^{+/-} , HER2 ⁻	Ki67 low, endocrine responsive, often chemotherapy responsive
Luminal B	20%	ER ⁺ , PR ^{+/-} , HER2 ⁺	Ki67 high, variable to chemotherapy, HER2 are trastuzumab responsive, usually endocrine responsive
Triple Negative/Basal 1	10–15%	ER ⁻ , PR ⁻ , HER2 ⁻	EGFR ⁺ , often chemotherapy responsive
HER2	15–20%	ER ⁻ , PR ⁻ , HER2 ⁺	Ki67 high, trastuzumab responsive, chemotherapy responsive

1.4.2. Triple-Negative Breast Cancer

Triple negative breast cancer (TNBC) is also known as basal, shows no expression in any of the three molecular markers (ER, PR and HER2). Basal epithelial cell layer shows a high expression in this type of breast cancers thus, cytokeratins 5, 6, and 17 are expressed [58, 67, 69]. Approximately 80 percent of TNBC are basal-like [70]. TNBC can confine other types of breast cancer like claudin-low tumor, which are enriched with stem cells and have epithelial to mesenchymal transition characteristics [71]. 15 percent of all invasive breast cancers are TNBC and basal like breast cancer subtypes which have are graded histologically as highest grade [72].

1.4.3. HER-2 Positive Breast Cancer

HER2 positive breast cancer accounts for nearly 30 percent of all breast cancers and clinically shows poor prognosis [73, 74]. In healthy tissues HER2 has several physiological roles; cell survival, repair mechanism and differentiation are regulated by HER2 signalling [75]. The mechanisms effecting breast cancer development are very complex and are different between each individual tumors. The p53 pathway has a key role in development of cancer and in breast cancer progression it plays a crucial role. [76, 77]. Aggressiveness of the disease and overall survival rate is linked with p53 mutations with a frequency of 80 percent [78]. Also p53 pathway has importance in diagnosis, prognosis and ultimately in treating breast cancer [79].

Receptor Tyrosine Kinase (RTKs) is another pathway effecting breast cancer. RTKs include HER (also called epidermal growth factor receptor (EGFR)) family and Src-family tyrosine kinases [80]. EFGR needed for normal growth is a member of RTK family. EGFR's intracellular domain is made up of 542 amino acid residues, consisting of a transmembrane-anchoring part, amino-terminal extracellular domain and a carboxyl terminal domain which is in the intracellular part. It is the carboxyl terminal which has tyrosine kinase (TK) activity [81].

The family of EGFR consists of the following members: EGFR (also could be referred as HER1), ERBB2 (which is also known as HER2/neu), ERBB3 (HER-3), and ERBB4 (HER-4) [82]. When a ligand, such as epidermal growth factor (EGF), binds to EGFR

extracellular domain, the EGFR gets activated. Then the receptor dimerizes, causing the tyrosine kinase, an intrinsic protein, to be activated and autophosphorylation of tyrosine occurs. Once they are phosphorylated, these residues come to Src homology 2 (SH2) proteins and they get recruited, thus the intracellular signaling pathways are activated in the end of these sequences [83].

Then the rest happens similar to a domino effect; it could activate the Ras, which activates Raf, which then activates either one of the two pathways; phosphatidylinositol 3-kinase (PI3K)/Akt or mitogen-activated protein kinase (MAPK). The key regulator in the survival of the cell is PI3K/Akt pathway, while the proliferation of the cell is dependent on the MAPK pathway [84, 85]. Following this activation, transcription factors that play a key role (c-fos, NF- κ B, STAT, c-Jun, and c-myc) are activated. The Akt pathway can be mediated by antiapoptotic signals which are expressed at high level, the activation of mRNA translation and pro-apoptotic signals expressed at low level [83, 86, 87].

EGFR pathway plays an important role in cancer; its activation enhances growth and progression of cancer, it promotes proliferation and metastasis, and also it inhibits apoptosis. Furthermore, progression of the disease, insufficient survival and response to therapy is associated with expression of EGFR in tumors. Studies show that highly expressed EGFR was observed in breast cancer, but we should keep in mind that other mechanisms from EGFR expression also can be involved in EGFR signaling. TGF- α activation in an autocrine loop is related to EGFR and cancer development. In this way, the gene overexpression occurs without gene amplification [83, 88].

EGFR overexpression is frequently observed in cancer; at least 50 percent of triple-negative breast cancer cases overexpress EGFR [89]. 20 to 30 percent of breast cancers overexpress HER-2 gene, transmembrane receptor which is 185 kDa [90]. Another study indicates that 30 percent of inflammatory breast cancer (IBC) also expresses EGFR and clinically is one of the most aggressive subtype of breast cancer [89].

A recent study conducted on breast cancer showed that PR and ER positive breast cancers patients had less recurrence rate compared to patients with HER2-overexpressing and triple negative breast cancers (TNBC). Also, correlative results were observed for mastectomy patients [91]. HER-2, member of human EGFR family, can also be named as HER or ERBB, and it's overexpression has a key role in progression and development of certain

aggressive breast cancers types [92]. SKBR3 and AU565 are breast cancer cell lines studied for breast cancer models and are classified as HER2 subtype showing and overexpression in HER2 gene [93]. Combination therapy of pertuzumab and trastuzumab, which are humanized monoclonal antibodies, is the first line treatment for HER2 positive breast cancer patients. For patients showing hormone receptor positive response and HER2 positive, treatment procedure includes anti-HER2 therapy and hormonal therapy combination [68].

1.5. THE MECHANISM OF BREAST CANCER METASTASIS

Breast cancer spread through direct invasion, blood vessel, and lymphatic route. Usually distribute metastatic colonies throughout the brain, bones, liver and lungs. Highest frequency of metastatic lesions are found in bone by 83 percent, where as lung and liver are less affected by 27 percent [94]. Primary breast tumors invade nipple, nearby muscles of chest wall, skin fascia and parenchyma. Nipple invasion is found in 23 to 31 percent of all invasive carcinomas detected clinically. In metastatic breast cancer, the lymph node stations (known as axilla) are involved and account for 40 to 50 percent of clinically detectable cases [95-97].

Intravasation is the invasion of carcinoma cells into blood and lymphatic vessels after they stimulate angiogenesis stromal membrane of breast. Epidermal growth factor (EGF) stimulate the intravasation of cancer cells. Level of circulating tumor cells indicate clinical progression of breast cancer's which have been metastasized. Cancer cells must extravasate after entering tissues blood vessels and the close relation between cancer cells and macrophages suggest that cancer cells recruit macrophages for circulating tissue parenchyma [98, 99].

At initial of clinical outcome, nearly 30 percent of breast cancer patients have thousands of micro metastases, which are clumps of disseminated cancer cells [100, 101]. However, this should not be concluded as all of these patients will develop metastasis disease. These micro metastasis in lymph nodes are detected by antibodies reactive with cytokeratins. Single-cell micro metastasis is possible to be detected among 10⁵ mesenchymal cells in blood, lymph nodes or bone marrow. A hot topic in last few decades is cancer stem cells. Breast cancer can originate from breast cancer stem cells, so self-renewal ability of cancer

stem cells promote tumor proliferation and metastasis. In normal and malignant cells, stem cell enrichment is promoted by HER2 overexpression [102].

P53 is a one of the main regulators of metastasis and controls transcription genes in metastatic pathway. 40 percent of all breast cancer show TP53 mutations and this varies among subtypes: 80 percent in basal like, 72 percent in HER2-enriched, 12 percent in Luminal A, and 29 percent in Luminal B subtypes. Tumor regression is seen by restoring p53 function in tumors [103, 104]. In systemic treatment of metastatic breast cancer, a major obstacle is drug resistance, which ends up with treatment failure and mortality [105]. Thus, alternative methods are required for breast cancer treatment.

1.6. TREATMENT OF BREAST CANCER

1.6.1. Chemotherapeutic Drugs

Although chemotherapy options for breast cancer has advanced considerably, during recent years death rates were remained unaffected [106]. Frontline treatment are endocrine therapy for hormone receptor positive breast cancer, whereas for HER2 positive breast cancer the innovator drug is trastuzumab (Herceptin) [107]. Tamoxifen was the first drug that has the molecular-target ability, although it was developed as oral contraceptive, it has been used for ER⁺ breast cancers [108]. Trastuzumab chemotherapeutic drug was developed against HER2⁺ breast cancers and is the first oncogene-targeted drug [109]. Although trastuzumab is an effective drug against HER2⁺ breast cancer patients, not all of these patients are sensitive to trastuzumab. Furthermore, a major drawback against HER2⁺ breast cancer patients that are sensitive to trastuzumab patients is that they develop resistance in 1 year of treatment [110]. HER2⁺ breast cancer patients receive combination therapy of trastuzumab with either docetaxel or paclitaxel as a first-line treatment of metastatic tumors [111].

Lapatinib is another drug used against HER2⁺ breast cancer, which is a dual EGFR/HER2 kinase inhibitor, is effective on patients who have developed transtuzumab resistance [112]. Combination therapy of lapatinib and trastuzumab was more efficient that monotherapy [113]. Toxicity caused by drug along with severe-side effects are decaps in choosing the right treatment method. Awada *et al.* conducted a study showing that

trastuzumab and taxane combination therapy was more effective than lapatinib and taxane, along with lower drug toxicity and side-effects for HER2⁺ metastatic breast cancer patients [114].

A study on different chemotherapy drugs and EGFR inhibitors in response to a broad range cell lines of breast cancer, HER-2 overexpressing cells such as SKBR3 were sensitive to EGFR inhibitors like erlotinib and gefitinib and less sensitive to doxorubicin (DOX) chemotherapeutic drug. Table 1.2 shows concentration of drug inhibiting 50 percent of cell growth (IC₅₀ value) [115].

Table 1.2. Response of different breast cancer when treated with EGFR inhibitors and chemotherapy drugs [115].

	BT20	HCC1937	MDA- MB-231	BT474	SKBR3
Gefitinib, IC₅₀ (μM)	15.5 ± 1.4	8.4 ± 1.5	20.7 ± 1.1	0.25 ± 0.05	0.88 ± 0.31
Erlotinib, IC₅₀ (μM)	20.1 ± 2.7	26.2 ± 9.3	42.6 ± 3.1	3.1 ± 0.4	3.6 ± 0.4
Carboplatin, IC₅₀ (μM)	8.6 ± 4.8	11.6 ± 2.8	15.4 ± 3.3	>20	9.7 ± 5.3
Doxorubicin, IC₅₀ (nM)	34.7 ± 9.5	38.6 ± 1.6	59.6 ± 9.8	117.0 ± 40.0	27.0 ± 9.0
Docetaxel, IC₅₀ (nM)	2.4 ± 1.4	7.2 ± 2.5	3.0 ± 0.5	2.8 ± 0.3	1.2 ± 0.6

Another comprehensive study showed a heat map of maximum cell-growth inhibition of several compounds. HER2⁺ breast cancers cell lines that were linked to trastuzumab resistance were sequenced for several mutations. It is clearly seen that doxorubicin and bortezomib were effective compounds in breast cancer AU565 and SKBR3 cell lines. Low cell viability of the HER2⁺ breast cancers cell lines were marked as red (bottom row of Figure 1.3) [116].

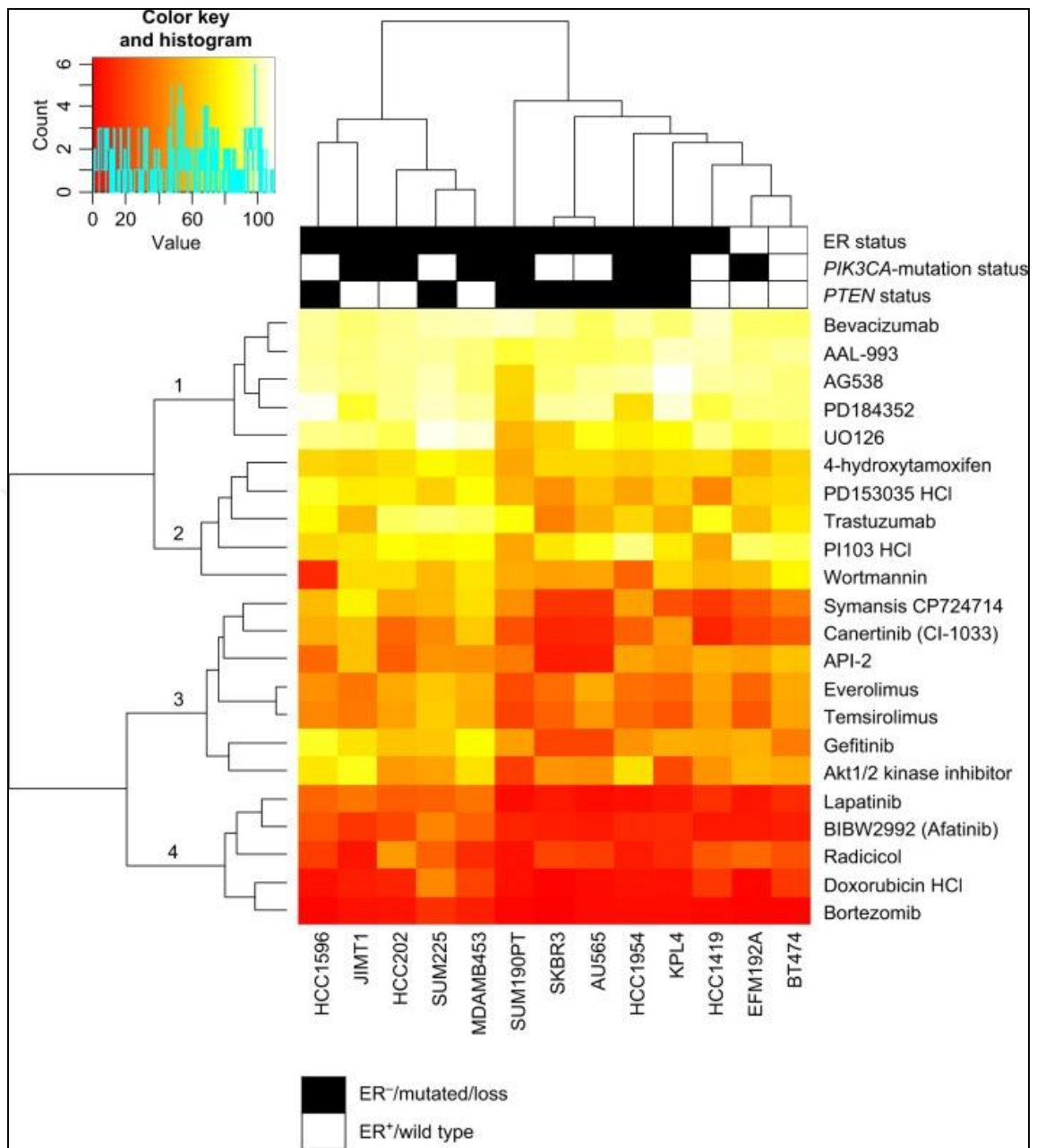


Figure 1.3. Heat map showing cell growth of different cells treated with different compounds [116].

1.6.2. Doxorubicin

DOX or known as anthramycin, an anthracycline antibiotic, is commonly utilized in cancer chemotherapy. DOX is an FDA approved chemotherapeutic drug and is usually prescribed in ovary, lung, breast, and stomach cancers. DOX acts in cancer cells by either intercalating into DNA, which causes disruption of topoisomerase II, or generating free radicals which damage DNA, membrane and proteins. DOX oxidizes into an unstable metabolite and when this is converted back to DOX, it releases reactive oxygen species (ROS) [117]. ROS lead to oxidative stress, DNA and membrane damage and thus the apoptotic pathway of cell death is triggered as given Figure 1.4.

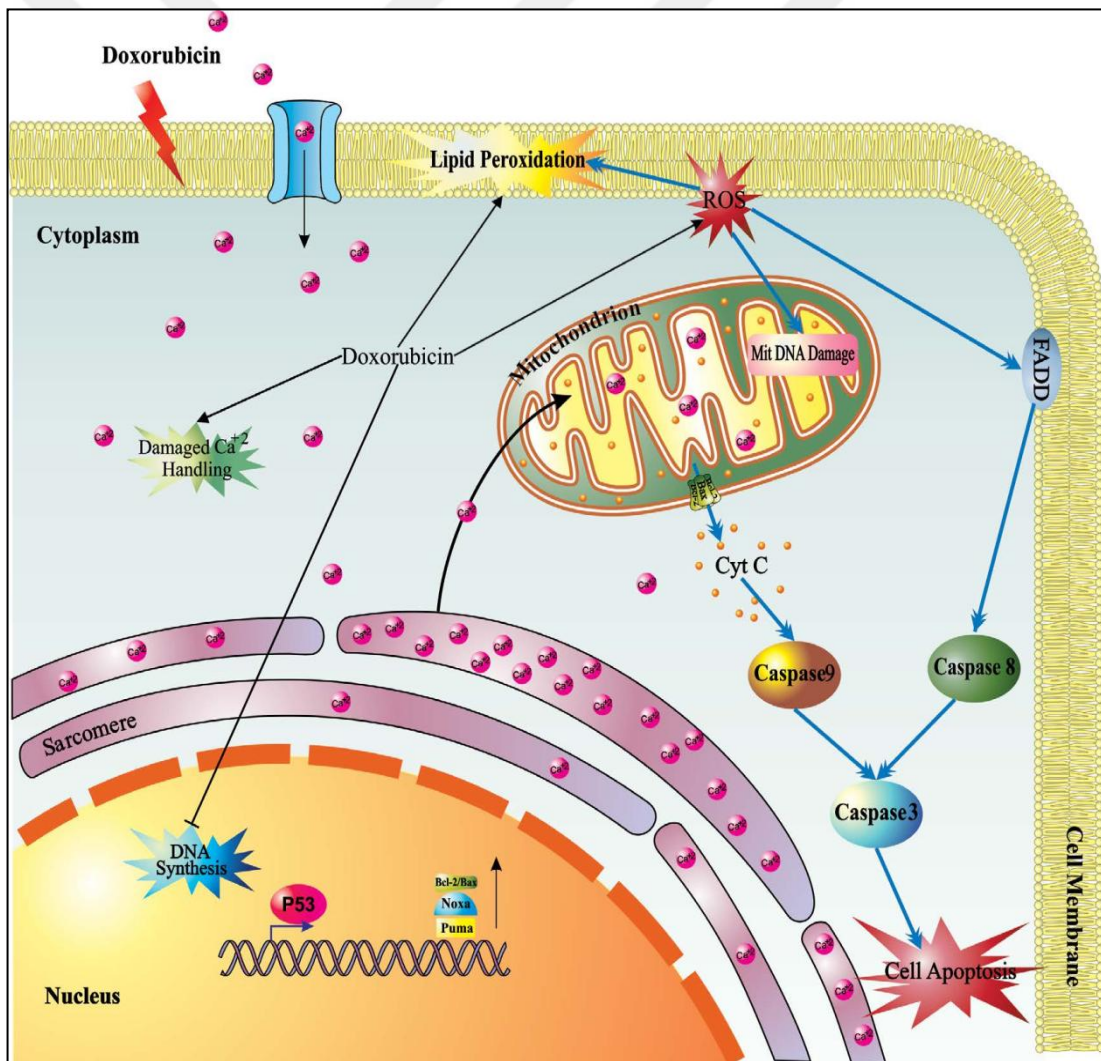


Figure 1.4. Effect of doxorubicin on cell death [118].

Poor oral bioavailability (nearly 5 percent) of DOX is due to low permeability of the drug. Catalyzed hydrolysis in the stomach and susceptibility of cytochrome P450 are other drawbacks of the drug and thus results in high presystemic metabolism [119]. Breast cancer treated with DOX leads to a decrease in concentration and time dependent Bcl-2 while increasing Bax levels [120].

DOX administered alone causes cardiotoxicity and mostly accumulate in liver, however, liposomal doxorubicin conjugates lead to a decrease of cardiotoxicity. Other studies showed that patients that are treated with liposomal DOX showed reduced of heart failure [106, 121].

Doxil is a liposomal formulation of DOX which is approved by the US Food and Drug Administration (FDA) [122]. Doxil, known as Caelyx in the rest of the world, is used for the treatment of AIDS-related Kaposi's sarcoma, ovarian carcinoma, multiple myeloma and in breast cancer patients with risk of cardiotoxicity for anthracycline drugs [123]. When Doxil is coupled with NGR peptides (a type of tumor homing peptide) it was observed that the antitumor activity was increased in orthotopic murine neuroblastoma models [124].

LipoDox, a generic version of Doxil, is a pegylated liposomal formulation of doxorubicin [125]. Myconet is a non-pegylated liposomal doxorubicin used clinically in treatment of solid tumors such as metastatic breast cancer and epithelial ovarian cancer. Preclinical studies show that Myconet had less toxic profile and clinical evidence confirmed this hypothesis [126, 127].

1.7. BIK, A PROAPOPTOTIC MEMBER OF BCL-2 FAMILY PROTEINS

In recent years gene delivery has shown hope for cancer treatment. Non viral breast cancer gene therapy methods include delivery of genetic material by physically or chemically [128]. PE1A-K2 is therapeutic nucleic acid which encodes E1A, which is a protein with known antitumor activity [129].

Another example of non-viral cancer therapy is, ZYC300 which is a pDNA that encodes the inactivated form of cytochrome P4501B1 (CYP1B1) carcinogen activator and Phase I clinical trials against ZYC300 treatment against renal diseases shows promise [130]. Protein drugs are one the most potent biotherapeutics with high potential in cancer

therapy. Among the most potent biotherapeutics, protein drugs show promising development in cancer treatment [131].

Over the past decades, proteins that play role in apoptosis have been investigated for cancer therapy. Among these apoptotic proteins, TRAIL and cytochrome c have been widely used as protein drugs [132]. These protein drugs show advantages such as high selectivity and therapeutic activity, and low toxic effect to healthy cells in comparison to chemotherapeutics. However, direct administration of these protein drugs have several drawbacks as rapid elimination and degradation, possible immune response, lack of bioavailability and poor cell permeability [133].

Apoptosis, programmed cell death, eliminates developmentally excess, mutated and damaged cells without causing inflammation. In cancer therapy, apoptosis is an important mechanism of cell death and thus, altering susceptibility of apoptosis enhances resistance to current used anticancer therapies. Genes, proteins, organelles and even ions regulates apoptosis [134].

B-cell lymphoma 2 (Bcl-2) family has a major part in apoptosis in cell. Altering Bcl-2 expression is a suggested mechanism for resistance in cytotoxic drugs. It is important to target anti-apoptotic Bcl-2 family in order to help apoptosis and fight chemotherapeutic drug resistance in cancer chemotherapy [135, 136]. Two major pathways that trigger apoptosis are intrinsic pathway, also called mitochondrial apoptotic pathway, and extrinsic pathway which is triggered when ligands called death ligands bind to death receptors [137].

In the extrinsic pathway, FAS and TRAIL death receptors are activated by their death ligands FAS and TRAIL or TNF α (tumor necrosis factor), respectively. This activation of TRAIL receptor forms a complex which activates caspase 8 and thus it activates either caspase 3 or intrinsic pathway [135, 137]. Figure 1.5 shows the apoptotic pathway and the roles of Bcl-2 family proteins.

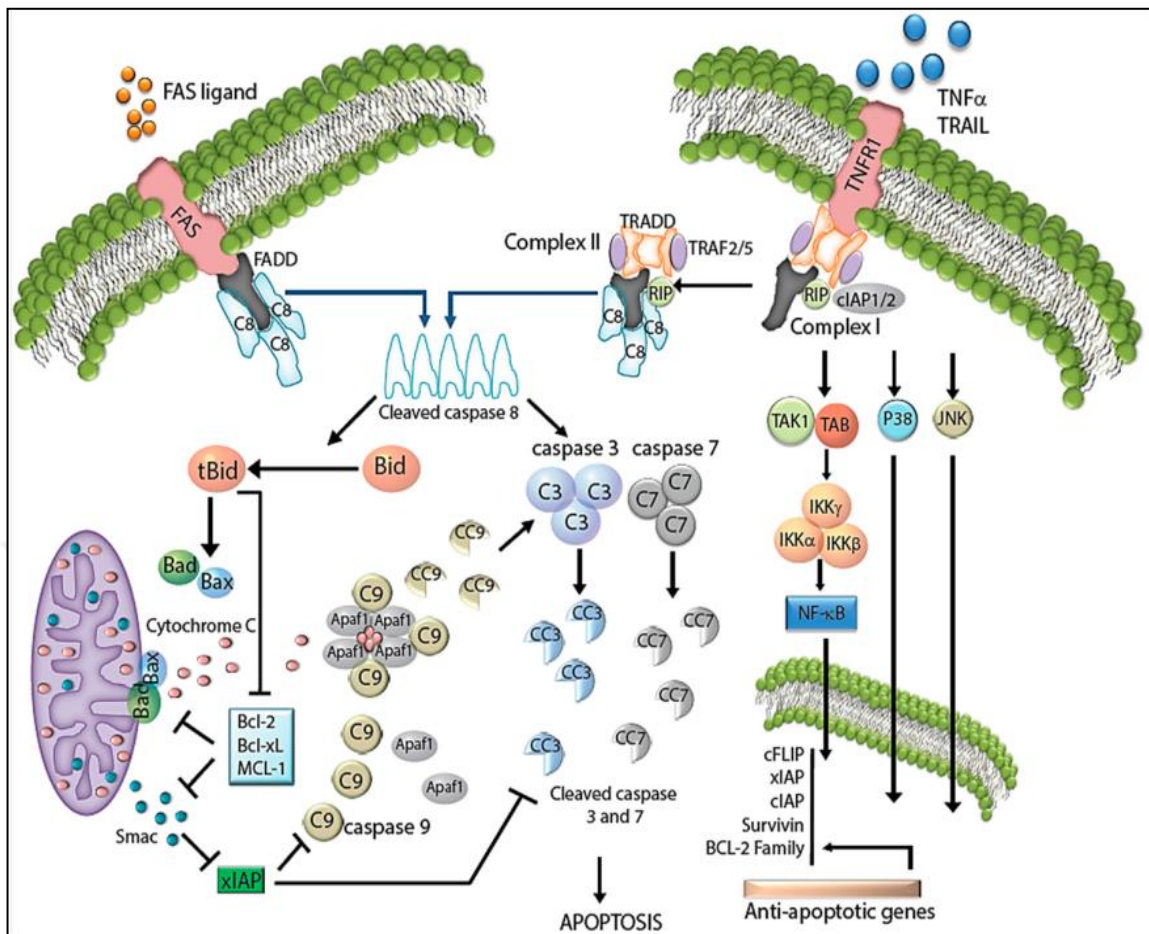


Figure 1.5. Bcl-2 family proteins affecting apoptotic pathway [137].

A signal such as radiation, cytotoxic drug, and cellular stress activates the intrinsic pathway. In intrinsic pathway, the Bcl-2 family play a key role and can be listed as in 3 groups with 25 members in total; multidomain pro-apoptotic, BH3-only pro-apoptotic and multidomain anti-apoptotic [138].

Bcl-2 family are known for their Bcl-2 homology domains; these are motifs with short sequences that are less than 20 amino acid residues [135]. As shown in Figure 1.6, Bcl-X_L, Mcl-1 and Bcl-2 are well known multidomain anti-apoptotic Bcl-2 family members, and Bad, Bak, and Bax are multidomain pro-apoptotic members [134]. Bid, Bik, Bim, and Noxa are members of pro-apoptotic BH 3 family [139].

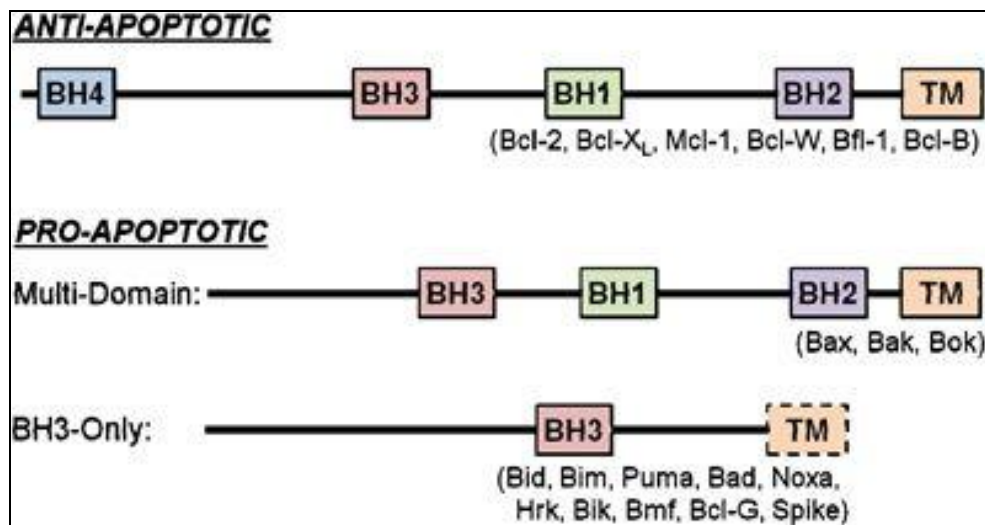


Figure 1.6. Comparisons of domain structures for the proteins of Bcl-2-family [139].

The pro-apoptotic protein Bax and Bak activates via changing their structure with a cytotoxic internal stimuli. These two proteins then migrate to the mitochondria, forces to open pores on surface of mitochondria and then proteins such as cytochrome c is released which mediates cell death. Thus, permeabilization of mitochondrial membrane is termed as “point of no return” for apoptosis. Once the cytochrome c is in the cytoplasm, it binds to caspase adaptor molecule, Apaf-1, activating caspase 9. This active caspase 9 causes executioner caspase 3 and 7 to be activated and in a very short time cell death occurs. Due to Bcl-2 family’s important role in regulating apoptosis, researchers focus on Bcl-2 inhibitors and several preclinical studies show promising results for solid tumors [137, 140, 141].

Bik, also known as Bcl-2 interacting killer, is a 18 kDa potent pro-apoptotic protein which is an essential initiator of apoptosis and forms a heterodimer with anti-apoptotic proteins like Bcl-2 and Bcl-X_L. Bik protein functions either by inducing activity of pro-apoptotic molecule or by inhibiting anti-apoptotic Bcl-2 proteins. Studies show that Bik sensitize tumor cells to apoptosis mediated by chemotherapy drugs such as doxorubicin [142].

Researchers also showed that a mutant form of Bik gene inhibited nearly 50 percent of ex vivo tumor assays. Threonine (T) 33 and serine (S) 35 of Bik residues were replaced with aspartic acid (D), Bik gene was mutated to **BikDD**, and this resulted in a constitutively phosphorylating form [138, 142]. BikDD and breast cancer correlation shows that there is a high death in triple negative breast cancer [143].

1.6. DRUG DELIVERY SYSTEMS

Standard chemotherapy administration lead to drug resistance and become inefficient throughout time, thus combination of nanotechnology with chemotherapeutics show promise for cancer treatment [144]. Drugs can be delivered either systemically (orally, transmuscularly, transnasally or transdermally) or directly to the target tissue or organ [145].

Delivering the drug in a controlled manner directly to the target tissue or organ within the intended therapeutic time is the main goal of sophisticated drug delivery systems. In order to maintain these features, polymers were used as drug carriers in drug delivered systems (DDS). These polymers could be natural (such as collagen, dextran and cellulose) or synthetic (such as polylactic acid and polyethylene glycol) and easily modified, so it will improve drug delivered systems [145-147].

DDS has several advantages: it extends bioavailability of the drug; the administered drug is reduced; and it prevents the drug's side effects. Furthermore, it improves utilization of the drug as well as patient compliance. However, there are several drawbacks of these systems such as being expensive and problems with degrading the product [148].

Other major problems of DDS is distribution of drug to healthy tissues and nonefficient accumulation. Nanotechnology in the area of oncology shows exciting possibilities and many countries encourage researchers to develop solutions in this area [149]. Therefore, it is important to produce biodegradable and target specific drug delivered systems so that the drug only goes to the target tissue/organ and does not cause toxicity in the other body parts. Figure 1.7 shows the main components of polymeric drug delivery systems [150].

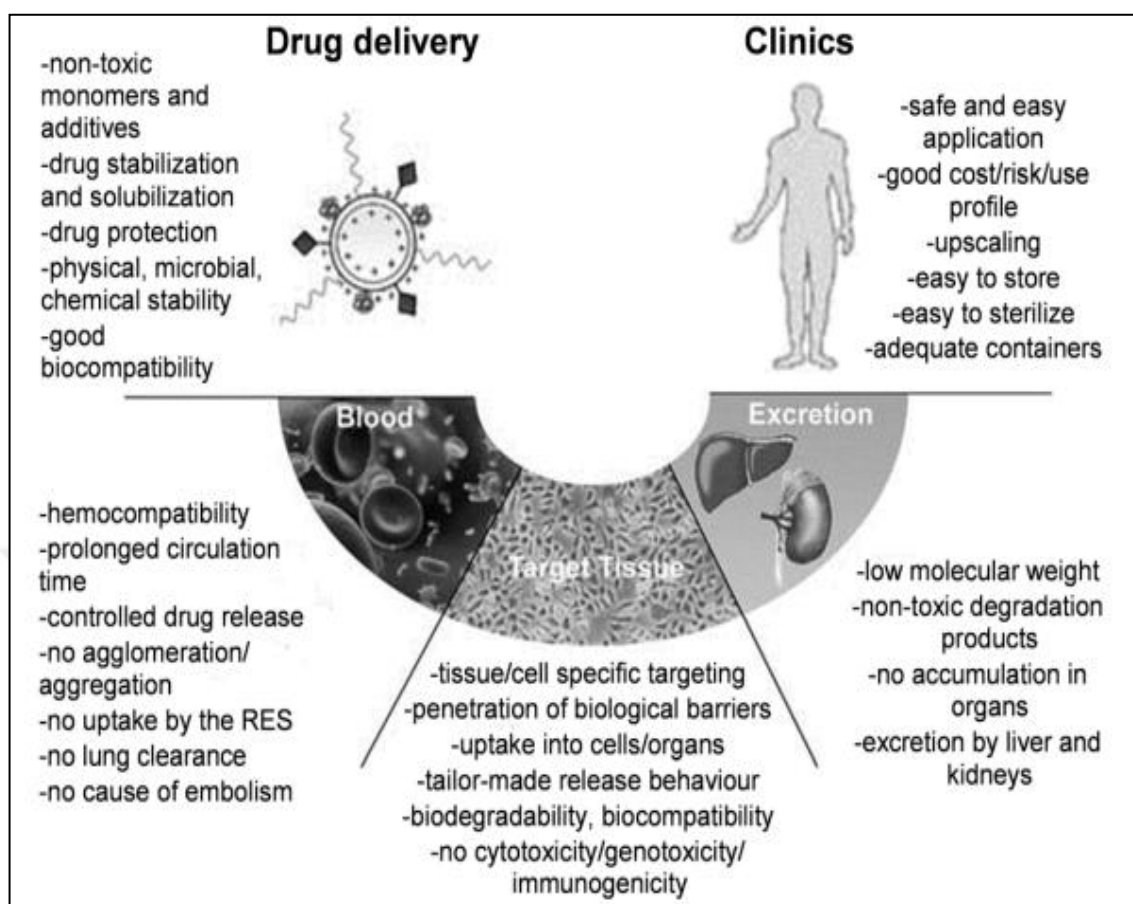


Figure 1.7. Components polymeric drug delivery systems [150].

Long term circulation times in blood vessels is possible if the liposome or other nanoparticles are coated with poly (-ethylene glycol) (PEG). Liposomes are nanoparticle platforms studied clinically in breast cancer [106]. Studies showed that liposomal doxorubicin had less cardiotoxicity to patients compared with doxorubicin administered alone [151]. Thus, the drawbacks caused by drugs or active agents in treatment of cancer could be overcome or at least minimized by loading drug into nanocarrier formulations [152]. Figure 1.8 shows the biophysicochemical properties of nanoparticles used as DDS in cancer therapy.

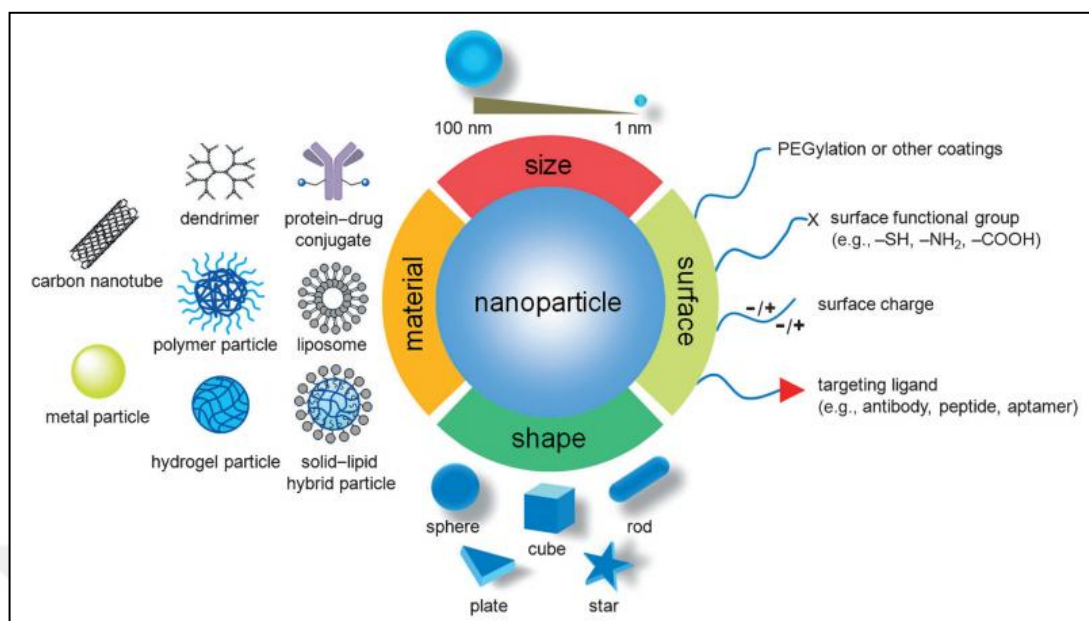


Figure 1.8. Biophysical properties of nanoparticles that have been explored as carriers for drug delivery in cancer therapy [153].

1.8. NANOCARRIERS

1.8.1. Copolymers in Design and Development of Nanocarriers

The scientific landscape for diagnosis and treatment of diseases are altered with the development of advanced nanoscale technologies. Nanoparticles have the ability to copy or change biological processes [154]. Using nanoparticle technology in drug delivery is not a new idea as it can be dated back to the early 1980s where development and investigation of polyalkylcyanoacrylate nanoparticles [155].

The polymeric nanoparticles are a hot topic in drug delivery because they are stable structures and are modified easily. Nanoparticles made from these polymers are advantageous because of their small size and biodegradability [154].

These characteristics allow the nanoparticle to extravasate through tumor is epithelium and penetrate microcapillaries. The particle size, surface properties of nanoparticles, drug loading, drug release and targeted drug delivery are important characteristics for drug delivery when nanoparticles are used [154, 156].

Drug delivery technology had advanced through the integral role of polymers. These polymers provide controlled release of therapeutic agents in constant doses over long periods, cyclic dosage, and tunable release of drugs. Although PEG has been used widely in therapeutic applications, the development of the immunogenic response to PEG imposes the need for the development of new polymers [157]. Polymers with functional groups have great importance in drug delivery systems. These polymers, with functional groups in side chains, can be prepared by polymer analogous reactions with other polymer precursors or by directly from the 2-oxazoline monomer with the required (amino, aldehyde or carboxyl) group [158].

Poly(2-oxazolines) are polymers that have the advantage of being able to develop next generation polymer therapeutics. This is because of their biocompatibility, solubility, variety in size and chemically functional properties. These polymers are applicable in drug and gene delivery systems. A drug is encapsulated to these polymeric structures and released over time through diffusion. Water soluble poly(2-oxazolines) with increasing hydrophobicity are: poly(2-methyl-2-oxazoline), poly(2-ethyl-2-oxazoline) and poly(2-isopropyl-2-oxazoline) [159, 160].

One of these polymers are poly(2-ethyl-2-oxazoline) (PetOx) which show advantages. In the last decade, more attention has been drawn to polycationic gene delivery vectors because they are easily prepared, have versatile chemical structure and lack of immune response *in vivo* [161].

Water soluble polycations condenses negatively charged DNA or RNA. Polyethylenimines (PEI) are widely studied cationic polymers as nonviral vectors capable of delivering plasmid DNA in *in vitro* and *in vivo* conditions [162]. Highly positively charged PEI condense and protect DNA from nuclease digestion in serum and also have advantage of easily chemical modification in structure [163]. Figure 1.9 shows the schematic diagram as PEI forming a DNA complex when subjected to DNA [164].

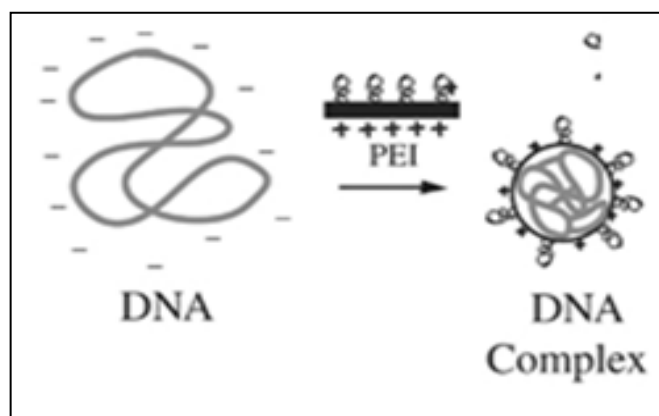


Figure 1.9. Structure of polyethylenimines in receptor-targeted polycation complexes [164].

DOPE, a cationic lipid acting as a helper co-lipid, increases transfection activity. Mochizuki *et al.* showed that DOPE mixed with cationic lipid displayed same transfection efficacy as commercially available transfection reagent Lipofectamine 2000 [165]. DOPE is a cone shaped fusogenic lipid [166]. DOPE is a neutral phospholipid that can alternate structurally by pH change [165, 167] and shows low toxicity and high stability of particle that is being delivered [168].

Polyesters are one of the most important biodegradable synthetic polymers. Polylactic acid (PLA), poly- ϵ -caprolactone (PCL), polyglycolic acid (PGA) are types of polyesters [169]. PLA hydrolyzes into hydroxyl-carboxylic acid in aquatic environment through ester bond cleavage and later metabolize into carbon dioxide and water through a citric acid cycle. Because of their low toxic, biodegradable, and biocompatible characteristics PLA has been approved by FDA for application in drug carriers, tissue engineering and medical materials [170]. PLA also shows properties as mechanical strength and processability [171].

Studies showed tha PLA nanoparticles have tendency to be used in gene therapy for ocular diseases [172]. Although, PLA shows disadvantages such as long degradation time, weak hydrophilicity, and low drug loading of polar drugs, these can be overcome through copolymerization of PLA with other copolymers [170]. Figure 1.10 shows some of the nanoparticles formed from amphiphilic block copolymers containing PLA.

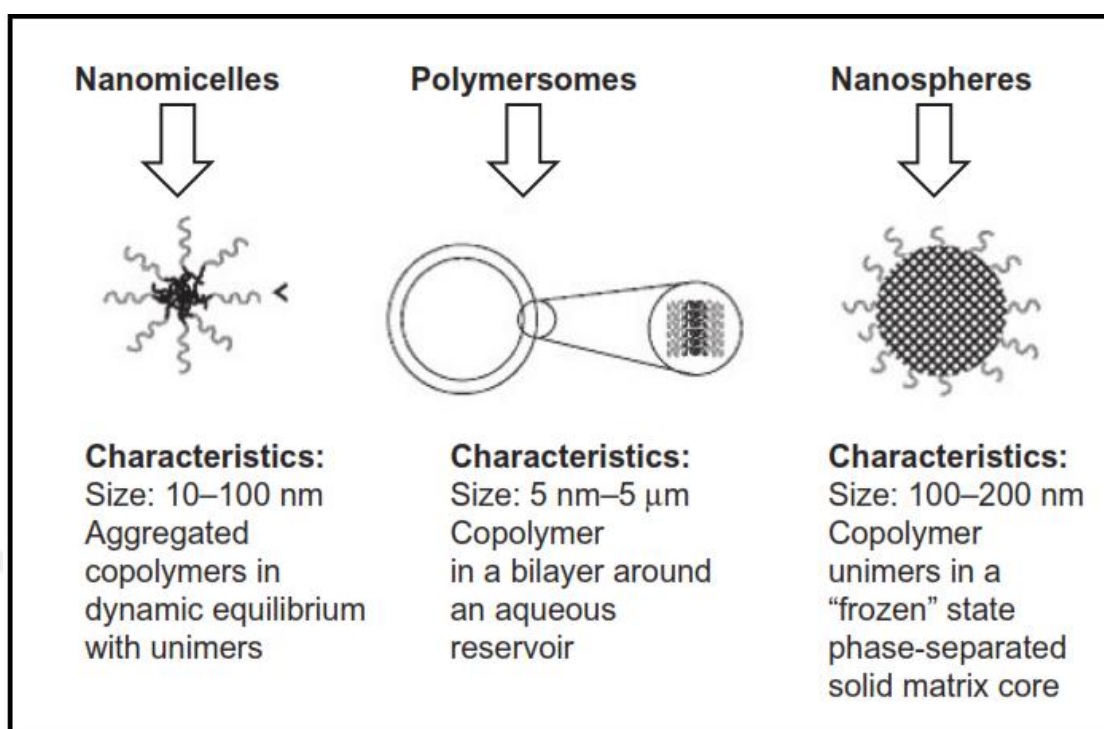


Figure 1.10. Nanoparticles formed from amphiphilic block copolymers containing PLA and their general characteristics [170].

Another polyester that could be used in DDS is PCL which has the advantage of having low degradation rate and thus, it is preferred in long term drug delivery devices [173]. PCL is also biocompatible like PLA [174] and mechanical strength property enables it to be used as surgical repair material [175]. PCL could be blended with other polymers easily and small drug molecules can easily enter these polymers [148]. PCL is a lipophilic and semi-crystalline polymer, which forms the core of micelle formulations and solubilize lipophilic drugs [176].

1.8.2. Liposomes

The history of liposomes goes back to 1965 and the suggestion of these nanoparticles to be used as drug carriers was in 1974 by Gregoriadis [177]. Liposomes are spherically small sized nanoparticles, which are ideal for enhanced accumulation in tumors and long systemic circulation [178]. Due to their phospholipid composition, liposomes show biocompatible, biodegradable, low toxicity and low immunogenicity characteristics [179].

These are the main attributes for a nanoparticle to be used in drug delivery systems. Liposomes hydrophobic and hydrophilic structures allow a wide range of lipophilic drugs to be encapsulated. Furthermore, certain modifications on the surface of liposomes with hydrophilic polymers have improved the circulation time of liposomes [180]. Liposomes are considered as one of the most prospective candidates showing well established technology for industrial scalability. However, in oral delivery of liposomes the major hurdle is the degradation of liposomes due to bile salts and intestinal lipases and aggregation in gastric environment [119]. Liposomes are used as nanoparticles to encapsulate drugs and giving the advantages of increased solubility, prevention from premature release into bloodstream, and protection from degradation [106]. Although, liposomes show great potential in anticancer drug delivery, there are limitations in clinical trials for controlled drug release. These limitations are overcome with the development of advanced liposomal formulations by drug release strategies triggered by external stimuli and surface modification of polymers [181]. Loading capacity of liposomes could be enhanced by addition of compounds to its structure. One effective method is by addition of triglyceride, which has the ability to enhance loading drug/agent capacity of liposomes [182]. The transfection efficiency of P18-PEtOx-DOPE liposomes could be enhanced by PEI [183]. Liposomes modified with hydrophilic polymers such as PEG improve circulation time and stability of the liposome. A protective shell is formed and this increases the stability of a colloidal dispersion [184]. However, PEG immunogenicity and efficiency is still an concerning issue [144]. Figure 1.11 shows the structure of liposomes nanocarriers.

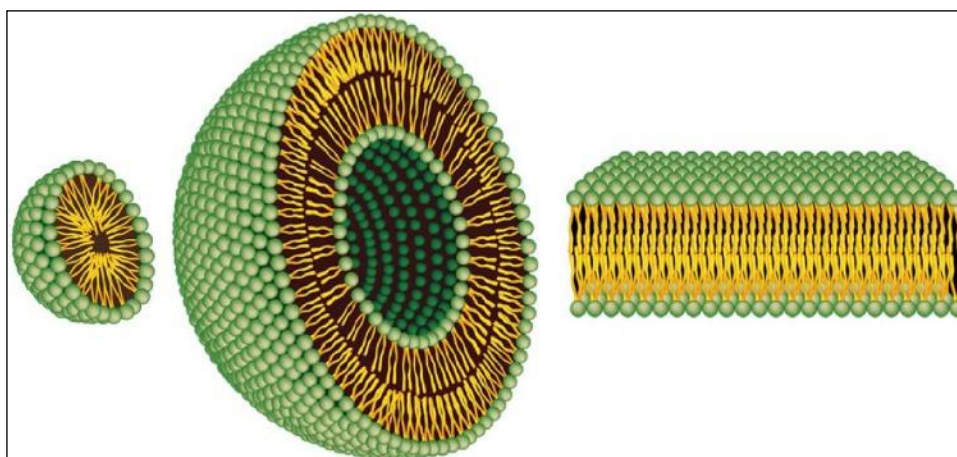


Figure 1.11. Representation of a micelle (left), a liposome (center), and a lipid bilayer (right) [185].

1.8.3. Micelles

Polymer micelles are amphiphilic block copolymers which form core-shell when left in aqueous environment and are ideal for carrying water insoluble chemotherapeutic [106]. In comparison to liposomes which have lipid bilayer, micelle structures are composed of one lipid layer (as given earlier in Figure 1.9). The apolar section of lipid layer is inward of micelle structures thus only polar section interact with the surrounding environment. This means that, the space for carrying the drug of interest in micelles is more limited than that of liposomes [185].

Micelles have advantages as increasing permeability and half-life of drugs [186]. Micelles fabricated by antibodies are used in HER2⁺ breast cancer [187]. Taxol drug delivered in HER2 antibody micelle complex showed high efficacy in comparison to simple lipid based protein [188].

A study conducted by et al. on metastatic breast cancer patients showed that paclitaxel drug loaded to polymeric micelles formulations response rate was 58.5 percent comparing with drugs that are in Phase I and II clinical trials [189].

Dox-Pluronic micelle SP1049C is currently in clinical trails and is used in metastatic cancer therapy [190]. The need of PEG was overcome by micelle nanocarriers based on PEOx-PLA-g-PEI, which showed successful delivery of DNA and chemotherapeutics [144].

1.8.4. Polymersomes

Polymersomes are nanoscale vesicles, in aqueous media amphiphilic copolymers self-assemble into polymersome structures. Polymersomes are more flexible than micelles and have the ability to deform to pass through narrow passages because of the low ratio of their surface area to membrane thickness [191].

Polymeric nanoparticles, made of natural or synthetic polymers, have high stability rate, easily changeable polymer characteristics and surface chemistry. These characteristics give them great advantages in the field of controlled drug release and tumor targeting.

Studies show that chemotherapeutic drugs loaded on biodegradable polymeric nanoparticles had tumor selective biodistribution with exploitable circulation time [192].

Polymersomes have been used to encapsulate chemotherapeutic drugs such as paclitaxel and DOX [191]. DOX has the ability to stay in the interior of polymersome until it degrades [154]. Studies show that DOX drug and poly (2-ethyl-2-oxazoline) Pet (Ox) conjugate had enhanced antitumor efficacy [193].

1.9. SMART TARGETING OF NANOPARTICLES

When developing a drug, it is important that it effect the pathologic tissues not the healthy tissues. In order to eliminate off-target effect of the active therapeutic agents on healthy tissues, there should be specific targeting to pathologic tissues. Thus, this is the main characteristics of ideal nanoparticle-based therapeutics. The usual approaches for cancer therapy (surgical approach, hormonal therapy or chemotherapy) are systemic and because they do not have targeting specificity and can cause tumor multidrug resistance, these approaches show detrimental side effects [194].

Thus it is important to find new approaches in targeted therapy for cancer. Using surface receptors and antigens which are overexpressed on tumors or angiogenic blood vessels, nanoparticles can be maintained interstitial space of tumors. Active targeting takes place once these nanoparticle are constructed to target specific receptors, are taken up by tumor cells. On the other hand, non-targeted nanoparticles accumulate on tumor site by enhanced permeability and retention (EPR) effect [195]. Figure 1.12 shows active and passive targeting of liposomes.

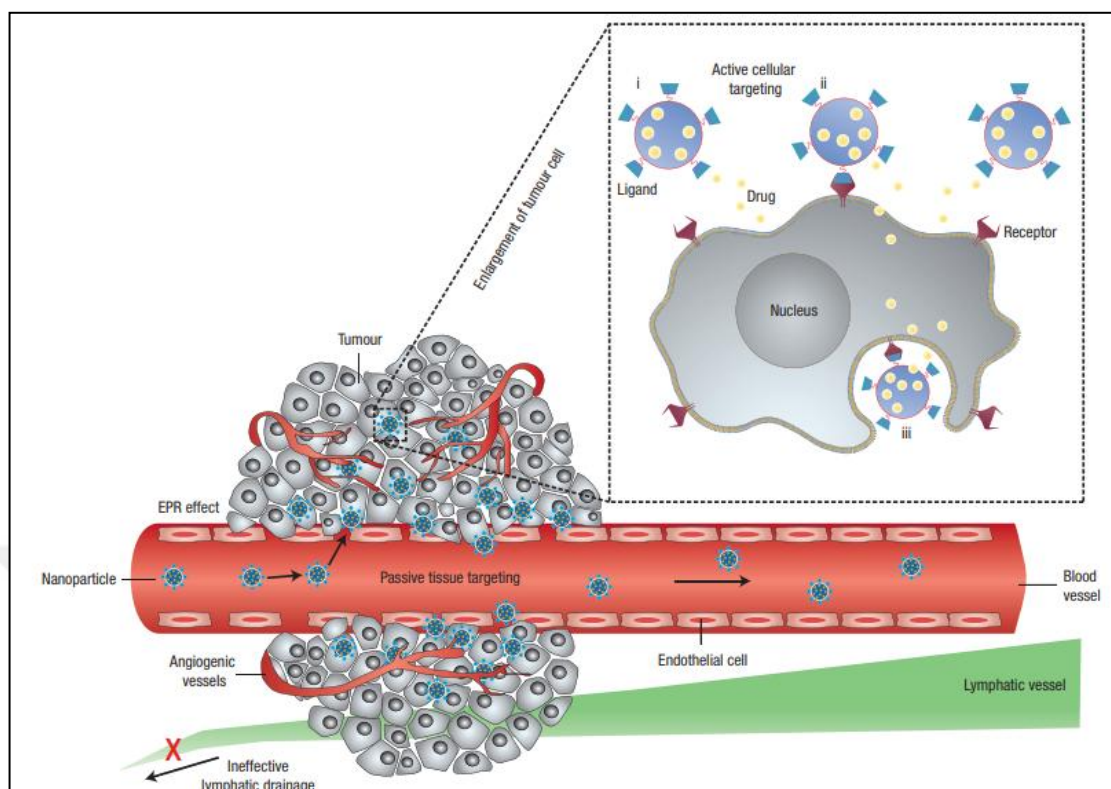


Figure 1.12. Representation of liposome nanocarriers that takes place in active and passive targeting of drug [195].

Small molecules, protein domains, peptides which are polypeptide based, antibodies and aptamers are targeting ligands that can be conjugated to nanoparticles surfaces. Small molecules could be easily conjugated to nanoparticles and their potential low cost are advantageous. However, most small molecule show drawbacks like not being able to bind to cell surfaces with specificity and high affinity when used as targeting ligands [155].

On the other hand, antibodies, protein domains, and homing peptides are poly-peptide based targeting ligands which could be systemically developed and generated using biological selection and expression systems. Stability, immunogenicity and complications for site-specific attachment with nanoparticles are major issues of these poly-peptide based targeting ligands [196, 197].

The pioneered research in using ligands for targeted drug delivery began with antibodies. However, the major challenges faced are antigen binding, circulation time and conjugation when antibodies are used as targeting agents of nanoparticles [198]. The size based sorting of poly-peptide based targeting ligands in descending order is as follows antibodies, peptides and small molecules [155].

Trastuzumab, which is a humanized monoclonal antibody targets HER2 extracellular domains and is made of magnetic nanocrystals. Another example of antibody used as targeting agent is MAB1609, which is a monoclonal Mouse IgG1 antibody that targets cytokeratin 7/8 extracellular domains. MAB1609 labeled to superparamagnetic iron oxide nanoparticles are used in targeted drug delivery [155].

Folic acid and RR-11a are small molecules that target HeLa cells and legumain and are used as targeting agents. Homing peptides are significant in the field of developing novel cancer therapeutics, for instances the peptides targeting mitochondria [194].

1.9.1. Tumor Targeting Peptides

The pioneered research of targeting homing peptides date to 1985 [155]. Toxic side effects and low specificity of many conventional chemotherapeutic agents used for cancer cells is documented for many years. Tumor homing peptides and engineered antibodies are some of the strategies used for targeting cancer cells for delivering chemotherapy drugs as well as diagnosis of cancer [199].

Homing peptides are in between of antibodies and small molecules in size comparison, antibodies being the largest among them. Also, these peptides have high specificity and affinity over the aforementioned targeting ligands. In the last decade, numerous studies were conducted on nanoparticles with homing peptides to be used as targeted studies.

EGF and Angiopoep-2 are examples of some of the natural peptides and derivatives of RGD peptides are one of the most popular homing peptides used to target $\alpha\beta3$ integrin [155]. Recent finding highlight the importance of peptide ligands in cancer targeted therapy [194].

Targeted drug delivery systems are important as it is wanted for chemotherapeutic drugs to effect only cancer cells not the healthy cells in the body. Engineered antibodies for targeting cancer cells have limited success because of the short *in vivo* life, their large size and low physicochemical stability. On the other hand, studies show that peptides are smaller in size, outstanding penetration to tissues and in addition it can very easily chemically conjugate to drugs [200]. Table 1.4 shows short homing peptides used as targeting ligands.

Table 1.3. Short homing peptides used for targeted nanoparticle [155].

Peptide	Sequence	Cyclic	Target	Nanoparticle
EGF	-	-	EGFR ECD	Vault nanoparticles
NGR	NGR	-	CD13 ECD	ELP micelles
iRGD	CRGDKGPDC	-	$\alpha_v\beta_3$, $\alpha_v\beta_5$	PLGA-PLL-PEG
TRAIL	hTRAIL(114–281)	-	DR4, DR5 ECD	HSA NPs
Pep 1	CHVLWSTRC	Yes	Pancreatic islet capillary endothelial cells	PLGA-b-PEG
RGD	cRGDfK	Yes	$\alpha_v\beta_3$ integrin	AuNPs
RGD	cyclic RGD	Yes	$\alpha_v\beta_3$ integrin	PEG-PEI
Tet-1	HLNILSTLWKYR	-	Motor neurons	PLGA
S2P	CRTLTVRKCC	-	Stabilin-2 ECD	Chitosan

Tumor homing peptide RGD (Arginine- Glycine- Aspartic acid) sequences target the $\alpha_v\beta_3$ integrin and NGR, consisting of Asparagine-Glycine-Arginine sequence, targets aminopeptidase N receptors which are overexpressed in tumor cells. Integrins are molecules that function in cell adhesion, they connect cytoskeleton with extra-cellular matrix or with neighbouring cells. The $\alpha_v\beta_3$ integrin is made up of 125 kDa α_v subunit and 105 kDa of β_3 subunit and it is known to bind ECM molecules with an RGD such as fibronectin [201]. One of the cancer specific peptide ligands is the dodecapeptide p160 (VPWMEPAYQRFL). This peptide was created from phage display [194].

Peptide p160, shows promise for improved targeted drug delivery systems, and derivatives of p160 peptides were studied for breast cancer. These peptides were 11 (RGDPAYQGRFL) and 18 (WXEAAYQRFL) which showed three fold higher affinity for MCF7 and MDA-MB-435 cell lines (which are breast cancer cell lines) [200]. Another tumor homing

peptide MC10 oligopeptide with Met-Ala-Arg-Ala-Lys-Glu sequence was found to be effective in targeting HER2 overexpressing cancers such as breast and ovarian cancer [202].

Peptide 18, synthetic analogue of p160, are more proteolytically stable in human serum. Once peptide 18 bind to cell surface receptors of breast cancer cells, it internalizes into cell via endocytosis. Recent studies show that peptide 18 was used for cancer detection and drug delivery due to its targeting capabilities to breast cancer [194]. One of these studies, showed a 5 fold decrease in tumor volume of NOD-SCID mice, inoculated with MDA-MB-435 breast cancer cells, when treated with peptide 18 labeled liposomal conjugated DOX [203].

Another study showed peptide 18 targeted liposomal DOX had 40 times less toxicity to MCF10A and HUVEC cells and showed increased selective delivery of DOX to breast cancer cells. Peptide 18 binds to keratin 1 (KRT1) on breast cancer cells, which is overexpressed compared with healthy mammary cells [194]. KRT1 also binds to derivatives of p160, which include peptide 11 and 18. Peptide 18 binding specifically to breast cancer (Figure 1.13).

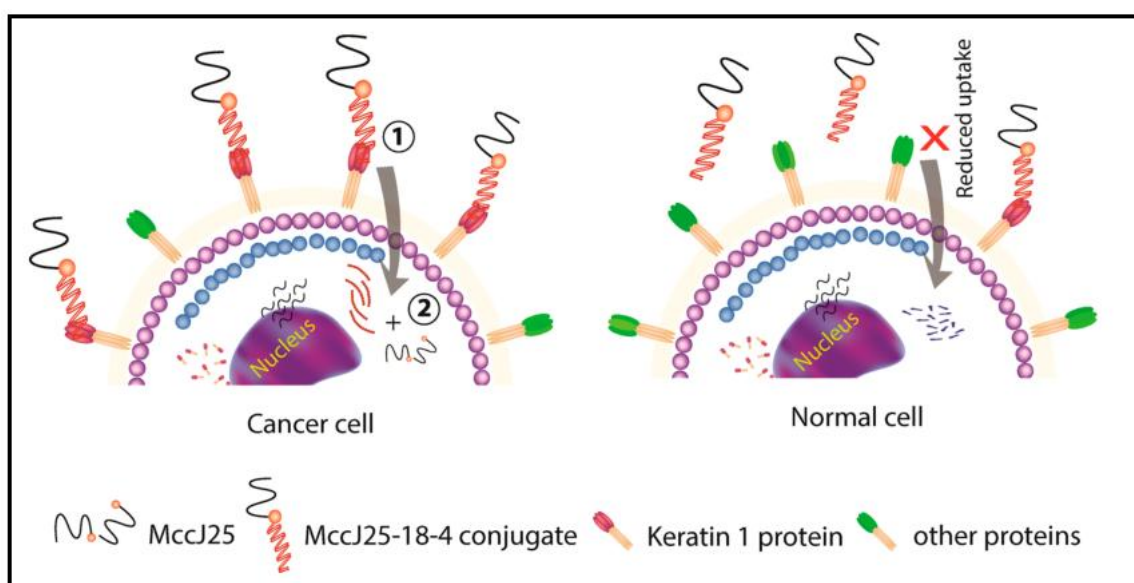


Figure 1.13. Schematic outline of peptide 18 binding specifically to breast cancer [194].

1.10. AIM OF THE STUDY

Breast cancer has the highest incidence among women and is still a major health problem. HER2 positive breast cancer account for 30 percent of these cases. Nanocarrier active target delivery is an important area in cancer targeted therapies. Peptide 18, a tumor homing peptide, shows high targeting specificity toward breast cancer. The aim of this thesis is to investigate a new approach to specifically target breast cancer using nanocarrier formulations. The binding affinity and target specificity of peptide 18 labeled PEtOx-DOPE liposomes, peptide 18 labeled PEtOx-b-PLA polymersomes, and peptide 18 labeled PEtOx-PEI-PCL micelle formulations was investigated for tumor selectivity. Peptide 18 deliver these nanocarriers to their target molecules in tumor cells and the therapeutic efficacy of targeted nanocarriers loaded with doxorubicin drug or proapoptotic BikDD gene was demonstrated. Another aim of the study was to complete the preclinical study by determining the antitumor efficacy of doxorubicin drug loaded peptide18-labeled nanocarriers to human HER2 positive breast cancer in CD-1 nude mice models.

2. MATERIALS

2.1. INSTRUMENTS

Laminar Flow Cabin (Heal Force Class II Biosafety Cabinet A2, China), CO₂ incubator (In-Vitro Cell ES NU-5800, NuAire, USA), Low-Speed Centrifuge (Gyrozen 416, Korea), 80°C freezer (New Brunswick, U410, Germany), Shaking Water Bath (Stuart SBS40, UK), Liquid Nitrogen Tank (Air Liquide Arpege 140, UK), High-Speed Centrifuge (Sigma Aldrich 3-18KS, Germany), Incubator Shaker (New Brunswick Innova 4330, USA), Inverted Microscope (Nikon Eclipse, TS100, Netherlands), Confocal Laser Scanning Microscope (Zeiss LSM 700, Germany), FACS Calibur (BD Biosciences, USA), MIKRO 22R Centrifuge (Hettich Zentrifugen, Germany), Magnetic Stirrer (Heidolph MR3004, Germany), pH Meter (Milwaukee Mi151, USA), Microplate reader (Bio-tek ELx800, USA), Vortex (Dragon Lab, MX-F, China), UV transilluminator (Vilber Lourmat, Germany), Heating Block (WiseTherm, HB-R, Switzerland), Weighing Machine (Shimadzu, AUW220D, Japan), Nano-Drop 2000 (Thermo Fisher Scientific, USA), Thermal Cycler (Biorad Mycycler 1709703, USA), CFX96 Real-Time PCR (Bio-Rad, C1000 Touch, USA), Guava easyCyte Flow Cytometers (Merck Milipore, Germany).

2.2. EQUIPMENT

Cell Culture Flasks T-25, T-75, and T-150 (SPL Life Sciences, Korea), 15 mL and 50mL Falcon tubes (Isolab, Germany), Filter 0.22/0.45 µm (Santorius Stedim Biotech, Germany), Cell Culture Dish, 100mm (SPL Life Sciences 200200, Korea), Cryo Tubes (TPP 89020, Switzerland), Cell Culture plates 6-well, and 96-well (TPP, Switzerland), Microcentrifuge Tubes 0.5, 1.5, and 2 mL (Isolab, Germany), Pipette Tips 10, 200, and 1000 µL (SPL Life Sciences, Korea), Serological pipettes 5, 10, 25, and 50 mL (Isolab, Germany), Electronic pipette (CAPP aid, Denmark), Micropipettes 10, 20, 100, 200, and 1000 µL (Eppendorf Research, Germany), Bright-Line Hemacytometer (Sigma Aldrich, Germany), Cell Scraper (Greiner bio one, USA), Multipipette 100 µL (Eppendorf Research, Germany), Graduated Cylinder 100, and 1000 mL (Isolab, Germany), Inoculation Loops (Isolab, Germany),

Erlenmeyer Flasks 500, and 1000 mL (Isolab, Germany), 8-well Chamber Slide (Thermo Fisher Scientific, USA).

2.3. DRUGS

Doxorubicin HCl (Koçak Farma L01DB01, Turkey), Adrimisin (Saba L01DB01, Turkey).

2.4. PEPTIDES

MC10 [5,6-TAMRA]-MARAKEGGGC (Biopeptide, USA), PEPTIDE 11 [5,6-TAMRA-Beta-Ala]-RGDPAYQGRFL (Biopeptide, USA), PEPTIDE 18 [5,6-TAMRA-Beta-Ala]-WXEAAAYQRFL (Biopeptide, USA).

2.5. CHEMICALS

2.5.1. Chemicals used for Cell Culture

RPMI 1640 Medium (Gibco BE12-702F, Thermo Fisher Scientific, USA), DMEM high glucose (Gibco 41966, Thermo Fisher Scientific, USA), Ham's F-12K (Kaighn's) Medium (Gibco 21127022, Thermo Fisher Scientific, USA), MEGM (Mammary Epithelial Growth Medium) Bullet Kit (Lonza CC-3150, Switzerland), DMEM low glucose (Gibco 31885, Thermo Fisher Scientific, USA), McCoy's 5A (Gibco 26600-023, Thermo Fisher Scientific, USA), DMEM:F12 Medium (Lonza BE12-719F, Switzerland), Heat inactivated Fetal Bovine Serum (FBS) (Gibco 10500-056, Thermo Fisher Scientific, USA), Penicillin-Streptomycin (PS) (Gibco 15140-122, Thermo Fisher Scientific, USA), Dimethyl Sulphoxide (DMSO) (Santa Cruz Biotechnology sc-202581, USA), Phosphate Buffered Saline (PBS) (Lonza BE17-517Q, Switzerland), Trypsin-EDTA (Gibco 25200056, Thermo Fisher Scientific, USA), Heparin (Sigma Aldrich H3149, Germany), Endothelial cell growth supplement (ECGS) (Sigma Aldrich E2759, Germany), Heat Inactivated Horse Serum (Gibco 26050088, Thermo Fisher Scientific, USA), Human epidermal growth factor (Lonza CC-4107, Switzerland), Bovine insulin (Sigma Aldrich I6634, Germany), Hydrocortisone (Sigma Aldrich H0888, Germany), Cell Proliferation Reagent WST-1

(Roche 15290018, Thermo Fisher Scientific, USA), Opti-MEM (Gibco 31985-070, Thermo Fisher Scientific, USA), X-treme GENE HP DNA transfection Reagent (Roche 6366246001, Thermo Fisher Scientific, USA).

2.5.2. Chemicals used for Plasmid Isolation and Site-Directed Mutagenesis

Ampicillin (Santa Cruz Biotechnology sc-202951, USA), Kanamycin (Santa Cruz Biotechnology sc-263433A, USA), QuickChange Lightning Multi Site-Directed Mutagenesis Kit (Agilent technologies 210514, USA), PureLink™ HiPure Plasmid Maxiprep Kit (Thermo Fisher Scientific K210007, USA), Isopropanol (Sigma Aldrich 19516, Germany), Purelink™ Quick Gel Extraction Kit (Thermo Fisher Scientific K0100-12, USA), UltraPure Agarose (Invitrogen 16500500, ThermoFisher Scientific, USA), 100 bp DNA ladder (NEB N32315, USA), Luria Broth (LB) Broth (Sigma Aldrich L3522, Germany), 5-bromo-4-chloro-3-indolyl- β -D-galactopyranoside (X-Gal) (Peqlab 37-2620, Austria), Isopropyl β -D-1-thiogalactopyranoside (IPTG) (Peqlab 37-2020, Austria), LB Agar (Sigma Aldrich 19344 Germany), Glycerol, *NotI* enzyme (NEB R0189S, USA), NEBuffer 3.1 (NEB B7203S, USA), T4 DNA ligase (Thermo Fisher Scientific EL0011, USA).

2.5.3. Chemicals used for Flow Cytometry and Confocal Microscopy

Formaldehyde Solution (Sigma Aldrich 15512 Germany), DAPI (AppliChem A4099, Germany), Paraformaldehyde (Merck Milipore 104005, Germany), ClearMount™ Mounting Solution (Invitrogen 00-8010, ThermoFisher Scientific, USA).

2.5.4. Chemicals used for Cell Cycle and Cell Death

Propidium Iodide (PI) (Biolegend 421301, USA), RNase (Sigma Aldrich, Germany), Triton-100X (MP Biomedical 9002931, France), Annexin V-FLUOS Staining Kit (Roche 11988549001, Switzerland).

2.5.5. Chemicals used for Real-time PCR

Sensiscript Reverse Transcription (RT) kit (Qiagen, 205213, USA), HS_RRN18s_QuantiTect Primer Assay (Qiagen QT00199367, USA), Trizol Reagent (Thermo Fisher Scientific 15596-018, USA), Absolute Ethanol (AppliChem A3928, Germany), QuantiTect SYBR Green PCR Kit (Qiagen, 204145, USA).

2.5.6. Chemicals used for animal studies

Matrigel (Corning, USA).

2.6. PLASMIDS

pEGFP-Bik (Addgene plasmid 10952, USA) (Figure 2.1), pCMV6-XL5-Bik (Origene SC119390, USA) (Figure 2.2), pCAG-GFPd2 (Addgene plasmid 14760, USA) (Figure 2.3).

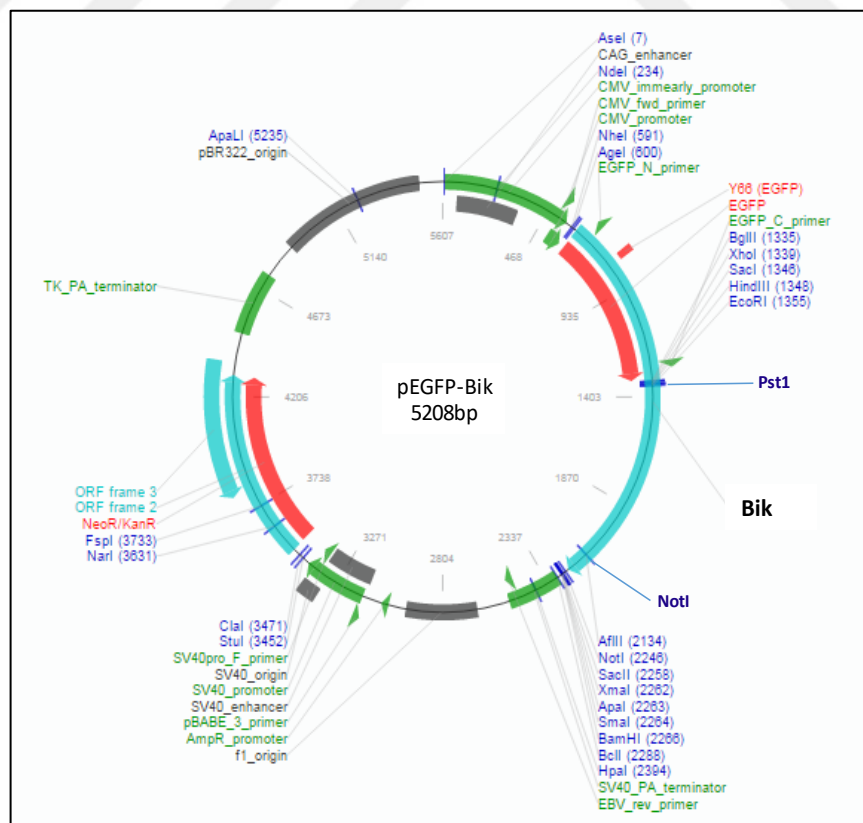


Figure 2.1. Map of pEGFP-Bik plasmid [204].

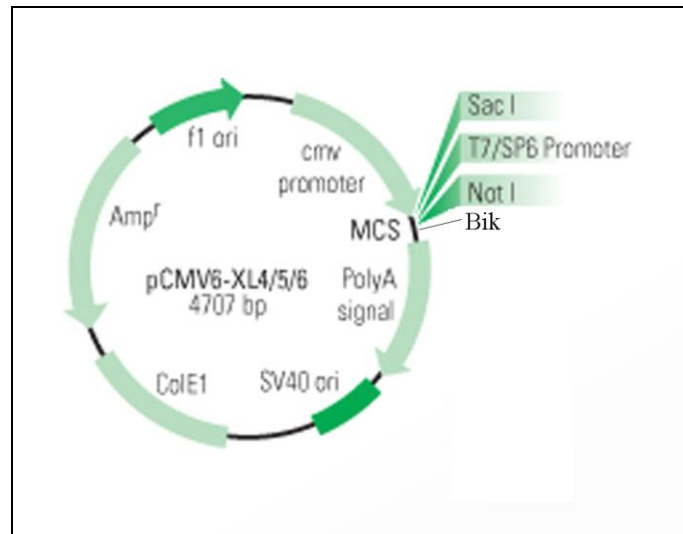


Figure 2.2. Map of pCMV6-XL-Bik plasmid, modified from [205].

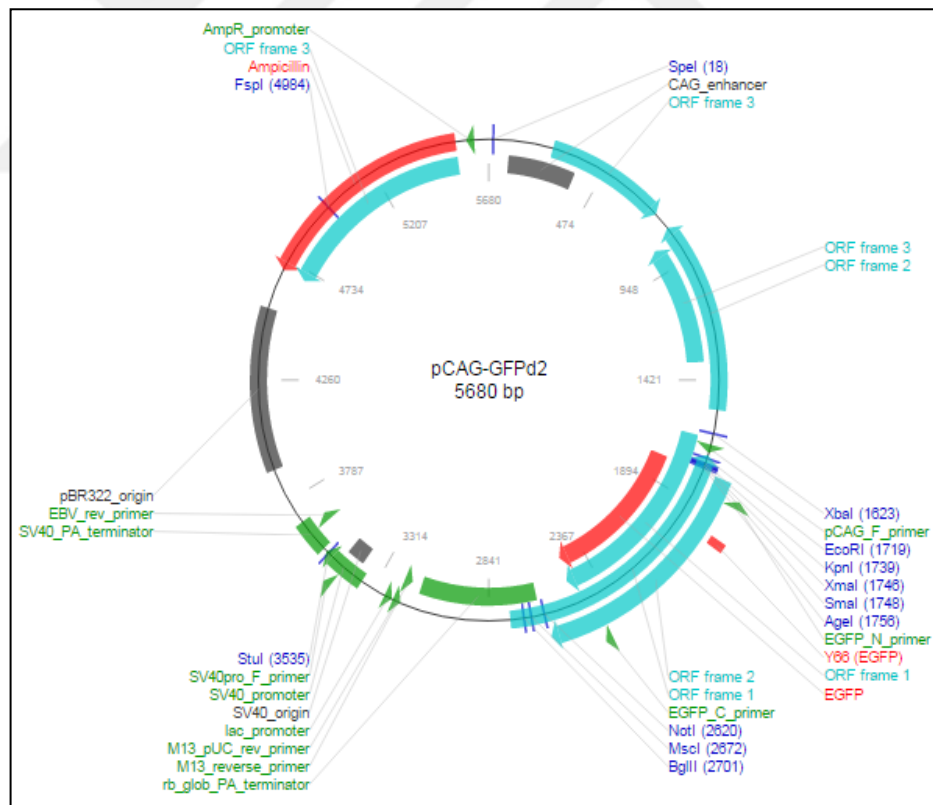


Figure 2.3. Map of pCAG-GFPd2 plasmid [206].

2.7. CELL LINES

Human Embryonic Kidney Epithelial Cell Line (HEK293, ATCC CRL-1573, USA), Human Umbilical Vein Endothelial Cell (HUVEC, ATCC CRL-1730, USA), Human Breast Epithelial Cell Lines (MCF10A, ATCC CRL-10317, USA) and (MCF12A, ATCC CRL-10782, USA), Breast Cancer Cell Lines (AU565, ATCC CRL-2351, USA) and (SKBR3, ATCC HTB-30, USA), Mesenchymal Stem Cells (MSC) isolated and differentiated from human adipose tissues [Abdik, 2018].

2.8. MOUSE RACE

CD-1 nu/nu female mice obtained from Charles River Laboratory by Kobay company, Turkey.

3. METHODS

3.1. CELL CULTURE

3.1.1. Cell Thawing

In order to resuscitate each frozen cell line, cryo tubes were thawed by rapidly warming to 37°C, after taken from the liquid nitrogen tank. Then, 1 mL of cell suspension was added drop wise drop to 2 mL of pre-warmed complete growth medium and the mixture was spinned at 300 \times g for 5 minutes. Pellet was resuspended in complete growth medium and transferred to tissue culture flask. After 24 hours incubation, the medium was changed with fresh complete growth medium to remove any residual of DMSO. All cells were incubated in a humidified incubator at 37°C, 95 percent (v/v) air and 5 percent (v/v) CO₂ conditions.

3.1.2. Cell Lines and Culturing Conditions

AU565 cells were grown in RPMI 1640 medium supplemented with 10 percent (v/v) FBS, 100 units/mL Penicillin, and 100 µg/mL Streptomycin. SKBR3 cells were cultured in McCoy's 5A medium containing 10 percent (v/v) FBS, 100 units/mL Penicillin, and 100 µg/mL Streptomycin. MCF10A cells were maintained in MEBM Bullet kit containing two percent (v/v) FBS, 100 units/mL Penicillin, and 100 µg/mL Streptomycin. MCF12A cells were cultured in DMEM:F12 medium supplemented with 20 ng/mL human epidermal growth factor, 0.01 mg/mL bovine insulin, 500 ng/mL hydrocortisone, 5 percent (v/v) horse serum, 100 units/ml Penicillin, and 100 µg/mL Streptomycin. HUVEC cells were maintained as a monolayer culture in F-12K Medium containing 0.1 mg/mL heparin, 0.03 mg/mL ECGS, 10 percent (v/v) FBS, 100 units/mL Penicillin, and 100 µg/mL Streptomycin. HEK293 and MSC cells were cultured in DMEM high glucose (10 percent (v/v) FBS, 100 units/mL Penicillin, and 100 µg/mL Streptomycin) and DMEM low glucose (10 percent (v/v) FBS, 100 units/mL Penicillin, and 100µg/mL Streptomycin), respectively. All cells were cultured in the humidified incubator at 37°C, 95 percent (v/v) air and 5 percent (v/v) CO₂ conditions.

3.1.3. Cell Subculturing

AU565 cells that reached 60 percent confluency were subjected to passaging, the rest of the cells were passaged at 70- 80 confluency. Cell monolayer was washed once with 1 x PBS and prior to incubation with 0.05 percent (w/v) trypsin-EDTA at 37°C for 5 minutes. Complete growth medium was added to cell suspension in order to eliminate trypsin activity. Then, the cell suspension was centrifuged at 300 x g for 5 minutes, the pellet was resuspended in their appropriate complete growth medium and cells were seeded in appropriate cell culture flasks.

3.1.4. Calculation of Cell Number

Following cell subculturing protocol (described in Section 3.1.3), 10 µL of cell suspension was loaded into the hemocytometer. The inverted light microscope using 4 x objective was used to count the middle quarter of the hemocytometer.

$$\frac{\text{Cell number}}{\text{mL}} = \text{Counted cell number} \times \text{dilution factor} \times \text{depth of hemocytometer} \quad (3.1)$$

3.1.5. Cryopreservation of Cells

Freezing mix solution was prepared by mixing 10 percent (v/v) DMSO and 90 percent (v/v) FBS. Cells were washed with 1 x PBS, dislodged by trypsin and counted as it was described in Section 3.1.4. Cell pellet was resuspended in 1 mL of freezing mix solution with cell density of 1 x 10⁶ cells/mL in each cryovial. Cells were immediately stored at -80°C freezer for overnight before transferring to a liquid nitrogen tank for the long-term storage.

3.2. SYNTHESIS AND CHARACTERIZATION OF PROAPOPTOTIC BIK GENE

3.2.1. Plasmid Isolation

pEGFP-C3-Bik, pCMV6-XL5-Bik and pCAG-GFPd2 plasmids were streaked on LB agar plates containing 100 µg/mL kanamycin and ampicillin, respectively. After overnight incubation at 37°C, single colony was selected from agar plates, transferred to 250 mL LB broth containing appropriate antibiotics and followed 37°C overnight incubation in a shaker with 150 *x rpm*. After the bacterial cultures had grown, all of the cultures were spinned at 4,000 *x g* for 10 minutes. Bacterial pellet was resuspended gently with 10 mL of resuspension buffer containing RNase A. Next, 10 mL of lysis buffer was added, mixed until the solution became homogenous and incubated at room temperature for 5 minutes. After the incubation process, 10 mL of precipitation buffer was added into the mixture and centrifuged at 12,000 *x g* for 10 minutes at room temperature. Meanwhile, equilibration columns were washed with 30 mL of equilibration buffer.

Then the supernatant was loaded onto equilibrated column and the solution in the column was allowed to drain by gravity flow. 60 mL of wash buffer was added into the column and the purified DNA was collected in 50 mL falcon tubes by adding 15 mL of elution buffer to the column. Thereafter, 10.5 mL of isopropanol was added to the eluate and the mixture was centrifuged at 12,000 *x g* for 30 minutes at 4°C. After the centrifugation process, supernatant was discarded, pellet was washed with 3 mL of 70 percent ethanol and re-centrifuged at 12,000 *x g* for 5 minutes at 4°C. Afterwards, the pellet was air dried, suspended in 200 µL of TE buffer and the concentration of the plasmids were measured using nanodrop before storing at -20°C. pEGFP-C3-Bik, pCMV6-XL5-Bik and pCAG-GFPd2 plasmids with appropriate concentrations were sent to Makrogene Company (Korea) for sequencing. M13 Forward and M13 Reverse universal primers were selected. For long term storage of plasmid, bacterial stocks were made by adding 500 µL of overnight culture to 500 µL of 50 percent glycerol and stocks were stored at -80°C.

3.2.2. Bik Plasmid Cloning by Restriction Enzyme Digest

3.2.2.1. Restriction Digestion

pCMV6-XL5-Bik (5200 bp) into pCAG-GFPd2 (5680 bp) plasmid DNAs were digested with *NotI* restriction enzyme. 1 U of *NotI* restriction enzyme, 1x Buffer, RNase/DNase free water, and 1 μg of plasmid DNA were incubated for 1 hour at 37°C. *NotI* restriction enzyme cuts pCAG-GFPd2 and pCMV6-XL5-Bik at 5'-GC[↓]GGCCGC-3' and 3'-CGCCGG[↑]CG-5' sites, to form sticky ends. Table 3.1 shows the components for digestion of Bik and pCAG-GFPd2 plasmid by *NotI* restriction enzyme. After digestion, the insert and vector were size separated by agarose gel electrophoresis and visualised using UV illuminator.

Table 3.1. Components for *NotI* restriction enzyme digest.

	Bik (insert DNA)	pCAG-GFPd2 (vector DNA)
1 μg of DNA	6.67 μL	4 μL
10 x Buffer	5 μL	5 μL
Enzim (1U)	0.5 μL	0.5 μL
RNase/DNase free water	37.8 μL	40.5 μL
Total	50 μL	50 μL

3.2.2.2. Plasmid DNA Purification After Digestion

The insert DNA (Bik) and vector DNA (pCAG-GFPd2) was isolated by gel purification method. Agarose gel was cut and placed in a 1.5 mL eppendorf tubes. Samples were weighted and 3 times volume of L3 solution was added to each eppendorf. Gel was incubated for 10 minutes at 50°C until the gel melts and 1 gel volume of isopropanol was added to the samples. Next, sample were loaded on a column and centrifuged at 12,000 $\times g$ for 1 minute. 500 μL of W1 solution was added to each sample and centrifuged at 12,000 $\times g$ for 1 minute. After centrifugation step, samples were incubated with 50 μL of elution

solution for 1 minute and centrifuged at $12,000 \times g$ for 1 minute. Concentration of samples were measured using nanodrop.

3.2.2.3. Ligation

Insert DNA and vector DNA were ligated using 1 U of T4 DNA ligase at 22°C for 10 minutes or at 18°C for overnight. The following mixture was prepared, and the insert DNA and vector DNA ratio was 1:1. Table 3.2. shows the components for ligation of insert and vector DNA. Ligated product was visualized on agarose gel electrophoresis.

Table 3.2. Components for ligation

	Overnight incubation at 18°C	10 minutes Incubation at 22°C
Insert	15 μL	7 μL
Vector	1 μL	1 μL
1 U of T4 DNA ligase	1 μL	1 μL
T4 buffer	2 μL	2 μL
PEG	1 μL	1 μL
RNase/DNase free water (complete to 20 μL volume)	-	8 μL

3.2.3. Transformation

For transformation of bacteria, XL-Gold competent cells were gently thawed on ice and 45 μL was aliquoted into 1.5 mL eppendorf tubes that were prechilled previously. 2 μL of β -mercaptoethanol was added into the competent cells, and after gently swirling tubes were incubated for 10 minutes on ice, with 2 minutes swirling interval. Then, 0.1 ng/ μL of pUC18 plasmid (positive control) and 1 μL of plasmid of interest was added onto competent cells following an incubation on ice for 30 minutes. Next, each tubes was incubated at 42°C for 30 seconds for “heat shock” treatment followed by immediate 2 minutes ice incubation. NYZ⁺ broth containing 0.5 percent of NaCl and yeast extract, 1 M

of MgCl₂, 1 M of MgSO₄, 1 percent of N₂ amines, 2 M of glucose, was preheated and 500 µL was added to samples following and incubation for 1 hour at 37°C in a bacterial shaker with 225 *x rpm*. Transformation mixture was spread on LB agar (20mM IPTG, 80 µg/mL X-Gal, and 100 µg/mL ampicillin) plates and incubated for overnight at 37°C. Selected white colonies were transferred to 0.5 mL of LB Broth and cultured at 37°C shaker for overnight. Plasmid isolation and sequencing of pCAG-GFPd2-Bik was conducted as described in Section 3.2.1.

3.3. SITE-DIRECTED MUTAGENESIS

Site-directed mutagenesis of the plasmid carrying Bik gene was performed according manufacturer's protocol of QuikChange Lightning Multi Site-Directed Mutagenesis Kit. Threonine 33 and Serine 35 of Bik gene was changed to aspartic acid by using the BikDD Forward primer: 5'-GTTCTTGGCATGGACGACGATGAAGAGGACC-3' and BikDD Reverse primer: 5'-GGTCCTCTTCATCGTCGTCATGCCAAGAAC-3'. The following components shown in Table 3.3 were used to perform thermal cycling.

Table 3.3. Site-directed mutagenesis components.

Components	Sample (BikDD)	Positive control
10× Quick Change Lightning Multi reaction buffer	2.5 µL	2.5 µL
Quick Solution	-	-
dNTP mix	1 µL	1 µL
Mutagenic primers	2 µL (50 ng each)	1 µL
dsDNA Template	1 µL (100 ng)	1 µL
QuikChange Lightning Multi enzyme blend	1 µL	1 µL
RNase/DNase free water	17.5 µL	18.5 µL
Final volume	25 µL	25µL

Thermal cycling reaction was carried out at 95°C for 2 minutes as the initial denaturation step, followed by 30 cycles at 95°C for 20 seconds, 55°C for 30 seconds, and 65°C for 150 seconds. Final extension step was conducted at 65°C for 5 minutes. Reaction mixture was incubated on ice for 2 minutes before adding 1 µL of *Dpn I* restriction enzyme to each sample. This is necessary for digesting the methylated DNA and the samples were thereafter incubated on ice for 5 minutes. Transformation of desired mutant plasmid was performed using XL-Gold competent cells according to manufacturer's protocol (Agilent Technologies) mentioned in Section 3.2.3. 1 µL, 10 µL, and 100 µL of transformation mixture containing mutant BikDD gene was spread on the LB agar (20mM IPTG, 80 µg/mL X-Gal, and 100 µg/mL kanamycin) plates. Mutagenesis and transformation control (pUC 18) were spread on plates with ampicillin. Following an overnight incubation of more than 16 hours at 37°C, a white colony was selected from each LB agar plate, transferred into 300 mL LB broth with antibiotic appropriate for each sample and incubated at 37°C for overnight. Plasmid isolation and sequencing of mutant BikDD gene was performed as described in Section 3.2.1.

3.4. PREPARATION OF COPOLYMER AND NANOCARRIER FORMULATIONS

3.4.1. Copolymers

PEtOx-*b*-PLA, PEtOx-DOPE, PEtOx_{30%}-PEI-PCL (PPP30) and PEtOx_{60%}-PEI-PCL (PPP60) copolymers were prepared by Sevgi Gülyüz and Umut Ugur Özköse from TUBITAK-MAM. Later these copolymers were tagged with Peptide 18 for targeted studies.

3.4.2. Liposome

PEtOx-DOPE liposome was formulated and encapsulated with BikDD gene and doxorubicin drug by Dr. Ongun M. Saka and Dr. Burcu Devrim, respectively from Pharmaceutical Technology Department, Ankara University.

3.4.3. Polymersome

PEtOx-*b*-PLA polymersome were formulated and encapsulated with BikDD gene and doxorubicin drug by Dr. Umut Can Öz from Pharmaceutical Technology Department, Ankara University.

3.4.4. Micelles

PPP30 micelles were formulated and loaded with doxorubicin drug by Naile Öztürk and PPP60 micelles were formulated and encapsulated with BikDD gene by Dr. Aslı Kara, respectively from Hacettepe University.

3.4.5. Stability Studies of Nanocarriers

DNA stability studies for PPP60/BikDD micelle complex, and proapoptotic BikDD gene loaded PEtOx-*b*-PLA polymersome and PEtOx-DOPE liposome were conducted by each groups. Serum stability of doxorubicin drug and pro-apoptotic BikDD gene loaded nanocarriers were conducted by each individual group.

3.5. DETERMINATION OF PEPTIDE AND FLUORESCCEIN LOADED CONSTRUCTS BINDING AFFINITY BY FLOW CYTOMETRY

3.5.1. Binding Affinity of Peptides

AU565 and SKBR3 cells were seeded in a 6-well plate at a density of 3×10^5 cells/well and MCF10A, MCF12A and HUVEC cells were seeded at a density of 2.5×10^5 cells/well, due to cell size difference. After overnight incubation, all five cells were treated with 10 μ M (10^{-5} mol/L) tamra labeled MC10, P11 or P18 peptides for 1 hour. 1 x PBS was used to wash cell monolayer, trypsin-EDTA was used to dislodge cells, and 0.5 percent formaldehyde solution was used for fixing the cells. Using Becton Dickinson FACS Calibur flow cytometer, fluorescence intensity was measured at FL2-H

(excitation/emission, 546:576 nm). 20,000 events for each sample were acquired and the results were analyzed using CellQuestPro Program.

3.5.2. Binding Affinity of Fluorescein Loaded P18-Nanocarrier Formulations

3×10^5 cells/well of AU565 cells and 2.5×10^5 cells/well of MCF10A and MCF12A cells were seeded in a 6-well plates. The targeting efficiency of P18 peptide labelled P18-PEtOx-*b*-PLA polymersome (tPS), P18-PEtOx-DOPE liposome, P18-PPP30 micelles, and P18-PPP60 micelles were analyzed by incubating AU565 and MCF10A cells with the fluorescein loaded constructs. Cells were treated with P18-PEtOx-DOPE liposome, P18-PPP30 micelles, and P18-PPP60 micelles for 1 hour, and treated with tPS for 4 hours. Then, PBS was used to wash cells and fixed with 0.5 percent formaldehyde solution after scraping attached cells by cell scraper. Using Becton Dickinson FACS Calibur flow cytometer, fluorescence intensity was measured at FL1-H (excitation/emission, 488:525 nm) for cells incubated with fluorescein loaded constructs. Each sample was acquired from 20,000 events and CellQuestPro Program was used in analyzing the results.

3.6. DETERMINATION OF PEPTIDE AND FLUORESCHEIN LOADED CONSTRUCTS BINDING AFFINITY BY CONFOCAL MICROSCOPY

AU565 (2.4×10^4 cells/well), MCF10A (2×10^4 cells/well) and MCF12A (2×10^4 cells/well) cells seeded on 8-well chamber slides were incubated for 24 hours at 37°C. Following incubation time, cells were treated with peptides and fluorescein loaded constructs as mentioned previously in Section 3.5. After appropriate incubation time, PBS was used to wash cells thrice with five minutes time intervals and fixed with freshly prepared 4 percent paraformaldehyde solution for 20 minutes on ice. After this step, cells were again washed thrice with PBS, 5 μ g/mL of DAPI was used to stain the nucleus for five minutes, prior to another set of PBS washing and mounting. Confocal laser scanning microscopy with 63 \times oil immersion lens was used to visualize cells.

3.7. TRANSFECTION OF BIKDD GENE

AU565 cells were seeded into a 6-well plate (3×10^5 cells/well) and incubated for 24 hours. Cells were transfected with either pEGFP-C3-Bik, pCMV6-XL5-Bik, pCAG-GFPd2-Bik, or pEGFP-C3-BikDD using Xtreme Gene HP DNA transcription reagent in Opti-MEM according to manufacturer's protocol, with a 1:1 ratio of DNA:transfection reagent.

3.8. CELL VIABILITY ASSAY

3.8.1. The Cytotoxicity of Copolymers and Nanocarrier Formulations on Normal Cell Lines

The cell viability assay was assessed colorimetrically using WST1 reagent to determine the cytotoxic effect of copolymers, and nanocarrier (polymersome, liposome, and micelle) formulations on HUVEC, MSC, MCF10A, and HEK293 cells. In 96-well plate, HUVEC cells and MSC were seeded at a density of 2.5×10^3 cells/well, whereas cell density was 5×10^3 cells/well for MCF10A and HEK293 cells. DMSO was used to dissolve PEtOx-DOPE, PEtOx-*b*-PLA, or PEtOx-PEI-PCL copolymers at a concentration of 125, 150, and 500 mg/mL, respectively. In order to eliminate cell toxicity caused by DMSO, cells highest concentration to be used for copolymers were determined to be in a final dilution of 1:1000. After 24 hours, all cells were treated either with PetOx-DOPE, PetOx-*b*-PLA, or PEtOx-PEI-PCL copolymer and formulations at chosen concentrations for 24, 48, and 72 hours. Following incubation time, cells were subjected to WST-1 assay following manufacturer's protocol. Cells were subjected to a mixture of 45 μ L of complete growth medium and 5 μ L of WST-1 reagent and incubated at 37°C for 1 hour. Each well was measured using a microplate reader at 450 nm. Cell viability percentage was calculated selecting the absorbance value obtained from Cnt (non-treated) cells as 100 percent.

3.8.2. Determination of the Effect of Gene or Drug Loaded Nanocarrier Formulations on AU565 Cell Line

AU565 cells were seeded in 96-well plate with a cell density of 1×10^4 cells/well and incubated overnight at 37°C , 95 percent (v/v) air and 5 percent (v/v) CO_2 . After 24 hours, AU565 cells were treated with pro-apoptotic BikDD gene or DOX drug loaded nanocarrier formulations (described in Section 3.3) along with empty nanocarrier formulations at chosen concentrations for 24, 48, and 72 hours. Following incubation time cell viability was measured as described previously in Section 3.8.1.

3.9. DETECTION OF GENE EXPRESSION LEVELS OF EGFR AND BIKDD IN AU565 CELL LINE

3.9.1. RNA isolation for EGFR Gene Analysis

AU565 and SKBR3 cells were seeded into 6-well plates at a density of 3×10^5 cells/well. After 24 hours, cells were incubated with appropriate serum-free media for 4 hours in order to induce the quiescence. After incubation time, cells were washed once with $500 \mu\text{L}$ of $1 \times \text{PBS}$ (pH7.4), dislodged by adding $250 \mu\text{L}$ of Trizol reagent, transferred into 1.5 mL eppendorf tubes and mixed well with $50 \mu\text{L}$ of chloroform. Samples were incubated at room temperature for 15 minutes and then centrifuged at $12,000 \times g$ for 15 minutes at 4°C . The clear phase (top phase) containing RNA was transferred into new eppendorf tubes, pre-cooled isopropanol with the same amount of RNA was added and mixed well by inverting the tube several times following 10 minutes incubation on ice. Then, samples were centrifuge at $12,000 \times g$ for 10 minutes at 4°C , supernatant was disposed and $500 \mu\text{L}$ of 75 percent (v/v) ethanol was added to each tube following another centrifugation step by $7,500 \times g$ for 10 minutes at 4°C . Each tube was airdried, pellet was suspended in a RNase/DNase free water and concentration was measured using nanodrop.

3.9.2. RNA isolation for BikDD Gene Analysis

AU565 (3×10^5 cells/well) cells were seeded into 6-well plates and incubated for 24 hours in a humidified incubator at 37°C and 5 percent CO₂. Followed by transfected with BikDD gene either with commercially available transfection reagent or nanoconstructs carrying gene of interest as previously described in Section 3.7. Trizol reagent was used to extract RNA from attached cells as described in Section 3.9.1.

3.9.3. Reverse Transcriptase Polymerase Chain Reaction

RNA isolated from the cell line of interest were converted into cDNA products via Sensiscript Reverse Transcriptase kit. PCR reaction was performed at 37°C for 1 hour according to manufacturer's protocol (Table 3.4).

Table 3.4. RT-PCR reaction master mix

Reagents	Volume per reaction
10x Buffer	2 μ L
dNTP (5mM)	2 μ L
Oligo-dT primer (10 μ M)	2 μ L
RNase/DNase free water	Variable
Template	Variable
Senscript Reverse transcriptase enzyme	1 μ L
Total volume	20 μ L

3.9.4. Quantitative Polymerase Chain Reaction

The mRNA expression levels of EGFR and BikDD genes were detected using QuantiTect Primer Assay and SYBR PCR Kit. Primer sequences used for EGFR were: sense 5'-ACCTGCGTGAAGAAGTGTC-3' and antisense 5'-ATTCGTAGCATTATGGAGA-3'. Bik primer sequence were: sense 5'-GAGACATCTTGATGGAGACC-3' and antisense 5'-

TCTAAGAACATCCCTGATGT-3'. Reaction mixture includes 500 ng of cDNA, 1.25 μ L primer, 3 μ L RNase/DNase free water, and 6.25 μ L Syber Green PCR mix. Samples were studied in triplicate and reaction conditions were listed in Table 3.5. Results were analyzed using Bio-Rad CFX Manager software, where the absolute quantification was analyzed using the obtained standard curve from the cycler and relative quantification was normalized using 18S rRNA reference gene.

Table 3.5. Quantitative PCR conditions

Cycle	Temperature	Time	Phase
1	94°C	15 minutes	-
2	95°C	5 minutes	Initial denaturation
3 (39 repeat)	95°C	60 seconds	Denaturation
	55°C	60 seconds	Annealing
	72°C	60 seconds	Extension
4	72°C	10 minutes	Final extension
5 (80 repeat)	50-80°C 0.5 °C increase /12 seconds	-	Melt curve
6	4°C	∞	Cooling

3.10. CELL CYCLE ASSAY

AU565 cells were seeded in a 6-well plates at a density of 3×10^6 cells/well. After 24 hours of incubation, cells were subjected to 4 hours serum starvation prior to treatment with P18-PEtOx-*b*-PLA-DOX, P18-PEtOxDOPE-DOX, P18-PPP30-DOX, free DOX or empty nanocarrier formulations for 24 hours while the control group was non-treated cells. Following incubation with drugs, cell media containing dead cells were centrifuged $350 \times g$ for 5 minutes, while attached cells were washed with 1 x PBS and trypsinized at 37°C for 5 minutes. Pellets were fixed with 70 percent ethanol for at least 1 hour at 4°C. Following fixation, samples were washed with 1 x PBS and permeabilized with 0.1 percent triton-X for 20 minutes at room temperature. Next, samples were washed with 1 x PBS, centrifuged

at 350 x g for 5 minutes and pellet was treated with 50 μ g/mL RNase A for 30 minutes at 37°C. After performing another washing step, cells were stained with 5 μ g/mL of PI in 1x PBS and analyzed using Guava easyCyte flow cytometry.

3.11. DETERMINATION OF CELL DEATH BY ANNEXIN-V

AU565 cells were seeded in a 6-well plate at a density of 3×10^6 cells/well and incubated for 24 hours in a humidified incubator at 37°C and 5 percent CO₂ conditions. After incubation time, AU565 cells were subjected to either P18-PEtOx-*b*-PLA-DOX, P18-PEtOx-DOPE-DOX, P18-PPP30-DOX, free DOX or empty nanocarrier formulations for 48 and 72 hours and the control group were non-treated cells. Following incubation with the aforementioned drugs, cell media containing dead cells were collected in a 1.5 mL eppendorf tubes, cells monolayer was washed with 1 x PBS and trypsinized at 37°C for 5 minutes. Samples in each tube were centrifuged at 350 x g for 5 minutes at 4°C, cell pellets were suspended in 1 mL of 1 x PBS and counted. 1×10^5 cells of each sample was transferred into new 1.5 mL eppendorf tubes and cells were centrifuged at 350 x g for 5 minutes at 4°C. Pellet were suspended in 100 μ L of Annexin binding buffer and incubated under dark conditions for 15 minutes with 2 μ L Annexin V and/or PI solution. After incubation time, samples were supplied with 400 μ L of Annexin binding buffer and analyzed immediately by flow cytometry with 20,000 events. Gating parameters were set with untreated cells incubated with and without Annexin V or PI. Annexin V versus PI plots from gated cells show population of non-apoptotic (Annexin V⁻PI⁻), early (Annexin V⁺PI⁻), and late (Annexin V⁺PI⁺) apoptotic cells.

3.12. IN VIVO STUDIES

3.12.1. Animals

For in vivo anticancer activity assay, athymic CD-1 nu/nu female mice (5-6 weeks old) weighing 20 \pm 2g obtained from KOBAY (Ankara, Turkey) were performed at Yeditepe University. The CD-1 nu/nu female mice were housed at sterilized and filtered cages, and subjected to a constant temperature of 23 \pm 1°C, relative humidity of 60 \pm 10 percent. The

mice were maintained at 12 hours dark/light environmental conditions and fed with special diets for nude mice and water ad libitum. All animal procedures were conducted under the guidelines approved by Institutional Animal Care and Welfare Committee of Yeditepe University (Turkey).

3.12.2. Development of Orthotopic Breast Cancer Model in CD-1 Nude Female Mice and Drug Applications

In order to create orthotopic breast cancer models, AU565 cells were injected into the second mammary fat pad of CD-1 nu/nu female mice. AU565 cells cultured in RPMI 1640 medium supplemented with 10 percent (v/v) FBS, 100 units/mL penicillin, and 100 µg/mL streptomycin were injected orthotopically to each mice at a density of 8×10^6 cells with 1:1 ratio of matrigel. Following the third day of inoculation, mice were injected with DOX (5 mg/kg) loaded P18-PEtOx-DOPE liposome, DOX (1 mg/kg) loaded P18-PEtOx-*b*-PLA and P18-PPP30 micelle, or free DOX intraperitoneally every three days for a total of 8 injections. Control groups received same volume of PBS (vehicle group) or nanocarrier formulation as treated groups. The tumor size and weight of each animal was measured before every injection. Mice were examined for morbidity and mortality till the end of the study.

3.12.3. Tumor Volume Measurements

The tumor size of each animal were measured periodically by a caliper before each injection of the drug. The tumor volume (mm^3) was calculated after resection of tumors by the formula given below [207, 208] :

$$\textit{Tumor volume} = (\textit{Lenght} \times (\textit{Width})^2) \quad (3.2)$$

3.12.4. Histopathological Analysis

Mice were sacrificed by cervical dislocation method after 27 days and organs including brain, lung, heart, liver, spleen, stomach, intestines, kidney, ovary and tumor tissues were fixed at 10 percent formalin. The organs will be send to pathology for further investigation

and in order to characterize the tumor tissues, hematoxylin and eosin (H&E) staining was conducted.

3.13. STATISTICAL ANALYSIS

All data given in the results part (Section 4) were means \pm standard deviation (SD) values calculated from three to six independent experiment's. Parametric statistics from between groups were compared using two-tailed Student's t-test using GraphPad Prism 6 (GraphPad Software, USA) and differences were considered statistically at * $P \leq 0.05$, ** $P \leq 0.01$, *** $P \leq 0.001$, **** $P \leq 0.0001$.

4. RESULTS

4.1. DETERMINATION OF THE MODEL HER2-POSITIVE BREAST CANCER CELL LINE FOR THE STUDY

4.1.1. Cell Proliferation Rate of AU565 and SKBR3 Cells

To evaluate which of the breast cancer cell lines had a better cell proliferation rate and to select and standardize the optimal cell seeding density for AU565 and SKBR3 cell lines, growth rate for each cell line was analyzed using WST-1 as mentioned in Section 3.8. The model cell line that is ideal for this study was planned to be decided upon according to the findings of WST-1 analysis.

Growth assay was conducted using a standard curve from absorbance values obtained from cells seeded on 96 well plates overnight at 5×10^3 , 7.5×10^3 , 10×10^3 , 15×10^3 , and 20×10^3 cells/well cell densities. To analyse the growth curve of breast cancer AU565 and SKBR3 cell lines were seeded and incubated for 96 hours. The standard curve was used to convert the absorbance values into corresponding cell numbers. The cell proliferation of AU565 and SKBR3 cells for 24, 48, 72, and 96 hours are shown in Figure 4.1.

AU565 cells showed a significant increase of cell proliferation at 72, and 96 hours in comparison to the cell number recorded at 24 hours. However, SKBR3 cells showed a significant increase in cell number only at 96 hours compared to the cell number at 24 hours. AU565 cells had a higher proliferation rate than SKBR3 cells at all times. At 96 hours, AU565 had nearly 2,500 cells more than SKBR3 cells per well. Cell proliferation rate for both cell lines is an important factor considering the large amount of cells that would be needed in *in-vivo* studies. The doubling time of AU565 cells was found as 72 hours where as, for SKBR3 cells the doubling time was between 72 to 96 hours, suggesting that AU565 better meets the criteria as a cell line to be utilized in *in-vivo* experiments.

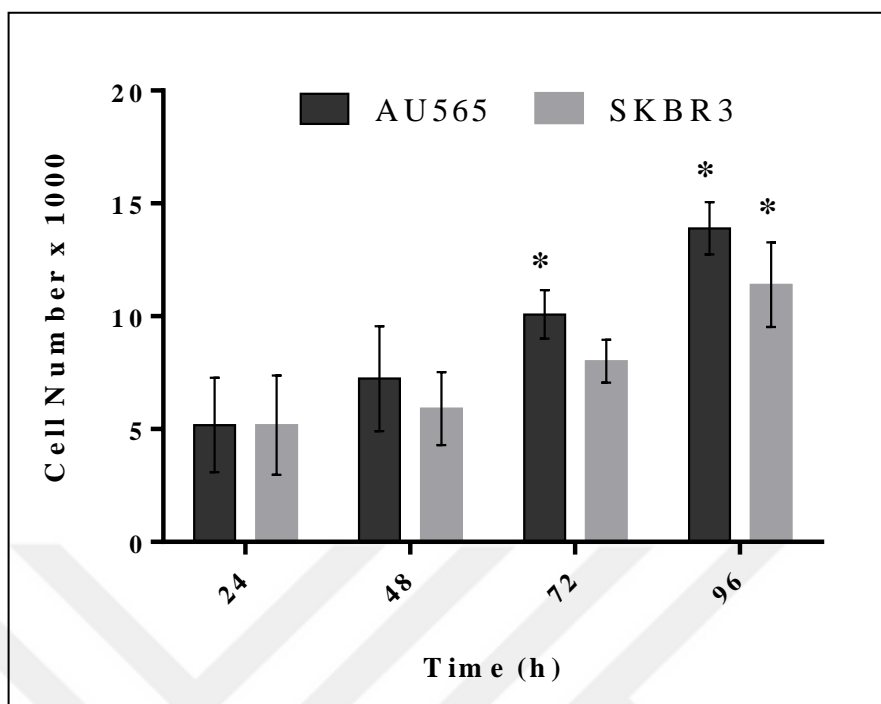


Figure 4.1. Determination of the cell proliferation rate of AU565 and SKBR3 cells. Both cells were not subjected to any treatment for 24, 48, 72, and 96 hours. The initial cell number/well was 5×10^3 and cell viability was measured by WST-1 assay. Each data point represents the average of three independent experiments \pm SD (* $P \leq 0.05$).

4.1.2. Gene Expression Level of EGFR in AU565 and SKBR3 Cells

In order to determine which EGFR positive breast cancer cell line had the highest EGFR expression, selected breast cancer AU565 and SKBR3 cell lines were analyzed for mRNA expression levels of EGFR by qPCR as mentioned before (Section 3.9). EGFR gene expression values for AU565 and SKBR3 cells were given in Figure 4.2.

The results of AU565 cells showed a 1.57 fold higher EGFR expression compared to SKBR3 cells. Thus, AU565 cell line is a better choice of a breast cancer model cell line for this study because EGFR overexpression is an important factor for the targeting of breast cancer cell lines.

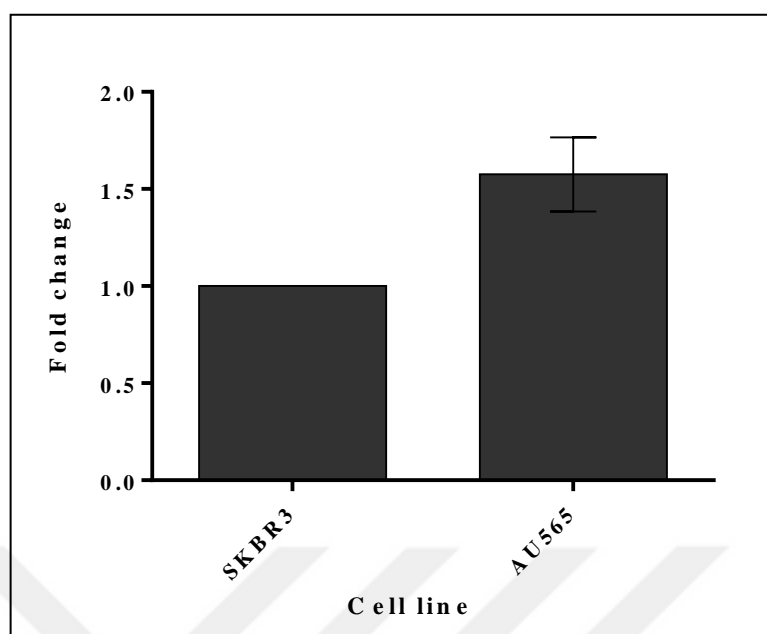


Figure 4.2. The relative EGFR/18sRNA mRNA levels in SKBR3 and AU565 cells was evaluated using qPCR. Each data point represents the average of three independent experiments.

4.2. BINDING AFFINITY OF PEPTIDE MC10, PEPTIDE 11 AND PEPTIDE 18 TO BREAST CANCER AND CONTROL CELL LINES DETERMINED BY FLOW CYTOMETRY

The specificity and binding affinity of peptides MC10, peptide 11 (P11) and peptide 18 (P18) to breast cancer SKBR3 and AU565 cell lines as well as to healthy epithelial breast MCF10A and MCF12A cell lines, and HUVEC cell lines were studied. 10 μ M (10^{-5} mol/L) of peptides MC10, peptide 11 (P11) and peptide 18 (P18) conjugated with TAMRA were used to treat all five cell lines for one hour. The binding affinity of three peptides to the cell surface of AU565, SKBR3, MCF10A, MCF12A and HUVEC cells were analyzed as described in Section 3.5.1.

Flow cytometry analysis of two breast cancer and three different control cell lines for TAMRA staining were given in Figure 4.3 and Table 4.1. Peptide MC10 exhibited binding affinity of 31.0 percent, 14.0 percent, 7.53 percent, 7.1 percent, and 5.4 percent for AU565, SKBR3, MCF10A, MCF12A and HUVEC cells, respectively.

On the other hand, P11 peptide showed low binding affinity to most of the cell lines tested. The binding affinity of P11 peptide was 27.0 percent to SKBR3, 24.0 percent to MCF10A, 18.5 percent to MCF12A, and 8.9 percent cells to HUVEC. However, a high binding affinity of P11 was evident to AU565 with 55.4 percent. Similarly, P18 peptide showed specific binding to AU565 cells with 69.0 percent, while it exhibited a binding affinity of 32.0 percent, 8.81 percent, 10.7 percent, 7.8 percent for SKBR3, MCF10A, MCF12A and HUVEC cells, respectively.

The results of these experiments indicated that peptide P18 could bind specifically to the AU565 cell line and show minimum binding to normal MCF10A, MCF12A and HUVEC cell lines. For for this study, the peptide with the highest binding affinity to cancer cell lines and the lowest binding affinity to normal cell lines is important. Therefore P18 was chosen as the targeting peptide to be used in the nanocarriers along with AU565 to be used in *in vitro* and *in vivo* studies as the model cell line. Later on in the study polymersome, liposome and micelle nanocarriers constructs will be tagged with P18 for targeting breast cancer AU565 cell lines.

Table 4.1. Average percentage binding affinity of peptide MC10, peptide 11, and peptide 18 to AU565, SKBR3, MCF10A, MCF12A, and HUVEC cells for three independent experiments (means \pm SD).

Cell Type	MC10	P11	P18
AU565	31.0 \pm 8.8	55.4 \pm 8.3	69.0 \pm 10.1
SKBR3	14.0 \pm 7.5	26.9 \pm 8.9	32.0 \pm 21.3
MCF10A	7.53 \pm 2.4	24.0 \pm 3.3	8.81 \pm 3.3
MCF12A	7.1 \pm 6.4	18.5 \pm 9.8	10.7 \pm 7.9
HUVEC	5.4 \pm 2.2	8.9 \pm 2.3	7.8 \pm 2.1

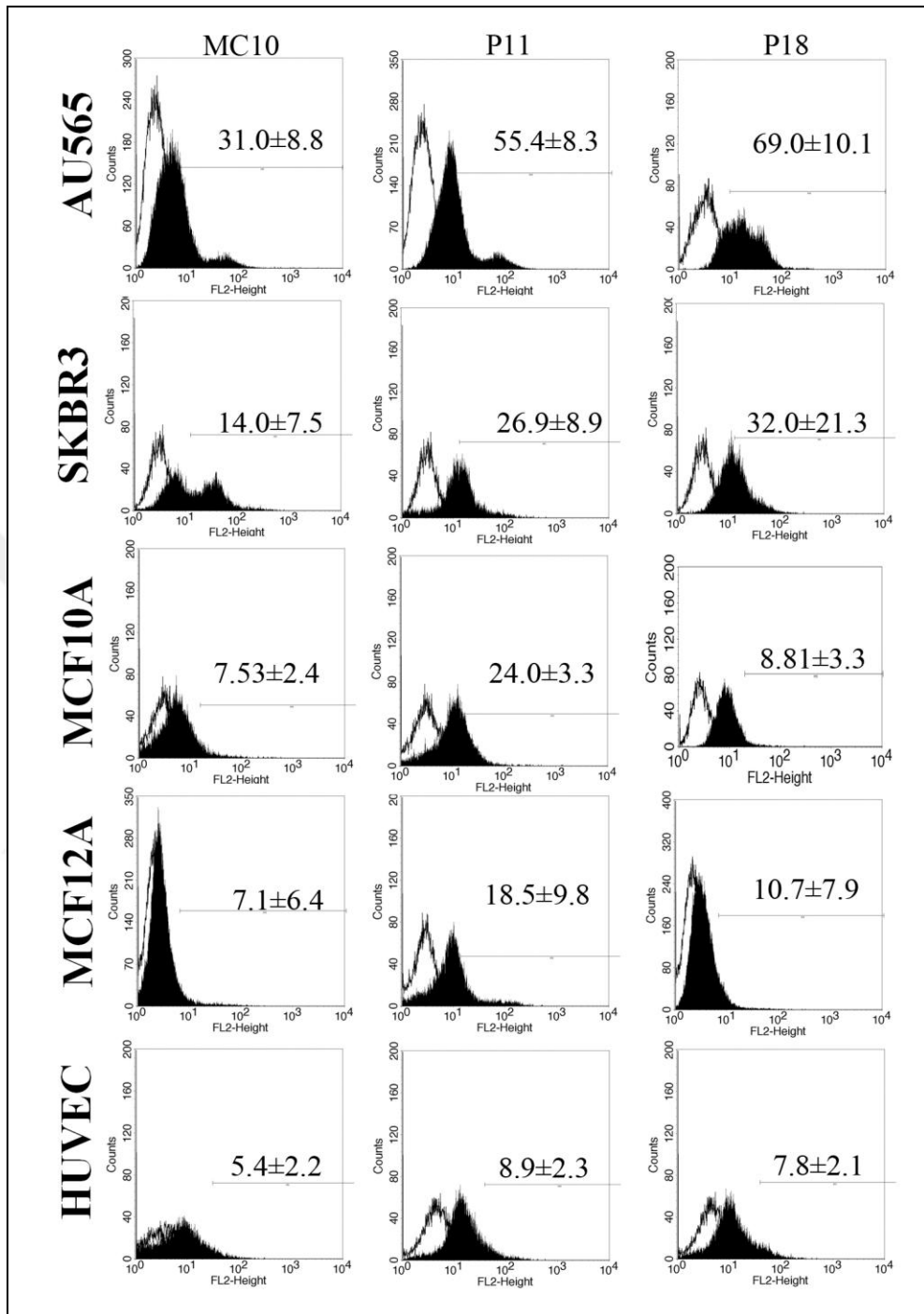


Figure 4.3. The representative histograms showing binding affinity of MC10, P11, and P18 on AU565, SKBR3, MCF10A, MCF12A, and HUVEC cell lines. Cells were treated with all peptides for 1 hour at 37°C.

4.3. DETERMINATION OF BINDING AFFINITY OF PEPTIDES ON BREAST CANCER AND CONTROL CELL LINE BY CONFOCAL MICROSCOPY

In order to confirm the flow cytometry results, confocal microscopy imaging was used to monitor binding affinity of MC10, P11 and P18 to AU565, MCF10A, and MCF12A cells. AU565 cells were seeded at a density of 2.4×10^4 cells/well while MCF10A and MCF12A cells were seeded at a density of 2×10^4 cells/well to 8-well chamber slides due to their size difference. After 24 hours, cells were incubated with 10 μ M of MC10, P11 and P18 for 1 hour as mentioned in Section 3.6.

The images of confocal microscopy used to analyze the samples were given in Figure 4.4, 4.5, and 4.6. Peptide bound cells were stained in red while the nucleus of cells were appeared in blue using DAPI staining. In agreement with the flow cytometry results, confocal microscopy images indicated that P18 was strongly bound to AU565 cells while, the binding affinity of peptides MC10, and P11 to AU565 cells was weaker as shown in Figure 4.4. In contrast, confocal microscopy images showed that MC10, P11, and P18 failed to bind to MCF10A cells (Figure 4.5). Similarly, the three peptides were bound to MCF12A cells with a very low binding affinity as shown in Figure 4.6.

Flow cytometry results in the previous section indicated that all three peptides bound to breast cancer AU565 cell line with high binding affinity. However, there was a low binding affinity detected on normal breast epithelial MCF10A and MCF12A cells and the confocal microscopy images confirmed these results.

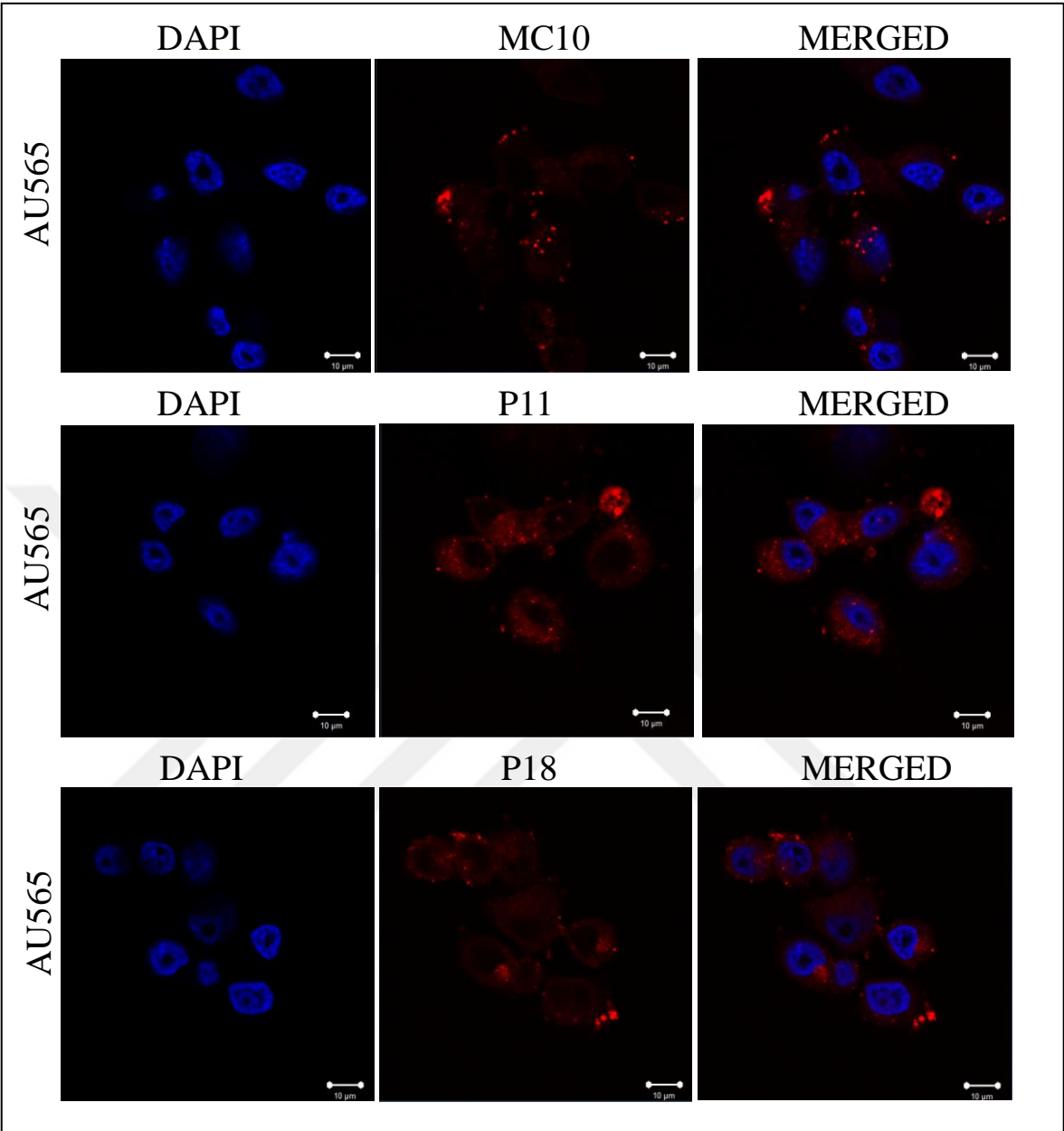


Figure 4.4. Peptide MC10, P11, and P18 binding affinity on AU565 cell line by confocal microscopy. Bar: 10 μm.

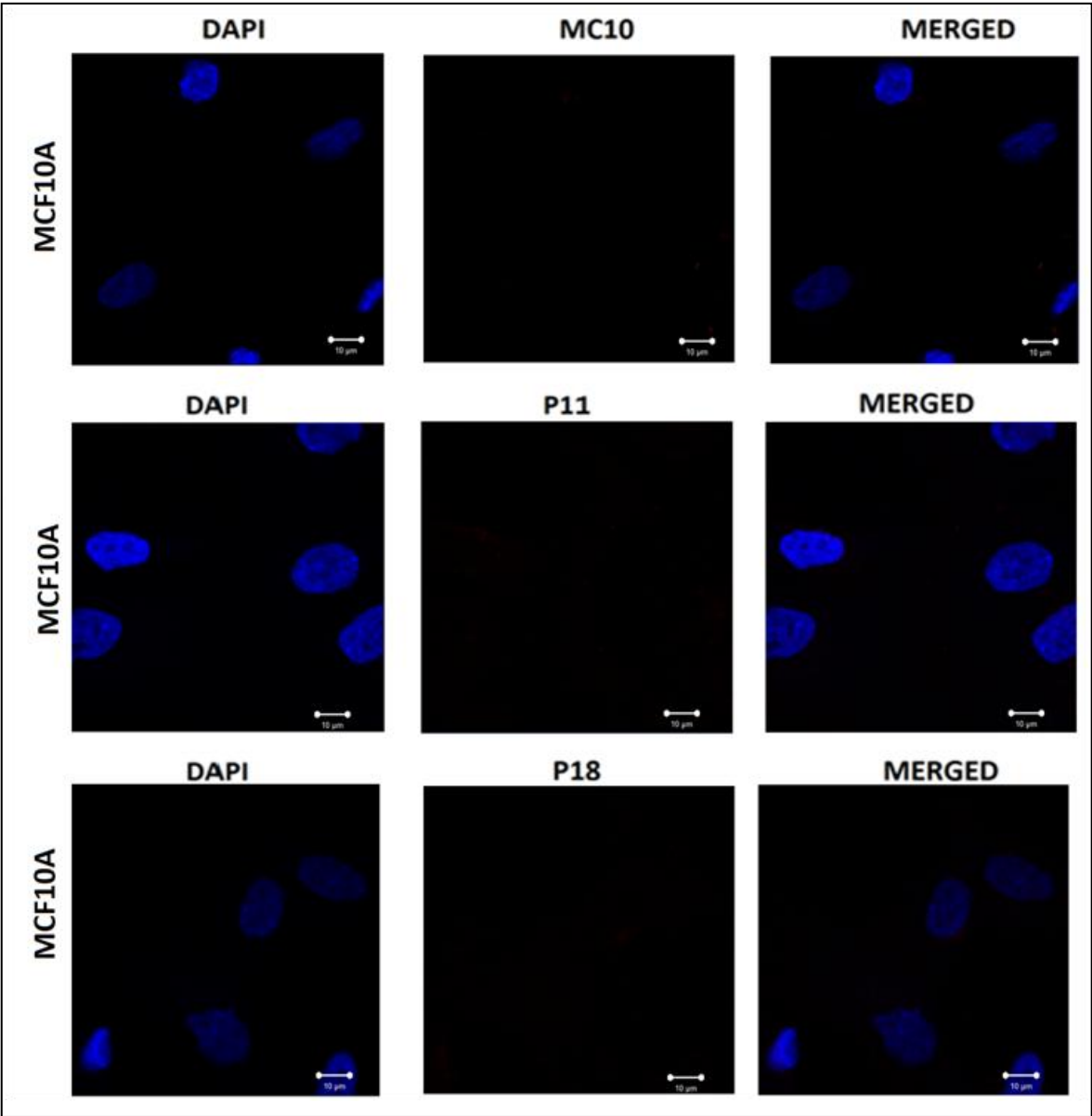


Figure 4.5. Peptide MC10, P11, and P18 binding affinity on MCF10A cell line by confocal microscopy. Bar: 10 µm.

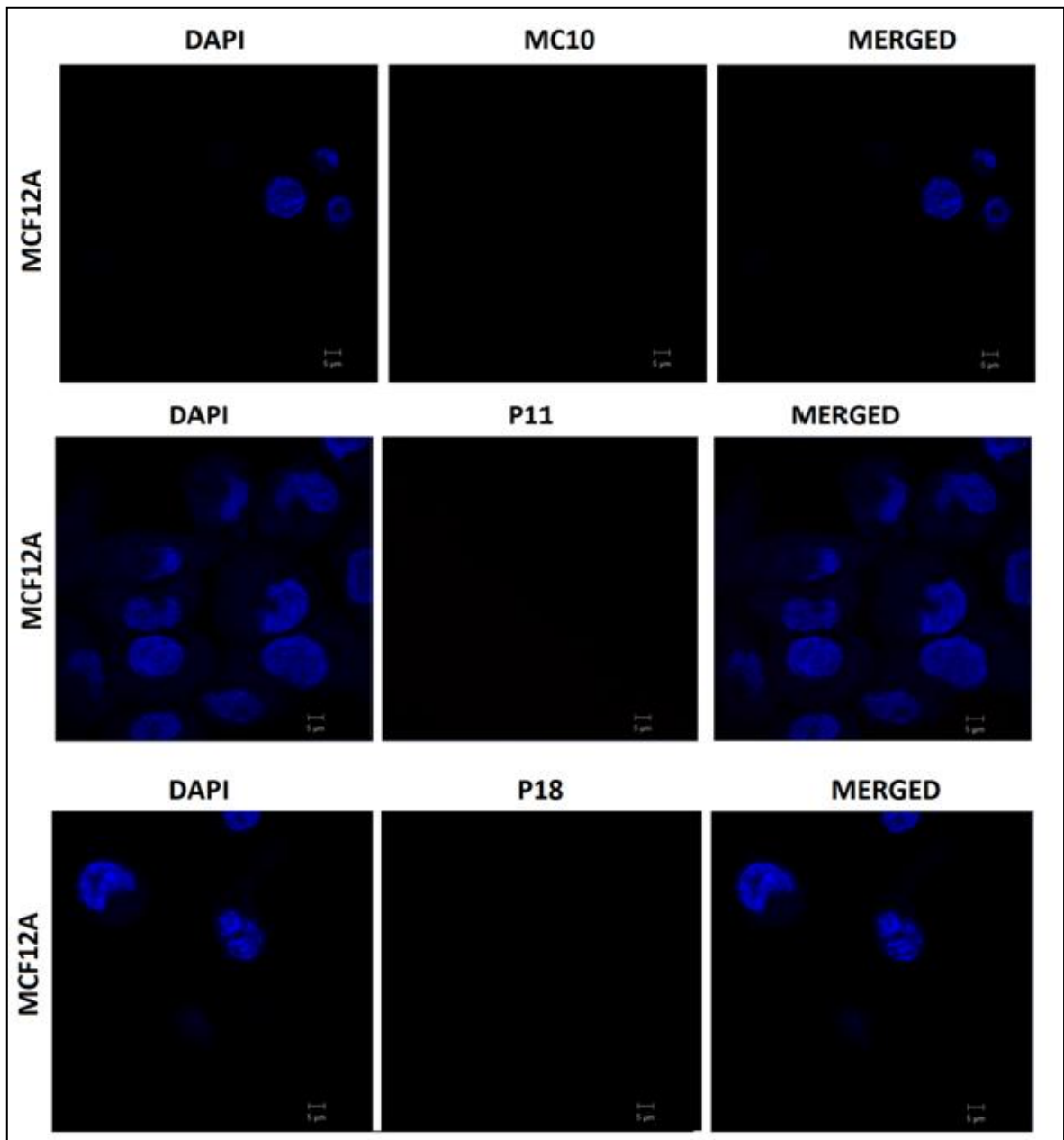


Figure 4.6. Peptide MC10, P11, and P18 binding affinity on MCF12A cell line by confocal microscopy. Bar: 5 μ m.

4.4. DETERMINATION OF THE PROAPOPTOTIC PLASMID AND SITE-DIRECTED MUTAGENESIS OF BIK TO BIKDD GENE

4.4.1. Gene Expression Level of Bik in AU565 Cell Line

In order to determine which of the three Bik plasmids had the most potent Bik expression, AU565 cells were transfected with pEGFP-C3-Bik, pCMV6-XL5-Bik, and pCAG-GFPd2-Bik plasmids. pCMV6-XL-Bik into pCAG-GFPd2 plasmid DNAs were digested with *NotI* restriction enzyme and ligated into pCMV6-XL-Bik as mentioned in Section 3.2.2. Changes in Bik expression values in AU565 cells were evaluated with qPCR as mentioned in Section 3.9. The relative Bik/18sRNA mRNA expression values were given in Figure 4.7. Real-time PCR analysis of Bik expression levels in AU565 cells after transfection showed Bik/18sRNA ratio of 50, 48 and 1 for pEGFP-C3-Bik, pCMV6-XL5-Bik, pCAG-GFPd2-Bik vectors. Thus, pEGFP-C3-Bik plasmid was chosen to be utilized in generation of mutant BikDD gene by site-directed mutagenesis.

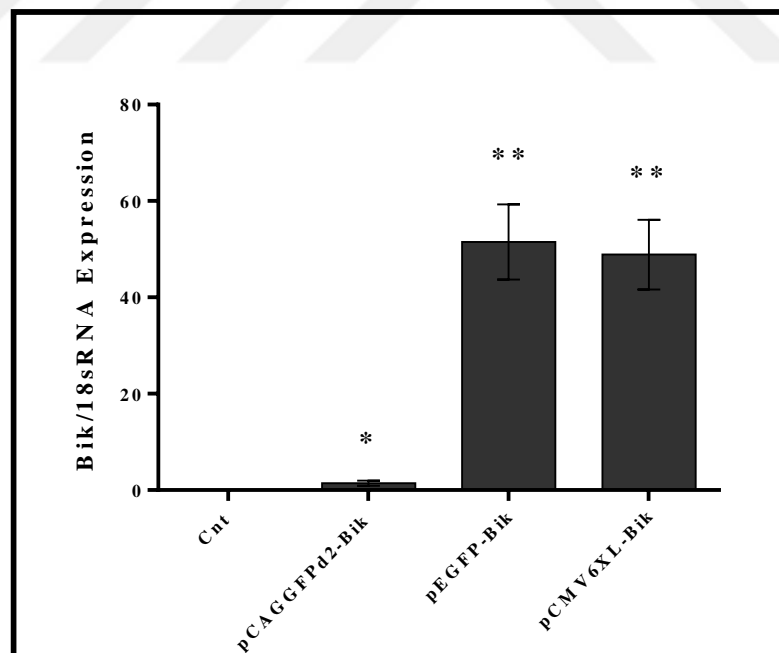


Figure 4.7. Relative Bik/18sRNA mRNA expression using qPCR for non-transfected control (Cnt) and AU565 cell line transfected with pEGFP-C3-Bik, pCMV6-XL5-Bik, and pCAG-GFPd2-Bik plasmids. Each data point represents the average of three independent experiments \pm SD (* p <0.05, ** p <0.01).

4.4.2. Chromatogram Analysis of Site-Directed Mutagenesis

Proapoptotic BikDD gene, the double mutant form of Bik gene, was used as pro-apoptotic gene to induce apoptosis in breast cancer cell lines [209]. Following site-directed mutagenesis performed as described in Section 3.3. DNA sequence analysis of the BikDD gene in pEGFP-C3-Bik vector was performed by Macrogen. Figure 4.8 shows the results of the chromatogram for mutagenesis of pEGFP-C3-BikDD plasmid, the black arrows shows that Threonine (T) at 33th position and Serine (S) at 35th position were mutated to Aspartic acid (D) and Bik gene was converted to BikDD successfully.

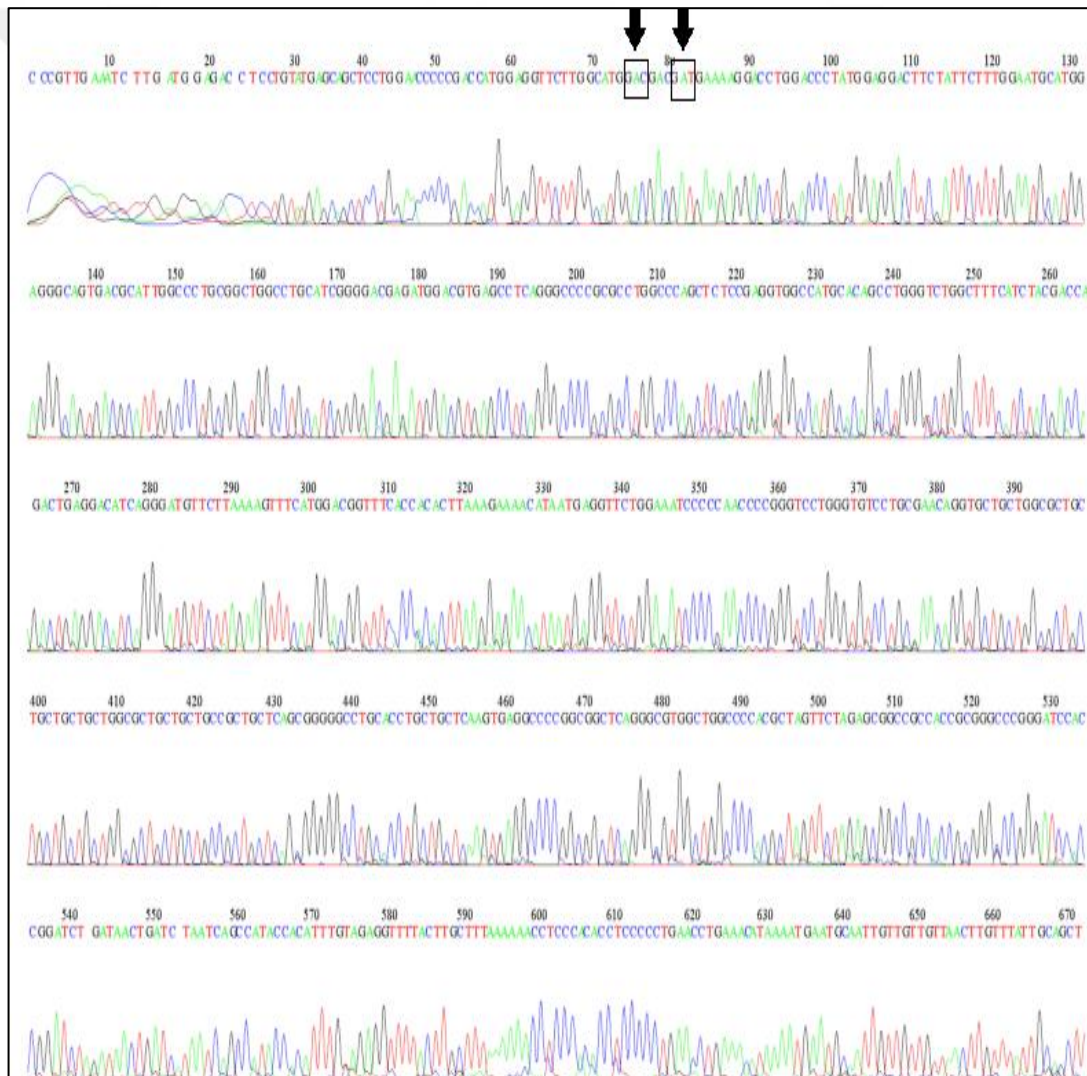


Figure 4.8. Chromatogram results of pEGFP-BikDD vector. The black arrows indicate the site of mutation T→D and S→D.

4.5. GENE EXPRESSION LEVELS OF BIKDD IN AU565 CELL LINE

In order to find out the mRNA expression level of Bik in AU565 cells transfected with pEGFP-BikDD, real time PCR was conducted as mentioned earlier in Section 3.9. Figure 4.9 shows the relative Bik/18sRNA mRNA expression levels in non-transfected cells (Cnt) and AU565 cells transfected with mutant BikDD and mock vector pEGFP-C3 (C3). AU565 cells transfected with 2 μ g of pEGFP-BikDD showed a 7 fold increase compared to AU565 cells transfected with mock vector.

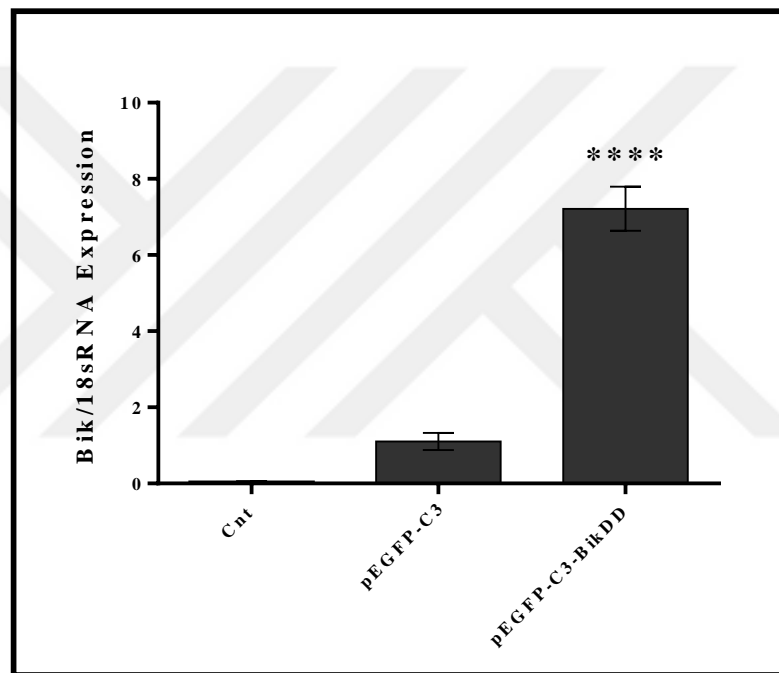


Figure 4.9. Relative Bik/18sRNA mRNA expression using qPCR for non-transfected (Cnt) and AU565 cells transfected with pEGFP-C3-BikDD, and mock vector pEGFP-C3 (C3). Each data point represents the average of three independent experiments \pm SD (* p <0.05).

4.6. LIPOSOME DELIVERY OF BIKDD OR DOXORUBICIN TO AU565 CELLS

4.6.1. Analysis of Cellular Cytotoxicity for PEtOx-DOPE Copolymer and Liposomes

In order to determine the cytotoxic effect of PEtOx-DOPE copolymer and liposome formulations, HUVEC, HEK293, MSC, and MCF10A cells were subjected to 25, 50, 75, 100, and 150 $\mu\text{g}/\text{mL}$ concentrations of PEtOx-DOPE copolymer and liposome for 24, 48, and 72 hours. Cytotoxicity was evaluated by WST-1 cell proliferation assay as described in Section 3.8.1. Absorbance value of control cells (DMSO for copolymer and non-treated for liposome formulations) were set as 100 percent, and cell viability percentage was calculated accordingly.

The cell viability of HUVEC cells after treatment with PEtOx-DOPE copolymer and liposome formulation were shown in Figure 4.10. In comparison to control cells, there was a 10 percent proliferation of HUVEC cells at 25, 50, and 75 $\mu\text{g}/\text{mL}$ concentration of PEtOx-DOPE copolymer treatment at 72 hours. However, HUVEC cells treated with 150 $\mu\text{g}/\text{mL}$ concentration of PEtOx-DOPE copolymer showed a significant toxicity by 30 percent at 72 hours. According to Figure 4.11b, HUVEC cells treated with lower concentrations (25- 75 $\mu\text{g}/\text{mL}$) of PEtOx-DOPE liposome formulation showed no significant decrease at 24, 48, and 72 hours. However, a significant toxicity of nearly 40 percent and 50 percent in the viability was observed at 100 and 150 $\mu\text{g}/\text{mL}$ of PEtOx-DOPE liposomes, respectively at 72 hours.

Figure 4.11 shows the effect of PEtOx-DOPE copolymer and liposome on cell viability of HEK293 cell line. In general, no significant reduction was observed on HEK293 cells treated with different concentrations of PEtOx-DOPE copolymer. At all time point, a slight ($p>0.05$) toxicity of 8 percent to 19 percent was detected on HEK293 cells when treated with 25-150 $\mu\text{g}/\text{mL}$ PEtOx-DOPE copolymer. On the contrary, significant toxicity of 40 and 46 percent on cell viability of HEK293 cells was recorded when treated with 100 and 150 $\mu\text{g}/\text{mL}$ concentrations of PEtOx-DOPE liposomes after 72 hours post treatment.

Figure 4.12 shows the cytotoxic effect of PEtOx-DOPE copolymer and liposome on MSCs. Although, no significant toxicity was detected for 24 hours, PEtOx-DOPE copolymer showed toxicity in MSCs with a percentage of 19, 23, and 25 percent at

concentrations of 75-150 $\mu\text{g}/\text{mL}$ for 48 hours. On the other hand, toxicity percentage of 26 and 32 percent at 100 and 150 $\mu\text{g}/\text{mL}$ of PEtOx-DOPE liposomes to MSC was detected at 48 hours. However, at 72 hours the cell viability of MSC were pulled back to almost control levels with a percentage of 10 to 18 percent decrease in cell viability

Cytotoxic effect of PEtOx-DOPE copolymer and liposome formulation on MCF10A cells was given in Figure 4.13. PEtOx-DOPE copolymer did not cause any significant cytotoxicity on MCF10A cells at all time points; toxicity of 12 percent with the highest dose of 150 $\mu\text{g}/\text{mL}$ of PEtOx-DOPE copolymer was observed at 72 hours. PEtOx-DOPE liposomes induced significant proliferation of MCF10A cells with a percentage of 39 percent at 150 $\mu\text{g}/\text{mL}$ for 72 hours. Altogether, these results demonstrate that until 75 $\mu\text{g}/\text{mL}$ PEtOx-DOPE copolymer and liposome showed almost no cytotoxic effect on healthy HUVEC, HEK293, MSC, and MCF10A cells.

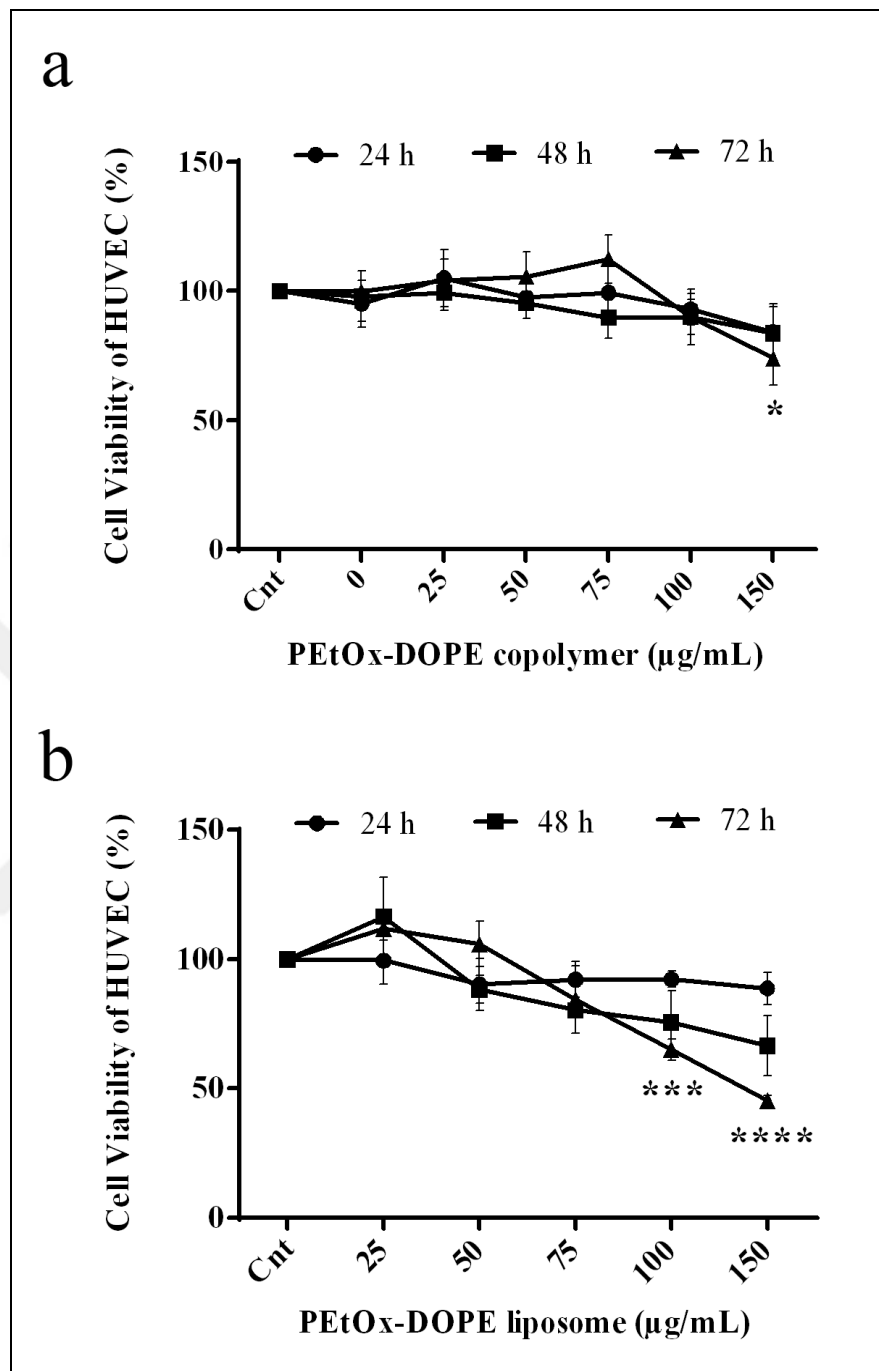


Figure 4.10. Effect of PEtOx-DOPE (a) Copolymer and (b) Liposome on HUVEC cell line viability. 25- 150 µg/mL of PEtOx-DOPE copolymer and liposome were used to treat HUVEC cells until 72 hours. Cell viability was assessed at each 24 hour interval by measuring the absorbance change using a microplate reader at 450 nm. Data represents average of three independent experiments \pm SD (* $P \leq 0.05$, *** $P \leq 0.001$, **** $P \leq 0.0001$).

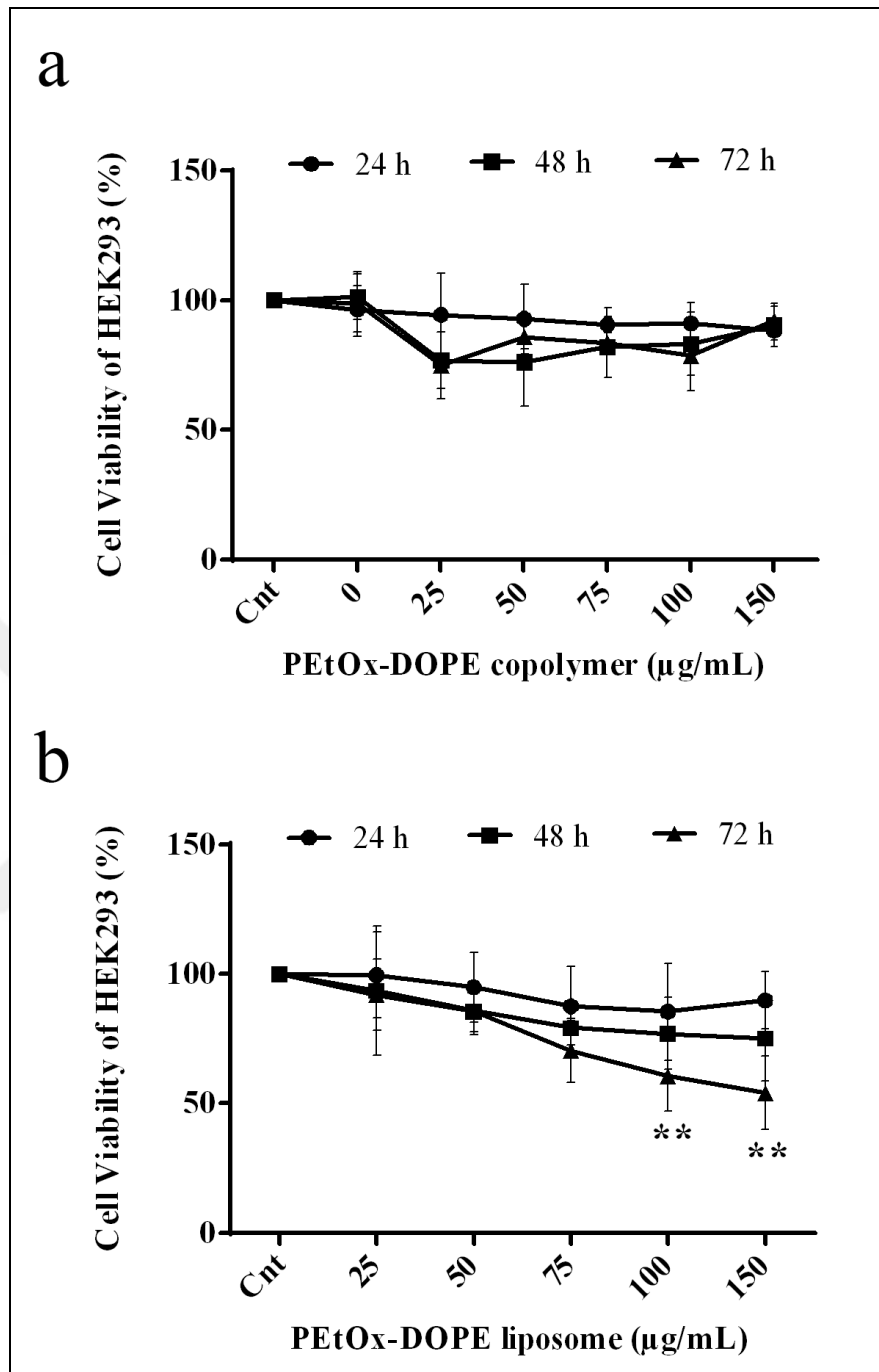


Figure 4.11. Effect of PEtOx-DOPE (a) Copolymer and (b) Liposome on HEK293 cell line viability. 25- 150 $\mu\text{g/mL}$ of PEtOx-DOPE copolymer and liposome were used to treat HEK392 cells until 72 hours. Cell viability was assessed at each 24 hour interval by measuring the absorbance change using a microplate reader at 450 nm. Data represents average of three independent experiments \pm SD (** $P \leq 0.01$).

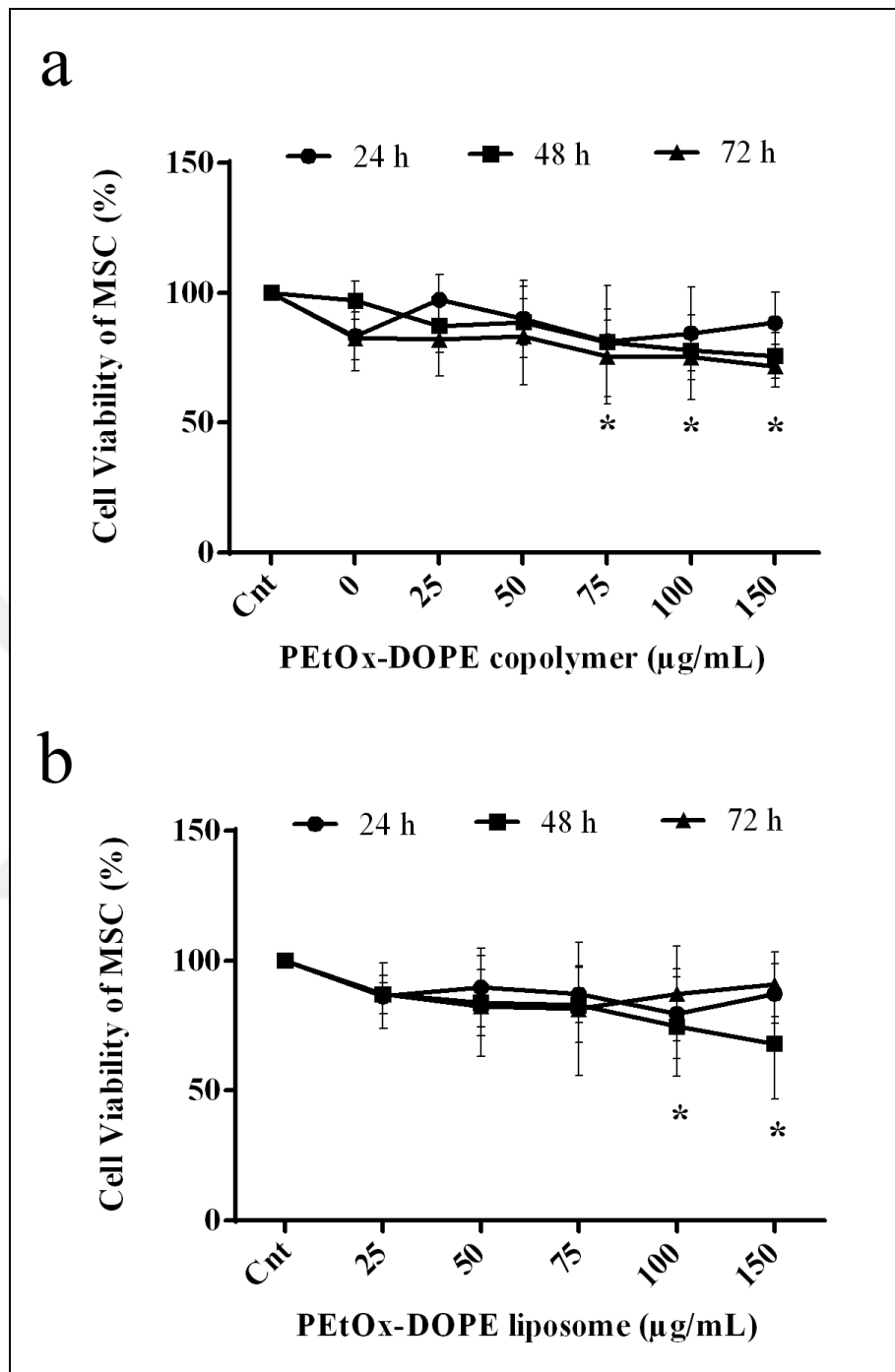


Figure 4.12. Effect of PETox-DOPE (a) Copolymer and (b) Liposome on MSC line viability. 25- 150 µg/mL of PETox-DOPE copolymer and liposome were used to treat MSC cells until 72 hours. Cell viability was assessed at each 24 hour interval by measuring the absorbance change using a microplate reader at 450 nm. Data represents average of three independent experiments \pm SD (* $P \leq 0.05$).

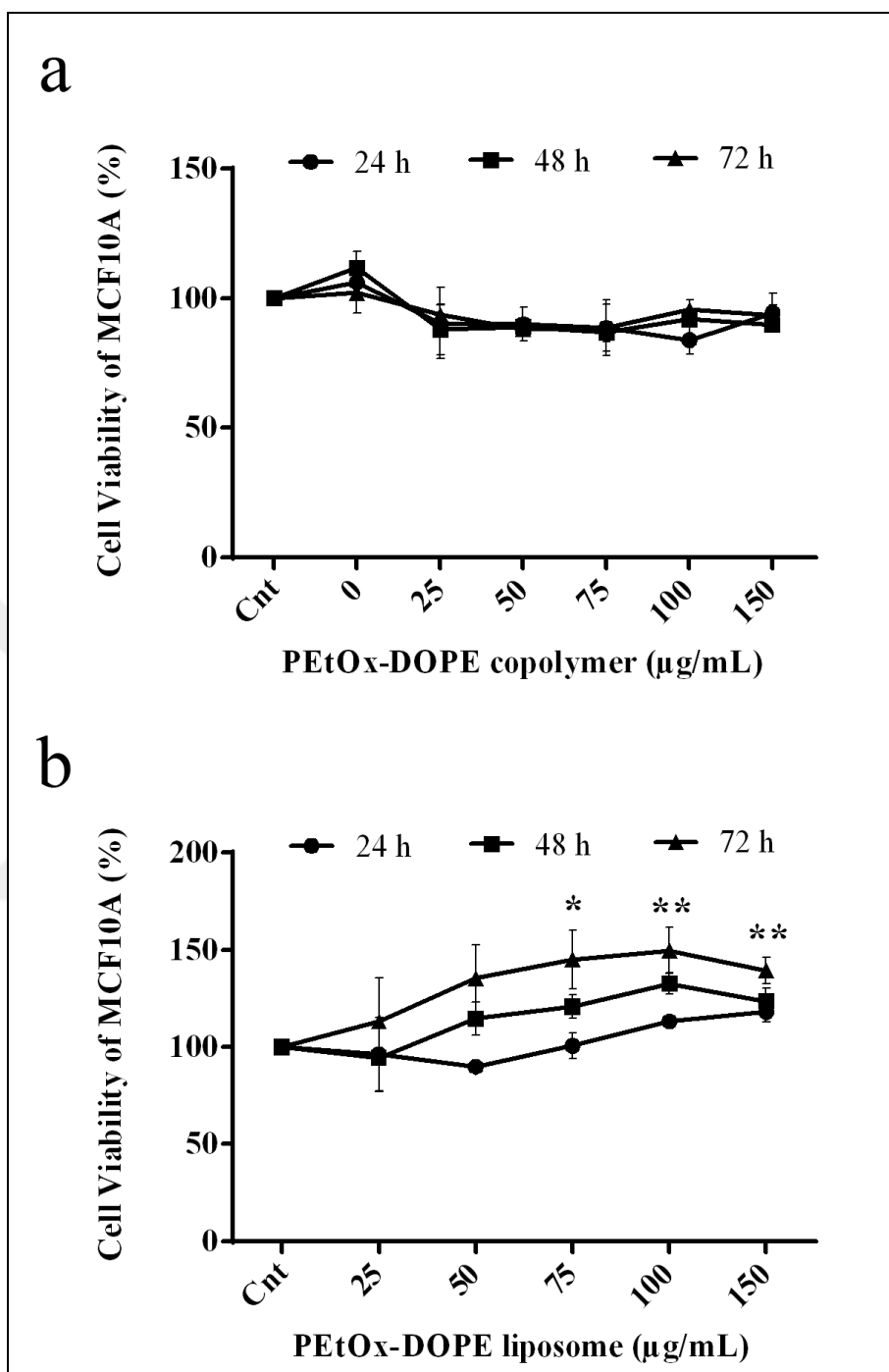


Figure 4.13. Effect of PEtOx-DOPE (a) Copolymer and (b) Liposome on MCF10A cell line viability. 25- 150 $\mu\text{g/mL}$ of PEtOx-DOPE copolymer and liposome were used to treat MCF10A cells until 72 hours. Cell viability was assessed at each 24 hour interval by measuring the absorbance change using a microplate reader at 450 nm. Data is the mean ($n=3$) \pm SD (* $P \leq 0.05$, ** $P \leq 0.01$).

4.6.2. Binding Affinity of P18 Labeled PEtOx-DOPE Liposomes to the Breast Cancer and Control Cell Lines

In order to answer the question whether peptide 18 labeled PEtOx-DOPE (P18-PEtOx-DOPE) liposomes showed a specific binding toward breast cancer cells; the binding affinity of P18-PEtOx-DOPE liposomes to AU565 and MCF10A cell lines were analyzed. P18-PEtOx-DOPE liposomes loaded fluorescein stain were used to treat AU565 and MCF10A cell lines for 1 hour as mentioned in Section 3.5.2.

Flow cytometry results demonstrated that the binding affinity of P18-PEtOx-DOPE liposomes by MCF10A, and AU565 cell line was 14.5 percent, and 79.7 percent, respectively (Figure 4.14). Results show that P18-PEtOx-DOPE liposomes exhibited specific binding to AU565 cancer cells.

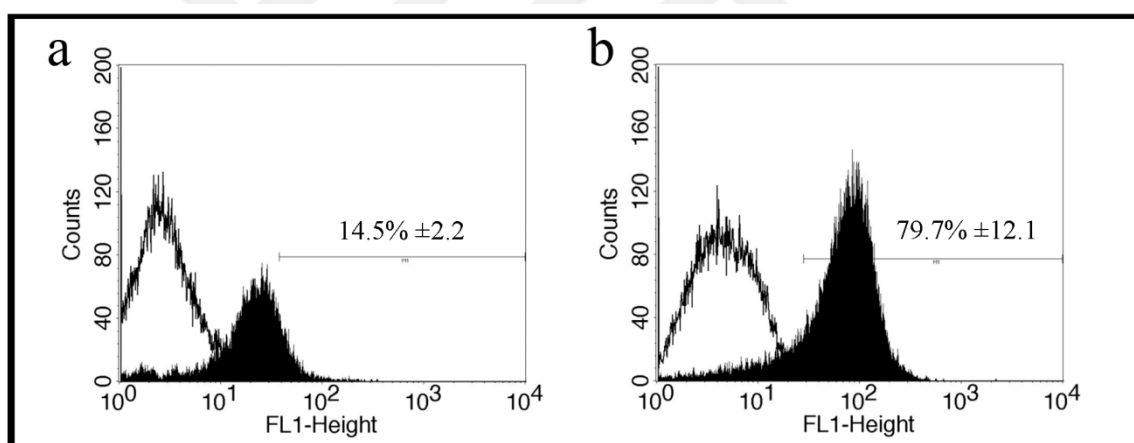


Figure 4.14. The representative histograms showing binding affinity of P18-PEtOx-DOPE liposome on (a) MCF10A and (b) AU565 cell lines. Fluorescein labeled P18-PEtOx-DOPE liposomes were used to treat cells for 1 hour at 37°C.

4.6.3. Cellular Uptake of P18 Labeled PEtOx-DOPE Liposomes to the Breast Cancer and Control Cell Lines

Confocal microscopy imaging was employed to monitor the binding affinity of P18-PEtOx-DOPE liposomes to the control MCF10A and AU565 cells. Cells were seeded to 8-

well chamber slides and allowed to attached for 24 hours prior to the treatment with liposomes as mentioned before (Section 3.6).

The images of confocal microscopy used to analyze the samples were given in Figure 4.15. P18-PEtOx-DOPE liposome bound cells were stained in green while the nucleus of cells were appeared in blue due to DAPI staining. In agreement with the flow cytometry results, confocal microscopy images indicated that P18-PEtOx-DOPE liposome was strongly bound to and internalized by AU565 cells, while it failed to bind to MCF10A cells.

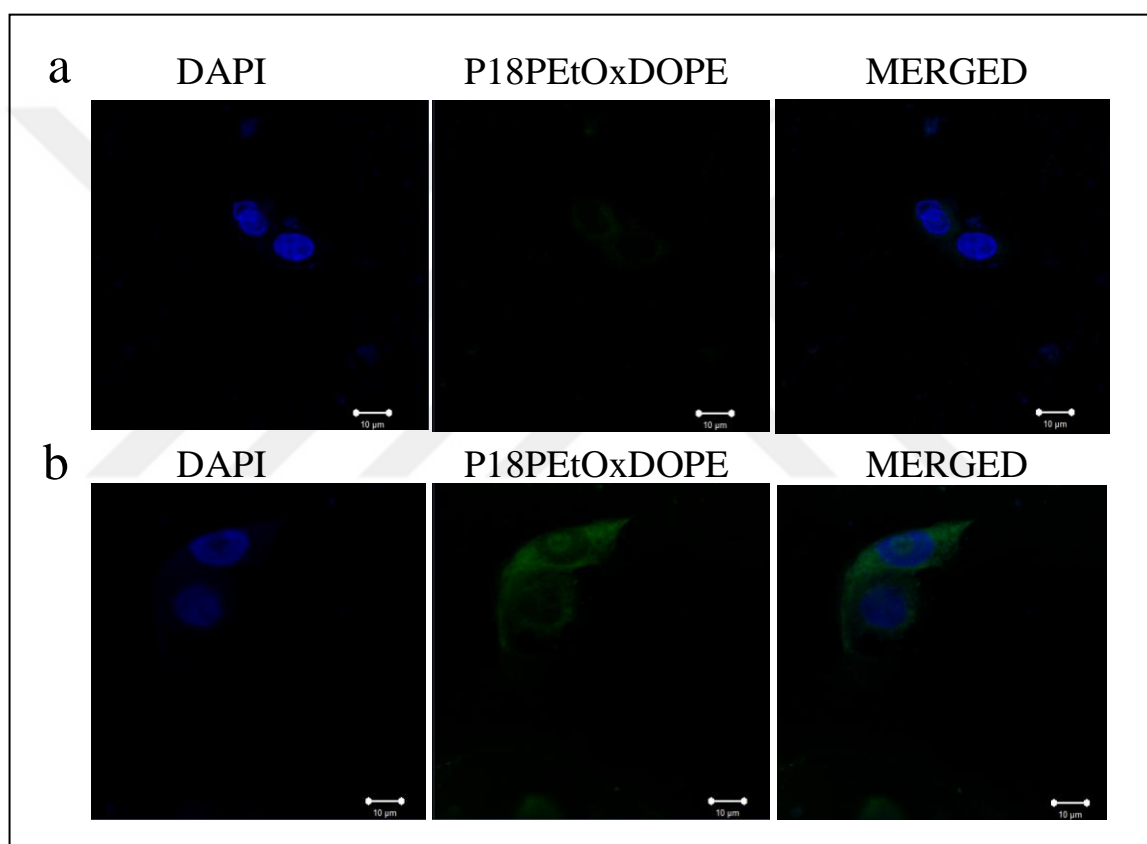


Figure 4.15. P18-PEtOx-DOPE liposome binding affinity on (a) MCF10A and (b) AU565 cell lines by confocal microscopy. Images were taken at 63 x magnification. Scale bar represents 10 µm.

4.6.4. Cell Viability of AU565 Cells Treated with BikDD or Doxorubicin Loaded to P18-Labeled PEtOx-DOPE Liposomes

In order to find out the therapeutic effect of proapoptotic BikDD gene on cell viability of AU565 cells, cells were subjected to increasing concentrations of BikDD loaded targeted

(P18) and empty PEOx-DOPE liposomes for 24, 48, and 72 hours. Dose-dependent effect on AU565 cell viability and proliferation was conducted using WST-1 as mentioned before (Section 3.8.2).

Figure 4.16 shows the effects of P18 targeted PEOx-DOPE-BikDD and empty PEOx-DOPE liposomes on the proliferative ability of AU565 cells for 72 hours post-treatment. At 24 hours, there was a 25 percent decrease in cell viability of AU565 cells when treated with 4 μg of P18-PEOx-DOPE-BikDD liposomes, while there was a proliferative effect of 10 percent on AU565 cell when treated with the same concentration of empty P18-PEOx-DOPE liposome (Figure 4.16a).

AU565 cells treated with 8 μg of P18-PEOx-DOPE-BikDD showed a significant decrease in cell viability with 30 percent at 48 hours. However, empty liposome had no significant effect on cell viability of AU565 cells at 8 μg treatment of PEOx-DOPE liposome (Figure 4.16b).

There was a significant decrease of 25 percent to 20 percent in cell viability of AU565 cells at 4, 8, and 12 μg of P18-PEOx-DOPE-BikDD at 72 hours (Figure 4.16c). In conclusion, the highest therapeutic effect was observed in AU565 cells when treated with 4 μg of P18-PEOx-DOPE-BikDD at 24 and 72 hours.

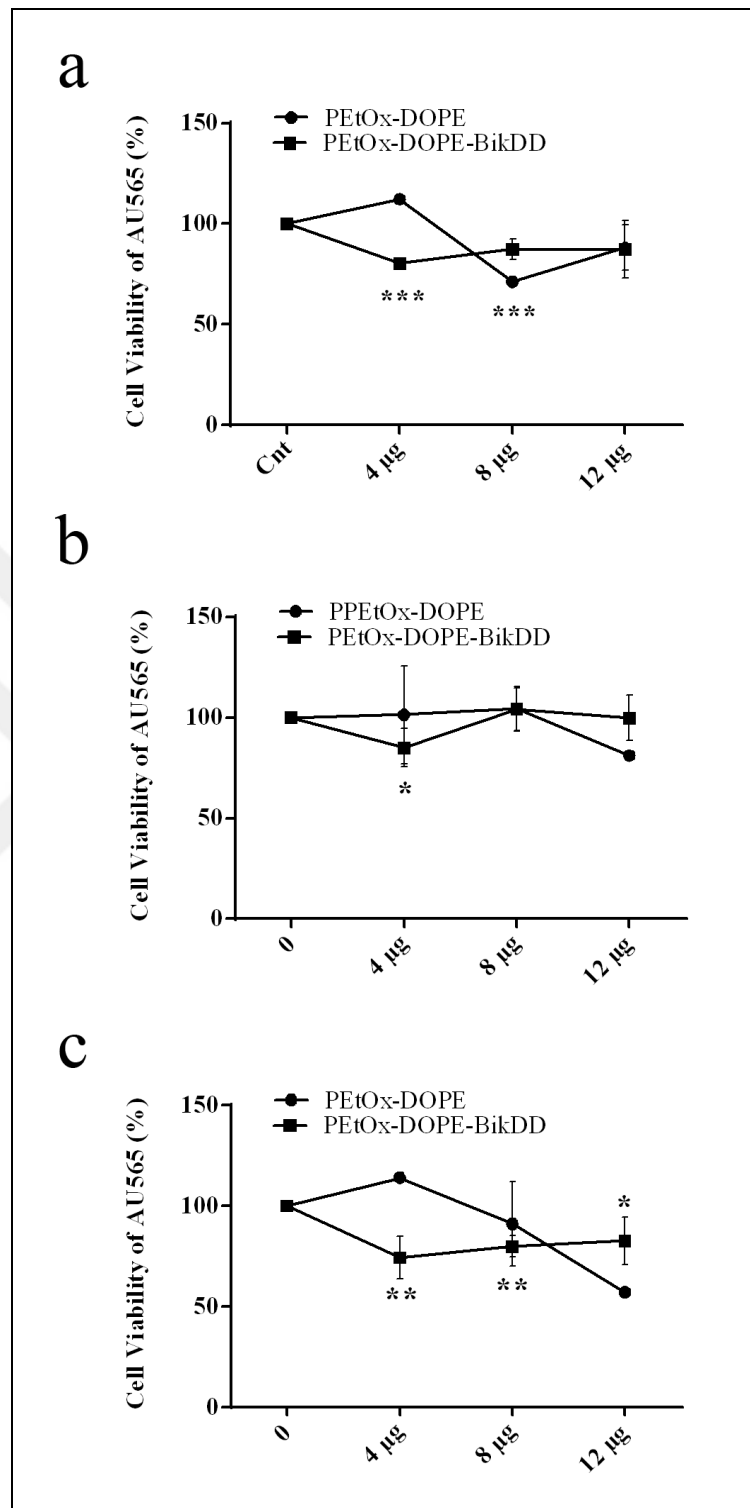


Figure 4.16. Determination of the cytotoxic effect of P18-PEtOx-DOPE-BikDD on AU565 cells. 4, 8, and 12 μ g of BikDD gene in P18-PEtOx-DOPE was to treat AU565 cells for (a) 24, (b) 48, and (c) 72 hours. At each 24 hours interval, cell viability was assessed by measuring the absorbance change by microplate reader at 450 nm. Data is mean of (n=3) \pm SD (* $P \leq 0.05$, ** $P \leq 0.01$, *** $P \leq 0.001$).

The therapeutic effect of doxorubicin loaded P18-PEtOx-DOPE liposomes on cell viability of AU565 cells were analyzed by using WST-1 assay as described in Section 3.8.2.

AU565 cells were subjected to increasing concentrations of free DOX, P18-PEtOx-DOPE-DOX, and PEtOx-DOPE liposomes for 24, 48, and 72 hours were given in Figure 4.17. The cytotoxic effect of 0.1- 10 $\mu\text{g}/\text{mL}$ of P18-PEtOx-DOPE-DOX on AU565 cells shows a dose dependent decrease with time. In comparison to (0 $\mu\text{g}/\text{mL}$) non-treated cells, there was a significant decrease in AU565 cell viability following 2.5, 5, and 10 $\mu\text{g}/\text{mL}$ of P18-PEtOx-DOPE-DOX liposome, and free DOX treatment at 24 hours (Figure 4.17a).

At 48 hours, significant decrease in cell viability of AU565 cells started from dosage of 1 $\mu\text{g}/\text{mL}$ of P18-PEtOx-DOPE-DOX liposome, and free DOX. Significant decrease in cell viability of AU565 cells was recorded as 75 percent, 81 percent, 80 percent, 87 percent, and 86 percent when treated with 1, 2.5, 5, and 10 $\mu\text{g}/\text{mL}$ of free DOX (Figure 4.17b).

After 72 hours, significant decrease in cell viability of AU565 cells was recorded as 36 percent, 65 percent, 83 percent, 99 percent, and 98 percent when treated with 0.05, 1, 2.5, 5, and 10 $\mu\text{g}/\text{mL}$ of P18-PEtOx-DOPE-DOX liposome. The effect of free DOX treatment in AU565 cells showed a significant decrease of 65 percent, 75 percent, 77 percent, 90 percent, 92 percent, 98 percent, and 99 percent when treated with 0.05, 0.1, 0.5, 1, 2.5, 5, and 10 $\mu\text{g}/\text{mL}$ of DOX (Figure 4.17c).

The therapeutic dosage to be used for *in vivo* studies was selected as 2.5 $\mu\text{g}/\text{mL}$ for P18-PEtOx-DOPE-DOX liposomes, as it was the minimal dose that showed the maximum effect.

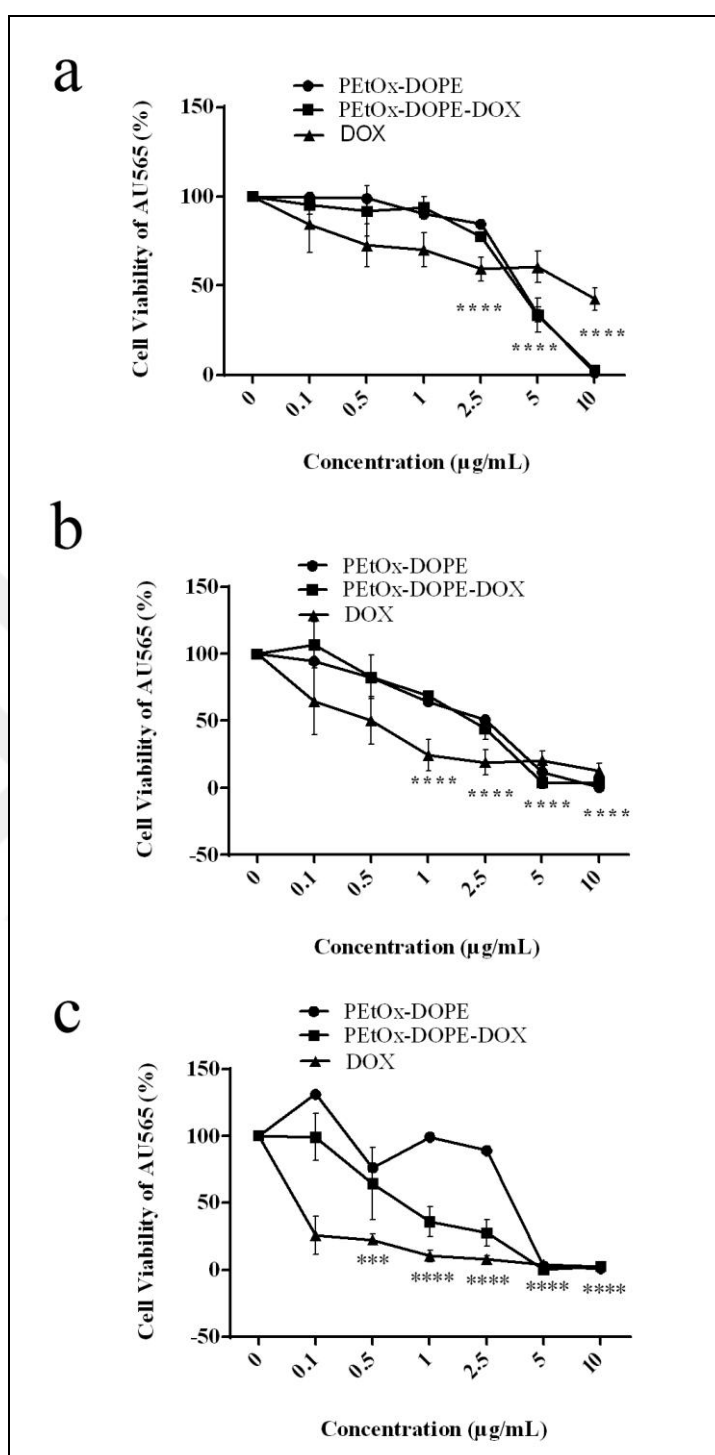


Figure 4.17. Determination of the cytotoxic effect of P18-PEtOx-DOPE-DOX on AU565 cells. 0.1 - 10 µg/mL of P18-PEtOx-DOPE-DOX were used to treat AU565 cells for (a) 24, (b) 48, and (c) 72 hours. At each 24 hours interval cell viability was assessed by measuring the absorbance change using a microplate reader at 450 nm. Data represents average of three independent experiments \pm SD (** $P \leq 0.01$, *** $P \leq 0.001$, **** $P \leq 0.0001$).

4.6.5. Bik Levels in AU565 Cells Treated with BikDD Loaded P18-Labeled PEtOx-DOPE Liposome

In order to find out the mRNA expression level of BikDD in AU565 cells transfected with P18-PEtOx-DOPE-BikDD liposomes, real time PCR was conducted as mentioned earlier in Section 3.9. Figure 4.18 shows the relative Bik/18sRNA mRNA expression levels in non-transfected (Cnt) AU565 cells, and AU565 cells transfected with 4, and 8 μg P18-PEtOx-DOPE-BikDD. AU565 cells transfected with 4 μg , and 8 μg of BikDD in P18-PEtOx-DOPE-BikDD liposomes showed a 5, and 20 fold increase in Bik gene expression when compared to the non-treated control cells (Cnt).

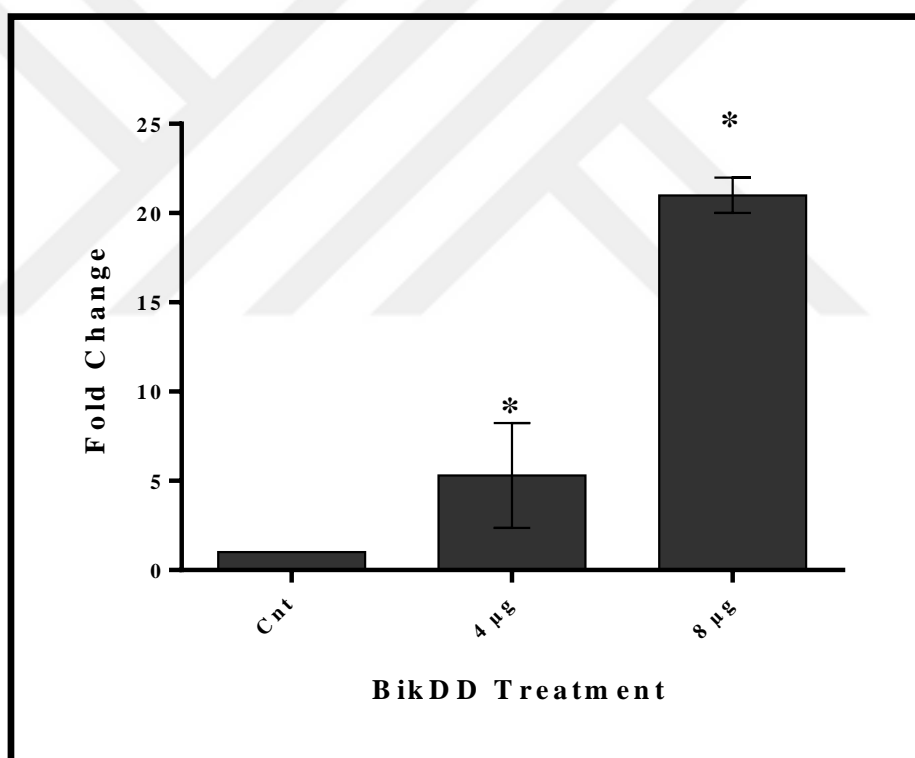


Figure 4.18. Relative Bik/18sRNA mRNA expression using qPCR for non-transfected (Cnt) and AU565 cells transfected with 4 and 8 μg of P18-PEtOx-DOPE-BikDD. Data represents mean (n=3) \pm SD (*p<0.05).

4.6.6. Effect of Doxorubicin Loaded P18-PEtOx-DOPE Liposomes on Cell Cycle

In order to find out the effect of P18-PEtOx-DOPE-DOX liposomes on cell cycle arrest, AU565 cells were treated with P18-PEtOx-DOPE liposomes, free DOX and P18-PEtOx-DOPE-DOX liposomes for 24 hours and cell cycle assay was conducted as mentioned in Section 3.10.

Figure 4.19 shows the effect of P18-PEtOx-DOPE-DOX on AU565 cells treated for 24 hours. The average proportion of G₀/G₁ phase for non-treated AU565 cells was 70 percent, and AU565 cells treated with PEtOx-DOPE liposomes, free DOX, and P18-PEtOx-DOPE-DOX liposomes was 64 percent, 61 percent, and 47 percent, respectively. The average proportion of S phase for non-treated AU565 cells was 6 percent. AU565 cells treated with PEtOx-DOPE liposomes, free DOX, and P18-PEtOx-DOPE-DOX liposomes average proportion of S phase was 12 percent, 22 percent, and 7 percent, respectively.

The population of cells in G₂/M phase was 23 percent, 17 percent, and 44 percent, after the treatment of AU565 cells with PEtOx-DOPE liposomes, free DOX, and P18-PEtOx-DOPE-DOX liposomes, respectively for 24 hours. For the control group (non-treated AU565 cells), the frequency of G₂/M cell cycle phase was found as 23 percent. The percentage of AU565 cells in G₂/M phase was induced while the percentage of cells in G₀/G₁ phase was decreased when AU565 cells were treated with P18-PEtOx-DOPE-DOX liposomes in comparison to the non-treated cells. These data indicate that P18-PEtOx-DOPE-DOX liposomes treatment arrested the cell cycle of AU565 cells in G₂/M phase at 24 hours.

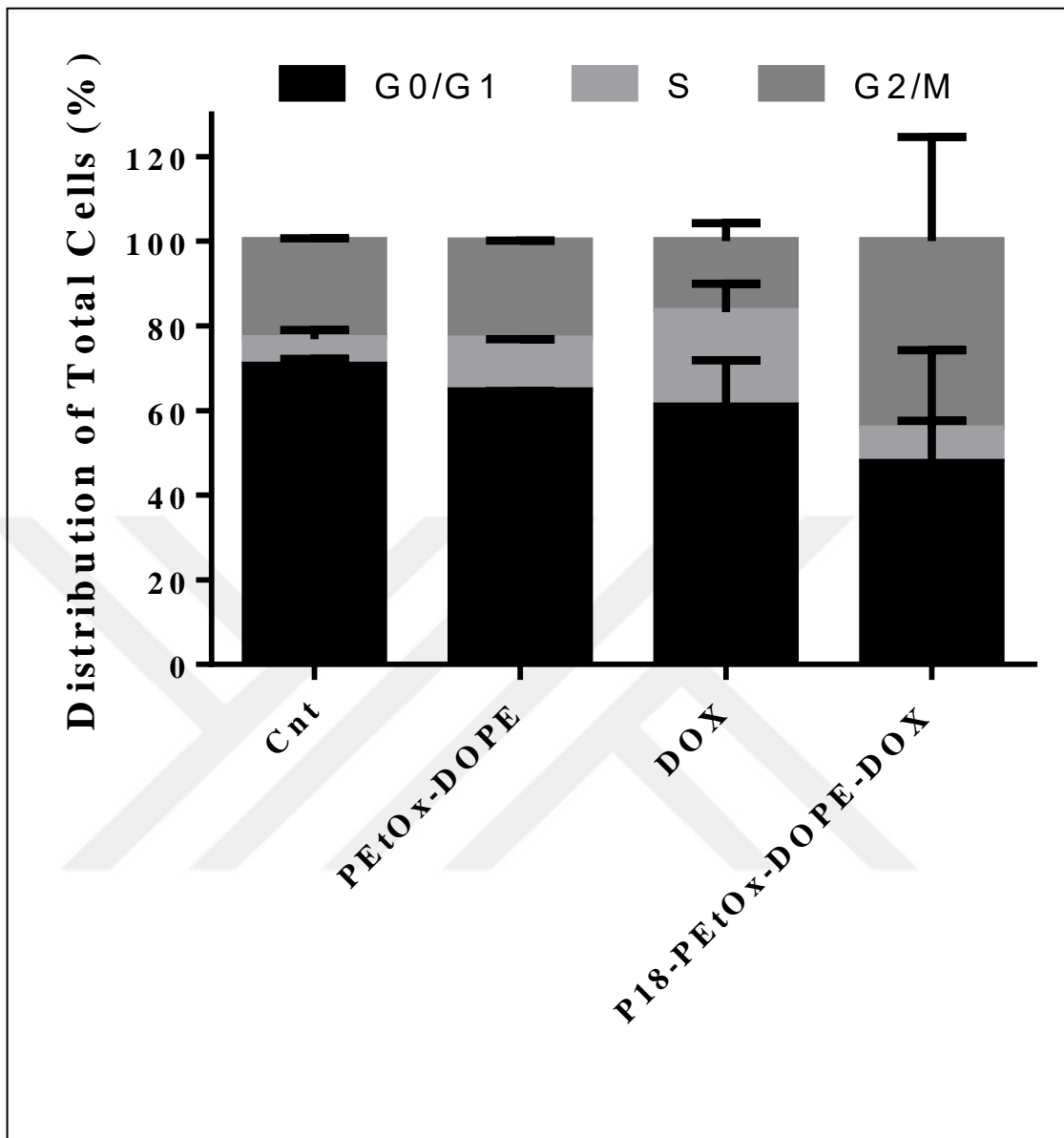


Figure 4.19. Cell cycle profiles of AU565 cells examined by flow cytometry. Non-treated AU565 cells (Cnt) and AU565 cells subjected to 2.5 $\mu\text{g}/\text{mL}$ of free DOX, empty PEtOx-DOPE liposomes, and P18-PEtOx-DOPE-DOX liposomes for 24 hours.

4.6.7. Effect of Doxorubicin Loaded P18-PEtOx-DOPE Liposomes on Cell Death

In order to analyze whether the decrease in cell viability in AU565 cells treated with P18-PEtOx-DOPE-DOX liposomes (Section 4.8.4) was due to apoptotic cell death, Annexin V-PI staining was conducted according to the procedure mentioned in Section 3.11.

Figure 4.20 shows the apoptotic response of AU565 cells to 2.5 $\mu\text{g}/\text{mL}$ doxorubicin loaded P18-PEtOx-DOPE liposomes at 48 hours. An average of 29 percent of Annexin-V stained AU565 cells were detected after treatment with empty PEtOx-DOPE liposomes for 48 hours. 11 percent of annexin V- positive cells were identified as the early apoptotic cells while 18 percent were found to be in late apoptosis. An average of 49 percent of Annexin-V stained AU565 cells were detected after treatment with P18-PEtOx-DOPE-DOX liposomes for 48 hours. 3 percent of annexin V- positive cells were identified as the early apoptotic cells while 46 percent were found to be in late apoptosis. Similarly, an average of 58 percent of Annexin-V stained AU565 cells were recorded after treatment of free DOX for 48 hours, with a 9 percent in early apoptosis and 49 percent in late apoptosis.

Figure 4.21 shows the apoptotic cell death for AU565 cells treated with doxorubicin loaded P18-PEtOx-DOPE liposomes for 72 hours. Empty PEtOx-DOPE liposomes treatment of AU565 cells resulted in 22 percent early apoptosis and 19 percent late apoptosis at 72 hours. P18-PEtOx-DOPE-DOX liposomes treatment of AU565 cells resulted in 6 percent early apoptosis and 69 percent late apoptosis at 72 hours, thus an average of 75 percent of Annexin-V stained AU565 cells were detected. Free DOX treatment of AU565 cells resulted in an average of 80 percent of Annexin-V positive stained cells which showed a 30 percent early apoptosis and 46 percent were late apoptosis features.

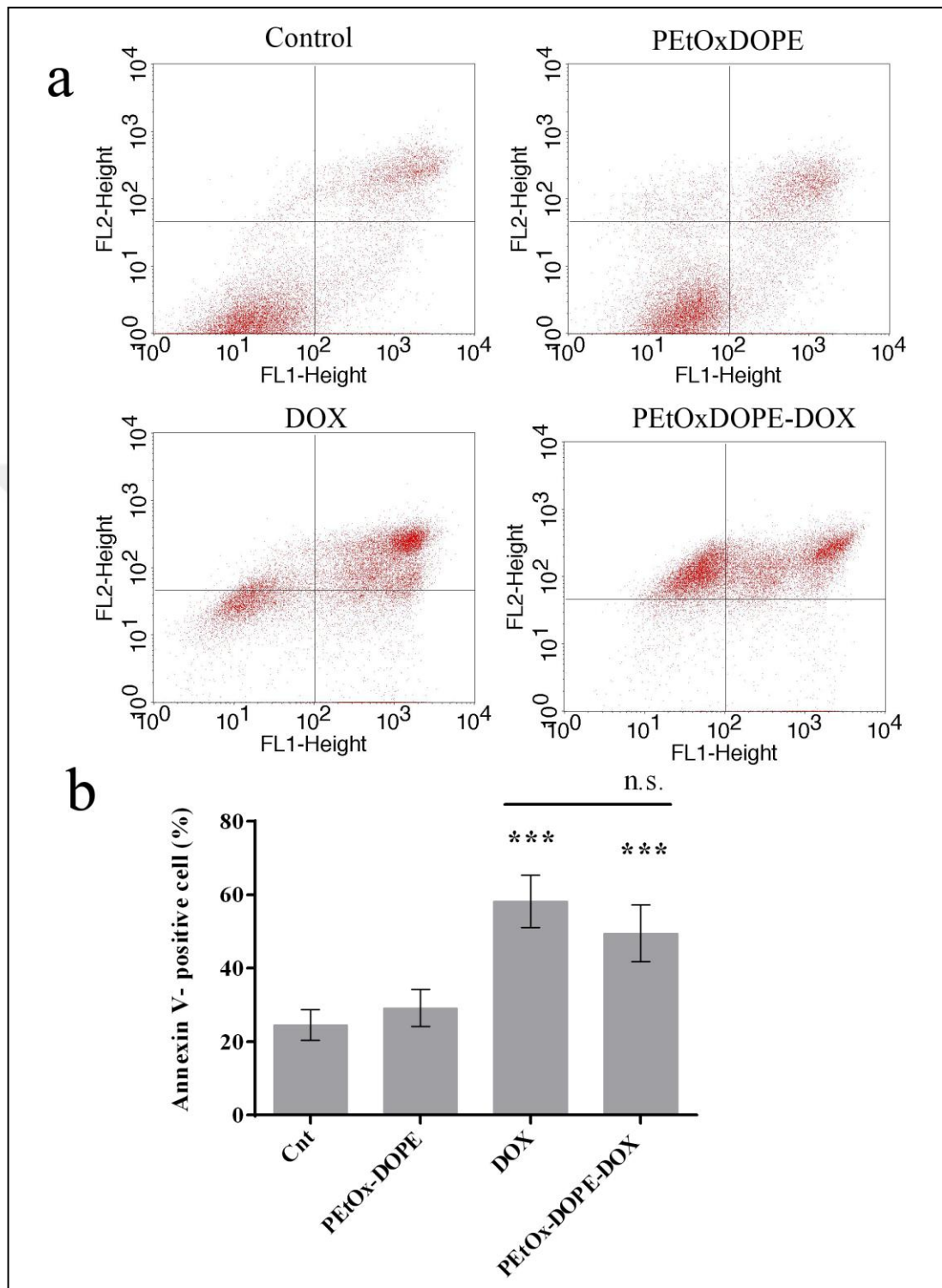


Figure 4.20. Effect of P18-PEtOx-DOPE-DOX liposomes on AU565 cell death at 48 hours. Annexin V/PI staining was used to analyze the cell death of AU565 cells subjected to 2.5 $\mu\text{g/mL}$ of DOX loaded P18-PEtOx-DOPE liposomes or free DOX. Representative (a) Histograms and (b) Graphical representation of percentage for cell death were shown.

Data point represents the average \pm SD (n=3) (**p<0.01).

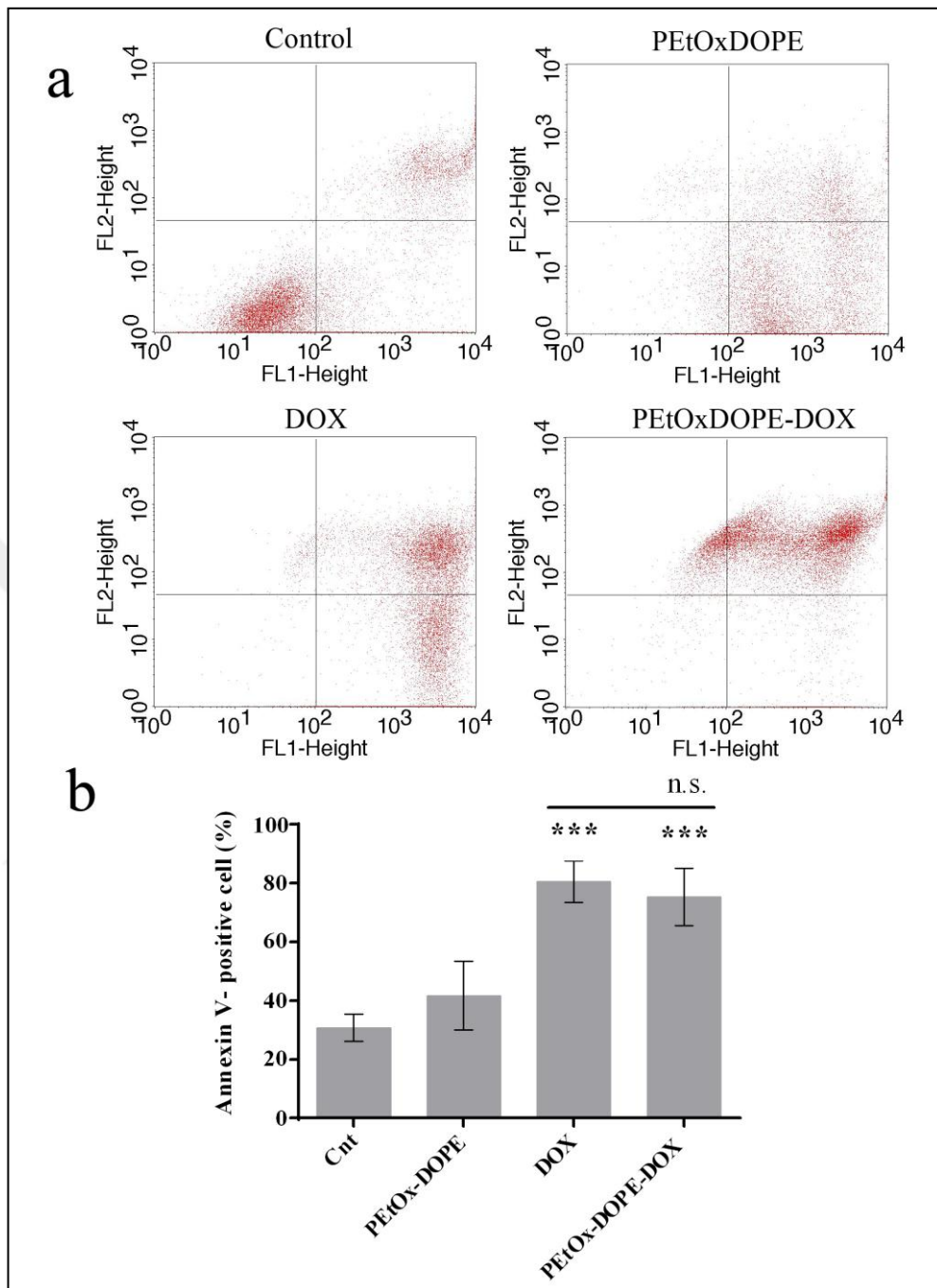


Figure 4.21. Effect of P18-PEtOx-DOPE-DOX liposomes on AU565 cell death at 72 hours. Annexin V/PI staining was used to analyze the cell death of AU565 cells subjected to 2.5 $\mu\text{g}/\text{mL}$ of DOX loaded P18-PEtOx-DOPE liposomes or free DOX. Representative (a) Histograms and (b) Graphical representation of percentage for cell death were shown.

Data point represents the average \pm SD (n=3) (**p<0.01, ***p<0.001).

4.7. POLYMERSOME DELIVERY OF BIKDD OR DOXORUBICIN TO AU565 CELLS

4.7.1. Analysis of Cellular Cytotoxicity of PEtOx-*b*-PLA Copolymer and Polymersome

In order to determine the cytotoxic effect of PEtOx-*b*-PLA copolymer and polymersome formulations, HUVEC, HEK293, MSC, and MCF10A cells were subjected to 25, 50, 75, 100, and 125 $\mu\text{g}/\text{mL}$ concentrations of PEtOx-*b*-PLA copolymer and polymersome for 24, 48, and 72 hours. Cytotoxicity was determined by WST-1 assay following manufacturer's protocols as described in Section 3.8.1. Absorbance value of control cells (DMSO for copolymer and non-treated for liposome formulations) were set as 100 percent, and cell viability percentage was calculated accordingly.

The cell viability of HUVEC cells after treatment with PEtOx-*b*-PLA copolymer and polymersome formulation were shown in Figure 4.22. PEtOx-*b*-PLA copolymer did not cause any significant cytotoxicity (only up to 10 percent) in HUVEC cells. However, HUVEC cells treated with the highest concentration of 125 $\mu\text{g}/\text{mL}$ PEtOx-*b*-PLA copolymer showed a significant toxicity by 25 percent at 48 and 72 hours (Figure 4.22a). PEtOx-*b*-PLA polymersome lead to an insignificant increase in the proliferation of HUVEC cell line with a percentage of 7 to 15 percent at doses until 100 $\mu\text{g}/\text{mL}$ for 24 and 48 hours except for cells treated with 125 $\mu\text{g}/\text{mL}$ of PEtOx-*b*-PLA copolymer which showed a significant toxicity of 15 percent. This decrease was however pulled back to the control levels at the end of the 72 hour-time point (Figure 4.22b).

PEtOx-*b*-PLA copolymer led to slight proliferation of HEK293 cells with a percentage of 2 to 7 percent at concentrations of 25-100 $\mu\text{g}/\text{mL}$ for all time points while no significant toxicity was detected at 125 $\mu\text{g}/\text{mL}$ concentration. Similarly, an increase in cell proliferation with a percentage of 4 percent to 19 percent was detected for 48 hours when HEK293 cells were treated with PEtOx-*b*-PLA polymersome. However, this increase was pulled back to control levels for 72 hours (Figure 4.23a-b).

PEtOx-*b*-PLA copolymer also led to a slight cell proliferation (9 to 12 percent) at 24 hours, (4 to 7 percent) at 48 hours in MSCs. Treatment of MSCs with PEtOx-*b*-PLA

polymersomes showed similar response to treatment with its copolymer, cell proliferation rates ranged from 3-16 percent at all time points (Figure 4.24a-b). In other words, PEtOx-*b*-PLA copolymer and polymersome showed no toxicity to MSCs.

No significant toxicity (a percentage of 7 to 9 percent) of MCF10A cell was detected at all concentrations of PEtOx-*b*-PLA copolymer and polymersomes at 24 hours. At 48 hours, slight proliferation of MCF10A cells with a percentage of 2- 13 percent was evident for 25-100 $\mu\text{g/mL}$ PEtOx-*b*-PLA copolymer and polymersomes-treatments. However, at 72 hours the cell viability values were comparable with the control levels for MCF10A cells (Figure 4.25a-b). Overall, the results revealed no significant toxicity of PEtOx-*b*-PLA copolymer and polymersomes towards human normal breast epithelial MCF10A cell line.

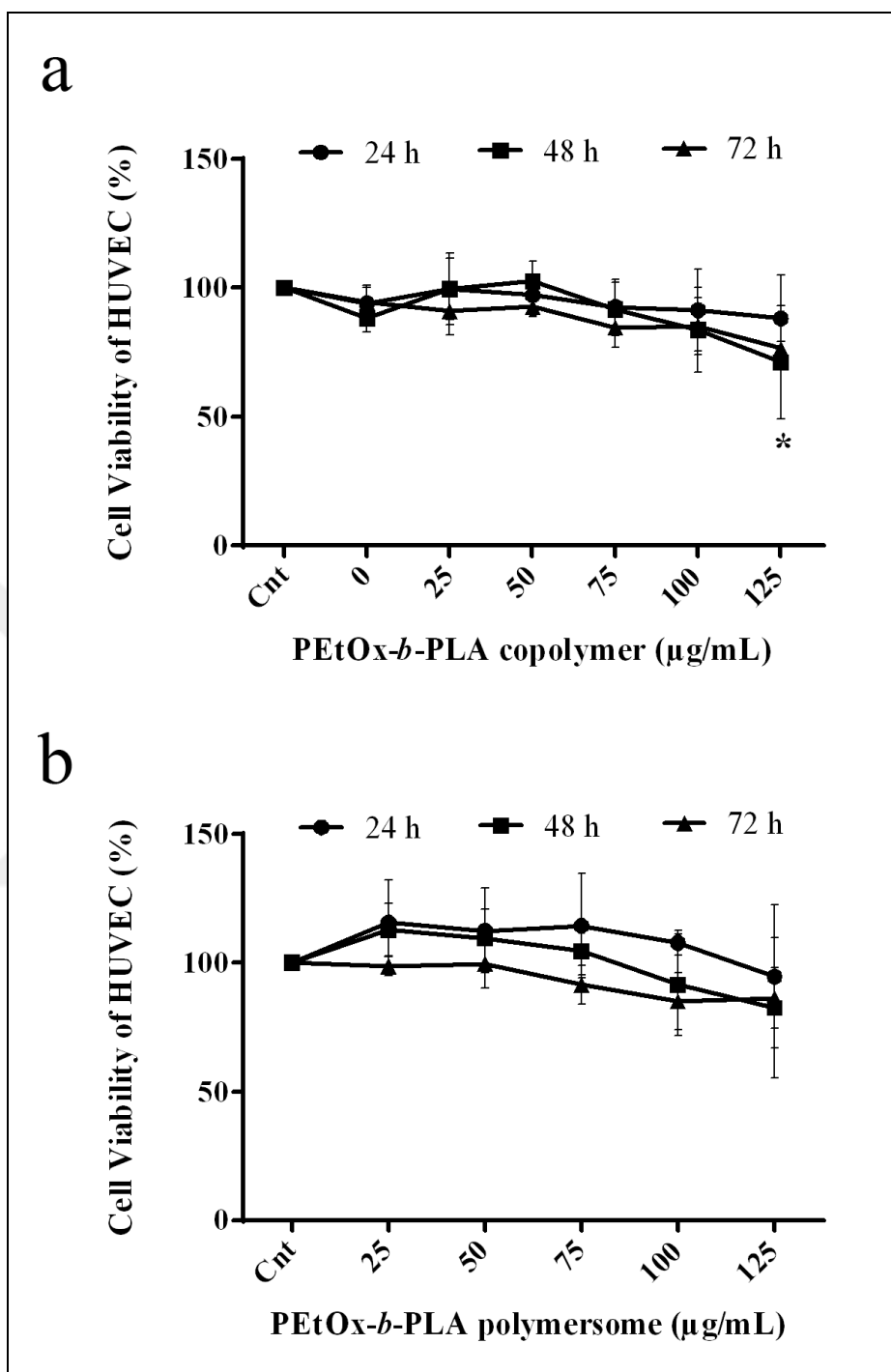


Figure 4.22. Effect of PEtOx-*b*-PLA (a) Copolymer and (b) Polymersome on HUVEC cell line viability. 25- 125 $\mu\text{g/mL}$ of PEtOx-*b*-PLA copolymer and polymersome were used to AU565 cells for 24, 48, and 72 hours. At each 24 hours interval cell viability was assessed by measuring the absorbance change using a microplate reader at 450 nm.

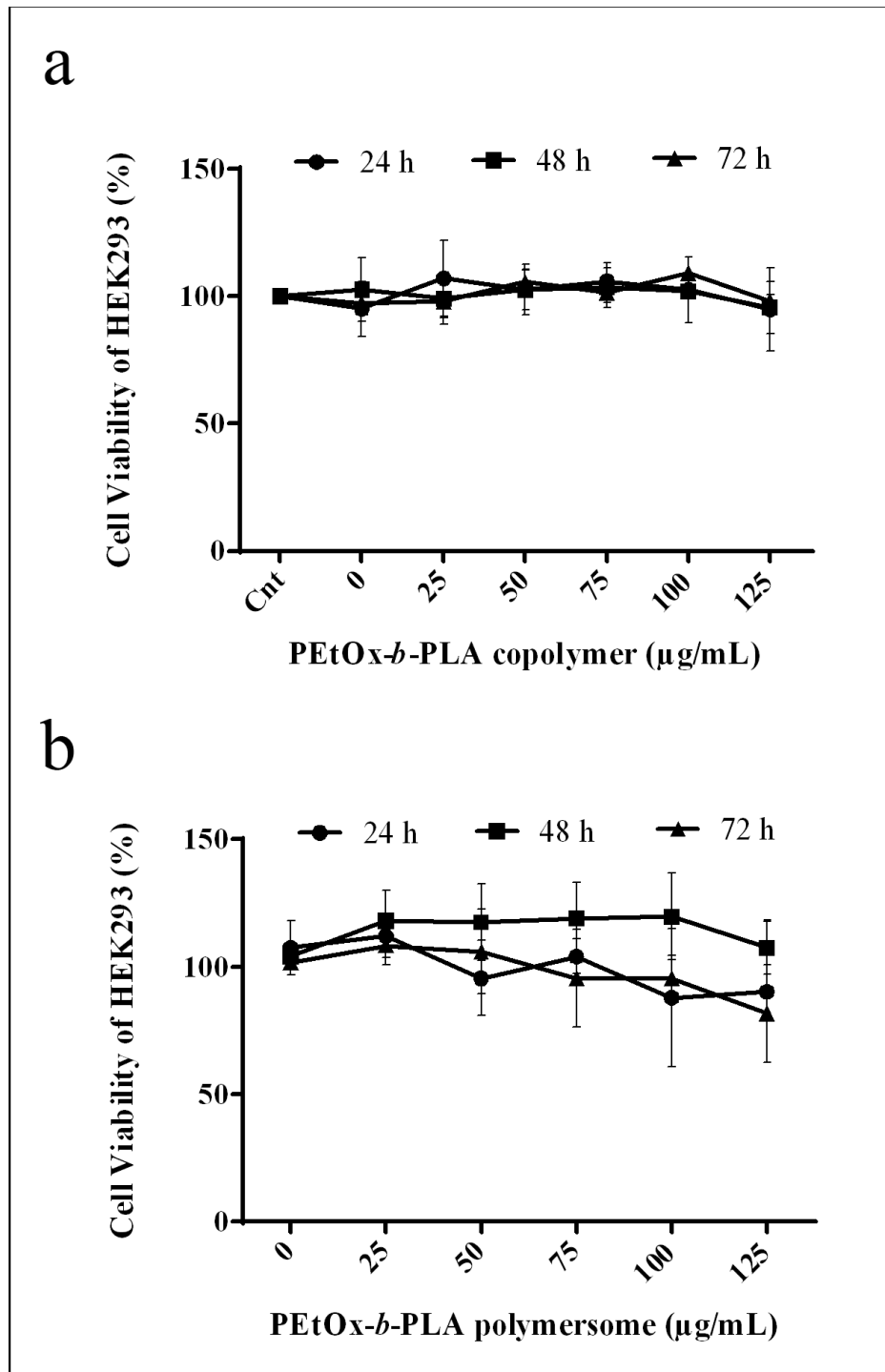


Figure 4.23. Effect of PEtOx-*b*-PLA (a) Copolymer and (b) Polymersome on HEK293 cell line viability. 25- 125 $\mu\text{g/mL}$ of PEtOx-*b*-PLA copolymer and polymersome treating AU565 cells for 24, 48, and 72 hours. At each 24 hours interval cell viability was assessed by measuring the absorbance change using a microplate reader at 450 nm.

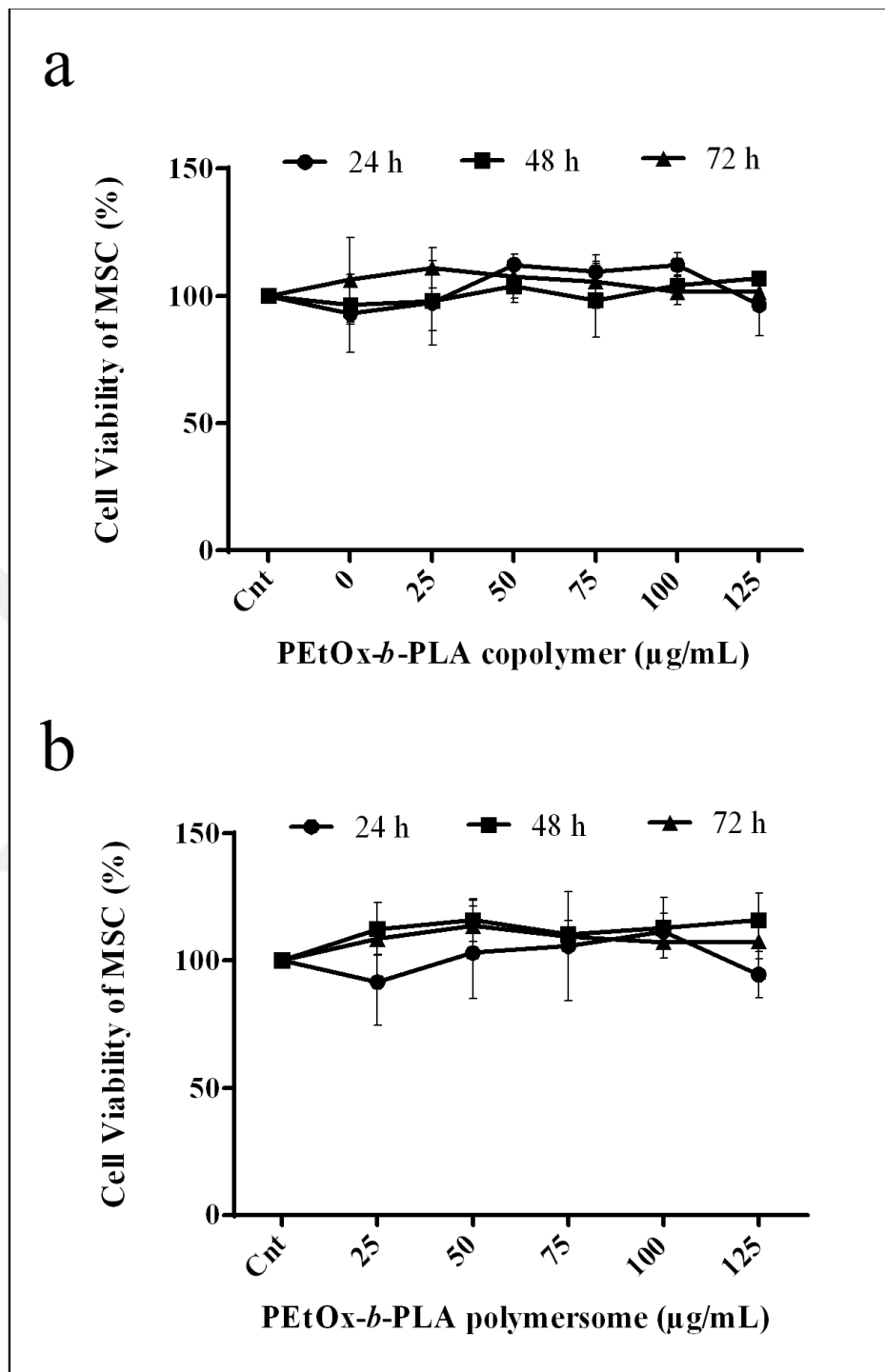


Figure 4.24. Effect of PEtOx-*b*-PLA (a) Copolymer and (b) Polymersome on MSC cell line viability. AU565 cells were treated with 25- 125 $\mu\text{g/mL}$ of PEtOx-*b*-PLA copolymer and polymersome were used in treatment of AU565 cells for 24, 48, and 72 hours. At each 24 hours interval cell viability was assessed by measuring the absorbance change using a microplate reader at 450 nm.

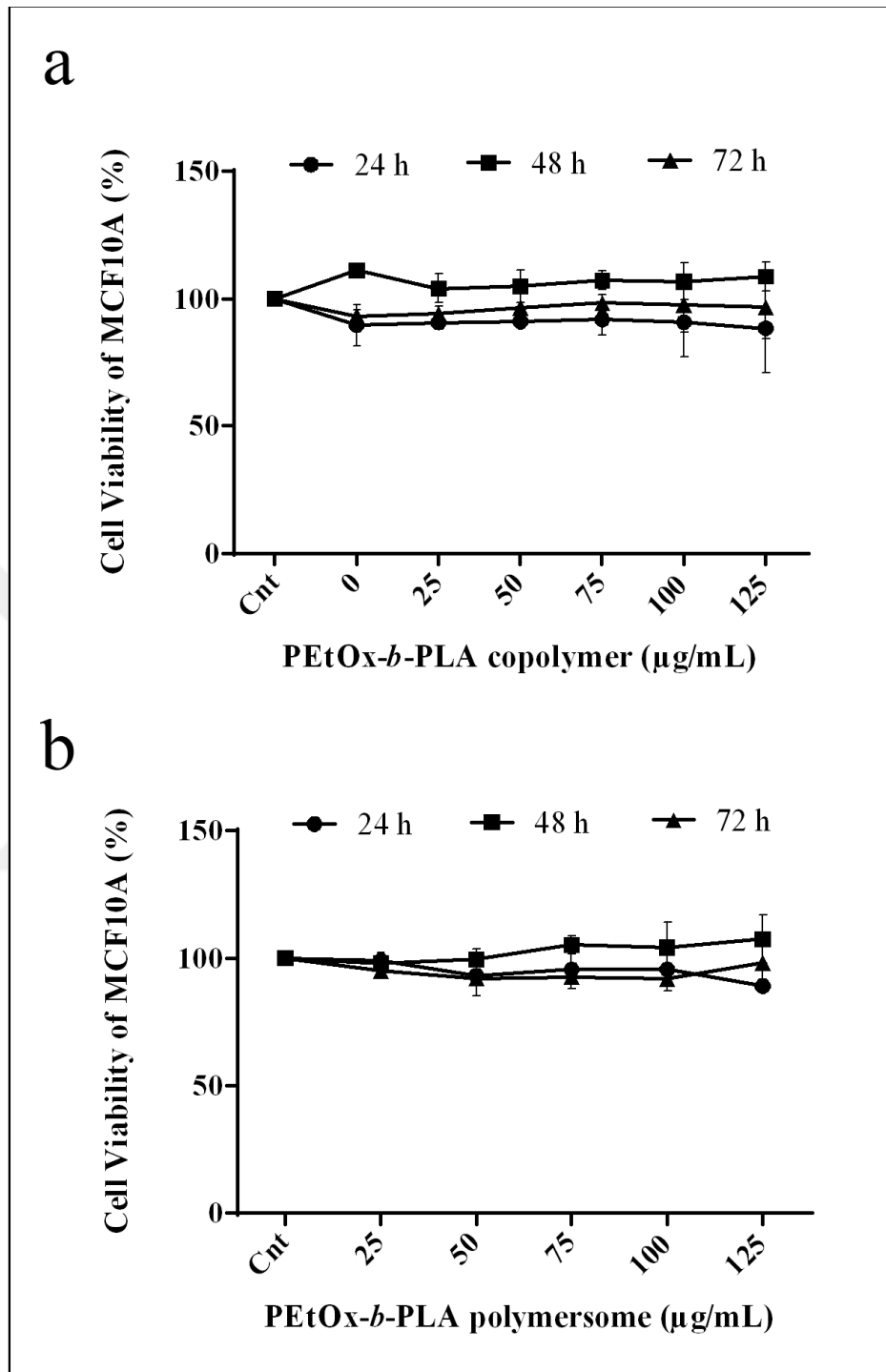


Figure 4.25. Effect of PEtOx-*b*-PLA (a) Copolymer and (b) Polymersome on MCF10A cell line viability. PEtOx-*b*-PLA copolymer and polymersome at 25- 125 µg/mL were used in treatment of AU565 cells for 24, 48, and 72 hours. At each 24 hours interval cell viability was assessed by measuring the absorbance change using a microplate reader at 450 nm.

4.7.2. Binding Affinity of P18-Labeled PEOx-*b*-PLA Polymersome to the Breast Cancer and Control Cell Lines

In order to answer the question whether peptide 18 labeled PEOx-*b*-PLA polymersome conjugates showed a specific binding towards breast cancer cells; the binding affinity of peptide 18 labeled PEOx-*b*-PLA polymersome conjugates to breast cancer AU565 cells in comparison to normal breast epithelial MCF10A cells were analyzed. AU565 and MCF10A cells were seeded on 6 well plate with a density of 3×10^5 cells/well, and 2.5×10^5 cells/well, respectively. P18-PEOx-*b*-PLA polymersomes loaded with fluorescein dye were used to treat AU565 and MCF10A cells for 4 hours at 37°C as mentioned in Section 3.5.2.

During *in vitro* binding affinity studies, flow cytometry analysis was conducted in order to monitor the uptake of P18-PEOx-*b*-PLA polymersomes conjugates. The binding affinity of P18-PEOx-*b*-PLA polymersomes to MCF10A, and AU565 cells assessed as 7.24 percent and 58.6 percent, respectively (Figure 4.26) suggesting that P18-PEOx-*b*-PLA polymersome exhibited high affinity and specific binding to breast cancer AU565 cells.

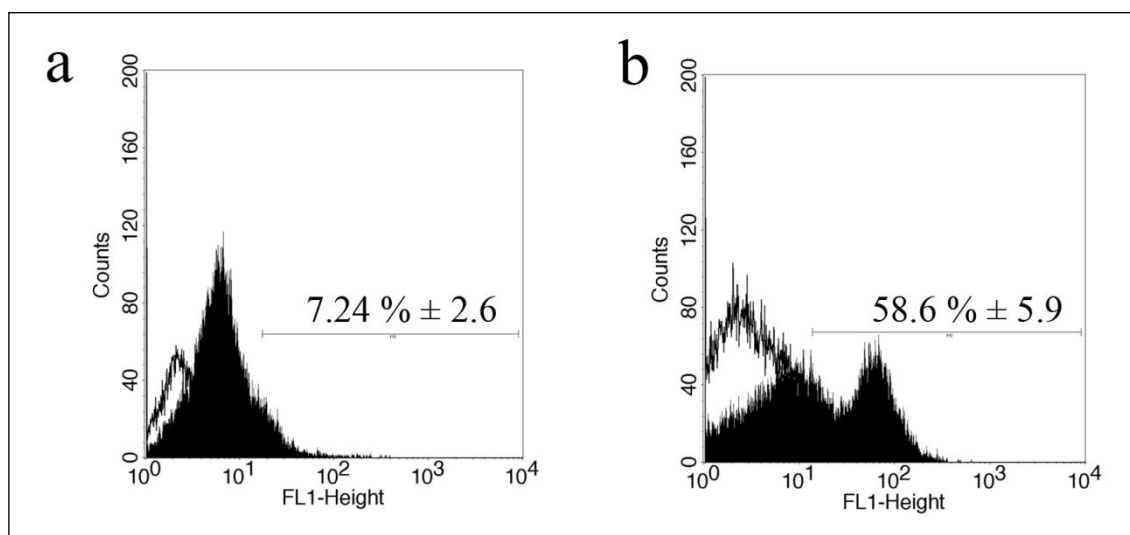


Figure 4.26. The representative histograms showing the binding affinity of P18-PEOx-*b*-PLA polymersome on (a) MCF10A and (b) AU565 cell line. Fluorescein labeled P18-PEOx-*b*-PLA polymersomes were used to treat cells for 4 hours at 37°C.

4.7.3. Cellular Uptake of P18-Labeled PEOx-*b*-PLA Polymersome to the Breast Cancer and Control Cell Lines

Confocal microscopy imaging was employed to monitor cellular uptake of P18-PEtOx-*b*-PLA polymersome to control MCF10A and breast cancer AU565. AU565 and MCF10A cells were seeded to 8-well chamber slides and allowed to attached for 24 hours prior to 4 hour-treatment as mentioned before (Section 3.6).

The images of confocal microscopy used to analyze the cellular uptake of samples were given in Figure 4.27. The nucleus of cells were appeared in blue (DAPI staining) while P18-PEtOx-*b*-PLA polymersome bound cells were stained in green. In agreement with the flow cytometry results, confocal microscopy images indicated that the incubation of AU565 cells with P18-PEtOx-*b*-PLA polymersome resulted in fluorescent staining of these cells while the incubation of MCF10A cells with the construct did not lead to the fluorescein labeling of MCF10A cells.

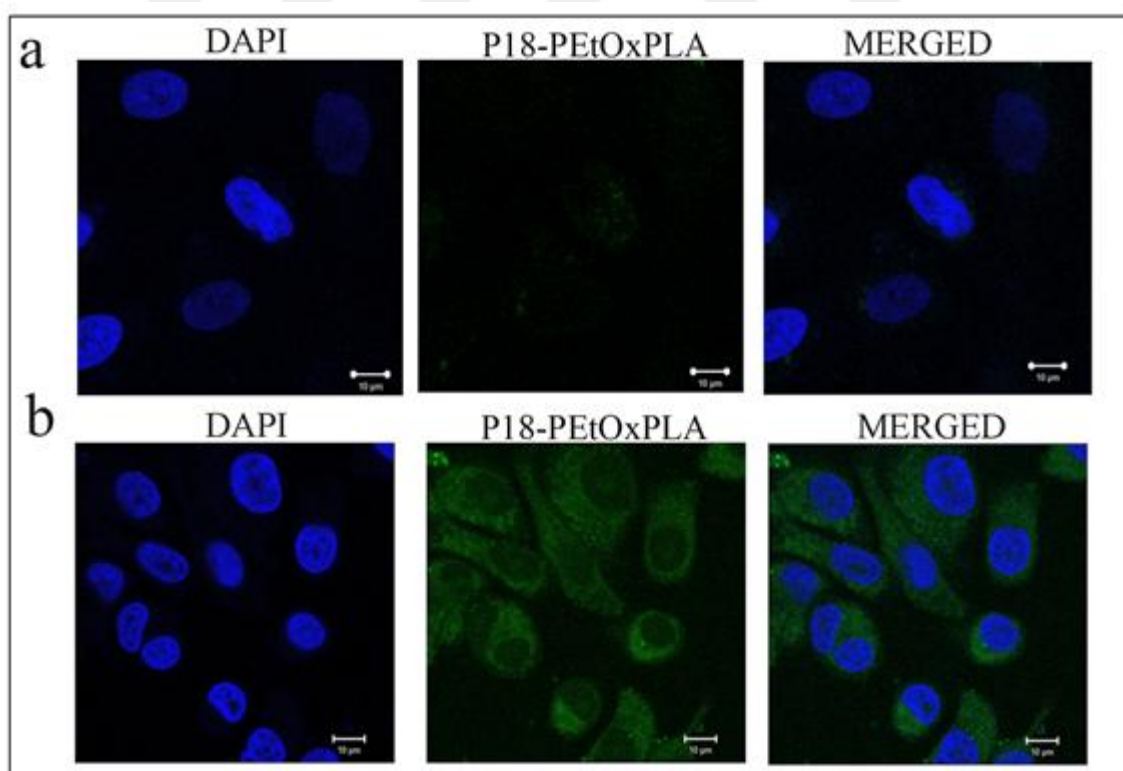


Figure 4.27. P18-PEtOx-*b*-PLA polymersome binding affinity on (a) MCF10A and (b) AU565 cell lines by confocal microscopy. Images were taken at 63 x objectives and scale bar represents 10 µm.

4.7.4. Cell Viability of AU565 Cells Treated with BikDD or Doxorubicin Loaded P18-Labeled PEtOx-*b*-PLA Polymersome

In order to find out the therapeutic effect of proapoptotic BikDD gene on the cell viability of AU565 cells, cells were subjected to increasing concentrations of BikDD loaded targeted (P18) and empty PEtOx-*b*-PLA polymersomes for 24, 48, and 72 hours. Cell viability and proliferation of AU565 cells was conducted using WST-1 as described previously (Section 3.8.2).

Figure 4.28 demonstrated the effects of 2, 5, and 10 μg P18-PEtOx-*b*-PLA-BikDD and un loaded empty PEtOx-*b*-PLA polymersome on the proliferative ability of AU565 cells at 72 hours post-treatment. The P18-PEtOx-*b*-PLA-BikDD treatment resulted in a dose dependent decrease in AU565 cell viability at 24 hours. In comparison to the non-treated (Cnt) AU565 cells, there was a 2 percent ($p < 0.05$), 7 percent ($p < 0.05$), and 18 percent ($p > 0.05$) decrease in cell viability of AU565 cells at 2, 5, and 10 μg of BikDD in P18-PEtOx-*b*-PLA-BikDD, respectively. A proliferative effect of 5 percent, 13 percent, and 14 percent ($p < 0.05$) in cell viability was detected at 2, 5, and 10 μg of empty PEtOx-*b*-PLA polymersome treatment, respectively (Figure 4.28a).

AU565 cells treated with 5 μg of P18-PEtOx-*b*-PLA-BikDD showed a significant decrease in cell viability with 28 percent at 48 hours, while empty polymersome had no significant effect (Figure 4.28b).

There was a decrease of nearly 11 percent in cell viability of AU565 cells at 2, and 10 μg of P18-PEtOx-*b*-PLA-BikDD at 72 hours. However, there was also a 6 percent, and 18 percent insignificant decrease in the cell viability of AU565 cells at 2, and 10 μg of empty PEtOx-*b*-PLA polymersome at 72 hours (Figure 4.28c).

In conclusion, the highest therapeutic effect was observed in AU565 cells when treated with 5 μg of P18-PEtOx-*b*-PLA-BikDD at 48 hours, thus 5 μg of P18-PEtOx-*b*-PLA-BikDD was selected to be used for *in vivo* studies.

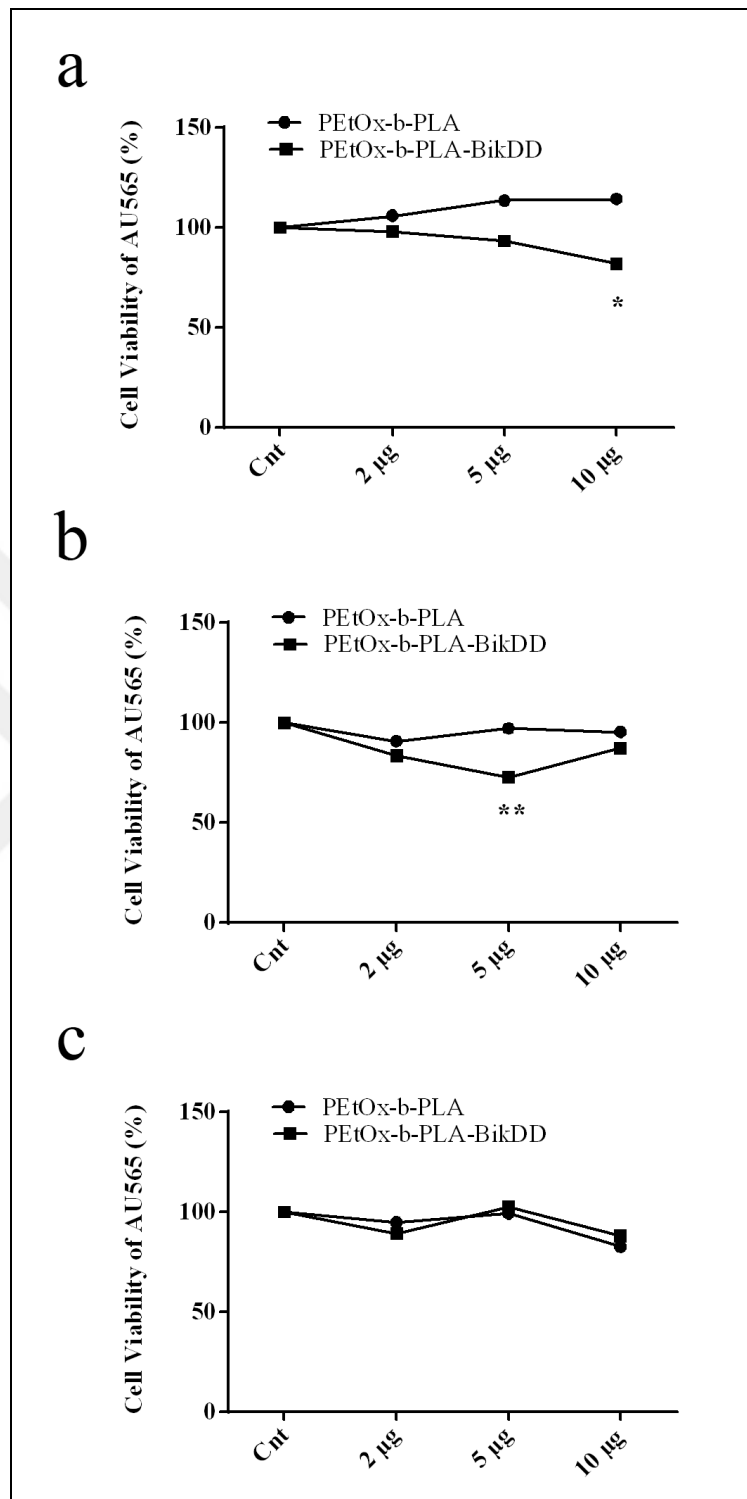


Figure 4.28. Determination of the cytotoxic effect of P18-PEtOx-b-PLA-BikDD on AU565 cells. 2, 5, and 10 µg of BikDD gene in P18-PEtOx-b-PLA was used to treat AU565 cells for (a) 24, (b) 48, and (c) 72 hours. At each 24 hour time interval, cell viability was assessed by measuring the absorbance change by microplate reader at 450 nm. Data is the mean of (n=3) ± SD (* P ≤ 0.05, ** P ≤ 0.01, *** P ≤ 0.001).

In order to determine the cytotoxic effect of P18-PEtOx-*b*-PLA-DOX on cell viability of AU565 cells, cells were subjected to increasing concentrations of P18-PEtOx-*b*-PLA-DOX for 24, 48, and 72 hours. Dose-dependent effect on AU565 cell viability and proliferation was determined using WST-1 assay as mentioned earlier (Section 3.8.2). Cell viability of AU565 cells treated with P18-PEtOx-*b*-PLA-DOX, empty PEtOx-*b*-PLA polymersome, and free DOX at post-treatment were shown in Figure 4.29.

At 0.05- 10 $\mu\text{g/mL}$ concentrations, P18-PEtOx-*b*-PLA-DOX was led to a gradual decrease in AU565 cells viability. In comparison to control cells, there was a significant 75 percent, 70 percent, 65 percent, 45 percent, 20 percent, 40 percent, and 10 percent decrease after 0.05, 0.1, 0.5, 1, 2.5, 5, and 10 $\mu\text{g/mL}$ treatment of P18-PEtOx-*b*-PLA-DOX for 24 hours. Treatment of AU565 cells with free DOX for 24 hours showed a parallel decrease in the cell viability (Figure 4.29a).

At 48 hours a significant decrease in cell viability of AU565 cells was evident for the concentrations between 0.05 $\mu\text{g/mL}$ to 10 $\mu\text{g/mL}$ of P18-PEtOx-*b*-PLA-DOX, which was found to be comparable to the free DOX treatment (Figure 4.29b). For the 72 hours treatment, the significant decrease in cell viability of AU565 cells was recorded as 36 percent, 65 percent, 83 percent, 99 percent, and 98 percent at 0.05, 1, 2.5, 5, and 10 $\mu\text{g/mL}$ of P18-PEtOx-*b*-PLA-DOX. Similarly free DOX treatment for 72 hours resulted in dose dependent significant decrease in AU565 cell viability with 65 percent, 75 percent, 78 percent, 90 percent, 92 percent, 96 percent and 98 percent at 0.05, 0.1, 0.5, 1, 2.5, 5, and 10 $\mu\text{g/mL}$ (Figure 4.29c).

The therapeutic dosage to be used for cell death studies was selected as 1 $\mu\text{g/mL}$ for P18-PEtOx-*b*-PLA-DOX polymersome, as it was the minimal dose that showed the maximum effect.

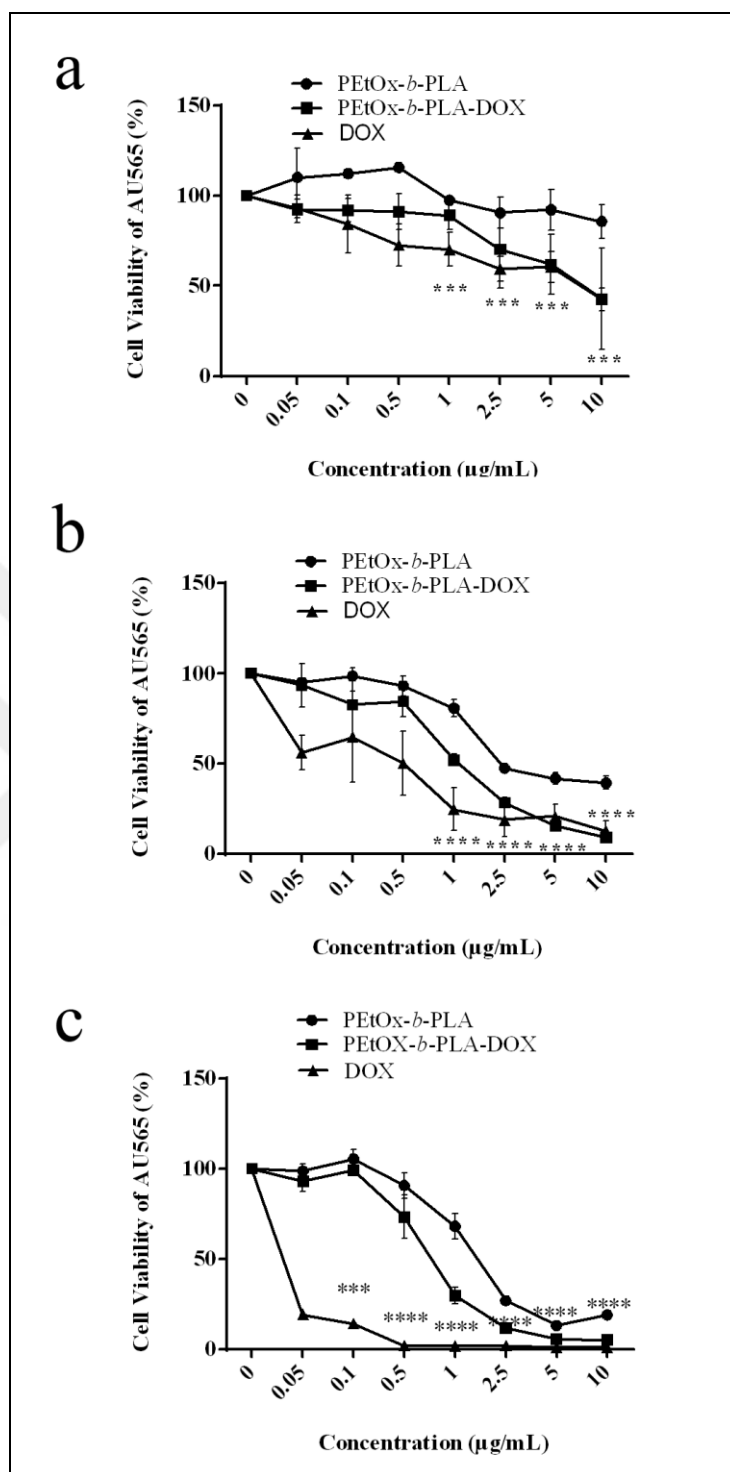


Figure 4.29. Determination of the cytotoxic effect of P18-PEtOx-*b*-PLA-DOX polymersome on AU565 cells. 0.05- 10 µg/mL of P18-PEtOx-*b*-PLA-DOX polymersome treatment along with free DOX was done for (a) 24, (b) 48, and (c) 72 hours. At each 24 hour intervals cell viability was assessed by measuring the absorbance change using a microplate reader at 450 nm. Data represents the mean (n=3) ± SD (***) $P \leq 0.001$, ****) $P \leq 0.0001$).

4.7.5. Bik Levels in AU565 Cells Treated with BikDD Loaded P18-Labeled PEtOx-*b*-PLA Polymersomes

In order to find out the mRNA expression level of BikDD in AU565 cells transfected with P18-PEtOx-*b*-PLA-BikDD polymersome, real time PCR was conducted as mentioned earlier (Section 3.9). Figure 4.30 shows the relative Bik/18sRNA mRNA expression levels in non-transfected (Cnt) AU565 cells, and AU565 cells transfected with 5 μ g P18-PEtOx-*b*-PLA-BikDD polymersomes. AU565 cells transfected with 5 μ g of BikDD in P18-PEtOx-*b*-PLA-BikDD polymersomes showed a 5.5 fold increase in Bik gene expression when compared to the non-transfected control cells (Cnt).

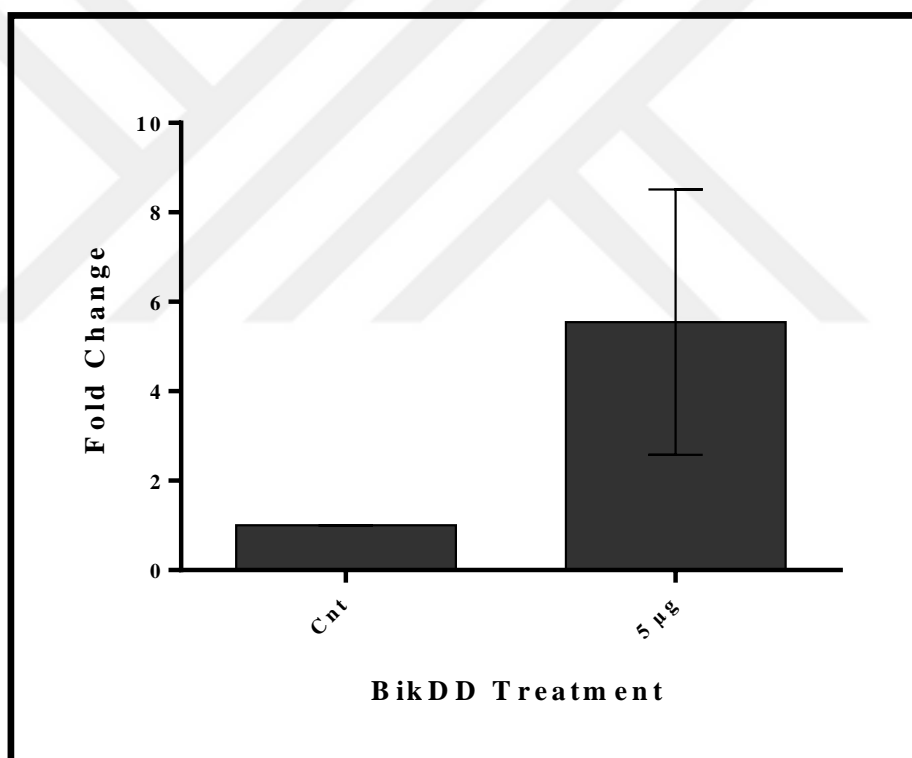


Figure 4.30. Relative Bik/18sRNA mRNA expression for non-transfected (Cnt) and AU565 cells transfected with P18-PEtOx-*b*-PLA-BikDD using qPCR. Data represents mean (n=3) \pm SD (*p<0.05).

4.7.6. Effect of Doxorubicin Loaded P18-Labeled PEtOx-*b*-PLA Polymersome on Cell Cycle

In order to find out the effect of P18-PEtOx-*b*-PLA-DOX polymersomes on cell cycle arrest, AU565 cells were treated with 1 $\mu\text{g}/\text{mL}$ of PEtOx-*b*-PLA polymersomes, free DOX and P18-PEtOx-*b*-PLA-DOX polymersomes. Cell cycle assay was conducted as mentioned in Section 3.10.

Figure 4.31 shows the effect of P18-PEtOx-*b*-PLA-DOX polymersomes on AU565 cells treated for 24 hours. The average proportion of G0/G1 phase for non-treated AU565 cells was 70 percent, and AU565 cells treated with PEtOx-*b*-PLA polymersomes, free DOX, and P18-PEtOx-*b*-PLA-DOX polymersomes was 67 percent, 69 percent, and 52 percent, respectively. The average proportion of S phase for non-treated AU565 cells was 6 percent. AU565 cells treated with PEtOx-*b*-PLA polymersomes, free DOX, and P18-PEtOx-*b*-PLA-DOX polymersomes average proportion of S phase was 12 percent, 19 percent, and 11 percent, respectively. The results of proportion of G2/M phase was 20 percent, 12 percent, and 37 percent, after treatment of AU565 cells with PEtOx-*b*-PLA polymersomes, free DOX, and P18-PEtOx-*b*-PLA-DOX polymersomes, respectively for 24 hours. For the control group (non-treated AU565 cells), the frequency of G2/M cell cycle phase was found as 23 percent.

The population of AU565 cells in G2/M phase was induced while the percentage of cells in G0/G1 phase was decreased when AU565 cells were treated with P18-PEtOx-*b*-PLA-DOX polymersomes in comparison to the non-treated cells. These data indicate that P18-PEtOx-*b*-PLA-DOX polymersomes treatment arrested the cell cycle of AU565 cells in G2/M phase at 24 hours.

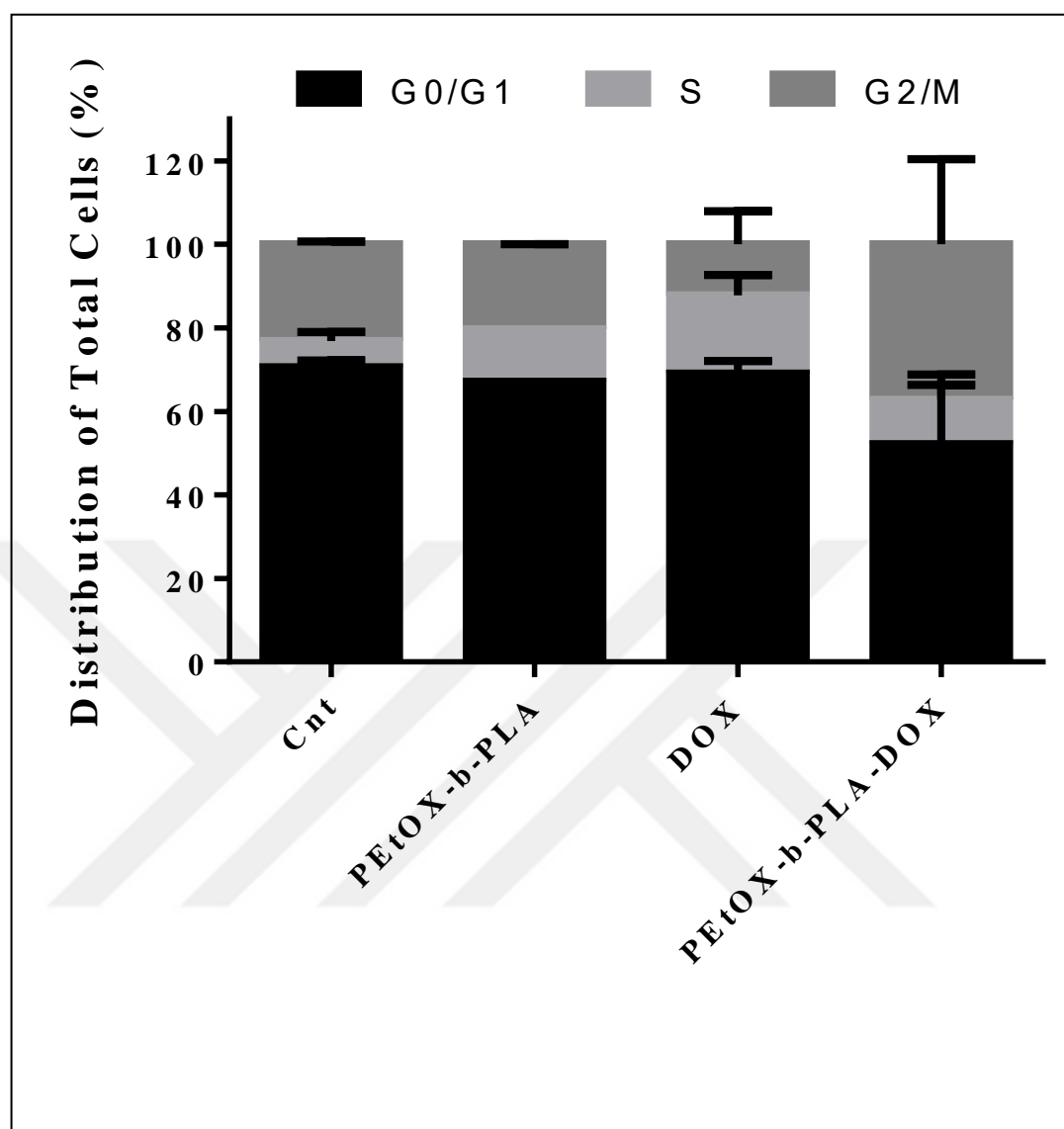


Figure 4.31. Cell cycle profiles of AU565 cells examined by flow cytometry. Non-treated AU565 cells (Cnt) and AU565 cells subjected to 1 $\mu\text{g}/\text{mL}$ of free DOX, empty PEtOx-b-PLA polymersome, and P18-PEtOx-b-PLA-DOX polymersomes for 24 hours.

4.7.7. Effect of Doxorubicin Loaded P18-Labeled PEOx-*b*-PLA Polymersome on Cell Death

To analyze whether the decrease in cell viability in AU565 cells treated with P18-PEOx-*b*-PLA-DOX polymersomes (Section 4.9.4) was due to apoptotic cell death, Annexin V-PI staining was conducted according to the procedure described (Section 3.11). Figure 4.32 and Figure 4.33 shows the apoptotic cell death of AU565 cells treated with doxorubicin loaded P18-PEOx-*b*-PLA polymersomes for 48, and 72 hours, respectively.

An average of 21 percent of Annexin-V stained AU565 cells were detected after treatment with empty PEOx-*b*-PLA polymersomes for 48 hours. 9 percent of annexin V- positive cells were identified as the early apoptotic cells while 12 percent were found to be in late apoptosis. An average of nearly 42 percent ($p < 0.05$) of Annexin-V stained AU565 cells were detected after treatment with 1 $\mu\text{g}/\text{mL}$ P18-PEOx-*b*-PLA-DOX polymersomes for 48 hours, where significant change of 19 percent cells were in early apoptosis while 23 percent were in late apoptosis. On the other hand, an average of 55 percent ($p < 0.01$) of Annexin-V stained AU565 cells were recorded after 1 $\mu\text{g}/\text{mL}$ free DOX treatment for 48 hours, in which 19 percent cells were found to be in early apoptosis while 36 percent were in late apoptosis (Figure 4.32).

Figure 4.33 shows the apoptotic cell death detected for AU565 cells treated with doxorubicin loaded P18-PEOx-*b*-PLA-DOX polymersomes for 72 hours. Empty PEOx-*b*-PLA polymersomes treatment resulted in 10 percent early apoptosis and 17 percent late apoptosis in AU565 cells at 72 hours. AU565 cells treated with 1 $\mu\text{g}/\text{mL}$ P18-PEOx-*b*-PLA-DOX polymersomes went into 29 percent early apoptosis and 41 percent late apoptosis at 72 hours giving a total of 71 percent ($p < 0.05$) of Annexin-V stained AU565 cells. 88 percent ($p < 0.01$) of Annexin-V positive cells were detected when AU565 cells were treated with 1 $\mu\text{g}/\text{mL}$ free DOX where 30 percent of cells were found to be in early apoptosis while 58 percent of cells were detected to be in late apoptosis (Figure 4.33).

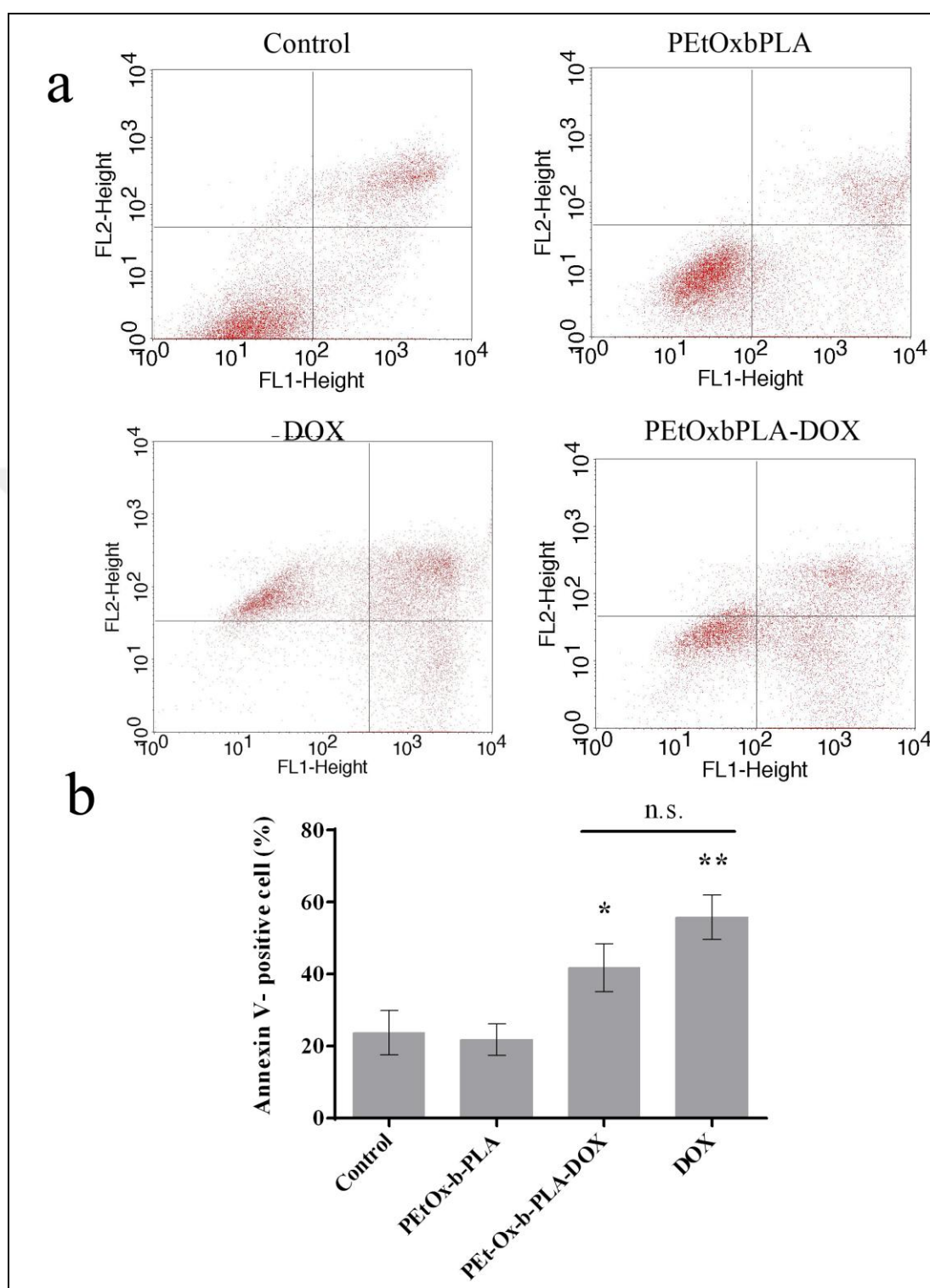


Figure 4.32. Effect of P18-PEtOx-b-PLA-DOX polymersome on AU565 cell death at 48 hours. Annexin V/PI staining was used to analyze the cell death of AU565 cells subjected to 1 $\mu\text{g}/\text{mL}$ of DOX loaded PEtOx-b-PLA polymersome or free DOX. Representative (a) Histograms and (b) Graphical representation of percentage for cell death were shown. Data point represents the average \pm SD (n=3) (*p<0.05).

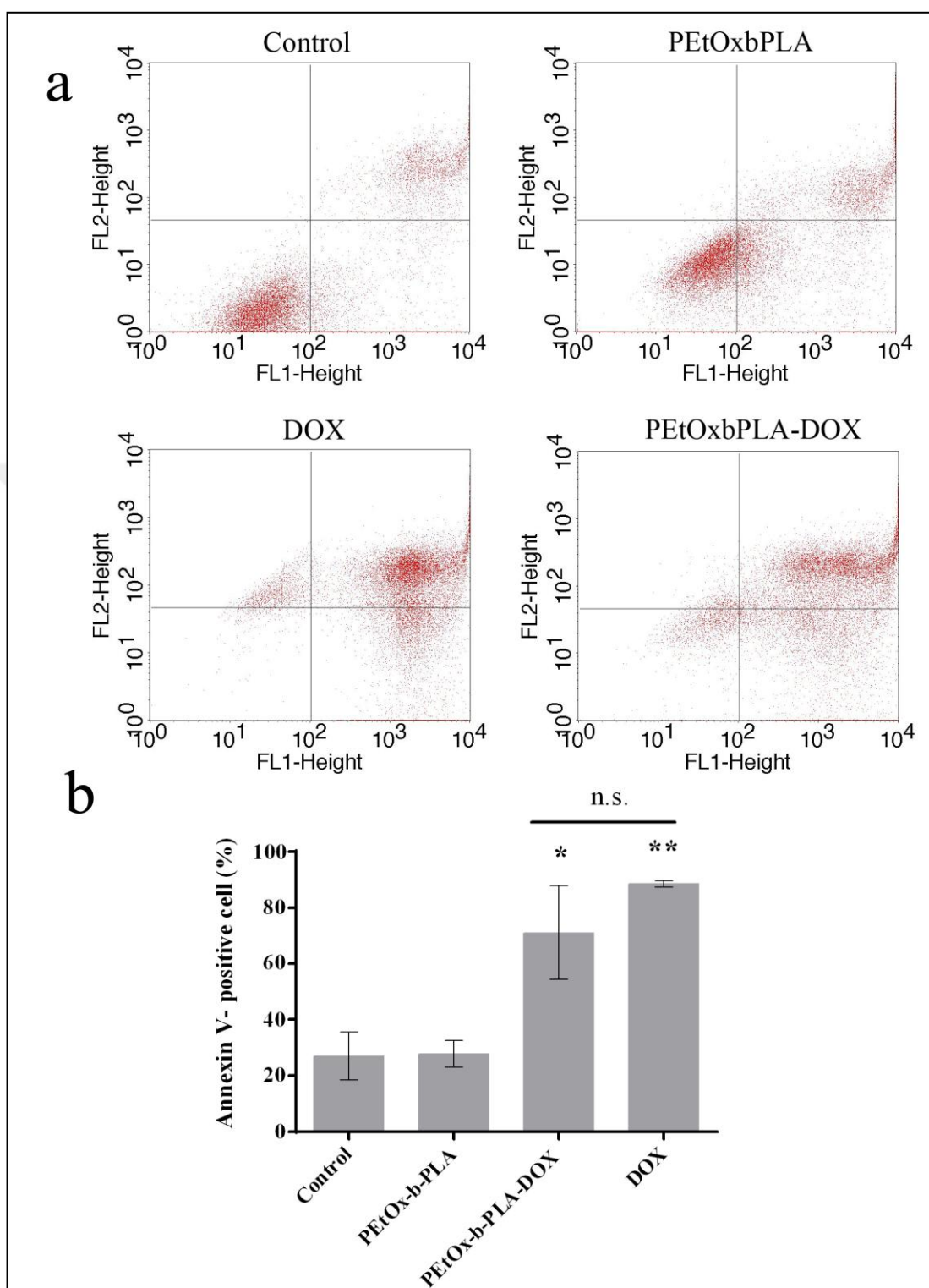


Figure 4.33. Effect of P18-PEtOx-b-PLA-DOX polymersome on AU565 cell death at 72 hours. Annexin V/PI staining was used to analyze the cell death of AU565 cells subjected to 1 $\mu\text{g}/\text{mL}$ of DOX loaded PEtOx-b-PLA polymersome or free DOX. Representative (a) Histograms and (b) Graphical representation (b) of percentage for cell death were shown.

Data point represents the average \pm SD (n=3) (*p<0.05).

4.8. MICELLE DELIVERY OF BIKDD OR DOXORUBICIN TO AU565 CELLS

4.8.1. Analysis of Cellular Cytotoxicity for PEtOx-PEI-PCL Copolymer and Micelles

In order to detect the safe dosage, HUVEC, HEK293, MSC, and MCF10A cells were treated with 100- 500 $\mu\text{g/mL}$ of PEtOx-PEI-PCL copolymer and micelles formulations for 24, 48, and 72 hours. Cytotoxicity was measured by WST-1 cell proliferation assay as described in Section 3.8.1. The percentage of cell viability was calculated setting the absorbance value obtained from Cnt (DMSO for copolymer and non-treated for micelle formulations) as 100 percent.

The cell viability of HUVEC cells after treatment with PEtOx-PEI-PCL copolymer and micelles formulations were shown in Figure 4.34. In comparison to control cells, no significant toxicity was detected in HUVEC cells treated with PEtOx-PEI-PCL copolymer for all time points (Figure 4.34a). On the other hand, slight toxicity of 10 to 15 percent was detected when HUVEC cells were treated with 200 - 500 $\mu\text{g/mL}$ of PEtOx-PEI-PCL micelles formulations (Figure 4.34b). Figure 4.35 shows the effect of PEtOx-PEI-PCL copolymer and micelle on cell viability of HEK293 cells. Although, PEtOx-PEI-PCL copolymer showed a significant toxicity at 100- 300 $\mu\text{g/mL}$ of PEtOx-PEI-PCL copolymer at 48 hours for HEK293 cells, at 72 hours the cell viability was pulled back to control levels (Figure 4.35a). PEtOx-PEI-PCL micelle formulations showed significant toxicity in HEK293 cells with a percentage of 45, 50, and 60 percent at concentrations of 300, 400, and 500 $\mu\text{g/mL}$ for 72 hours (Figure 4.35b). Figure 4.36 shows the effect of PEtOx-PEI-PCL copolymer and micelle on cell viability of MSC. PEtOx-PEI-PCL copolymer did not cause any significant cytotoxicity on MSC cells at all time points (Figure 4.36a). PEtOx-PEI-PCL micelle induced proliferation of MSC cells with a percentage of 25 and 30 percent at 100, and 200 $\mu\text{g/mL}$ for 72 hours (Figure 4.36b). The effect of PEtOx-PEI-PCL copolymer and micelle on cell viability of MCF10A cells were shown in Figure 4.37. PEtOx-PEI-PCL copolymer did not cause any significant cytotoxicity on MCF10A cells at all time points; toxicity of nearly 15 percent with 100 and 300 $\mu\text{g/mL}$ of PEtOx-PEI-PCL copolymer was observed at 48 hours (Figure 4.37a). Toxicity of 20- 30 percent on cell viability of MCF10A cells was recorded when treated with 300 and 500 $\mu\text{g/mL}$ concentrations of PEtOx-PEI-PCL micelle after 24 hour post treatment (Figure 4.37b).

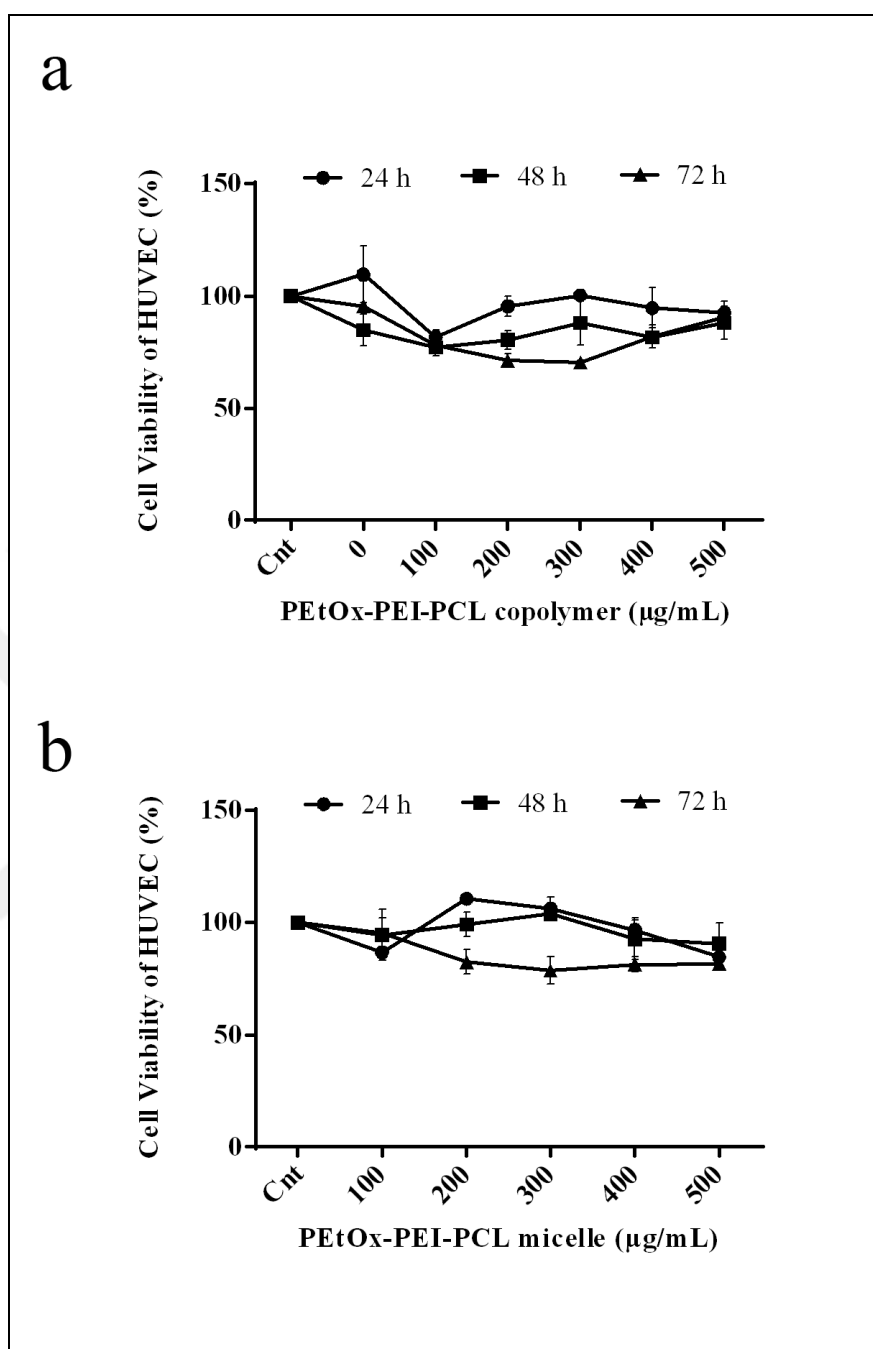


Figure 4.34. Cytotoxicity of PEtOx-PEI-PCL (a) Copolymer and (b) Micelles against HUVEC. 100, 200, 300, 400, and 500 $\mu\text{g/mL}$ of PEtOx-PEI-PCL copolymer and micelles were used to treat HUVEC until 72 hours incubation. At each 24 hour interval, cell viability was assessed by measuring the absorbance change using a microplate reader at 450 nm.

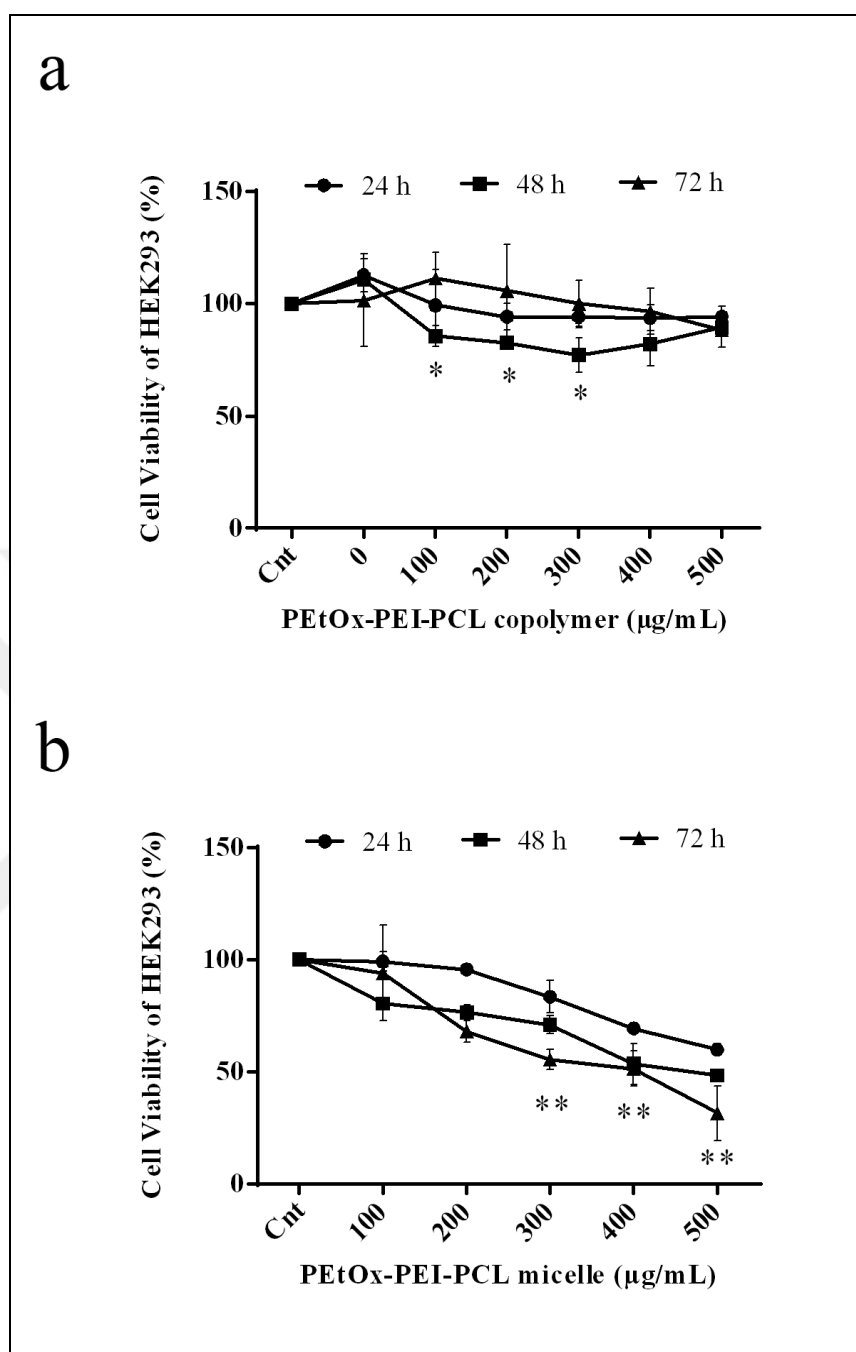


Figure 4.35. Cytotoxicity of PEtOx-PEI-PCL (a) Copolymer and (b) Micelles against HEK293 cells. 100, 200, 300, 400, and 500 $\mu\text{g/mL}$ of PEtOx-PEI-PCL copolymer and micelles were used to treat HEK293 cells until 72 hours incubation. At each 24 hour interval, cell viability was assessed by measuring the absorbance change using a microplate reader at 450 nm. Data represents the average ($n=3$) \pm SD (* $P \leq 0.05$, ** $P \leq 0.01$).

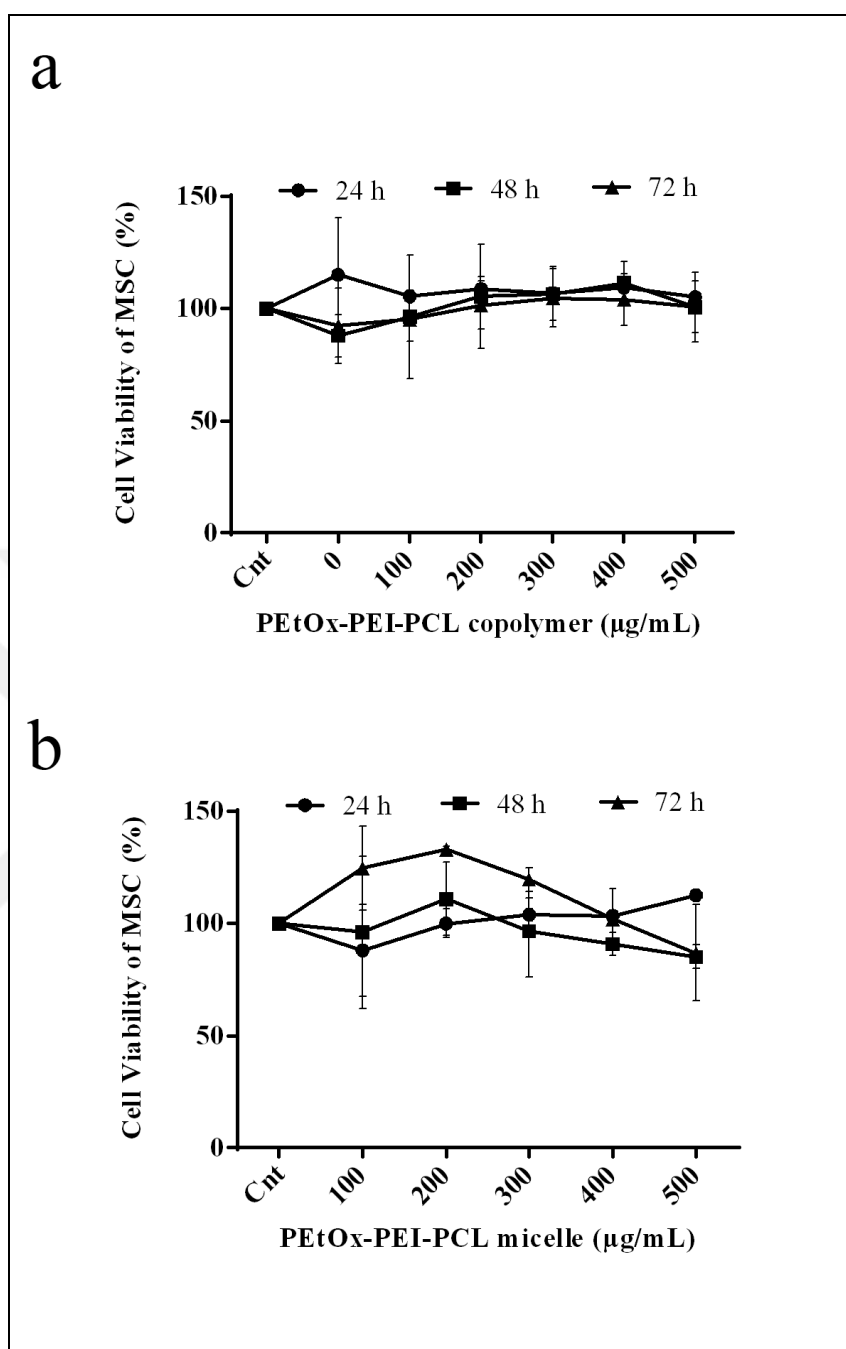


Figure 4.36. Cytotoxicity of PEtOx-PEI-PCL (a) Copolymer and (b) Micelles against MSC cells. 100, 200, 300, 400, and 500 $\mu\text{g/mL}$ of PEtOx-PEI-PCL copolymer and micelles were used to treat MSC cells until 72 hours incubation. At each 24 hour interval, cell viability was assessed by measuring the absorbance change using a microplate reader at 450 nm.

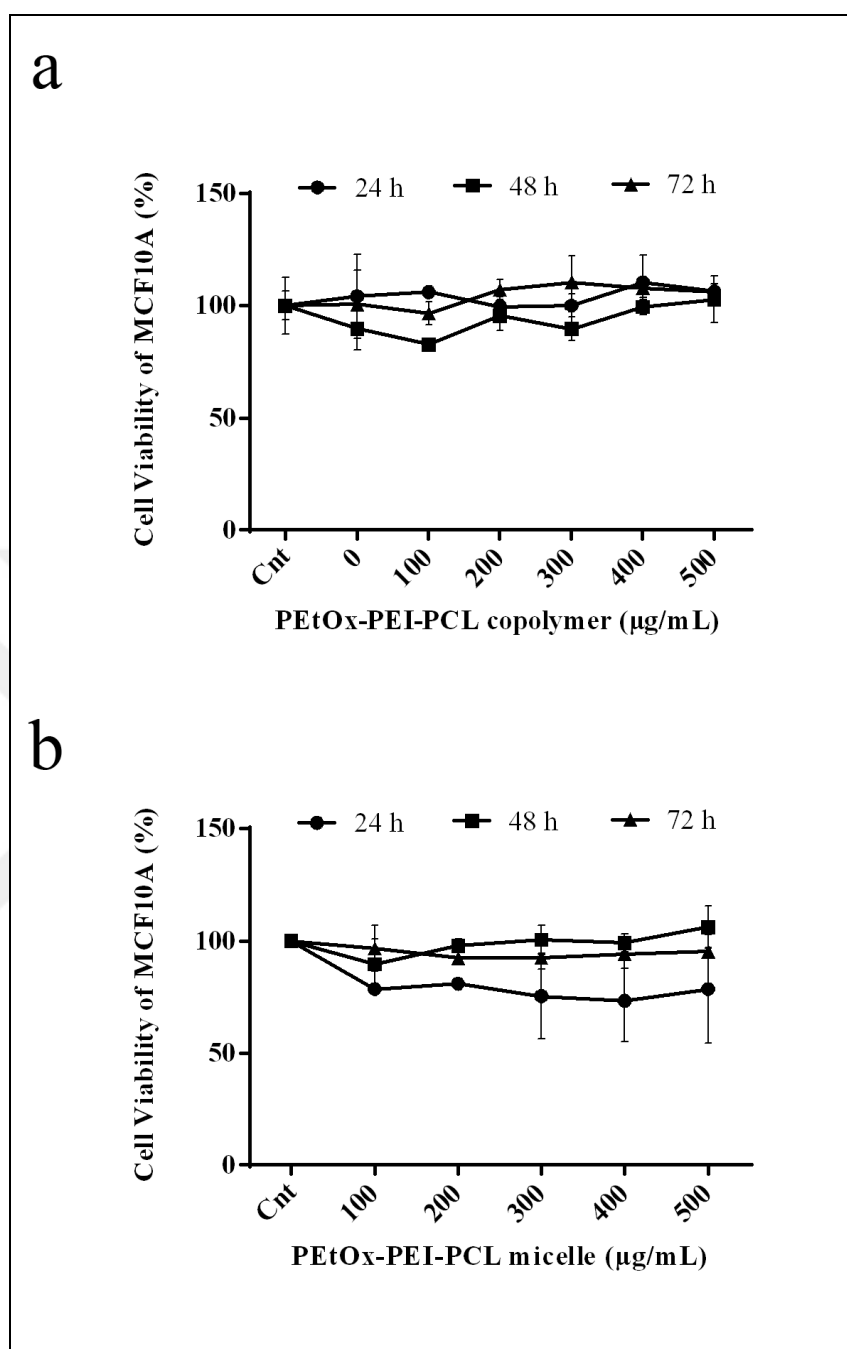


Figure 4.37. Cytotoxicity of PEtOx-PEI-PCL (a) Copolymer and (b) Micelles against MCF10A cells. 100, 200, 300, 400, and 500 $\mu\text{g/mL}$ of PEtOx-PEI-PCL copolymer and micelles were used to treat MCF10A cells until 72 hours incubation. At each 24 hour interval, cell viability was assessed by measuring the absorbance change using a microplate reader at 450 nm.

4.8.2. Binding Affinity of P18-Labeled PEtOx-PEI-PCL Micelles to the Breast Cancer and Control Cell Lines

In order to answer the question whether peptide 18 labeled PEtOx-PEI-PCL (P18-PEtOx-PEI-PCL) micelles showed a specific binding towards breast cancer cells; the binding affinity of P18-PEtOx-PEI-PCL micelles to AU565 and MCF10A cells were analyzed using flow cytometry. AU565 and MCF10A cells were seeded on 6 well plate with a density of 3×10^5 cells/well, and 2.5×10^5 cells/well, respectively. P18-PEtOx-PEI-PCL micelles loaded fluorescein stain were used to treat AU565 and MCF10A cell lines for 1 hour at 37°C as mentioned in Section 3.5.2.

Figure 4.38 shows the binding affinity of P18-labeled PEtOx-PEI-PCL micelles to MCF10A and AU565 cells. According to the flow cytometric analysis, P18-PEtOx-PEI-PCL micelles showed a binding affinity of 14.4 percent and 85.6 percent to MCF10A and AU565 cells, respectively. Results show that P18 PEtOx-PEI-PCL micelles exhibited specific binding to AU565 cancer cells

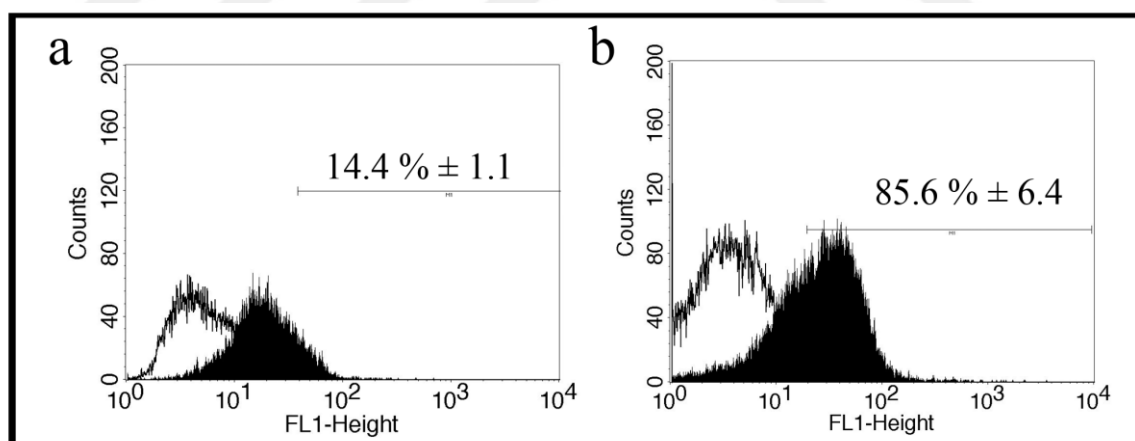


Figure 4.38. The representative histograms showing binding affinity of P18-PEtOx-PEI-PCL micelles on (a) MCF10A and (b) AU565 cells. Fluorescein labeled P18-PEtOx-PEI-PCL micelles was used to treat cells for 1 hour at 37°C.

4.8.3. Cellular Uptake of P18-Labeled PEtOx-PEI-PCL Micelles to the Breast Cancer and Control Cell Lines

Confocal microscopy imaging was employed to monitor the efficiency for cellular uptake of P18 labeled PEtOx-PEI-PCL micelles to control breast epithelial MCF10A and breast cancer AU565 cells that were seeded at 2.4×10^4 and 2×10^4 density, respectively into 8 well chamber slides (Section 3.6). Samples were visualized using confocal microscopy.

Confocal imaging indicated that peptide 18 labelled PEtOx-PEI-PCL bound to AU565 cells strongly while low binding was detected on MCF10A cells as shown in Figure 4.39. While, most of green fluorescence of fluorescein accumulated in cytoplasm of AU565 cells treated with P18-PEtOxPEIPCL micelles and much weaker fluorescein was showed in MCF10A cells. All cell nuclei (blue) were identified by DAPI staining.

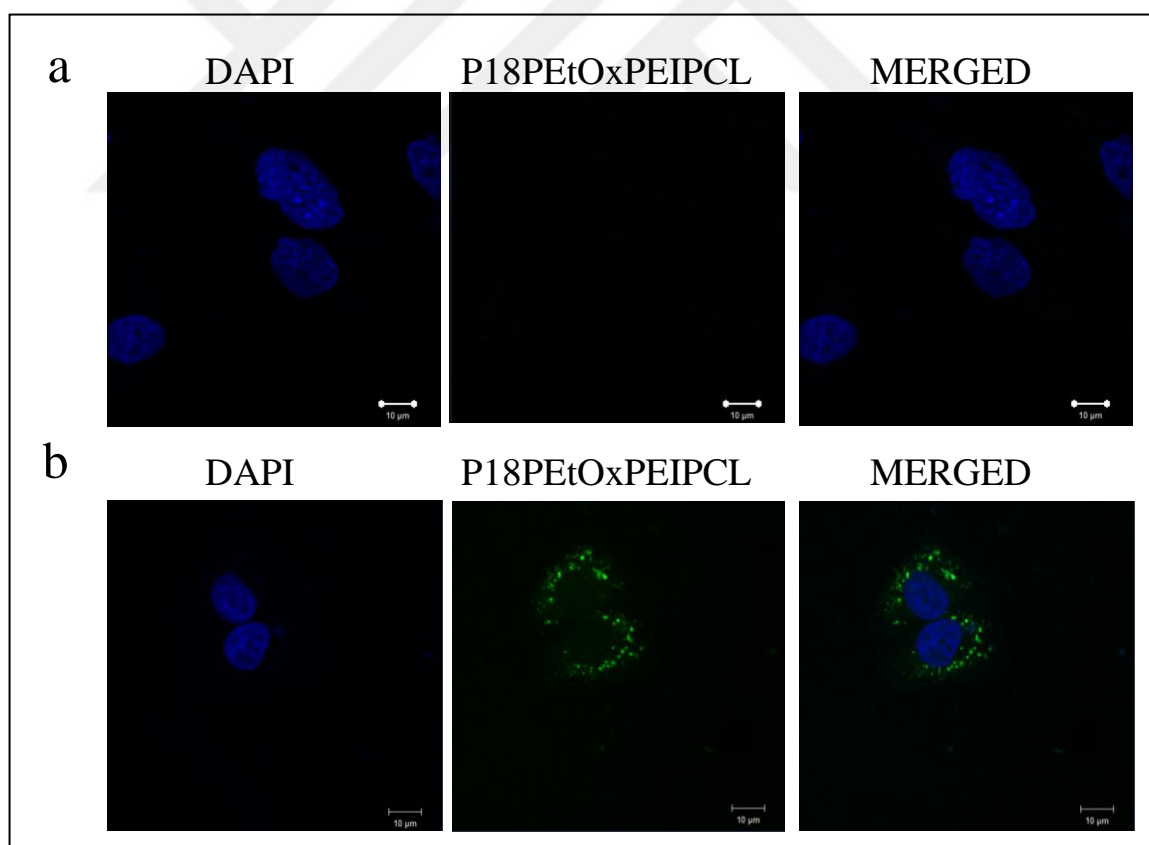


Figure 4.39. P18-PEtOxPEIPCL micelles binding affinity on (a) MCF10A and (b) AU565 cell lines by confocal microscopy. 63 x objectives were used to take images and scale bar is 10 μm.

4.8.4. Cell Viability of AU565 Cells Treated with BikDD or Doxorubicin Loaded P18-Labeled PEtOx-PEI-PCL Micelle

The lethal effect of proapoptotic BikDD gene on cell viability of AU565 cells was determined by treating AU565 cells with BikDD loaded targeted (P18) and empty PEtOxPEI_{60%}PCL (PPP60) micelle complex for 24, 48, and 72 hours. Cell viability and proliferation of AU565 cells was conducted using WST-1 as mentioned in Section 3.8.2. The absorbance values of control cells at each time interval was considered as 100 percent for the viability analysis.

The impact of 4, 6, and 8 μg of BikDD in P18-PPP60 micelle/BikDD complex and empty PPP60 micelle on cell viability of AU565 cells until 72 hours post-treatment was demonstrated in Figure 4.40. The effect of P18-PPP60 micelle/BikDD complex caused a dose dependent decrease in AU565 cell viability at 24 hours. In comparison to non-treated (Cnt) AU565 cells, there was a 6 percent, 18 percent, and 33 percent decrease in cell viability of AU565 cells at 4, 6, and 8 μg of BikDD in P18-PPP60-BikDD, respectively. Similarly, there was a decrease of 10 percent, 9 percent, and 26 percent in cell viability of AU565 cells at 4, 6, and 8 μg of empty PPP60 micelle, respectively (Figure 4.40a).

AU565 cells treated with 6 and 8 μg of BikDD in P18-PPP60-BikDD micelle complex showed a significant decrease in cell viability with 23, and 49 percent at 48 hours. In contrast, empty micelle had no significant effect (15, and 12 percent) on cell viability of AU565 cells at 6 and 8 μg treatment of empty micelle (Figure 4.40b).

There was a significant decrease of 34, 35, and 56 percent in cell viability of AU565 cells at 4, 6, and 8 μg of BikDD in P18-PPP60-BikDD micelle complex at 72 hours. However, there was a decrease of 23, 19, and 35 percent in cell viability of AU565 cells at 4, 6, and 8 μg of empty PPP60 micelle (Figure 4.40c).

In conclusion, the highest therapeutic effect was observed in AU565 cells when treated with 8 μg of BikDD in P18-PPP60-BikDD micelle complex at all time points.

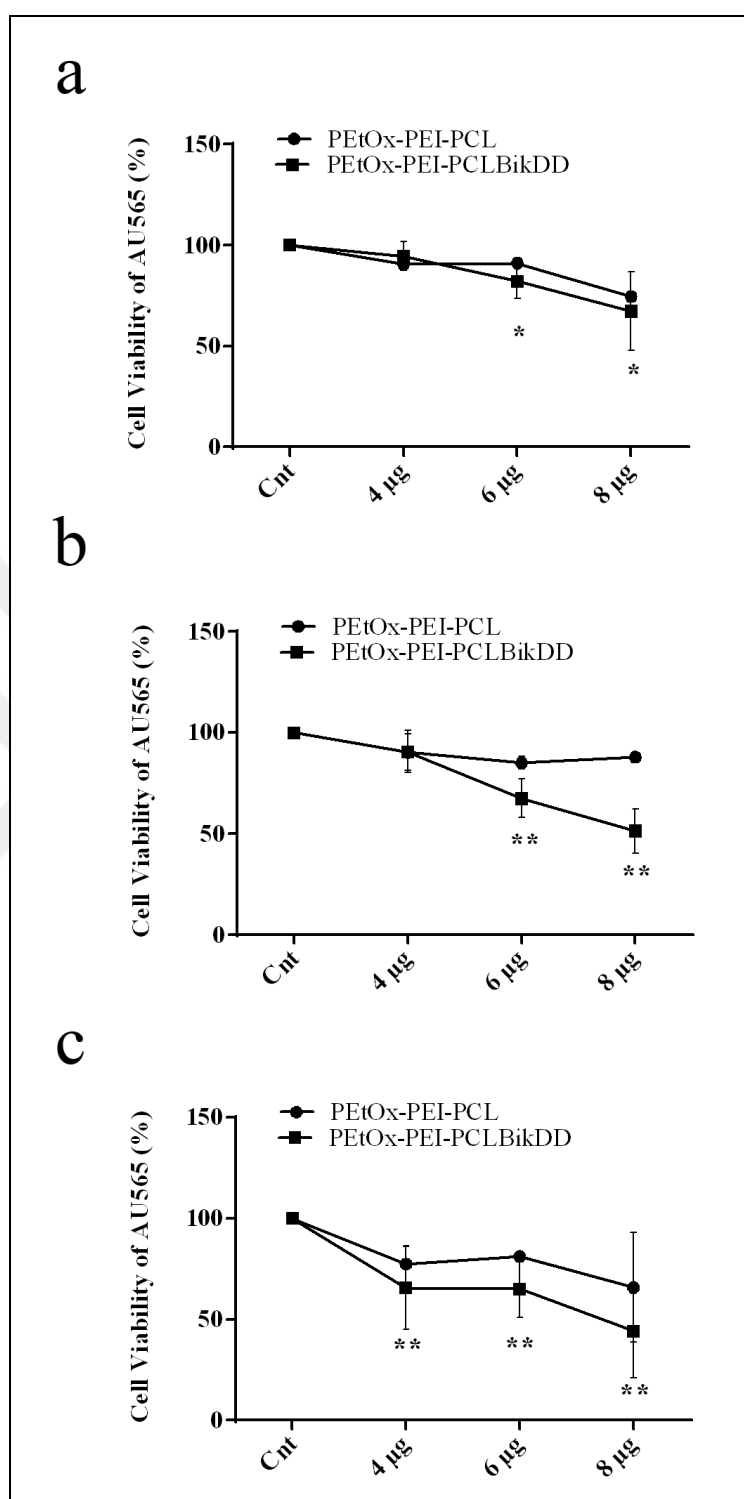


Figure 4.40. Determination of the cytotoxic effect of P18-PEtOxPEIPCL-BikDD on AU565 cells. 2, 5, and 10 µg of BikDD gene in P18-PEtOxPEIPCL was to treat AU565 cells for (a) 24, (b) 48, and (c) 72 hours. At each 24 hours interval, cell viability was assessed by measuring the absorbance change by microplate reader at 450 nm. Data is mean of (n=3) ± SD (* P ≤ 0.05, ** P ≤ 0.01, *** P ≤ 0.001).

In order to determine the therapeutic effect of doxorubicin loaded P18 targeted PEtOxPEI_{30%}PCL (PPP30) micelles on cell viability of AU565 cells, cells were treated with 0.1, 0.5, 1, 2.5, 5, 10, and 20 µg/mL of DOX loaded P18 targeted (P18) and empty PPP30 micelles for 24, 48, and 72 hours. WST-1 assay was used to determine the dose-dependent effect on AU565 cell viability as mentioned in Section 3.8.2.

Figure 4.41 shows the effects of P18-PPP30-DOX and empty PPP30 micelle on cell viability of AU565 cells for 72 hours post-treatment. The cytotoxic effect of 0.1- 20 µg/mL of P18-PPP30-DOX on AU565 cells shows a dose dependent decrease with time. In comparison to control cells, there was a 20 percent, 23 percent, 25 percent, 25 percent, 35 percent, 38 percent, and 60 percent decrease for 0.1, 0.5, 1, 2.5, 5, 10, and 20 µg/mL of P18-PPP30-DOX for 24 hours. Likewise, a dose dependent decrease in AU565 cells was detected when subjected to free DOX. In comparison to control cells, there was a 13 percent, 30 percent, 41 percent, 46 percent, 38 percent, 31 percent, and 32 percent decrease for 0.1, 0.5, 1, 2.5, 5, 10, and 20 µg/mL of free DOX for 24 hours (Figure 4.41a).

At 48 hours, significant decrease in cell viability of AU565 cells started from dosage of 1 µg/mL P18-PPP30-DOX. In comparison to control cells, there was a 8 percent, 20 percent, 40 percent, 63 percent, 75 percent, 84 percent, and 95 percent decrease for 0.1, 0.5, 1, 2.5, 5, 10, and 20 µg/mL of P18-PPP30-DOX for 48 hours. In contrast, a significant decrease in cell viability of AU565 cells was evident for 0.05 µg/mL of free DOX treatment. In comparison to control cells, there was a 27 percent, 61 percent, 72 percent, 82 percent, 87 percent, 84 percent, and 88 percent decrease for 0.1, 0.5, 1, 2.5, 5, 10, and 20 µg/mL of free DOX for 48 hours (Figure 4.41b).

After 72 hours post treatment, significant decrease in cell viability of AU565 cells was recorded as 41 percent, 52 percent, 77 percent, 88 percent, 95 percent, and 99 percent when treated with 0.5, 1, 2.5, 5, 10, and 20 µg/mL of P18-PPP30-DOX. Similarly, significant decrease in cell viability of AU565 cells was recorded with treatment of 0.1- 20 µg/mL of free DOX (Figure 4.41c).

The therapeutic dosage to be used for cell death studies was selected as 1 µg/mL for P18-PPP30-DOX micelle, as it was the minimal dose that showed the maximum effect.

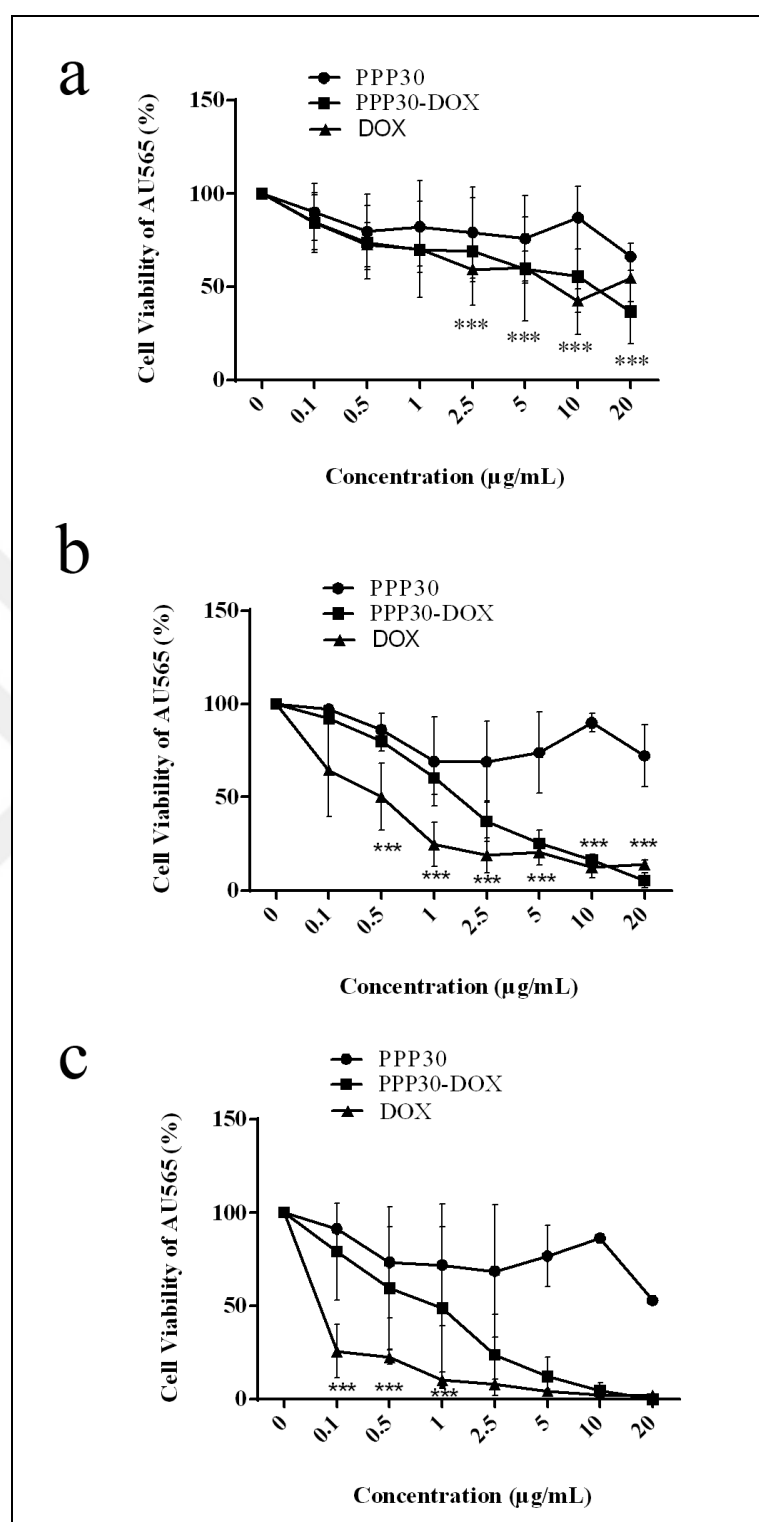


Figure 4.41. Determination of the cytotoxic effect of P18-PPP30-DOX micelle on AU565 cells. 0.1 to 20 µg/mL of P18-PPP30-DOX micelle were used to treat AU565 cells for (a) 24, (b) 48, and (c) 72 hours. At each 24 hour interval cell viability was assessed by measuring the absorbance change using a microplate reader at 450 nm. Data represents mean (n=3) ± SD (***) P ≤ 0.001, **** P ≤ 0.0001).

4.8.5. Bik Levels in AU565 Cells Treated with BikDD Loaded P18-Labeled PEtOx-PEI-PCL Micelles

In order to find out the mRNA expression level of BikDD in AU565 cells transfected with P18-PPP60 micelle/BikDD complex, real time PCR was conducted as mentioned earlier (Section 3.9). Figure 4.42 shows the relative Bik/18sRNA mRNA expression levels in non-transfected (Cnt) AU565 cells, and AU565 cells transfected with 4 and 8 μg P18-PPP60 micelle/BikDD complex. AU565 cells transfected with 4 μg and 8 μg of BikDD in P18-PPP60 micelle/BikDD complex showed a 16, and 33 fold increase in Bik gene expression when compared to the non-treated control cells (Cnt).

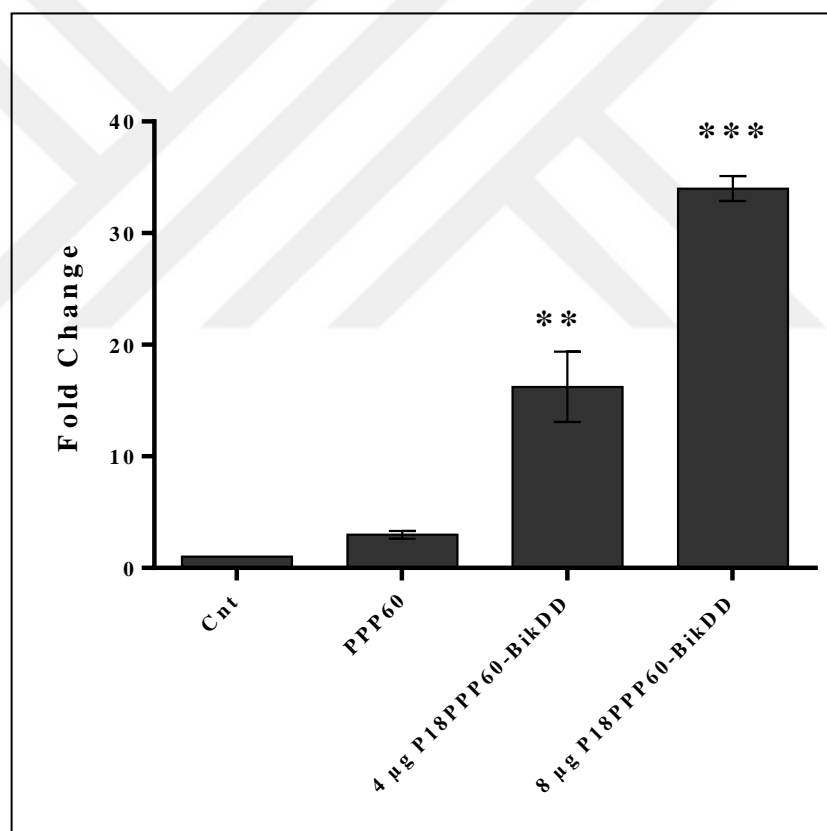


Figure 4.42. Relative Bik/18sRNA mRNA expression using qPCR for non transfected (Cnt) and AU565 cells transfected 4 and 8 μg of BikDD in P18PPP60 micelle/BikDD complex. Data represents mean ($n=3$) \pm SD (** $p<0.01$, *** $p<0.001$).

4.8.6. Effect of Doxorubicin Loaded P18-Labeled PEtOx-PEI-PCL Micelle on Cell Cycle

In order to determine the effect of P18-PPP30-DOX micelle on AU565 cell cycle arrest, cells were treated with P18-PPP30-DOX micelle for 24, 48, and 72 hours. PI staining was used to analyze the cell cycle of AU565 cells subjected to 1 $\mu\text{g/mL}$ of DOX loaded P18-PPP30 micelle or free DOX as mentioned earlier (Section 3.10).

Figure 4.43 shows the effect of P18-PPP30-DOX on AU565 cell cycle arrest. The average population of G0/G1 phase-cells for non-treated group was 66 percent, and G0/G1 phase cells treated with PPP30 micelle, free DOX, and P18-PPP30-DOX micelle was 55 percent, 69 percent, and 25 percent, respectively.

The average proportion of S phase for non-treated AU565 cells was 9 percent. AU565 cells treated with PPP30 micelle, free DOX, and P18-PPP30-DOX micelle average proportion of S phase was 9 percent, 19 percent, and 10 percent, respectively.

The population of cells in G2/M phase for 24 hours was 35 percent, 19 percent, and 65 percent, after the treatment of AU565 cells with PPP30 micelle, free DOX, and P18-PPP30-DOX micelle, respectively. For the control group (non-treated AU565 cells), the frequency of G2/M cell cycle phase was found as 24 percent. The percentage of AU565 cells in G2/M phase was induced while the percentage of cells in G0/G1 phase was decreased when AU565 cells were treated with P18-PPP30-DOX micelle in comparison to the non-treated cells. These data indicate that P18-PPP30-DOX micelle treatment arrested the cell cycle of AU565 cells in G2/M phase at 24 hours.

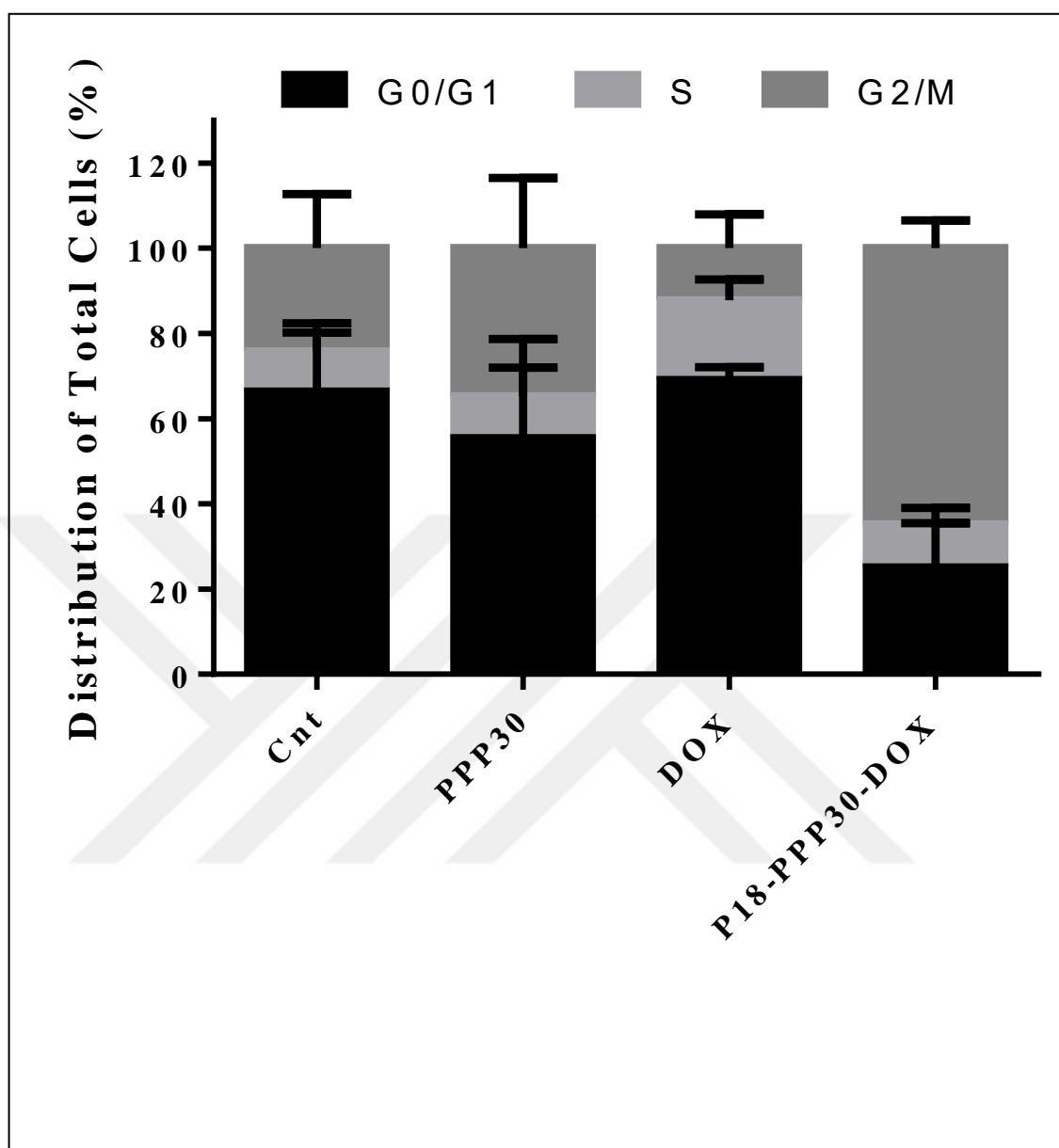


Figure 4.43. Cell cycle profiles of AU565 cells examined by flow cytometry. Non-treated AU565 cells (Cnt) and AU565 cells subjected to 1 $\mu\text{g}/\text{mL}$ of free DOX, empty PPP30 micelles, and P18-PPP30-DOX micelle for 24 hours.

4.8.7. Effect of Doxorubicin Loaded to P18-PEtOx-PEI-PCL Micelles on Cell Death

The cytotoxic effect of P18-PPP30-DOX micelle complex on AU565 cells suggested that cell viability may be relevance to induced apoptotic cell death. Thus, in order to detect apoptotic response of drug therapy on AU565 cells, Annexin V-PI staining was conducted as mentioned in Section 3.11. Figure 4.44 and Figure 4.45 shows the apoptotic cell death of doxorubicin loaded P18-PPP30 micelle formulations on AU565 cells at 48, and 72 hours, respectively.

An average of 25 percent of Annexin-V stained AU565 cells were detected after treatment with empty PPP30 micelle for 48 hours. 11 percent of annexin V- positive cells were identified as the early apoptotic cells while 14 percent were found to be in late apoptosis. An average of nearly 59 percent of Annexin-V stained AU565 cells were detected after 48 hours treatment with 1 $\mu\text{g}/\text{mL}$ of P18-PPP30-DOX micelle complex, where significant change of 14 percent cells were in early apoptosis while 42 percent were in late apoptosis. On the other hand, an average of 62 percent of Annexin-V stained AU565 cells were recorded after treatment of 1 $\mu\text{g}/\text{mL}$ free DOX for 48 hour, where significant change of 20 percent cells where in early apoptosis while 42 percent were in late apoptosis (Figure 4.44).

Figure 4.45 shows the apoptotic cell death for AU565 cells treated with doxorubicin loaded P18-PPP30 micelle for 72 hours. Empty PPP30 micelle treatment of AU565 cells resulted in 6 percent early apoptosis and 15 percent late apoptosis at 72 hours. AU565 cells treated with 1 $\mu\text{g}/\text{mL}$ P18-PPP30-DOX micelle complex resulted in 18 percent early apoptosis and 56 percent late apoptosis at 72 hours with a total of 74 percent of Annexin-V stained AU565 cells. 1 $\mu\text{g}/\text{mL}$ free DOX treatment of AU565 cells resulted in an average of 88 percent of Annexin-V positive stained cells.

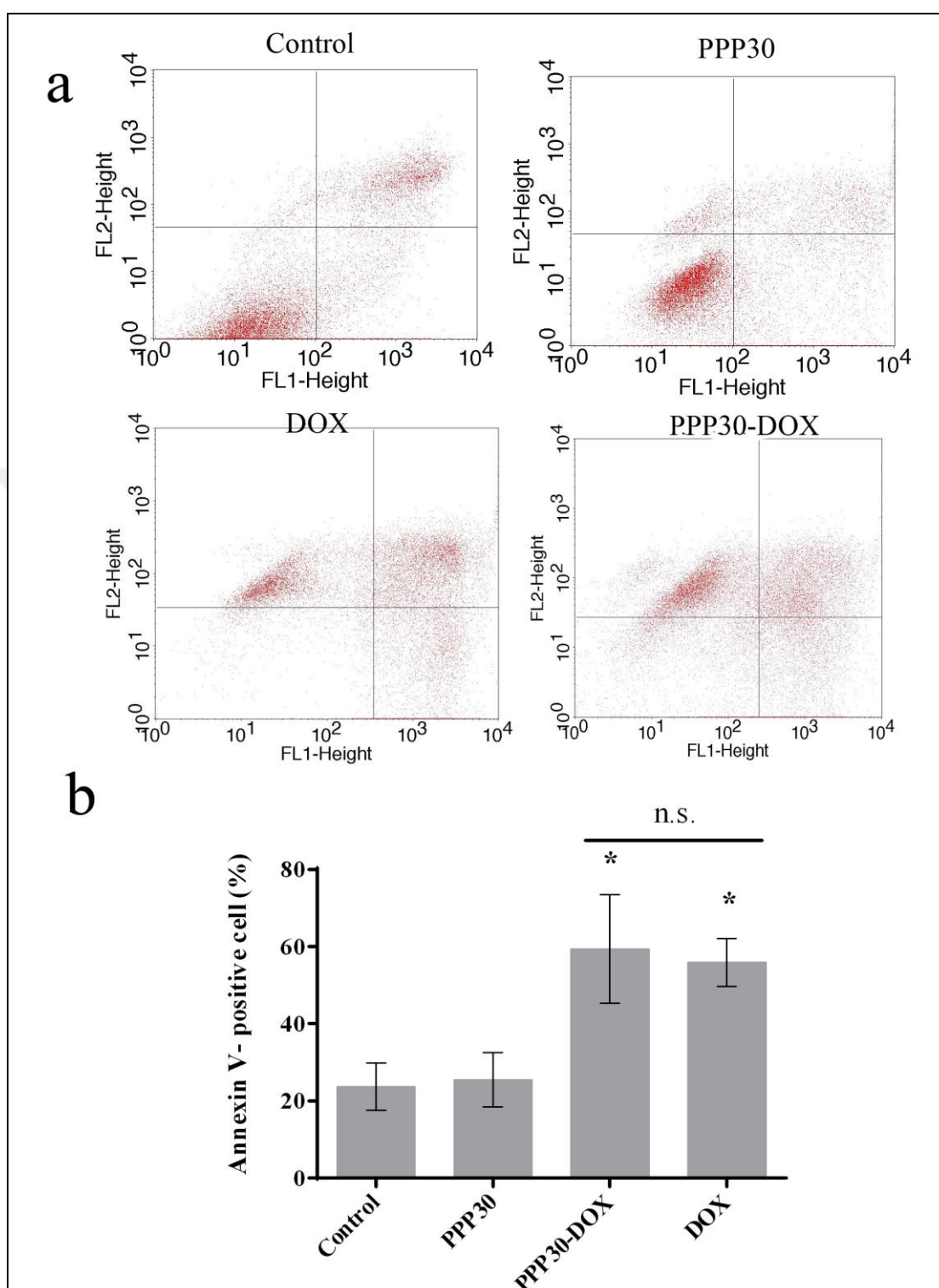


Figure 4.44. Effect of P18-PPP30-DOX micelle on AU565 cell death at 48 hours. Annexin V/PI staining was used to analyze the cell death of AU565 cells subjected to 1 $\mu\text{g}/\text{mL}$ of DOX loaded P18-PPP30 micelle or free DOX. Representative (a) Histograms and (b) Graphical representation of percentage for cell death were shown. Data represents mean (n=3) \pm SD (*p<0.05).

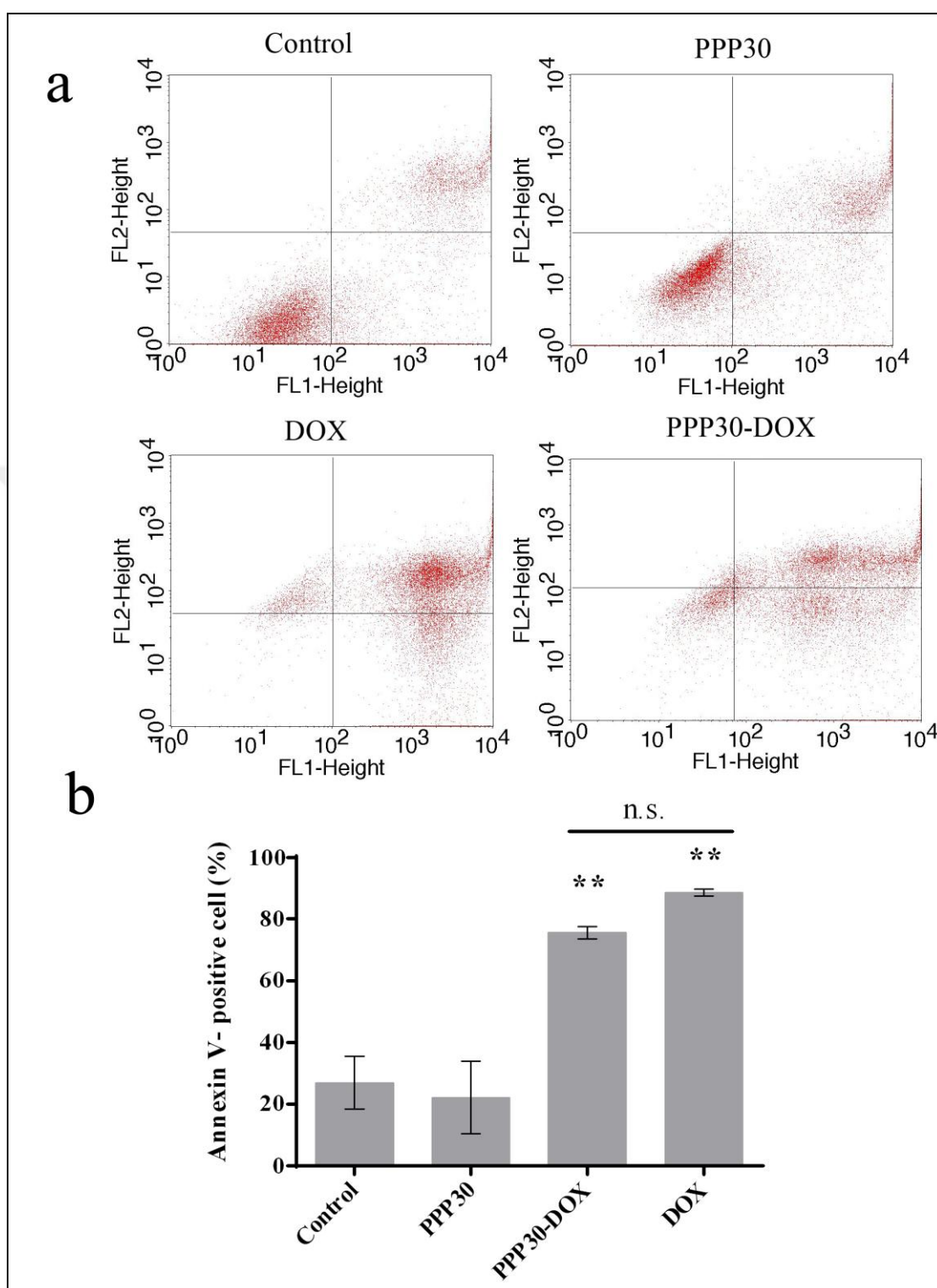


Figure 4.45. Effect of P18-PPP30-DOX micelle on AU565 cell death at 72 hours. Annexin V/PI staining was used to analyze the cell death of AU565 cells subjected to 1 $\mu\text{g}/\text{mL}$ of DOX loaded P18-PPP30 micelle or free DOX. Representative (a) Histograms and (b) Graphical representation of percentage for cell death were shown. Data represents mean (n=3) \pm SD (*p<0.05).

4.9. THERAPEUTIC EFFECT OF TARGETED NANOCARRIERS ON AU565 TUMOR MODELS

4.9.1. Therapeutic effect of P18-PEtOx-DOPE-DOX Liposomes on AU565 Tumor Models

Immunocompromised mice are used as tumor models in cancer research in order to circumvent immune rejection [210]. Athymic nude, severe combined immunodeficiency (SCID), and NOD-SCID mice are the most commonly used xenograft models [211]. For decades, athymic nude mice were most widely studied in forming xenograft models of human breast cancer cell lines [212]. Recent studies showed that NOD-SCID gamma (NSG) mice are highly permissive for engraftment of human metastatic cancer models [213]. NSG provided a better model when compared to SCID mice for studying human breast cancer metastasis [214]. CD-1 (nu/nu), athymic nude mice that have a mutation in their “nude” *foxn1* gene which is responsible for the hair follicle and thymic development [215]. Thus, these mice which are profoundly T cell deficient and have severely impaired immune response [216] provide a better model for observing the tumor when injected subcutaneously, due to the natural lack of hair [215].

In order to evaluate the therapeutic efficacy of P18-PEtOx-DOPE-DOX, breast cancer orthotopic models were formed in 6-8 weeks old CD-1 nude female mice as mentioned earlier in Section 3.12. CD-1 nude female mice bearing disseminated AU565 orthotopic tumors were treated intraperitoneally, once in every three days for a total of 8 injections, with PEtOx-DOPE liposomes, P18-PEtOx-DOPE-DOX liposomes, or DOX, all at the cumulative DOX dose of 5 mg/kg. The tumor size and weight of each animal was measured before every injection, and mice were examined for morbidity and mortality until sacrifice day (28th).

Figure 4.46 shows the representative pictures of CD-1 nude female mice, where the tumor development was recorded in vehicle control (PBS), PEtOx-DOPE liposomes, DOX, and P18-PEtOx-DOPE-DOX liposomes. All the animals were alive during the experimental period. All animals (n=6) in the vehicle control cohort receiving PBS, and empty PEtOx-DOPE liposomes developed tumors (Figure 4.46a-b). The incidence of tumor formation was four out of six in animals of the group subjected to 5 mg/kg of free DOX (Figure 4.4

6c), while tumor incidence was six out of six in the group of mice subjected to the treatment of 5 mg/kg P18-PEtOx-DOPE-DOX liposomes (Figure 4.46d).

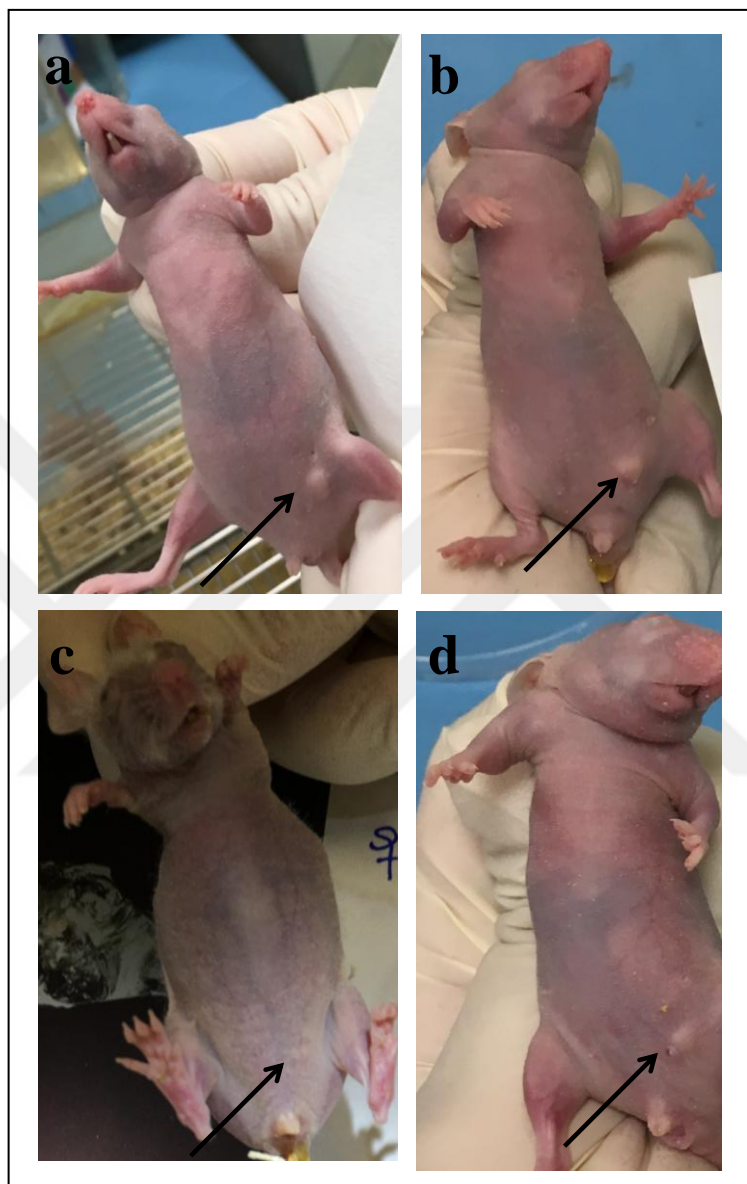


Figure 4.46. Effect of P18-PEtOx-DOPE-DOX liposomes on tumor growth. CD-1 nude female mice were implanted with AU565 (8×10^6) cells. Following the third day of inoculation, animals were divided randomly into four groups ($n=6$) and exposed to vehicle control (PBS), 5 mg/kg P18-PEtOx-DOPE-DOX liposomes, 5 mg/kg free DOX, and 5 mg/kg PEtOx-DOPE liposomes every three days. Representative pictures of CD-1 nude female mice exhibiting tumor development in mammary pad were shown for (a) Vehicle control cohort, (b) PEtOx-DOPE liposomes cohort, (c) Free DOX cohort, and (d) P18-PEtOx-DOPE-DOX liposomes cohort.

The body weight of CD-1 nude female mice recorded through 25 days showed that there was no weight loss in vehicle control, PEtOx-DOPE liposomes, and P18-PEtOx-DOPE-DOX liposomes treatment cohorts suggesting tolerable treatment dosage. On the contrary, animals in the free DOX cohorts had a loss of weight of average 1.9 g at day 25 although, the chosen dosage for free DOX was consistent with the literature (Figure 4.47).

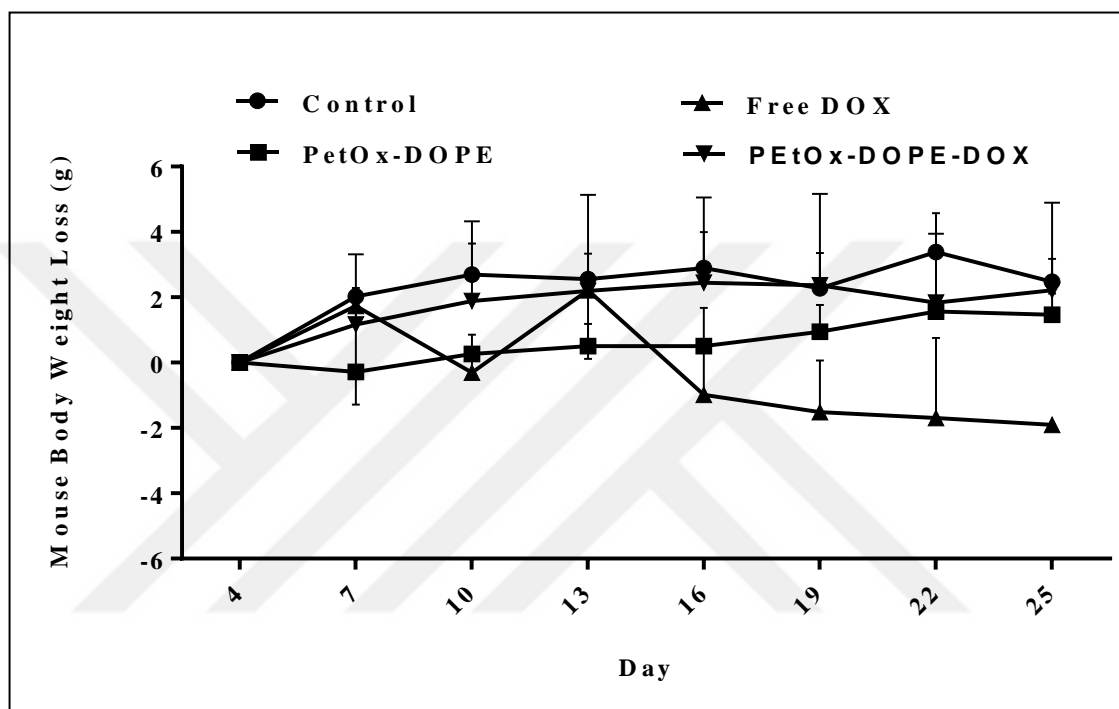


Figure 4.47. Effect of P18-PEtOx-DOPE-DOX liposomes on the CD-1 nude mice body weight.

Sacrificiation of animals took place following 25 days of drug treatment and nine different organs along with tumor tissues were isolated as mentioned in Section 3.12. The isolated tumors from animals in control (PBS), PEtOx-DOPE liposomes, DOX, or P18-PEtOx-DOPE-DOX liposomes was demonstrated in Figure 4.48a. The tumor weight hence the size isolated from P18-PEtOx-DOPE-DOX liposomes cohort were smaller compared to control and PEtOx-DOPE liposomes cohort. The tumor weight was 0.030 g, 0.033 g, 0.018 g, and 0.018 g in average for the control (PBS), PEtOx-DOPE liposomes, free DOX, and P18-PEtOx-DOPE-DOX liposomes cohorts, respectively. Importantly, treatment with free DOX and P18-PEtOx-DOPE-DOX liposomes significantly reduced tumor weight by 41 percent compared to control cohorts (Figure 4.48b). The tumor volume was 35 mm³, 18.5 mm³, 13.8 mm³, and 8.3 mm³ in average for the control (PBS), PEtOx-DOPE liposomes,

free DOX, and P18-PEtOx-DOPE-DOX liposomes cohorts, respectively. The treatment with free DOX and P18-PEtOx-DOPE-DOX liposomes significantly reduced tumor volume compared by 60 percent and 76 percent in comparison to control cohorts. (Figure 4.48c). Although P18-PEtOx-DOPE-DOX liposome treatment resulted in a more pronounced decrease in tumor weight and volume, there was no significant difference on these parameters for the tumors dissected from free DOX treated mice.

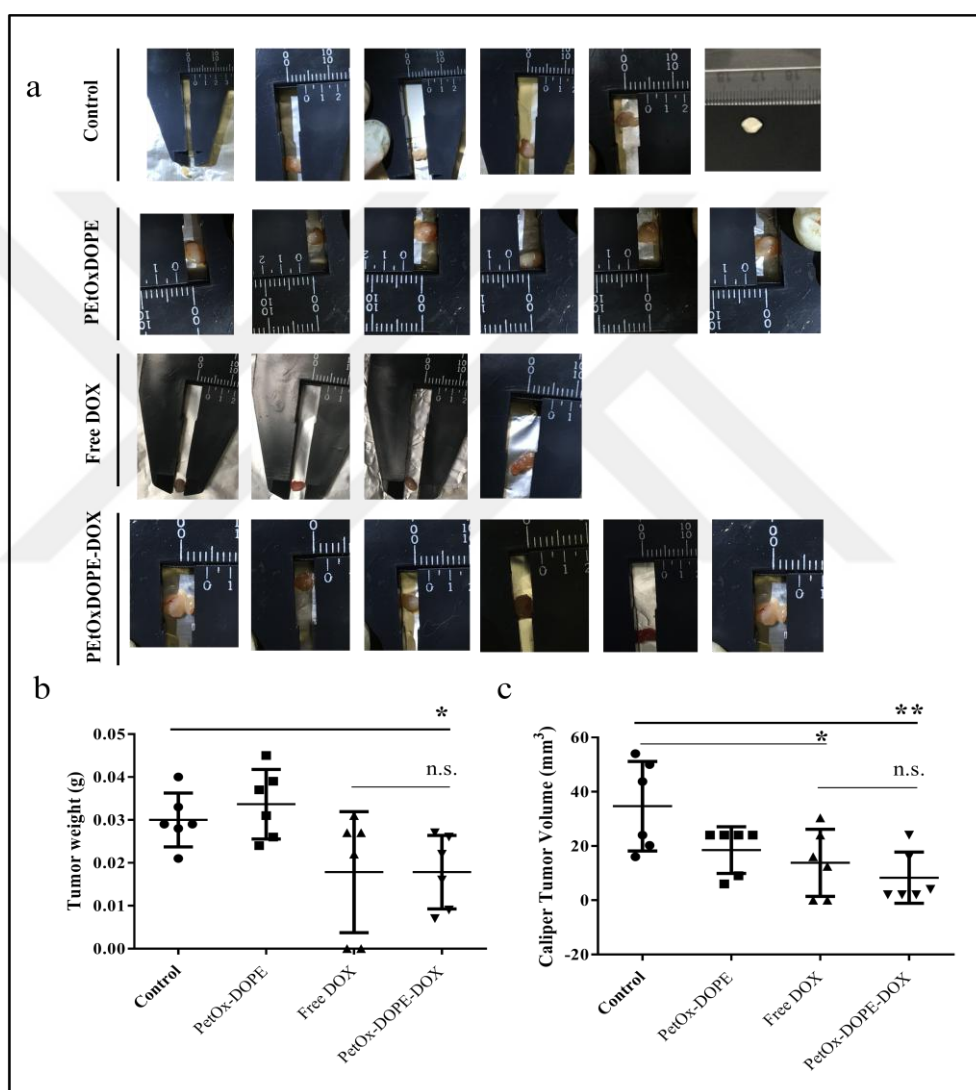


Figure 4.48. Antitumor effect of P18-PEtOx-DOPE-DOX liposomes on CD-1 nude mice models. (a) Pictures represent the tumor isolated from CD-1 nude mice in four different groups subjected to treatment with either vehicle control (PBS), PEtOx-DOPE liposomes, DOX, or P18-PEtOx-DOPE-DOX liposomes. Graph shows the distribution of the isolated (b) Tumor weights and (c) Tumor volume.

Following sacrifice and tumor isolation of animals, samples were stained by H&E for histopathological analysis (Figure 4.49). The characterization of the isolated tumor tissues of CD-1 nude female mice used in the study was shown in Table 4.2. All tumor types were characterized as adenocarcinoma, verifying AU565 orthotopic CD-1 nude mouse models were generated successfully. Histological and nuclear grading of all tumors in four different treatment groups were recorded as Grade 3. Tumor isolated from one of the animals in the P18-PEtOx-DOPE-DOX liposomes cohorts during sacrifice was recorded as no tumor, only minimal tumor bed during histopathological analysis. No signs of toxicity was detected for organs (brain, lung, heart, liver, spleen, stomach, intestines, kidney, and ovary) extracted from all four treatment cohorts. All the data given above suggest that P18-PEtOx-DOPE-DOX liposomes gave an anti-tumor response comparable to free-DOX.

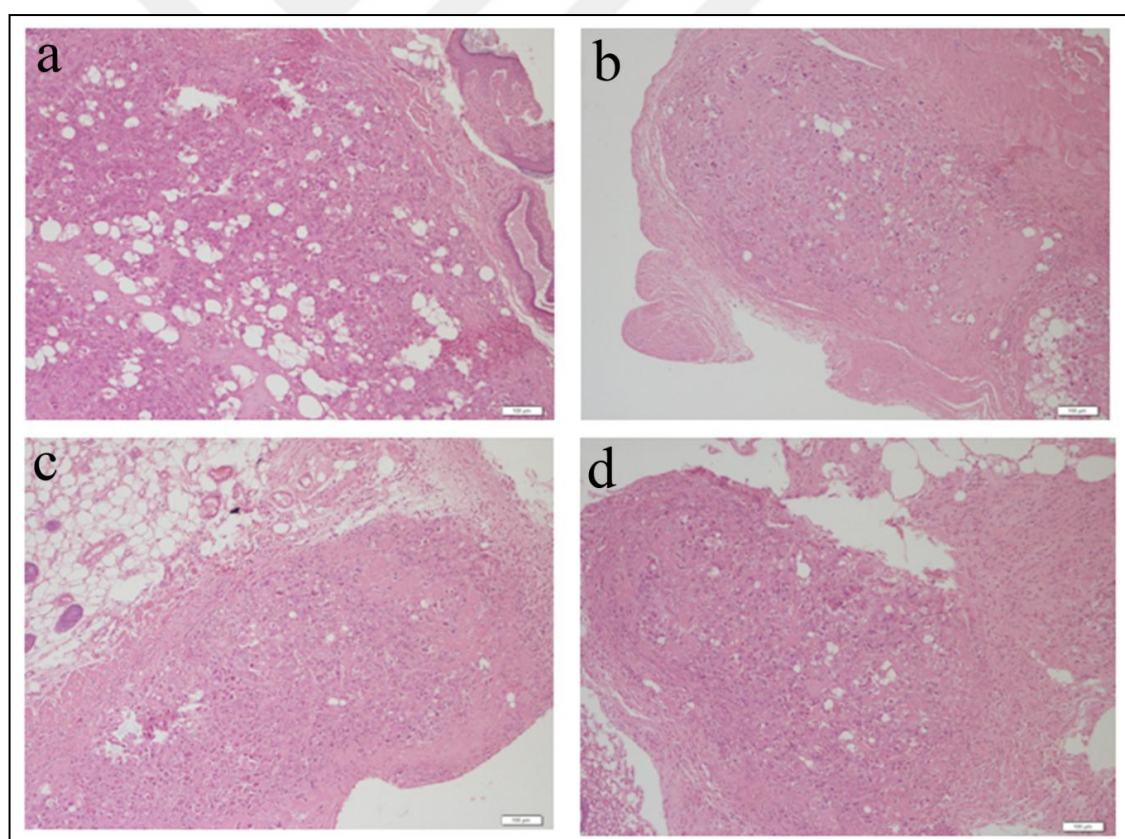


Figure 4.49. Histopathological analysis of the P18-PEtOx-DOPE-DOX liposomes tumor samples. H&E staining was used to stain the tumors isolated from CD-1 nude mice in four different groups subjected to treatment of either (a) Vehicle control, (b) Free DOX, (c) P18-PEtOx-DOPE-DOX liposomes, or (d) PEtOx-DOPE liposomes.

Table 4.2. Effect of P18-PEtOx-DOPE-DOX liposomes on tumor tissues of CD-1 nude mice used in the study.

	Animal	Tumor Type	Histologic/Nuclear Grading
Control	1	Adenocarcinoma	H3/N3
	2	Adenocarcinoma	H3/N3
	4	Adenocarcinoma	H3/N3
	6	Adenocarcinoma	H3/N3
	6	Adenocarcinoma	H3/N3
	6	Adenocarcinoma	H3/N3
PEtOx-DOPE	1	Adenocarcinoma	H3/N3
	2	Adenocarcinoma	H3/N3
	3	Adenocarcinoma	H3/N3
	4	Adenocarcinoma	H3/N3
	5	Adenocarcinoma	H3/N3
	6	Adenocarcinoma	H3/N3
Free DOX	1	-	-
	2	-	-
	3	Adenocarcinoma	H3/N3
	4	Adenocarcinoma	H3/N3
	5	Adenocarcinoma	H3/N3
	6	Adenocarcinoma	H3/N3
P18-PEtOxDOPEDOX	1	Adenocarcinoma	H3/N3
	2*	-	-
	3	Adenocarcinoma	H3/N3
	4	Adenocarcinoma	H3/N3
	5	Adenocarcinoma	H3/N3
	6	Adenocarcinoma	H3/N3

* no tumor, only minimal tumor bed was recorded during histopathological analysis

4.9.2. Therapeutic effect of P18-PEtOx-b-PLA-DOX Polymersomes on AU565 Tumor Models

Breast cancer orthotopic models were formed in 6-8 weeks old CD-1 nude female mice and the anti-tumor effect of P18-PEtOx-b-PLA-DOX polymersomes were analyzed as described in Section 3.12. Following fourth day of tumor formation, CD-1 nude female mice were treated intraperitoneally, once in every three days for a total of 8 injections, with PEtOx-b-PLA polymersomes, P18-PEtOx-b-PLA-DOX polymersomes, or DOX, all at the cumulative DOX dose of 1 mg/kg.

The tumor size and weight of each animal was measured before every injection, and mice were examined for morbidity and mortality until 28th day. Figure 4.50 shows the representative pictures captured to show effect of P18-PEtOx-b-PLA-DOX polymersomes on CD-1 nude female mice exhibiting tumor development. All animals (n=6) in vehicle control cohort, developed tumors (Figure 4.50a). The incidence of tumor formation was six out of six animals in the group of mice subjected to empty PEtOx-b-PLA polymersomes and 1 mg/kg of free DOX (Figure 4.50b-c). The incidence of tumor formation was five out of six animals in the group of mice subjected to the treatment of 1 mg/kg of P18-PEtOx-b-PLA-DOX polymersomes (Figure 4.50d).



Figure 4.50. Effect of P18-PEtOx-b-PLA-DOX polymersomes on tumor growth. CD-1 nude female mice were implanted with 8×10^6 AU565 cells. Following the third day of inoculation, animals were divided randomly into four groups ($n=6$) and exposed to vehicle control (PBS), 1 mg/kg P18-PEtOx-b-PLA-DOX polymersomes, 1 mg/kg free DOX, and 1 mg/kg PEtOx-b-PLA polymersomes every three days. Representative pictures of CD-1 nude female mice exhibiting tumor development in mammary pad were shown for (a) Vehicle control cohort, (b) PEtOx-b-PLA polymersomes cohort, (c) Free DOX cohort, and (d) P18-PEtOx-b-PLA-DOX polymersomes cohort.

The body weight of CD-1 nude female mice recorded through 25 days showed that there was no weight loss in vehicle control, PEtOx-b-PLA polymersomes, free DOX, and P18-PEtOx-b-PLA-DOX polymersomes treatment cohorts, thus suggesting tolerable treatment dosage (Figure 4.51).

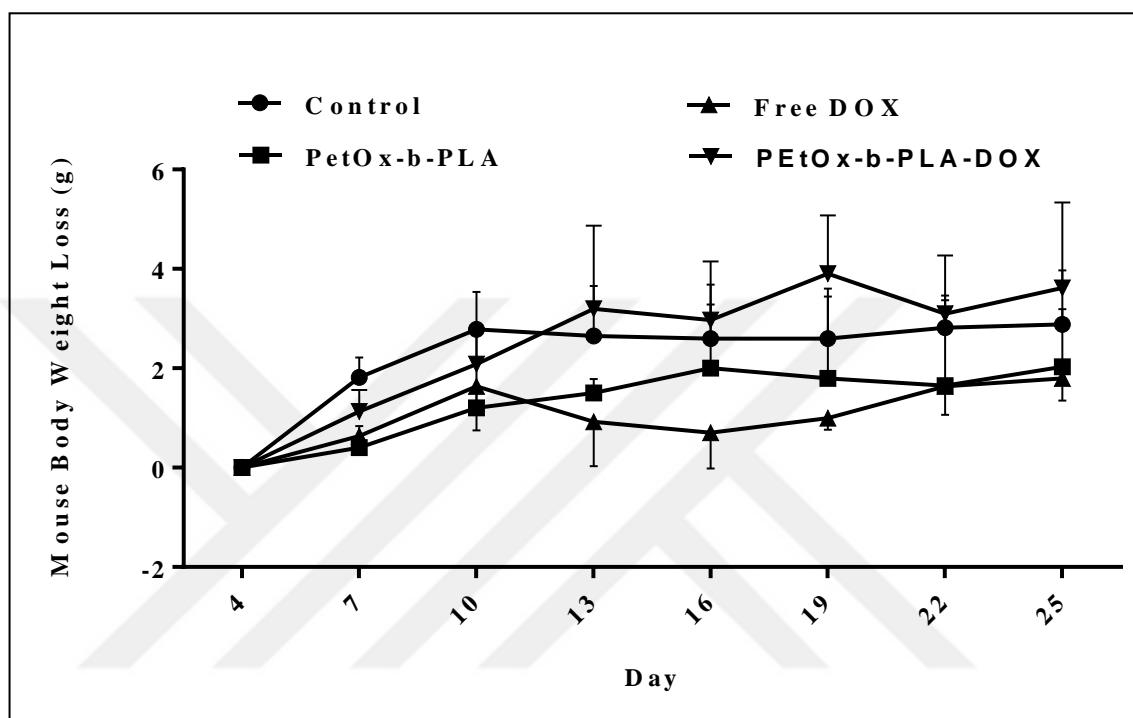


Figure 4.51. Effect of P18-PEtOx-b-PLA-DOX polymersomes on the CD-1 nude mice body weight.

On day 28, sacrifice of animals took place following drug treatment and nine different organs along with tumor tissues were isolated as mentioned earlier (Section 3.12). The images of isolated tumors from animals in vehicle control (PBS), PEtOx-b-PLA polymersomes, free DOX, and P18-PEtOx-b-PLA-DOX polymersomes were given in Figure 4.52a. The average tumor weight was 0.024 g, 0.033 g, 0.013 g, and 0.021 g for the control (PBS), PEtOx-b-PLA polymersomes, free DOX, and P18-PEtOx-b-PLA-DOX polymersomes cohorts, respectively. Treatment with free DOX reduced tumor weight by 46 percent compared to control cohorts. However, treatment with P18-PEtOx-b-PLA-DOX polymersomes showed a decrease ($p > 0.05$) of 4 percent in tumor weight compared to control cohorts (Figure 4.52b). The tumor volume was 31 mm^3 , 25 mm^3 , 20 mm^3 and 8 mm^3 in average for the control (PBS), PEtOx-b-PLA polymersomes, free DOX, and P18-PEtOx-b-PLA-DOX polymersomes cohorts, respectively. A significant decrease of 36

percent and 72 percent was observed in tumor volume of free DOX and P18-PEtOx-b-PLA-DOX polymersomes cohorts, respectively compared to vehicle control cohorts. Interestingly, tumor volume of P18-PEtOx-b-PLA-DOX polymersomes showed a significant decrease of 57 percent compared to free DOX cohorts (Figure 4.52c).

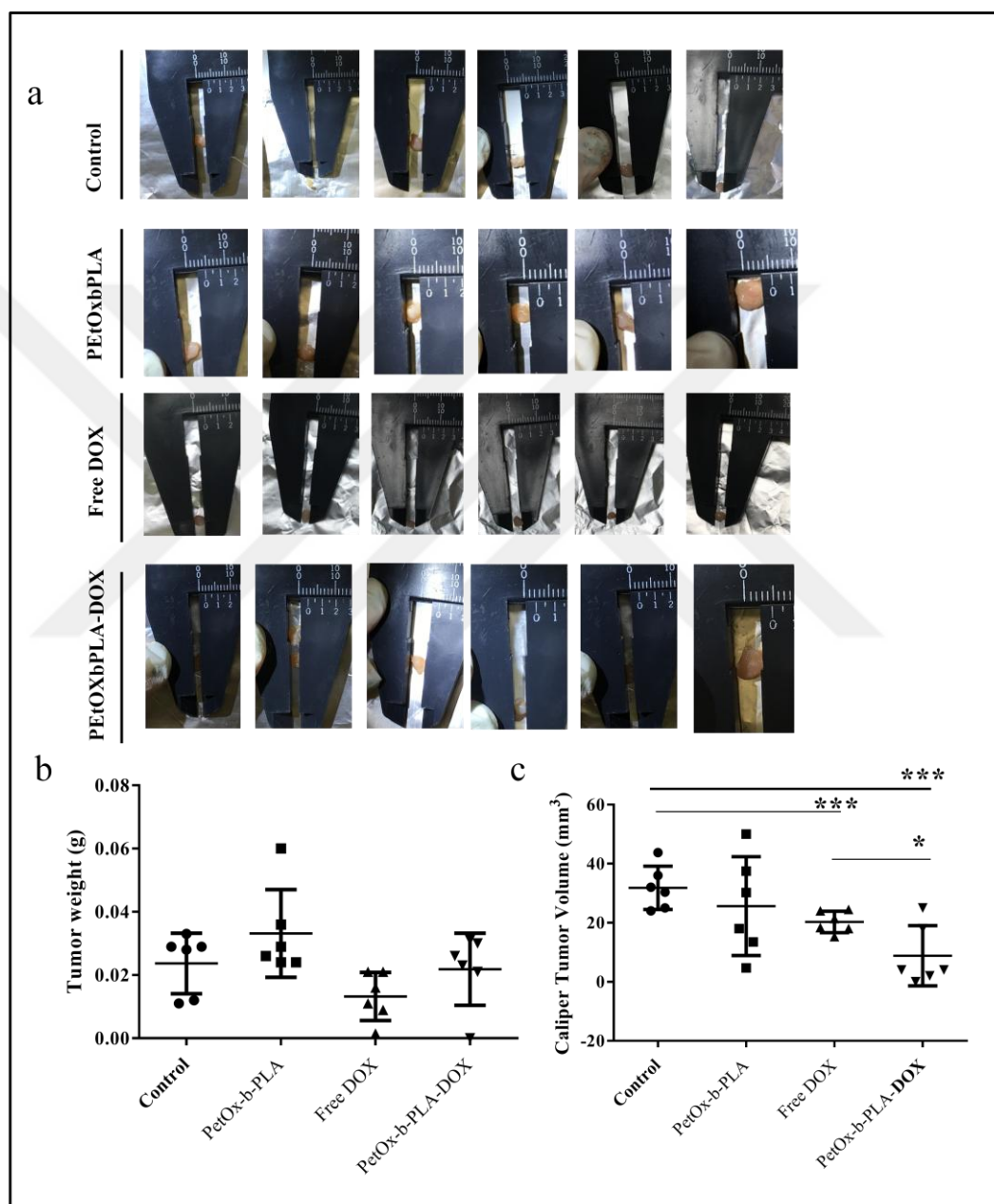


Figure 4.52. Antitumor effect of P18-PEtOx-b-PLA-DOX polymersomes on CD-1 nude mice models. (a) Pictures represent the tumor isolated from CD-1 nude mice in four different groups subjected to treatment with either vehicle control (PBS), or PEtOx-b-PLA polymersomes, or free DOX, or P18-PEtOx-b-PLA-DOX polymersomes. Graph shows the distribution of the isolated (b) Tumor weights and (c) Tumor volumes.

Following sacrifice and tumor isolation of animals, samples were stained by H&E for histopathological analysis (Figure 4.53). The characterization of the isolated tumor tissues of CD-1 nude female mice used in the study was shown in Table 4.3. The characterization of all tumor types as adenocarcinoma confirmed that AU565 orthotopic CD-1 nude mouse models were generated successfully. Histological and nuclear grading of all tumors in four different treatment groups were recorded as Grade 3. Toxicity was not detected from organs (brain, lung, heart, liver, spleen, stomach, intestines, kidney, and ovary) extracted from all four treatment cohorts. All the data given above suggest that P18-PEtOx-b-PLA-DOX polymersomes gave strong anti-tumor response comparable to free DOX. Table 4.3 shows the characterization of the isolated tumor tissues of CD-1 nude female mice used in the study by pathologist.

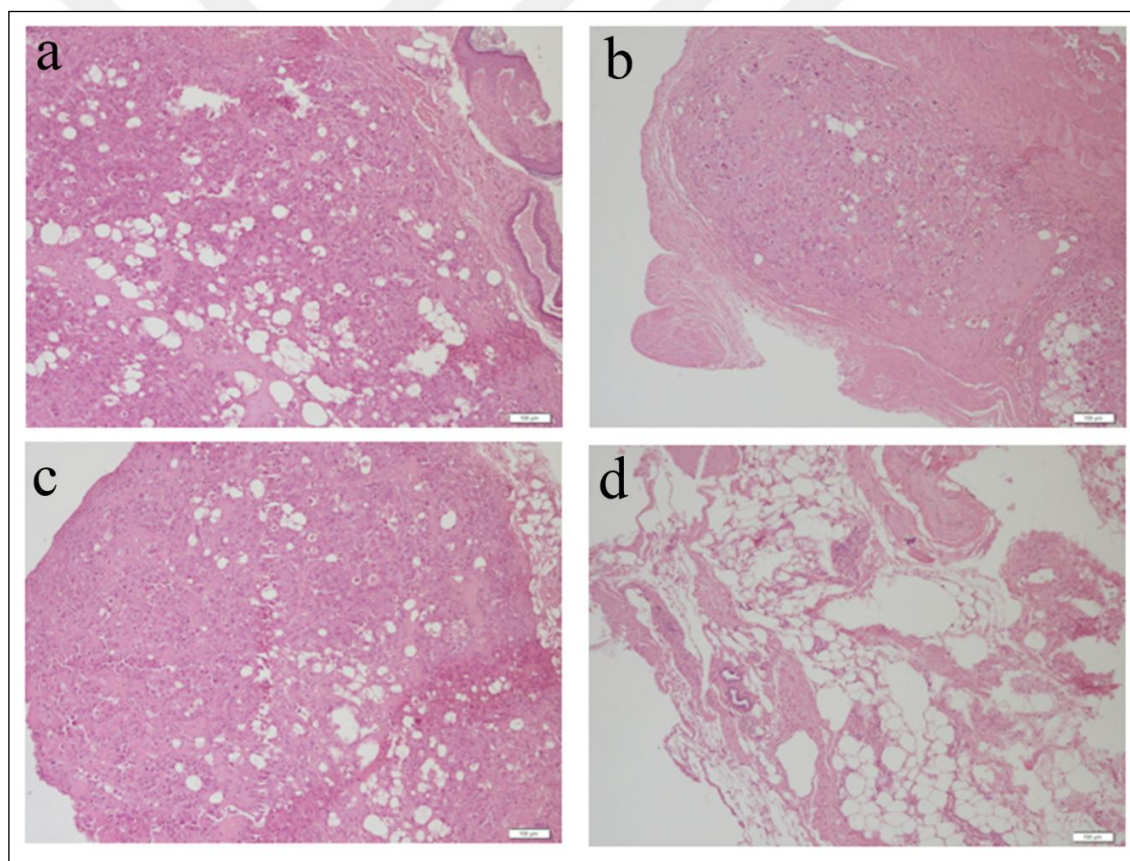


Figure 4.53. Histopathological analysis of the P18-PEtOx-b-PLA-DOX polymersomes tumor samples. H&E staining was used to stain the tumors isolated from CD-1 nude mice in four different groups subjected to treatment of either (a) Vehicle control, (b) free DOX, (c) P18-PEtOx-b-PLA-DOX polymersomes, and (d) PEtOx-b-PLA polymersomes.

Table 4.3. Effect of P18-PEtOx-b-PLA-DOX polymersomes on tumor tissues of CD-1 nude mice used in the study.

	Animal	Tumor Type	Histologic/Nuclear Grading
Control	1	Adenocarcinoma	H3/N3
	2	Adenocarcinoma	H3/N3
	3	Adenocarcinoma	H3/N3
	4	Adenocarcinoma	H3/N3
	5	Adenocarcinoma	H3/N3
	6	Adenocarcinoma	H3/N3
P18-PEtOx-b-PLA	1*	-	-
	2*	-	-
	3	Adenocarcinoma	H3/N3
	4	-	-
	5	Adenocarcinoma	H3/N3
	6	Adenocarcinoma	H3/N3
Free DOX	1	Adenocarcinoma	H3/N3
	2	Adenocarcinoma	H3/N3
	3**	-	-
	4	Adenocarcinoma	H3/N3
	5	Adenocarcinoma	H3/N3
	6	Adenocarcinoma	H3/N3
P18-PEtOx-b-PLA -DOX	1	-	-
	2	-	-
	3	Adenocarcinoma	H3/N3
	4	Adenocarcinoma	H3/N3
	5*	Adenocarcinoma	-
	6	Adenocarcinoma	H3/N3

* no tumor, only minimal tumor bed, ** no tumor but lymph node present

4.9.3. Therapeutic effect of P18-PEtOx-PEI-PCL-DOX Micelles on AU565 Tumor Models

In order to evaluate the therapeutic efficacy of P18-PEtOx-PEI-PCL-DOX (PPP30-DOX) micelles, breast cancer orthotopic models were formed in 6-8 weeks old CD-1 nude female mice as mentioned earlier in Section 3.12. CD-1 nude female mice bearing disseminated AU565 orthotopic tumors were treated intraperitoneally, once in every three days for a total of 8 injections, with empty PEtOx-PEI-PCL micelles, P18-PEtOx-PEI-PCL-DOX micelles, or DOX, all at the cumulative DOX dose of 1 mg/kg. The tumor size and weight of each animal was measured before every injection, and mice were examined for morbidity and mortality until sacrifice day (28th).

Figure 4.54 shows the representative pictures of CD-1 nude female mice, where the tumor development was recorded in vehicle control (PBS), PEtOx-PEI-PCL 0 micelles, free DOX, and P18-PEtOx-PEI-PCL-DOX micelles. All animals (n=6) in vehicle control cohort receiving PBS, and empty PEtOx-PEI-PCL micelles developed tumors (Figure 4.54a-b). The incidence of tumor formation was six out of six animals in the group of mice subjected to 1 mg/kg of free DOX (Figure 4.54c), likewise six out of six animals in the group of mice subjected to the treatment of 1 mg/kg P18-PEtOx-PEI-PCL-DOX micelles (Figure 4.54d).

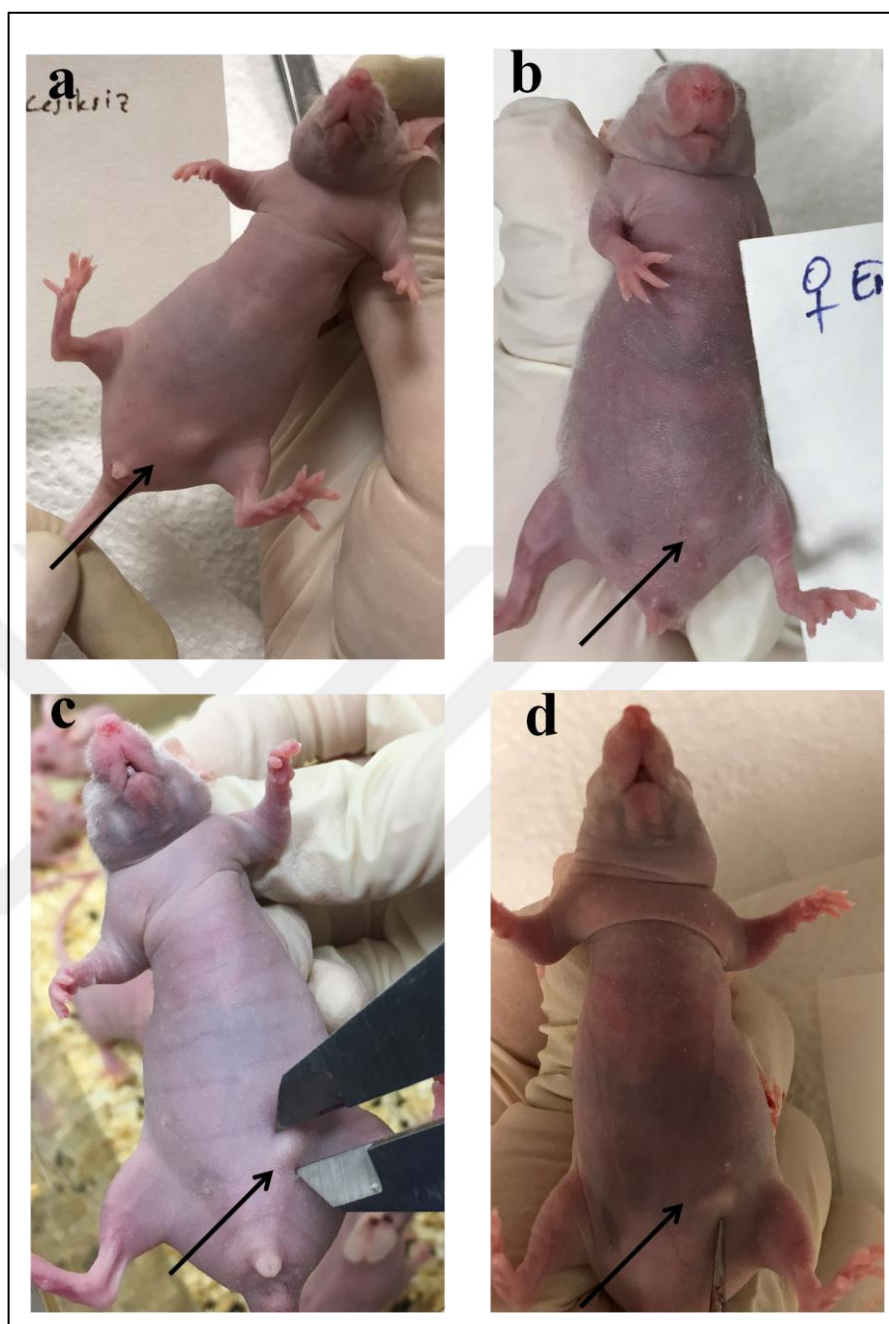


Figure 4.54. Effect of P18-PEtOx-PEI-PCL-DOX micelles on tumor growth. CD-1 nude female mice were implanted with 8×10^6 AU565 cells. Following the third day of inoculation, animals were divided randomly into four groups (n=6) and exposed to vehicle control (PBS), 1 mg/kg P18-PEtOx-PEI-PCL-DOX micelles, 1 mg/kg free DOX, and 1 mg/kg empty PPP micelles every three days. Representative pictures of CD-1 nude female mice exhibiting tumor development in mammary pad were shown for (a) Vehicle control cohort, (b) Empty PEtOx-PEI-PCL micelles cohort, (c) Free DOX cohort, and (d) P18-PEtOx-PEI-PCL-DOX micelles cohort.

The body weight of CD-1 nude female mice recorded through 25 days showed that there was no weight loss in vehicle control, empty PEtOx-PEI-PCL micelles, free DOX, P18-PEtOx-PEI-PCL-DOX micelles treatment cohorts suggesting tolerable treatment dosage (Figure 4.55).

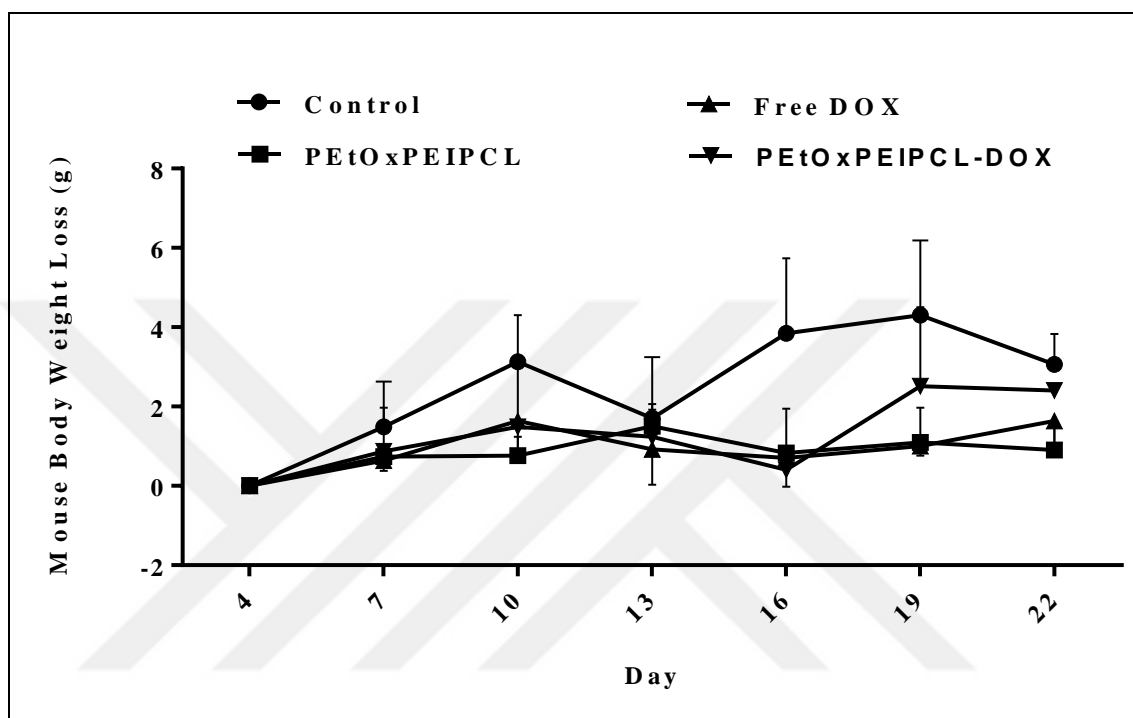


Figure 4.55. Effect of P18-PEtOx-PEI-PCL-DOX micelles on the CD-1 nude mice body weight.

On day 28, sacrifice of animals took place following drug treatment and nine different organs along with tumor tissues were isolated as mentioned earlier (Section 3.12). The isolated tumors from animals in vehicle control (PBS), PEtOx-PEI-PCL micelles, free DOX, and P18-PEtOx-PEI-PCL-DOX micelles was given in Figure 4.56a. The average tumor weight was 0.028 g, 0.0045 g, 0.013 g, and 0.013 g for the control (PBS), PPP30 micelles, free DOX, and P18-PEtOx-PEI-PCL-DOX micelle cohorts, respectively. Treatment with free DOX, empty PEtOx-PEI-PCL micelles, and P18-PEtOx-PEI-PCL-DOX micelles reduced tumor weight by 52.5 percent, 53.6 percent, and 84 percent compared to control cohorts, respectively (Figure 4.56b). The tumor volume was 25.8 mm³, 5.5 mm³, 20.3 mm³, 5.6 mm³, in average for the control (PBS), empty PEtOx-PEI-PCL micelles, free DOX, and P18-PEtOx-PEI-PCL-DOX micelle cohorts, respectively. Thus, treatment with free DOX, PEtOx-PEI-PCL micelles, and P18-PEtOx-PEI-PCL-DOX

micelles reduced tumor volume by 21 percent, 78.5 percent, and 64 percent compared to control cohorts, respectively. Interestingly, there was a significant decrease of 54.4 percent and 72.9 percent in P18-PEtOx-PEI-PCL-DOX and PEtOx-PEI-PCL micelle cohorts compared to free DOX cohorts (Figure 4.56c).

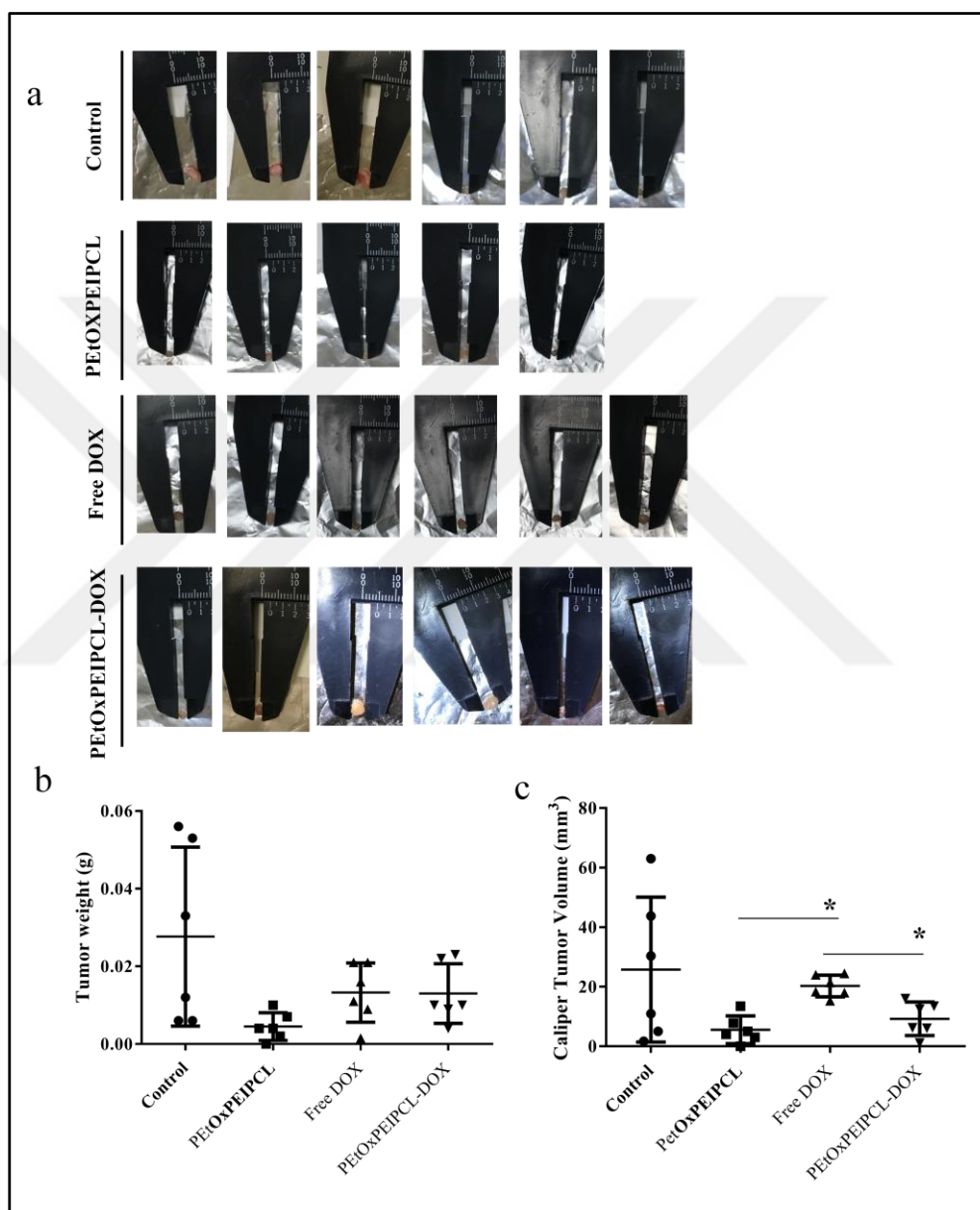


Figure 4.56. Antitumor effect of P18-PEtOx-PEI-PCL -DOX micelles on CD-1 nude mice models. (a) Pictures represent the tumor isolated from CD-1 nude mice in four different groups subjected to treatment with either vehicle control (PBS), or PEtOx-PEI-PCL micelles, or free DOX, or P18 PEtOx-PEI-PCL -DOX micelles. Graph shows the distribution of the isolated (b) Tumor weights and (c) Tumor volumes.

Following sacrifice and tumor isolation of animals, samples were stained by H&E for histopathological analysis (Figure 4.57). All tumor types were characterized as adenocarcinoma, verifying AU565 orthotopic CD-1 nude mouse models were generated successfully. Histological and nuclear grading of all tumors in four different treatment groups were recorded as Grade 3. Toxicity was not detected from organs (brain, lung, heart, liver, spleen, stomach, intestines, kidney, and ovary) extracted from all four treatment cohorts. All the data given above suggest that P18-PEtOx-PEI-PCL-DOX micelles gave strong anti-tumor response comparable to free DOX. Table 4.4 shows the characterization of the isolated tumor tissues of CD-1 nude female mice used in the study by pathologist.

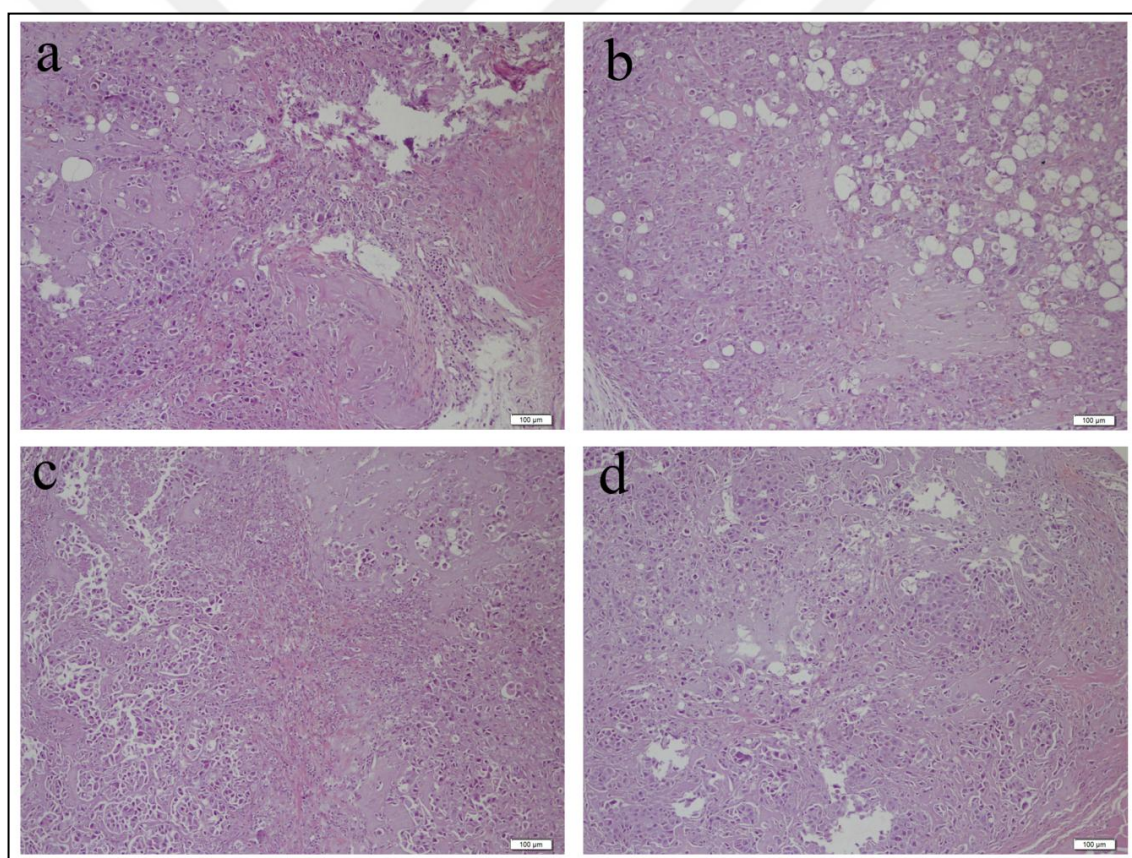


Figure 4.57. Histopathological analysis of the P18-PEtOx-PEI-PCL-DOX micelles tumor samples. H&E staining was used to stain the tumors isolated from CD-1 nude mice in four different groups subjected to treatment of either (a) Vehicle control, (b) free DOX, (c) P18-PEtOx-PEI-PCL-DOX micelle, and (d) Empty PEtOx-PEI-PCL micelles.

Table 4.4. Effect of P18-PEtOx-PEI-PCL-DOX micelles on tumor tissues of CD-1 nude mice used in the study.

	Animal	Tumor Type	Histologic/Nuclear Grading
Control	1	Adenocarcinoma	H3/N3
	2	Adenocarcinoma	H3/N3
	3	Adenocarcinoma	H3/N3
	4	Adenocarcinoma	H3/N3
	5	Adenocarcinoma	H3/N3
	6	Adenocarcinoma	H3/N3
PEtOx-PEI-PCL	1	Adenocarcinoma	H3/N3
	2*	-	-
	3	Adenocarcinoma	H3/N3
	4	Adenocarcinoma	H3/N3
	5	Adenocarcinoma	H3/N3
	6	Adenocarcinoma	H3/N3
Free DOX	1	Adenocarcinoma	H3/N3
	2	Adenocarcinoma	H3/N3
	3**	-	-
	4	Adenocarcinoma	H3/N3
	5	Adenocarcinoma	H3/N3
	6	Adenocarcinoma	H3/N3
P18-PEtOx-PEI-PCL-DOX	1	Adenocarcinoma	H3/N3
	2	Adenocarcinoma	H3/N3
	3	Adenocarcinoma	H3/N3
	4	Adenocarcinoma	H3/N3
	5	Adenocarcinoma	H3/N3
	6	Adenocarcinoma	H3/N3

* No tumor, ** No tumor but lymph node is present

4.9.4. Therapeutic effect of P18-PEtOx-DOPE-BikDD Liposomes on AU565 Tumor Models

Breast cancer orthotopic models were formed in 6-8 weeks old CD-1 nude female mice and the anti-tumor effect of P18-PEtOx-DOPE-BikDD liposomes were analyzed as mentioned earlier (Section 3.12). CD-1 nude female mice bearing disseminated AU565 (8×10^6 cells) orthotopic tumors, following fourth day of tumor formation, were treated intraperitoneally with PEtOx-DOPE liposomes, P18-PEtOx-DOPE-BikDD liposomes, or 5 μg of naked BikDD gene once in every three days for a total of 8 injections. The animals were examined for morbidity and mortality until sacrifice day (28th).

Figure 4.58 shows the representative pictures of the effect of P18-PEtOx-DOPE-BikDD liposomes on CD-1 nude female mice exhibiting tumor development. All animals (n=5) in all cohorts developed tumors.

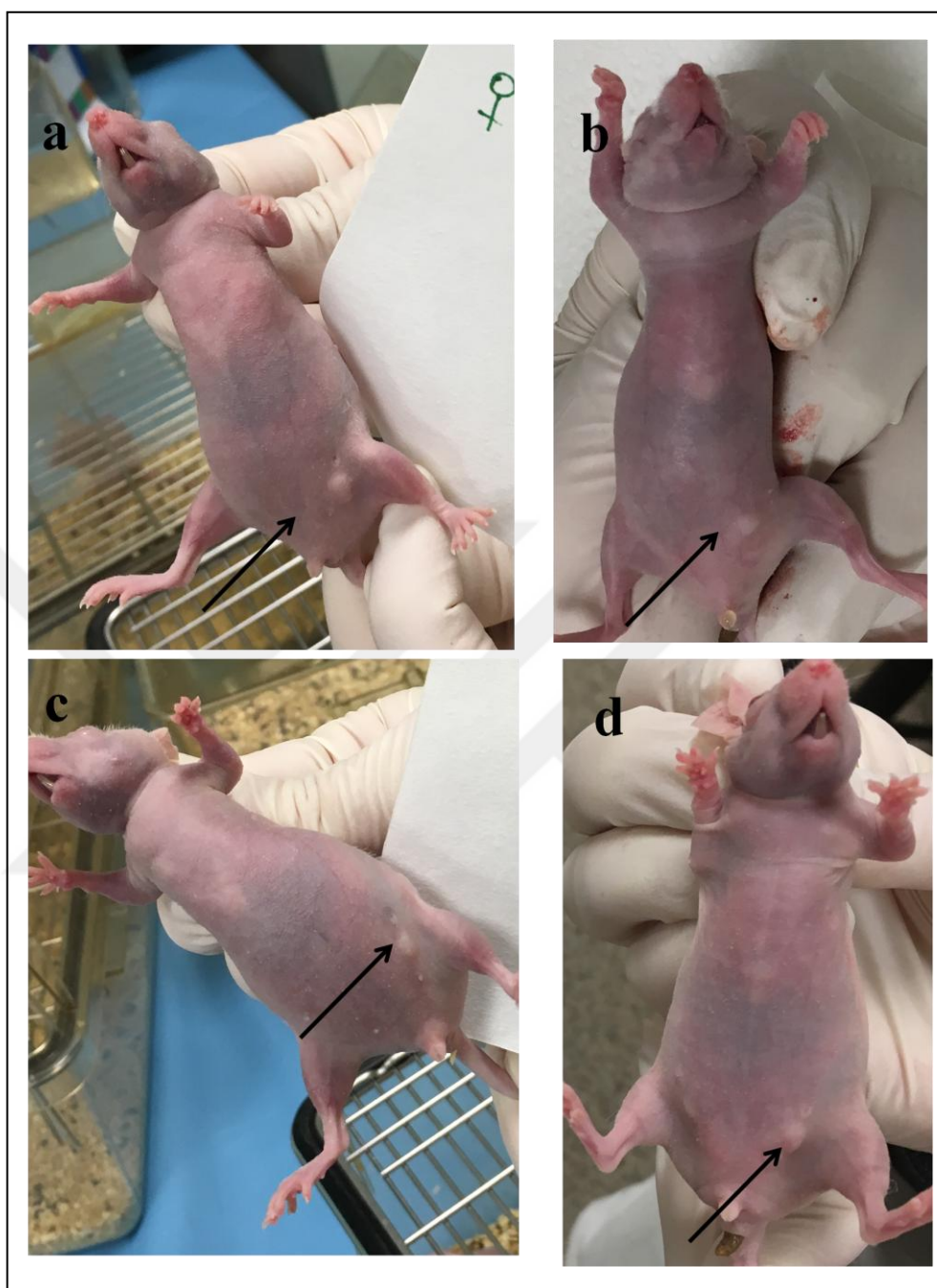


Figure 4.58. Effect of P18-PEtOx-DOPE-BikDD liposomes on tumor growth. CD-1 nude female mice were implanted with AU565 (8×10^6) cells. Following the third day of inoculation, animals were divided randomly into four groups ($n=5$) and exposed to vehicle control (PBS), 5 μg of BikDD in P18-PEtOx-DOPE-BikDD liposomes, 5 μg of naked BikDD gene, and 5 μg of empty PEtOx-DOPE liposomes every three days. Representative pictures of CD-1 nude female mice exhibiting tumor development in mammary pad were shown for (a) Vehicle control cohort, (b) PEtOx-DOPE liposomes cohort, (c) Naked BikDD gene cohort, and (d) P18-PEtOx-DOPE-BikDD liposomes cohort.

The body weight of CD-1 nude female mice recorded on the 5th and 7th injections showed that there was no weight loss in vehicle control, P18-PEtOx-DOPE-BikDD liposomes, naked BikDD gene, and empty PEtOx-DOPE liposomes treatment groups, suggesting tolerable treatment dosage (Figure 4.59).

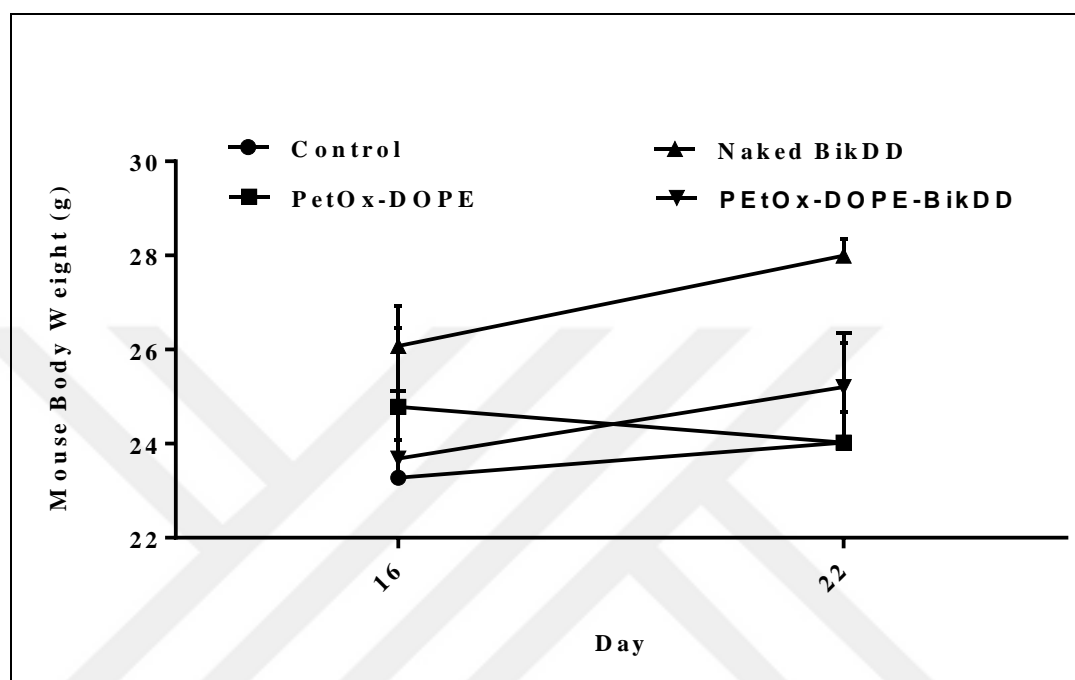


Figure 4.59. Effect of P18-PEtOx-DOPE-BikDD liposomes on the CD-1 nude mice body weight.

On day 28, sacrifice of animals took place following the drug treatments and nine different organs along with tumor tissues were isolated as mentioned earlier (Section 3.12). The images of isolated tumors from animals in vehicle control (PBS), PEtOx-DOPE liposomes, naked BikDD gene, and empty PEtOx-DOPE liposomes cohorts were given in Figure 4.60a. The average tumor weight was 0.02 g, 0.011 g, 0.0314 g, 0.001 g for control (PBS), empty PEtOx-DOPE liposomes, naked BikDD gene, and P18-PEtOx-DOPE-BikDD liposomes cohorts, respectively. Treatment with PEtOx-DOPE liposomes and P18-PEtOx-DOPE-BikDD liposomes reduced ($p > 0.05$) tumor weight by 48 percent and 49 percent, respectively compared to control cohorts. On the contrary, treatment with naked BikDD gene had shown a 32 percent increase ($p > 0.05$) in tumor weight compared to control cohorts (Figure 4.60b). The tumor volume was 15.9 mm^3 , 15.8 mm^3 , 18.5 mm^3 , and 12.7 mm^3 for control (PBS), empty PEtOx-DOPE liposomes, naked BikDD gene, and P18-PEtOx-DOPE-BikDD liposomes cohorts, respectively. A decrease ($p > 0.05$) of 20

percent was observed in tumor volume of P18-PEtOx-DOPE-BikDD liposomes cohorts compared to vehicle control cohorts, while an increase ($p>0.05$) of 14 percent was observed in tumor volume of naked BikDD gene cohorts compared to vehicle control cohorts (Figure 4.60c).

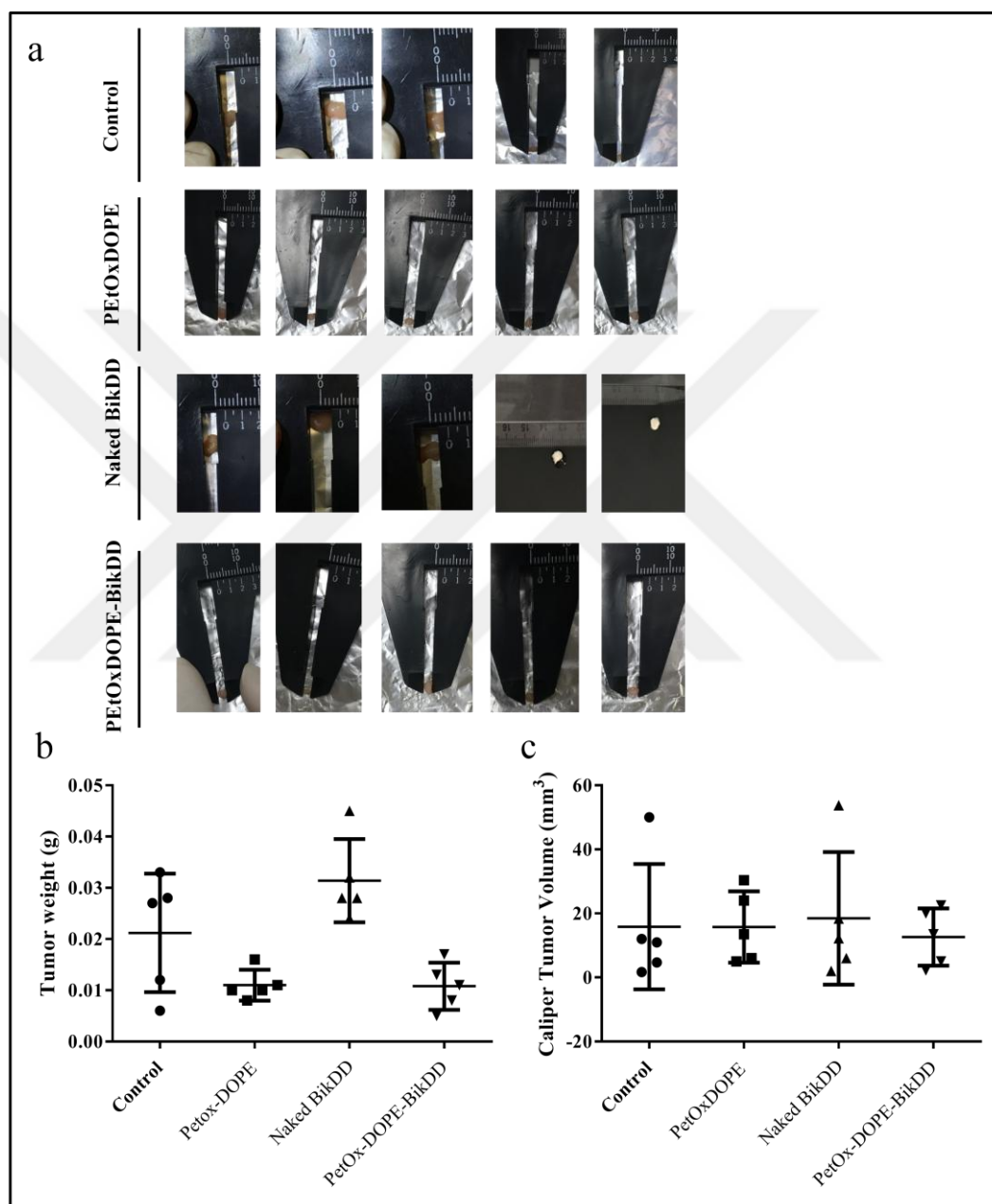


Figure 4.60. Antitumor effect of P18-PEtOx-DOPE-BikDD liposomes on CD-1 nude mice models. (a) Pictures represent the tumor isolated from CD-1 nude mice in four different groups subjected to treatment with either vehicle control (PBS), or PEtOx-DOPE liposomes, or naked BikDD, or P18- PEtOx-DOPE-BikDD liposomes. Graph shows the distribution of the isolated (b) Tumor weights and (c) Tumor volumes.

Following sacrifice and tumor isolation of animals, samples were stained by H&E for histopathological analysis (Figure 4.61). All tumor types were characterized as adenocarcinoma, verifying AU565 orthotopic CD-1 nude mouse models were generated successfully. Histological and nuclear grading of all tumors in four different treatment groups were recorded as Grade 3. Toxicity was not detected from organs (brain, lung, heart, liver, spleen, stomach, intestines, kidney, and ovary) extracted from all four treatment cohorts. The characterization of the isolated tumor tissues of CD-1 nude female mice from histopathological analysis was shown in Table 4.5.

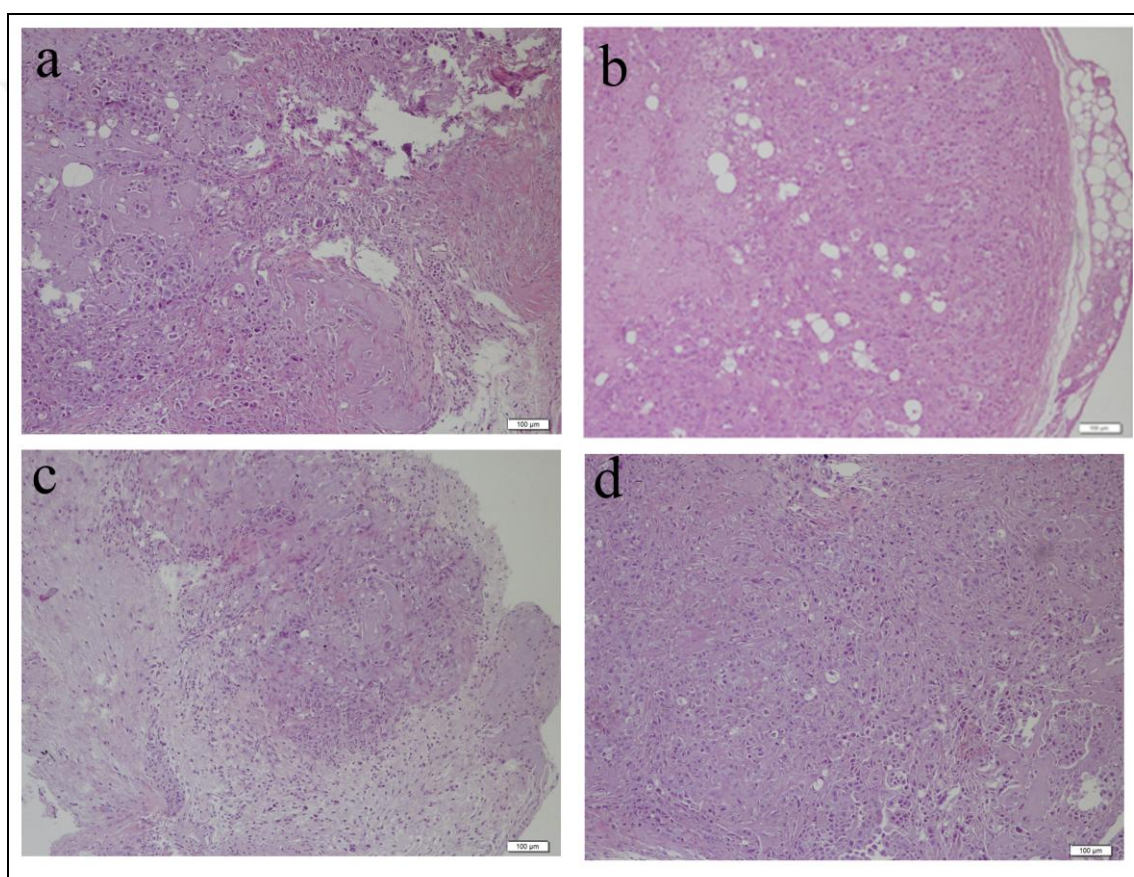


Figure 4.61. Histopathological analysis of the tumor samples of P18-PEtOx-DOPE-BikDD liposomes. H&E staining was used to stain the tumors isolated from CD-1 nude mice in four different groups subjected to treatment of either (a) Vehicle control, (b) Naked BikDD gene, (c) P18-PEtOx-DOPE-BikDD liposomes, and (d) Empty PEtOx-DOPE liposomes.

Table 4.5. Effect of P18-PEtOx-DOPE-BikDD liposomes on tumor tissues of CD-1 nude mice used in the study.

	Animal	Tumor Type	Histologic/Nuclear Grading
Control	1	Adenocarcinoma	H3/N3
	2	Adenocarcinoma	H3/N3
	3	Adenocarcinoma	H3/N3
	4	Adenocarcinoma	H3/N3
	5	Adenocarcinoma	H3/N3
PEtOx-DOPE	1	Adenocarcinoma	H3/N3
	2	Adenocarcinoma	H3/N3
	3	Adenocarcinoma	H3/N3
	4	Adenocarcinoma	H3/N3
	5	Adenocarcinoma	H3/N3
Naked BikDD gene	1	Adenocarcinoma	H3/N3
	2	Adenocarcinoma	H3/N3
	3	Adenocarcinoma	H3/N3
	4	Adenocarcinoma	H3/N3
	5	Adenocarcinoma	H3/N3
P18-PEtOx-DOPE- BikDD	1	Adenocarcinoma	H3/N3
	2	Adenocarcinoma	H3/N3
	3	Adenocarcinoma	H3/N3
	4	Adenocarcinoma	H3/N3
	5	Adenocarcinoma	H3/N3

All the data given above suggest that P18-PEtOx-DOPE-BikDD liposomes did not give a strong anti-tumor response in in vivo studies.

4.9.5. Therapeutic effect of P18-PEtOx-b-PLA-BikDD Polymersome on AU565 Tumor Models

In order to evaluate the therapeutic efficacy of P18-PEtOx-b-PLA-BikDD polymersome, breast cancer orthotopic models were formed in 6-8 weeks old CD-1 female nude mice as mentioned in Section 3.12. CD-1 nude female mice bearing disseminated AU565 (8×10^6 cells) orthotopic tumors were treated intraperitoneally, once in every three days for a total of 8 injections, with either empty PEtOx-b-PLA polymersomes, 5 μ g of naked BikDD gene, or 5 μ g of BikDD in P18-PEtOx-b-PLA-BikDD polymersome. The weight of each animal was measured only twice (fifth and seventh injection) during the experiment, as the treatment was done at fixed dosage; 5 μ g of BikDD gene. All animals were examined for morbidity and mortality until sacrifice day (28th).

Figure 4.62 shows the representative pictures of CD-1 nude female mice exhibiting tumor development. Following the third day of inoculation, animals were divided randomly into four groups (n=5) and exposed to vehicle control (PBS), 5 μ g of BikDD in P18-PEtOx-b-PLA-BikDD polymersome, 5 μ g of naked BikDD gene, and empty PEtOx-b-PLA polymersome every three days. All animals (n=5) in vehicle control cohort receiving PBS developed tumors (Figure 4.62a). Like wise, all animals (n=5) in empty PEtOx-b-PLA polymersome, naked BikDD gene and P18-PEtOx-b-PLA-BikDD polymersome cohorts also developed tumors (Figure 4.62b-d).

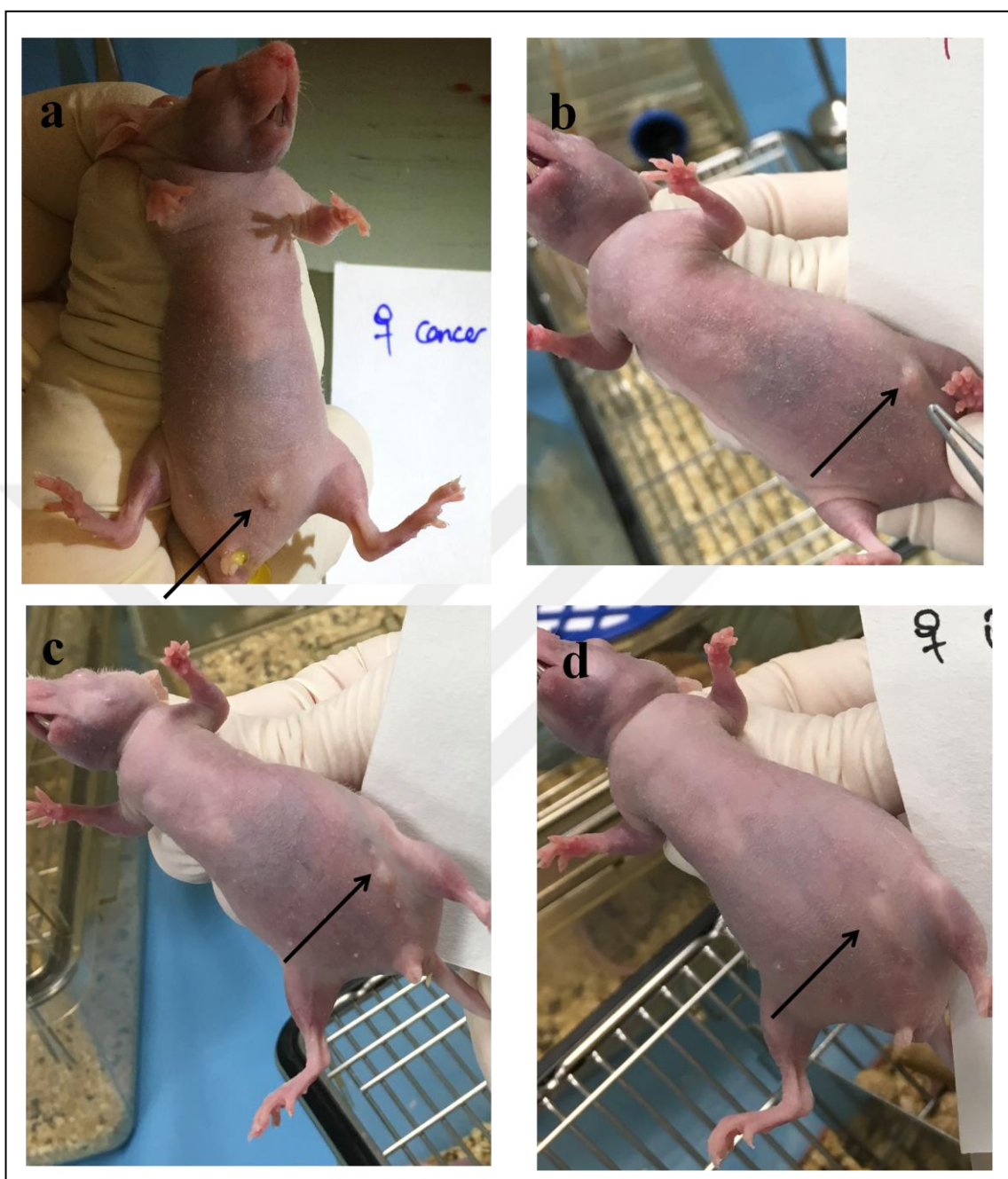


Figure 4.62. Effect of P18-PEtOx-b-PLA-BikDD polymersome on tumor growth. CD-1 nude female mice were implanted with 8×10^6 AU565 cells. Following the third day of inoculation, animals were divided randomly into four groups ($n=5$) and exposed to vehicle control (PBS), 5 μg of BikDD in P18-PEtOx-b-PLA-BikDD polymersome, 5 μg of naked BikDD gene, and empty PEtOx-b-PLA polymersome every three days. Representative pictures of CD-1 nude female mice exhibiting tumor development in mammary pad were shown for (a) Vehicle control cohort, (b) Empty PEtOx-b-PLA polymersome cohort, (c) Naked BikDD gene cohort, and (d) P18-PEtOx-b-PLA-BikDD polymersome cohort.

The body weight of CD-1 nude mice recorded before 5th and 7th injections which were on day 16 and day 22, respectively, showed no weight loss in vehicle control cohorts, empty PEtOx-b-PLA polymersome cohorts, naked BikDD gene cohorts, and P18-PEtOx-b-PLA-BikDD polymersome cohorts (Figure 4.63). This suggested that the chosen dosage was tolerable to all the animals.

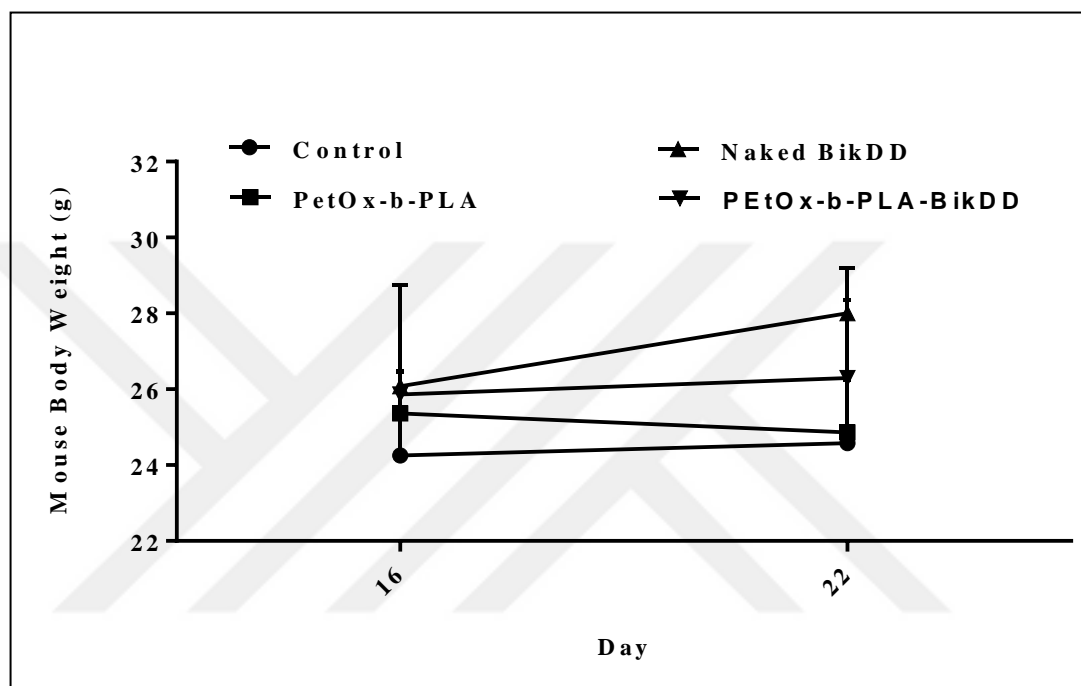


Figure 4.63. Effect of P18-PEtOxbPLA-BikDD polymersome on CD-1 nude mice body weight.

On day 28, sacrifice of animals took place following treatment and nine different organs along with tumor tissues were isolated as mentioned earlier (Section 3.12). The isolated tumors from animals in vehicle control (PBS), empty PEtOx-b-PLA polymersome, naked BikDD gene, and P18-PEtOx-b-PLA-BikDD polymersome was given in Figure 4.64a. The average tumor weight was 0.029 g, 0.0278 g, 0.0314 g, and 0.0296 g for the control (PBS), empty PEtOx-b-PLA polymersome, naked BikDD gene, and P18-PEtOx-b-PLA-BikDD polymersome cohorts, respectively. Treatment with naked BikDD gene, and P18-PEtOx-b-PLA-BikDD polymersome increased tumor weight by 8 percent and 2 percent, while treatment with empty PEtOx-b-PLA polymersome decreased ($p > 0.05$) tumor weight by 4 percent compared to control cohorts (Figure 4.64b). The tumor volume was 27.3 mm³, 24.7 mm³, 18.47 mm³, 6.6 mm³ in average for the control (PBS), empty PEtOx-b-PLA polymersome, naked BikDD gene, and P18-PEtOx-b-PLA-BikDD

polymersome cohorts, respectively. Thus, treatment with naked BikDD gene, empty PEtOx-b-PLA polymersome, and P18-PEtOx-b-PLA-BikDD polymersome decreased ($p>0.05$) tumor volume by 32 percent, 9 percent, 75 percent compared to control cohorts, respectively. Interestingly, there was decrease of 64 percent in P18-PEtOx-b-PLA-BikDD polymersome compared to naked BikDD gene cohorts (Figure 4.64c).

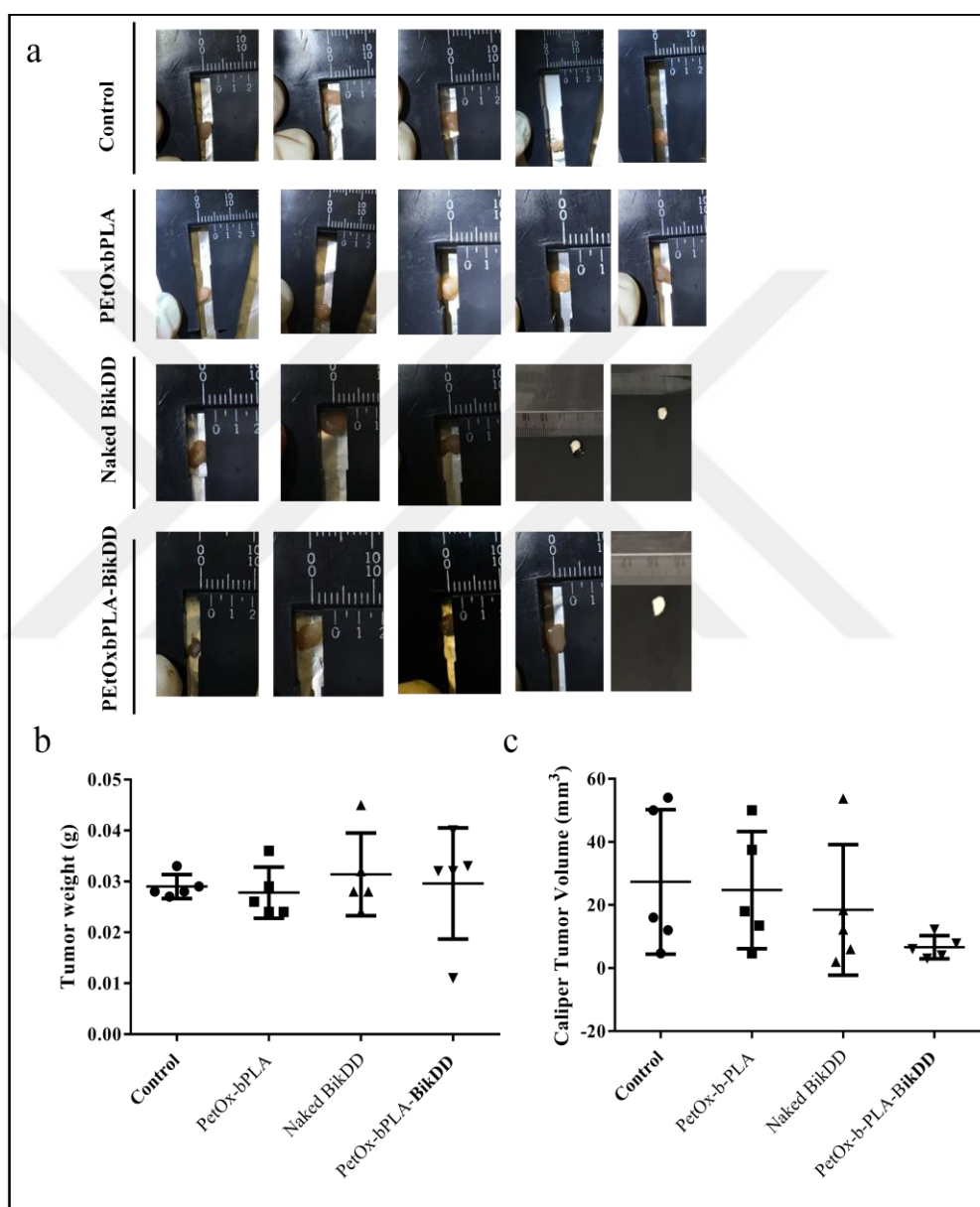


Figure 4.64. Antitumor effect of P18-PEtOx-b-PLA-BikDD polymersome on CD-1 nude mice models. (a) Pictures represent the tumor isolated from CD-1 nude mice in four different groups subjected to treatment with either vehicle control (PBS), or PEtOx-b-PLA polymersome, or naked BikDD, or P18-PEtOx-b-PLA-BikDD polymersome. Graph shows the distribution of the isolated (b) Tumor weights and (c) Tumor volumes.

Following sacrifice and tumor isolation of animals, samples were stained by H&E for histopathological analysis (Figure 4.65). The characterization of the isolated tumor tissues of CD-1 nude female mice used in the study was shown in Table 4.6. All tumor types were characterized as adenocarcinoma, verifying AU565 orthotopic CD-1 nude mouse models were generated successfully. Histological and nuclear grading of all tumors in four different treatment groups were recorded as Grade 3. Toxicity was not detected from organs (brain, lung, heart, liver, spleen, stomach, intestines, kidney, and ovary) extracted from all four treatment cohorts. All the data given above suggest that P18-PEtOx-b-PLA-BikDD polymersome did not give an anti-tumor response comparable to naked BikDD gene.

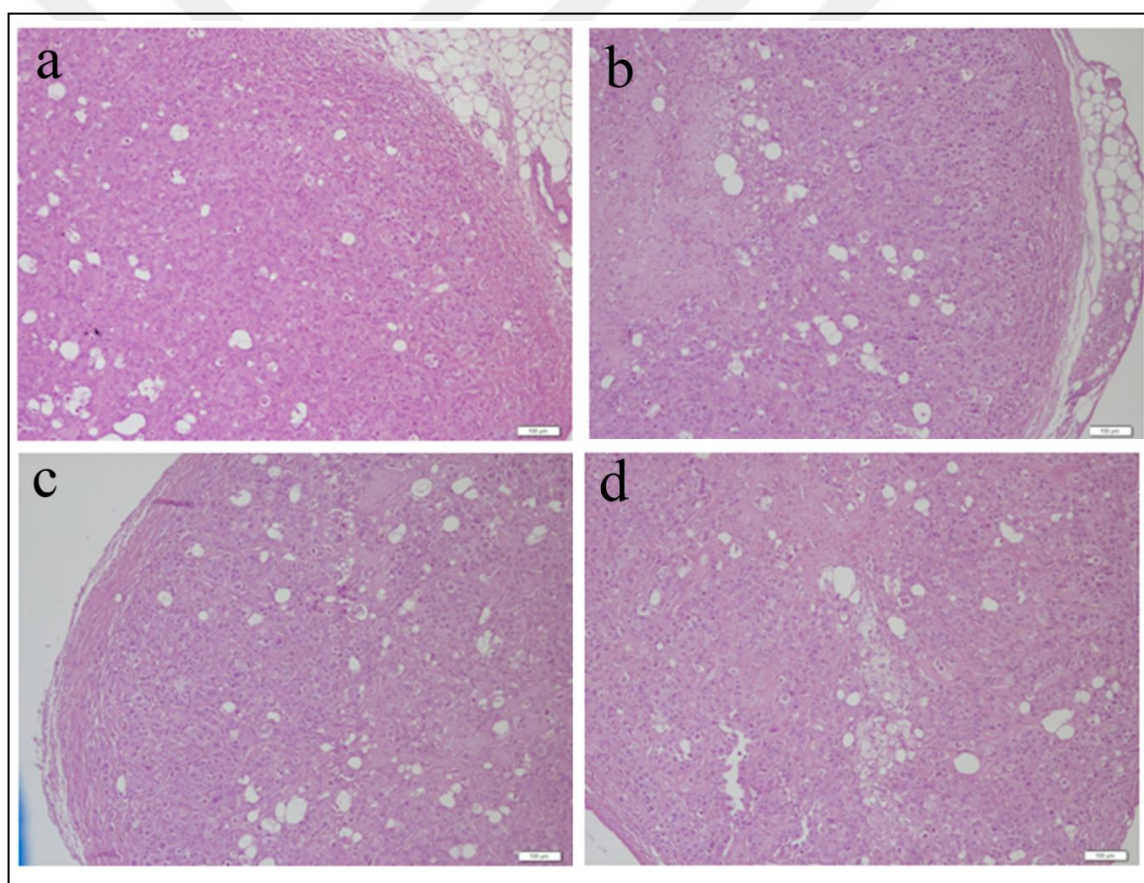


Figure 4.65. Histopathological analysis of the tumor samples of P18-PEtOx-b-PLA-BikDD polymersome. H&E staining was used to stain the tumors isolated from CD-1 nude mice in four different groups subjected to treatment of either (a) Vehicle control, (b) Naked BikDD gene, (c) P18-PEtOx-b-PLA-BikDD polymersomes, and (d) Empty PEtOx-b-PLA polymersomes.

Table 4.6. Effect of P18-PEtOx-b-PLA-BikDD polymersomes on tumor tissues of CD-1 nude mice used in the study.

	Animal	Tumor Type	Histologic/Nuclear Grading
Control	1	Adenocarcinoma	H3/N3
	2	Adenocarcinoma	H3/N3
	3	Adenocarcinoma	H3/N3
	4	Adenocarcinoma	H3/N3
	5	Adenocarcinoma	H3/N3
PEtOx-b-PLA	1	Adenocarcinoma	H3/N3
	2	Adenocarcinoma	H3/N3
	3	Adenocarcinoma	H3/N3
	4*	-	-
	5	Adenocarcinoma	H3/N3
Naked BikDD gene	1	Adenocarcinoma	H3/N3
	2	Adenocarcinoma	H3/N3
	3**	-	-
	4	Adenocarcinoma	H3/N3
	5	Adenocarcinoma	H3/N3
P18-PEtOx-b-PLA-BikDD	1	Adenocarcinoma	H3/N3
	2	Adenocarcinoma	H3/N3
	3	Adenocarcinoma	H3/N3
	4	Adenocarcinoma	H3/N3
	5	Adenocarcinoma	H3/N3

4.9.6. Therapeutic effect of P18-PEtOx-PEI-PCL-BikDD Micelles on AU565 Tumor Models

Based on the promising results from *in vitro* experiments, the *in vivo* antitumor efficacy was further investigated on CD-1 nude female mice bearing human breast tumors (8×10^6 AU565 cells). Following the third day of inoculation, the treatment was done by intravenously injecting PBS, naked BikDD gene, 8 μ g of BikDD in P18-PEtOx-PEI-PCL-BikDD micelles and empty PEtOx-PEI-PCL micelles into tumor bearing mice, every three days for a total of 8 injections as mentioned in Section 3.12. All mice were alive during the whole period of the experiment.

Figure 4.66 shows the representative pictures of CD-1 nude female mice, where the tumor development was recorded in vehicle control (PBS), PEtOx-PEI-PCL micelles, naked BikDD gene, and P18-PEtOx-PEI-PCL-BikDD micelles. All animals (n=6) in vehicle control cohort receiving PBS.

The body weight of CD-1 nude mice recorded before 5th and 7th injections which were on day 16 and day 22, respectively. There was no weight loss in vehicle control cohorts, empty PEtOx-PEI-PCL micelle cohorts, naked BikDD gene cohorts, and P18-PEtOx-PEI-PCL-BikDD micelle cohorts, indicating that the chosen dosage was tolerable to all the animals (Figure 4.67).

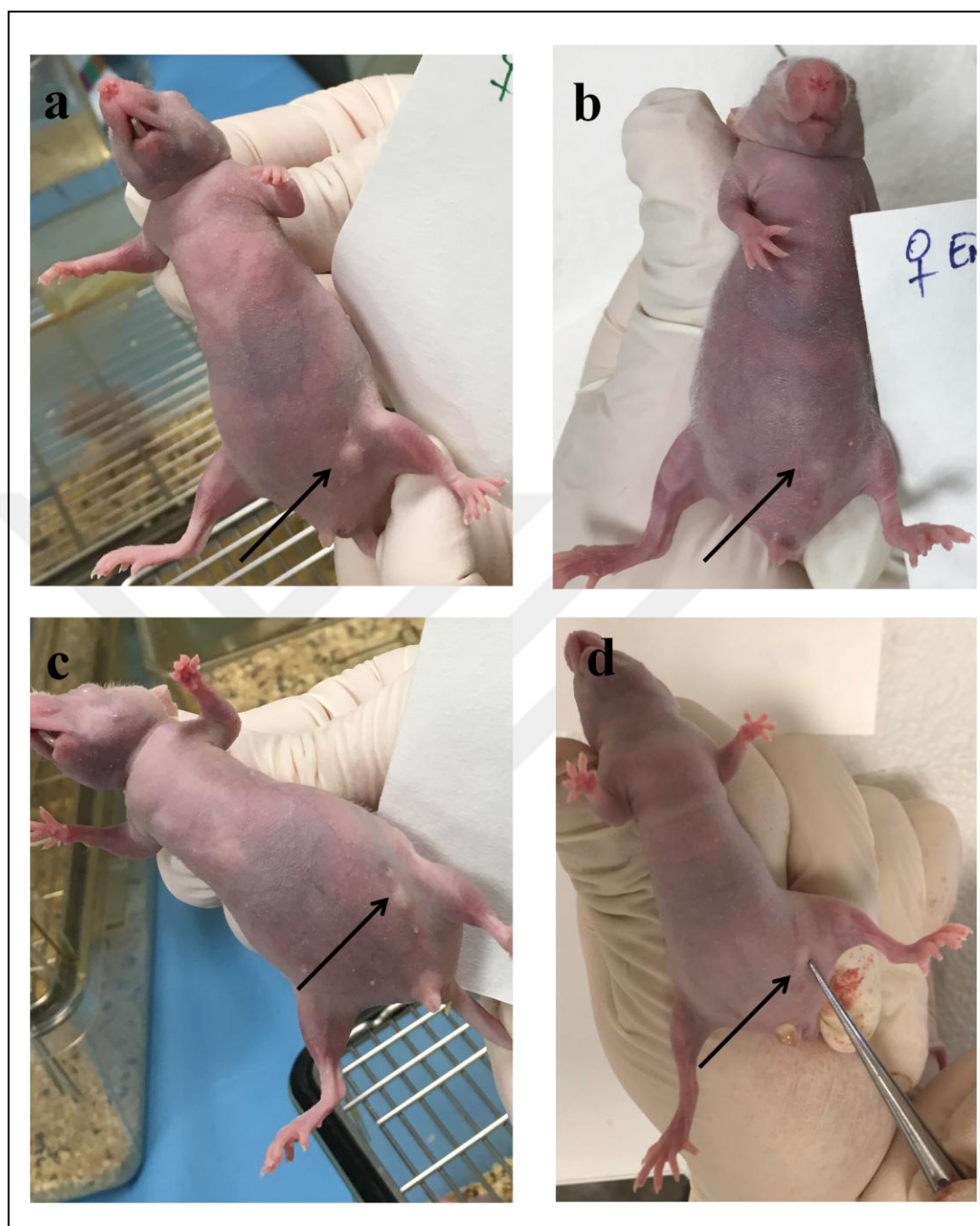


Figure 4.66. Effect of P18-PEtOx-PEI-PCL-BikDD micelles on tumor growth. CD-1 nude female mice were implanted with 8×10^6 AU565 cells. Following the third day of inoculation, animals were divided randomly into four groups (n=5) and exposed to vehicle control (PBS), 8 μ g of BikDD in P18-PEtOx-PEI-PCL-BikDD micelles, naked BikDD gene, and empty PEtOx-PEI-PCL micelles every three days. Representative pictures of CD-1 nude female mice exhibiting tumor development in mammary pad were shown for (a) Vehicle control cohort, (b) Empty PEtOx-PEI-PCL micelle cohort, (c) Naked BikDD gene cohort, and (d) P18-PEtOx-PEI-PCL-BikDD micelles cohort.

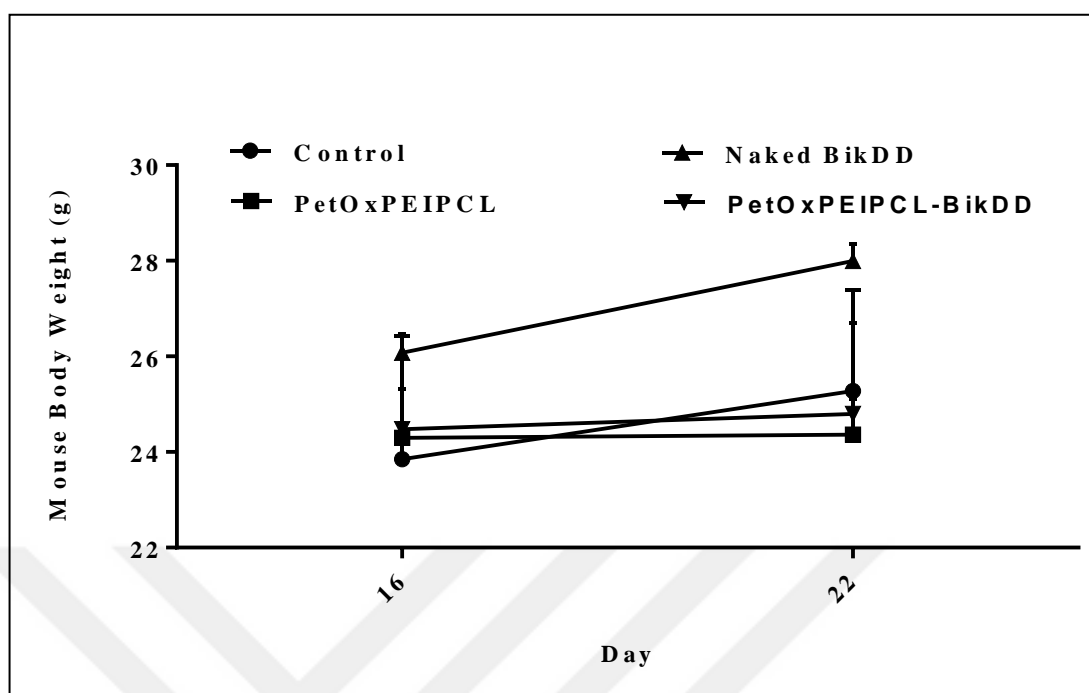


Figure 4.67. Effect of P18-PEtOx-PEI-PCL-BikDD micelle on CD-1 nude mice body weight.

On day 28, sacrifice of animals took place following drug treatment and nine different organs along with tumor tissues were isolated as mentioned earlier (Section 3.12). The isolated tumors from animals in vehicle control (PBS), empty PEtOx-PEI-PCL micelle, naked BikDD gene cohorts, and P18- PEtOx-PEI-PCL-BikDD micelle cohorts were given in Figure 4.68a. The graph showing the distribution of the isolated tumor weights of each treatment group was given in Figure 4.68b. The average tumor weight 0.032 g, 0.0028 g, 0.0314 g, and 0.0112 g was control (PBS), empty PEtOx-PEI-PCL micelle, naked BikDD gene, and P18-PEtOx-PEI-PCL-BikDD micelle cohorts, respectively. Treatment with naked BikDD gene and P18-PEtOx-PEI-PCL-BikDD micelle reduced ($p > 0.05$) tumor weight by 2 percent and 65 percent respectively, compared to control cohorts. Interestingly there was a significant reduction of 83 percent in tumor weight of empty PEtOx-PEI-PCL micelle cohorts in comparison to control cohorts (Figure 4.68b). The tumor volume was 29.95 mm^3 , 6.6 mm^3 , 18.47 mm^3 , and 5.4 mm^3 for control (PBS), empty PEtOx-PEI-PCL micelle, naked BikDD gene cohorts, and P18- PEtOx-PEI-PCL-BikDD micelle cohorts, respectively. A decrease ($p > 0.05$) of 38 percent, 81 percent, and 78 percent was observed in tumor volume of naked BikDD gene cohorts, P18-PEtOx-PEI-PCL-BikDD micelle cohorts, and empty PEtOx-PEI-PCL micelle cohorts compared to vehicle control cohorts.

A decrease ($p > 0.05$) of 70 percent and 64 percent was observed in tumor volume of P18-PEtOx-PEI-PCL-BikDD micelle cohorts, and empty PEtOx-PEI-PCL micelle cohorts compared to naked BikDD cohorts (Figure 4.68c).

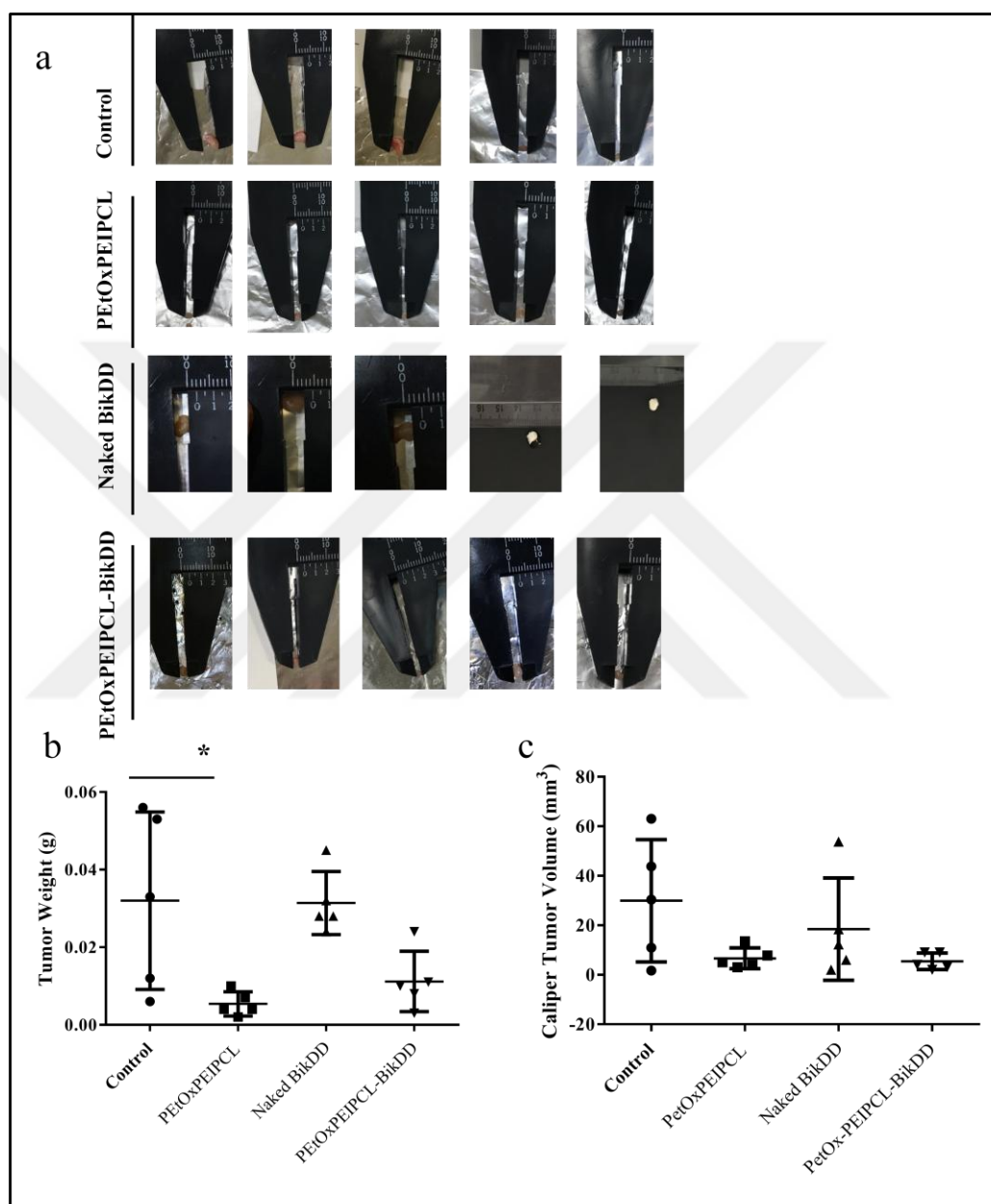


Figure 4.68. Antitumor effect of P18-PEtOx-PEI-PCL-BikDD micelle on CD-1 nude mice models. (a) Pictures represent the tumor isolated from CD-1 nude mice in four different groups subjected to treatment with either vehicle control (PBS), or empty PEtOx-PEI-PCL micelle, or naked BikDD gene, or P18-PEtOx-PEI-PCL-BikDD micelle cohorts. Graph shows the distribution of the isolated (b) Tumor weights and (c) Tumor volumes.

Following sacrifice and tumor isolation of animals, samples were stained by H&E for histopathological analysis (Figure 4.69). Table 4.7 shows the characterization of the isolated tumor tissues of CD-1 nude female mice used in the study by pathologist. All tumor types were characterized as adenocarcinoma, verifying AU565 orthotopic CD-1 nude mouse models were generated successfully. Histological and nuclear grading of all tumors in four different treatment groups were recorded as Grade 3. Toxicity was not detected from organs (brain, lung, heart, liver, spleen, stomach, intestines, kidney, and ovary) extracted from all four treatment cohorts. All the data given above suggest that P18-PEtOx-PEI-PCL-BikDD micelle did not show a strong anti-tumor response comparable to naked BikDD gene and control cohorts.

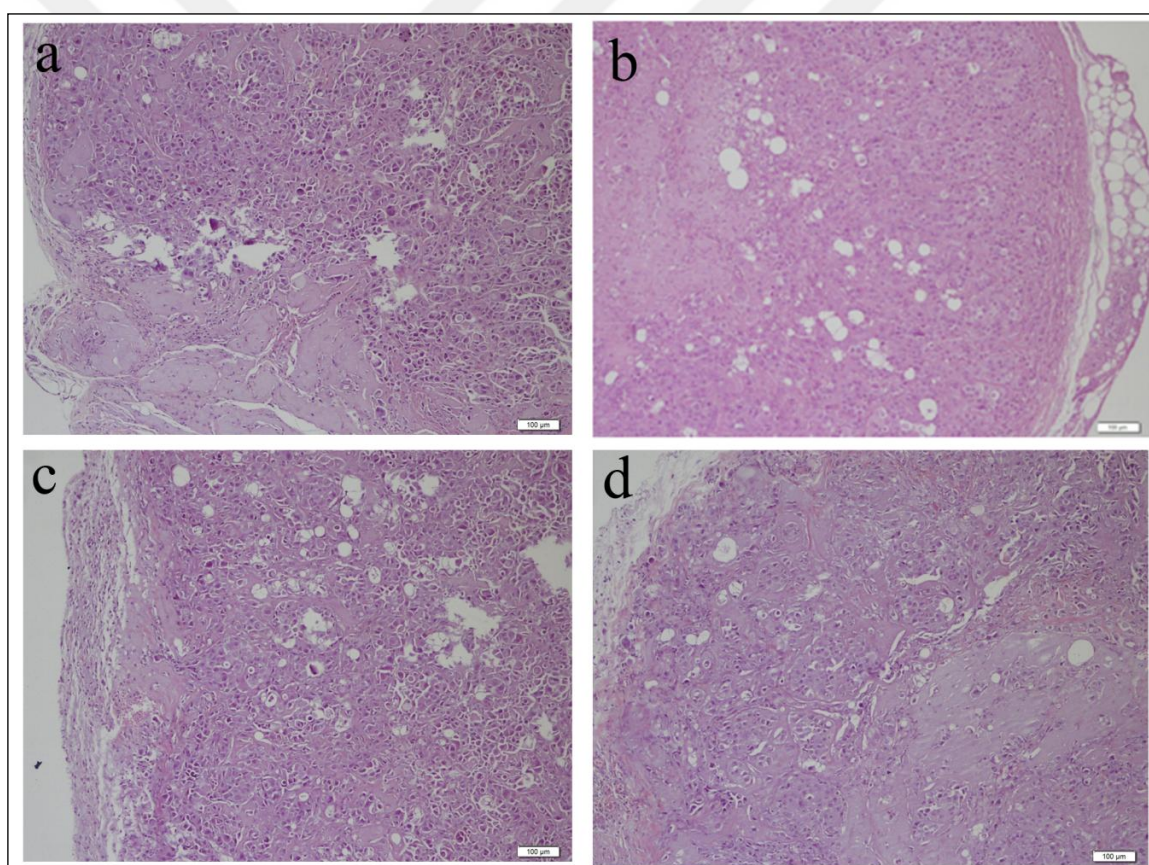


Figure 4.69. Histopathological analysis of the tumor samples of P18-PEtOx-PEI-PCL-BikDD micelles. H&E staining was used to stain the tumors isolated from CD-1 nude mice in four different groups subjected to treatment of either (a) Vehicle control, (b) Naked BikDD gene, (c) P18-PEtOx-PEI-PCL-BikDD micelle, and (d) Empty PEtOx-PEI-PCL micelle.

Table 4.7. Effect of P18-PEtOx-PEI-PCL-BikDD micelles on tumor tissues of CD-1 nude mice used in the study.

	Animal	Tumor Type	Histologic/Nuclear Grading
Control	1	Adenocarcinoma	H3/N3
	2	Adenocarcinoma	H3/N3
	3	Adenocarcinoma	H3/N3
	4	Adenocarcinoma	H3/N3
	5	Adenocarcinoma	H3/N3
PEtOx-PEI-PCL	1	Adenocarcinoma	H3/N3
	2	Adenocarcinoma	H3/N3
	3	Adenocarcinoma	H3/N3
	4	Adenocarcinoma	H3/N3
	5	Adenocarcinoma	H3/N3
Naked BikDD gene	1	Adenocarcinoma	H3/N3
	2	Adenocarcinoma	H3/N3
	3**	-	-
	4	Adenocarcinoma	H3/N3
	5	Adenocarcinoma	H3/N3
P18-PEtOx-PEI- PCL-BikDD	1	Adenocarcinoma	H3/N3
	2	Adenocarcinoma	H3/N3
	3	Adenocarcinoma	H3/N3
	4	Adenocarcinoma	H3/N3
	5	Adenocarcinoma	H3/N3

5. DISCUSSION

Breast cancer is still a major health problem seen and the main cause of death in females [44]. Nearly 30 percent of breast cancers are molecularly classified as HER2 positive breast cancer [217] and clinically show poor prognosis [74]. Conventional therapeutic approaches does not give a satisfactory therapeutic efficacy and HER2 positive breast cancer patients suffer systemic toxicity [218]. Breast cancer treatment landscape has been advanced in the last few decades. One of these advances are HER2 directed therapies which show effective clinical outcomes in early stage HER2 positive breast cancer patients [219]. Trastuzumab, FDA approved drug, is considered an effective therapeutic treatment against HER2 positive breast cancer and survival rate of patients show remarkable improvements [220]. It is the first oncogene targeted drug developed against HER2 positive breast cancer [109]. However, in the recent years the clinical application of Trastuzumab is limited because of the development of drug resistance [221]. This is overcome by treating HER2 positive breast cancer patients with trastuzumab and other chemotherapeutic drug combinations as the first line metastatic tumor treatments [111].

In the last few decades, nanoparticles in cancer targeted therapy research area has become the hot topic [222]. Standard administration of chemotherapeutic drugs can lead to drug resistance and thus become inefficient over time. The nanotechnology platform shows promise for cancer treatment when combined with chemotherapeutic drugs [144]. Drugs can be delivered directly to tissue or organ in a controlled manner and the main goal in sophisticated drug delivery systems is to deliver the drug directly to the target tissue or organ within the intended therapeutic time [223]. Due to lack of targeting specificity systemic approaches (hormonal therapy or chemotherapy) for cancer therapy can cause multidrug resistance and have detrimental side effects [194].

A century ago, Paul Ehrlich proposed the use of protein therapeutics specifically targeting diseases and his magic bullet theory has captured attention since that time [224]. Successful therapeutic strategies have been developed by using tumor targeting monoclonal antibodies in cancer treatment [225]. Although the most widely used clinically are antibodies [44], antibody properties such as large size, poor tissue penetration and high cost of manufacturing have limited the utility of therapeutic antibodies [226]. The therapeutic potential of peptides was discounted for many years due to their low solubility

properties. However, chemical modifications by cyclization or D-amino acid incorporation has overcome this challenge [227, 228]. Tissue penetrability, low manufacturing cost, minimal immunogenicity and easy modification for improving *in vivo* stability are peptide properties which make them ideal candidates for cancer therapeutics [229].

In the current study, we aimed to develop a new approach of targeted therapy for HER2 positive breast cancer AU565 cells using drug or gene loaded peptide targeted nanocarrier formulations and the *in vitro* and *in vivo* anticancer effects were shown. The choice of peptide (peptide 18) used as targeting label for nanocarriers in this thesis was a derivative of the tumor homing dodecapeptide p160, created by phage display [194]. Peptide 11 (P11) and peptide 18 (P18) are derivatives of p160 peptide that has shown specific targeting and binding to breast cancer cells [200]. P18 was found to be more proteolytically stable in human serum than other analogue of p160 peptide. P18 binds to keratin 1 (KRT1) which is overexpressed in breast cancer cell lines [194]. Previous studies showed that the binding profile of P11 and P18 to breast epithelial MCF10A cells were low, while these peptides showed a high binding affinity toward breast cancer cells MCF7 and MDAMB435 [200]. Similarly, results in this thesis showed that P18, yielded a three-fold higher binding profile to AU565 cells compared to MCF10A cells, while P11 displayed high binding affinity to both AU565 and MCF10A. Thus, P18 was chosen as the targeting peptide to be used in the nanocarrier formulations for targeting breast cancer AU565 cells.

Liposomes are nanocarriers that have lipid bilayer structures and carry drugs for prolonged circulation time [230]. For targeted drug delivery, liposomes are the most commonly investigated nanocarriers. This is due to their abilities of improving the biodistribution of compounds to target sites, stabilizing the therapeutic compound, and overcoming cellular uptake obstacles [231]. DOPE is a cationic helper colipid which increases the transfection activity and Mochizuki *et al.* showed that liposomes with DOPE composition displayed similar transfection efficacy as Lipofectamine 2000 [165]. In light of these findings, DOPE liposomes were used in this study. In the development of nanocarrier drug delivery systems, endothelial HUVEC cell line [232, 233], HEK293 [234, 235], and MSC [236, 237] cells are used routinely to evaluate the effect of nanocarrier material intended for drug delivery therapeutics on cell viability. In agreement with literature, results of this thesis show that there was minimal toxicity at low dosage of PEtOxDOPE liposomes on HUVEC, HEK293, and MSC cells, while an inductive effect on cell proliferation was

observed on MCF10A cells. As the PEtOxDPOE liposomes showed minimal toxicity to normal cells, target specificity of studies were then carried out by using P18 labeled PEtOxDPOE liposomes. We have investigated whether P18 labeled PEtOx-DOPE liposomes showed specific binding to breast cancer using AU565 and MCF10A cell lines. It was found that P18-PEtOx-DOPE liposomes exhibited specific binding to breast cancer using AU565 and MCF10A cells. Confocal microscopy images also confirmed our flow cytometry results, showing P18-PEtOxDPOE liposome was strongly bound to and internalized by AU565 cells. Our results are comparable to literature reporting favorable outcomes on P18-nanocarrier conjugates being a potential agent in breast cancer targeted therapies. MDAMB435 cells have shown high cellular uptake for P11 and P18 targeted polymeric micelles [200].

Another nanocarrier used in this study was polymersomes, which consists of amphiphilic copolymers and have the ability to load hydrophobic and hydrophilic drugs, thus characteristic of polymersomes is to improve the bioavailability of drug [191]. Studies show that carrier systems may be toxic to the stem cells and their effects on mesenchymal stem cells have been examined [238]. Furthermore, PEtOx-*b*-PLA copolymer displayed low toxicity profile on normal epithelial prostate PNT1A cell line [239] and HDF cells [240] suggesting that PEtOx-*b*-PLA polymersome maybe a safe nanocarrier for cargo of drugs. In agreement with literature, our results show that PEtOx-*b*-PLA copolymer and polymersomes showed no significant toxicity on HUVEC, HEK293, MSC, and MCF10A cells. PEtOx-*b*-PLA polymersomes labeled with P18 (P18-PEtOx-*b*-PLA) for targeted studies showed specific binding to AU565 cells when compared to normal MCF10A cells indicated by flow cytometry results and confocal images.

The final nanocarrier chosen in this study was micelles. Micelle nanovesicles are ideal for carrying water insoluble chemotherapeutic drugs [241]. These nanocarriers can increase the permeability and half-life of drugs [242]. PEI based polymers could be used to increase the gene transfection efficiency hence can be useful for the gene therapy studies [243]. According to the literature, the formation of amphiphilic cationic polymers based on PEI showed a reduced toxicity in HUVEC cells without compromising gene delivery efficiency [244, 245]. Similarly, PEtOx-PEI-PCL copolymer and micelle formulations showed no significant toxicity on MSC, HUVEC, and MCF10A cells. However, HEK293 cells treated with 300 to 500 $\mu\text{g/mL}$ of PEtOx-PEI-PCL micelle formulations showed a significant

toxicity, thus suggesting that the limit for safe dosage of PEtOx-PEI-PCL micelles is 300 $\mu\text{g}/\text{mL}$. The toxicity observed in HEK293 cells may be due to the fact that PEI has an endosomal escape pathway that causes the rupture of endosome membrane and non-specific interactions of PEI is known to cause toxic side effects [246]. Another major challenge in chemotherapy is the non-specific delivery of anticancer agents to healthy tissues leading to various side effects [247]. Thus, our results in this thesis show that P18-PEtOxDOPE liposome, P18-PEtOx-*b*-PLA polymersomes, and P18-PEtOx-PEI-PCL micelle formulations had a high binding affinity to AU565 cells compared to control MCF10A cells, suggesting that these nanocarrier formulations are target specific.

In recent years, gene therapy has brought hope for cancer treatment. Carcinogen activator ZYC300 [130] and apoptotic proteins such as TRAIL, cytochrome c, and granzyme B have been investigated for their anti-cancer effects in cancer therapy. However, direct administration of this protein drugs showed diminished therapeutic efficacy [133]. In recent years, BikDD gene has been identified as a pro-apoptotic protein and used in studies for treatment of breast [248], prostate [249], pancreatic [250], and lung [251] cancer treatment.

Studies showed that BikDD transfected to breast cancer MDA-MB-468 cells induced apoptosis by 40 to 80 percent more than the wild type Bik [143]. Consistently, it was demonstrated that P18-PEtOx-DOPE liposome formulations successfully delivered BikDD gene to AU565 cells (Figure 4.18), which resulted in a significant decrease in cell viability of AU565 cells (Figure 4.16), suggesting that P18-PEtOx-DOPE liposome could be an excellent nanocarrier system to be tested in *in vivo* studies. The high transfection efficiency of nanocarrier based DOPE formulations is suggested because of the fusogenic effect of non-lamellar phase [252]. Recent studies report that DOPE transfection efficiency and internalization are cell line dependent [253, 254]. However, our results showed that P18-PEtOx-DOPE-BikDD liposomes in CD-1 nude female mice were not effective as an antitumor agent, as no significant change was observed in tumor incidence, weight or volume was detected in P18-PEtOx-DOPE-BikDD liposomes cohorts compared to control cohorts. This could be due to insufficient dose of BikDD given per mouse due to low loading capacity of P18-PEtOx-DOPE liposomes. As maximum 300 μL of liquid can be injected to mice, the maximum gene dose that could be reached per mouse was 5 μg . However, Li *et al.* had shown strong antitumor response on breast cancer MCF7 nude mice

models by delivering 15 μg of BikDD gene per mice using SN liposomes [209], suggesting that delivering a higher gene dosage was essential for an antitumor response. Another reason for the failed antitumor effect of P18-PEtOx-DOPE-BikDD liposomes could be the choice of intraperitoneal injection method chosen for the study since other studies have shown the anti-tumor effect of BikDD carrying liposomal structures through tail vein injection [250, 255, 256].

There are only few reports on tumor-targeted polymersomes for controlled delivery of therapeutics proteins [133]. In this thesis, the proapoptotic BikDD gene was delivered using novel P18 labeled PEtOx-*b*-PLA polymersome formulations to HER2 breast cancer AU565 cell lines. Our results showed that delivery of BikDD gene by P18-PEtOx-*b*-PLA polymersome resulted in a significant decrease in cell viability of AU565 cells at 48 hours (Figure 4.28). However, under the same treatment conditions AU565 cells transfected with 5 μg of P18-PEtOx-*b*-PLA-BikDD polymersome showed a nonsignificant increase in Bik gene expression (Figure 4.30). Thus, delivery of BikDD gene by P18-PEtOx-*b*-PLA polymersome to AU565 cells were not as effective as the delivery of BikDD gene by P18-PEtOx-DOPE liposome. As mentioned previously, increasing the loading capacity of nanocarrier is a key point for these polymersomes as well. Similar to P18-PEtOx-DOPE-BikDD liposome *in vivo* results, P18-PEtOx-*b*-PLA-BikDD polymersome in CD-1 nude mice did not give an effective antitumor response, as no significant change in tumor volume or weight was detected. Extending the drug treatment duration [255] along with previously mentioned tail vein injections [250] and delivering higher BikDD gene dosage [143], could be more effective in *in vivo* gene delivery of P18-PEtOx-*b*-PLA-BikDD polymersomes.

PetOx-PEI block copolymers are potential candidate for nonviral gene therapy, where the *in vitro* studies revealed low cytotoxicity and high transfection efficiency in gene expression [257]. Consistently, P18-PEtOx-PEI-PCL micelle formulations successfully delivered proapoptotic BikDD gene to AU565 cells (Figure 4.42), which resulted in significant decrease of cell viability of AU565 cells (Figure 4.40). BikDD gene delivery by P18-PEtOx-PEI-PCL micelle higher therapeutic effect than BikDD gene delivery by P18-PEtOx-DOPE liposomes and P18-PEtOx-*b*-PLA polymersome formulations. This maybe due to the presence of PEI, as micelle of PEI based amphiphilic block copolymers show high DNA transfection activity [258]. Although, the *in vitro* studies suggested high antitumor

response of proapoptotic BikDD gene delivered by P18-PEtOx-PEI-PCL micelle to AU565 cells, the *in vivo* studies did not show an effective antitumor response in CD-1 nude female mice. No significant decrease was observed in tumor weight or volume of P18-PEtOx-PEI-PCL micelle/BikDD complex cohorts compared to control cohorts. On the contrary, significant decrease in tumor volume of empty PEtOx-PEI-PCL micelle was observed in comparison to control cohorts. This could be due to unsuccessful inoculation of CD-1 nude mice group that was assigned to receive injections of PEtOx-PEI-PCL micelle. Mice in this group have been separately inoculated with AU565 cells than the rest of the cohorts due to the late arrival of animals from Charles Rivers Laboratories. Thus for this reason, the *in vivo* studies for PEtOx-PEI-PCL micelle with control groups should be repeated.

Drug-loaded polymer nanocarriers effectively accumulate in tumors, with low systemic toxicity and long circulating half-life [259]. Doxorubicin is a potent chemotherapeutic drug that has shown efficacy for breast cancer therapy [260]. However, doxorubicin related cardiotoxicity is still an issue that needs to be overcome in breast cancer treatment, which is caused from apoptotic cell death of cardiomyocytes [261]. This side effect of doxorubicin is minimized by encapsulating the drug into liposomal nanocarriers and forming liposomal doxorubicin [262]. Pegylated liposomal doxorubicin (PLD) is *de facto* the first nanomedicine to be approved for cancer therapy [263]. PLD (Doxil) overcomes cardiocytotoxicity caused by nonliposomal doxorubicin [264]. Myconet, the non-pegylated other liposomal doxorubicin formulation, is used in treatment of metastatic breast cancer and the toxic profiles caused by doxorubicin is eliminated in this formulation [126, 127]. MM-302 (Hermione) is a pegylated antibody-liposomal doxorubicin that targets HER2 overexpressing tumors [265]. The antitumor activity of MM302 is superior than doxorubicin and pegylated liposomal doxorubicin demonstrated in preclinical models of HER2 positive breast cancer BT474 cells [266]. Studies also show that, P18-doxorubicin drug conjugate enhanced the selective delivery of doxorubicin breast cancer MCF-7 and MDA-MB-435 cells, with 40 times less toxicity to noncancerous cells [267]. In consideration of the advantage of delivering doxorubicin by targeted- nanocarriers, P18-PEtOx-DOPE liposome formulations were loaded with doxorubicin was studied in this thesis. The delivery of doxorubicin by P18-PEtOx-DOPE liposome formulations led to a potent anti-tumor efficacy in AU565 cells. Therapeutic effect of doxorubicin loaded P18-PEtOx-DOPE liposomes on cell viability of AU565 cells showed that 2.5 $\mu\text{g}/\text{mL}$ of P18-PEtOx-DOPE-DOX liposomes was the minimal dose with the maximum effect. 0.5 to 2.5

$\mu\text{g/mL}$ of P18-PEtOx-DOPE-DOX liposomes showed lower cytotoxicity compared with doxorubicin during 24, 48, and 72 hours incubation (Figure 4.17). This may be due to the fact that free DOX is an amphipathic and small molecule that can easily cross the cell membrane [268]. This explains why free DOX had higher cytotoxic efficiency than P18-PEtOx-DOPE liposome-DOX conjugate. Doxorubicin delivered by P18-PEtOx-DOPE liposomes arrested cell cycle of AU565 cells in G_2/M phase at 24 hours (Figure 4.19). This suggests that chemotherapeutic DOX inserts into minor grooves of nucleic acids and hinder their synthesis therefore inhibiting cell growth [269]. Our results demonstrated that the apoptotic cell death for AU565 cells treated with doxorubicin loaded P18-PEtOx-DOPE liposomes showed promising anti-tumor response (Figure 4.21). Throughout literature, orthotopic tumor models were formed by researchers for breast cancer cells [270]. The results presented in this thesis investigated the anti-tumor effect of doxorubicin loaded P18-PEtOx-DOPE liposomal formulations on AU565 tumor models. To our knowledge this thesis was the first study that used orthotopic HER2 positive AU565 breast cancer models in CD-1 nude female mice. Although, the chosen dosage (5mg/kg) for free DOX in this study was consistent with literature [271], our results showed that animals in the free DOX cohorts had a loss of weight. Furthermore the treatment with free DOX and P18-PEtOx-DOPE-DOX liposomes cohorts showed significant and comparable reduction in tumor weight and volume. The high antitumor activity of the nanocarrier formulations may be attributed to its extended time in circulation and higher accumulation potential in tumor through its EPR effect and high release of DOX from endosomes [154, 272]. Furthermore, the enhanced antitumor efficacy may be due to the effective preservation of encapsulated DOX preventing its leakage in blood stream in addition to its facilitated intracellular release of DOX.

The promising results of doxorubicin delivery by P18-PEtOx-DOPE liposomes to AU565 cells, had lead us to study the delivery of doxorubicin by P18-PEtOx-b-PLA polymersome formulations. Therapeutic effect of doxorubicin loaded P18-PEtOx-b-PLA polymersome on cell viability of AU565 cells showed that $1\ \mu\text{g/mL}$ of P18-PEtOx-b-PLA polymersome had effective therapeutic dose (Figure 4.29) and this dosage was more effective than P18-PEtOx-DOPE liposomes. Furthermore, our results indicate that $1\ \mu\text{g/mL}$ of P18-PEtOx-b-PLA-DOX polymersomes showed cell cycle arrest in AU565 cells at G_2/M phase for 24 hours (Figure 4.31) and the apoptotic cell death for AU565 cells treated with P18-PEtOx-b-PLA-DOX polymersomes showed promising anti-cancer response (Figure 4.32 and

Figure 4.33). In parallel to anticancer effect of P18-PEtOx-b-PLA polymersome *in vitro*, we further showed its anti-tumor effect in breast cancer orthotopic mouse models. Doxorubicin delivery of P18-PEtOx-b-PLA polymersome in CD-1 nude female mice was effective as an antitumor agent since a significant decrease in tumor volume was detected in P18-PEtOx-b-PLA polymersome cohorts compared to the control and free doxorubicin cohorts. In light of the promising *in vitro* and *in vivo* results of doxorubicin delivery of P18-PEtOx-DOPE liposomes and P18-PEtOx-b-PLA polymersome, the anti-tumor efficacy of doxorubicin delivered by novel P18-PEtOx-PEI-PCL micelle formulations was investigated in this study. Therapeutic effect of P18-PEtOx-PEI-PCL-DOX micelle complex on cell viability of AU565 cells showed that 1 $\mu\text{g}/\text{mL}$ of P18-PEtOx-PEI-PCL-DOX micelle had the maximum effect (Figure 4.41). Smaller size of micelle structures enables them to spontaneously penetrate into the body compartments [273] making them more advantageous than liposomes. Similar to effect of P18-PEtOx-b-PLA-DOX polymersome, P18-PEtOx-PEI-PCL-DOX micelle showed an arrest in G2/M phase of cell cycle in AU565 cells (Figure 4.43) and a comparable apoptotic cell death (Figure 4.44 and Figure 4.45). The animal studies performed showed an anti-tumor effect of P18-PEtOx-PEI-PCL-DOX micelle on AU565 tumor models. Doxorubicin delivery of P18-PEtOx-PEI-PCL micelles in CD-1 nude female mice was effective as an antitumor agent with a significant decrease in tumor volume in parallel with free doxorubicin cohorts.

In summary, the results in this thesis showed for the first time P18 targeted PEtOx-DOPE liposome, PEtOx-b-PLA polymersome, and PEtOx-PEI-PCL micelle formulations loaded with proapoptotic BikDD gene or doxorubicin drug enhanced the antitumor effect in breast cancer AU565 cells. A remarkable anti-cancer activity was observed for *in vitro* for P18PEtOx-DOPE-DOX liposome, P18-PEtOx-b-PLA-DOX polymersome, and P18PEtOx-PEI-PCL-DOX micelle HER2 positive breast cancer. Delivery of doxorubicin by these nanocarrier formulations led to the regression of *in vivo* AU565 tumor growth.

6. CONCLUSION AND FUTURE PERSPECTIVE

In this study, we have reported that P18 showed specific binding affinity to AU565 cells while low binding affinity to control MCF10A, MCF12A and HUVEC cells. Toxicology studies performed on the HUVEC, MSC, HEK293, and MCF10A showed that nanocarrier formulations did not affect the cell survival hence they would pose little toxicity if any to the healthy tissues. The increased Bik mRNA and protein expression in AU565 cell line indicated a high targeting efficiency for the P18-labeled nanocarrier formulations. Doxorubicin delivered to AU565 cells with polymersome and liposomes nanocarrier formulations had a therapeutic effect. The apoptosis results of P18 targeted nanocarriers loaded with doxorubicin drug; P18-PEtOx-DOPE-DOX, P18-PEtOx-*b*-PLA-DOX, and P18-PEtOx-PEI-PCL-DOX, showed promising results as it was as effective as doxorubicin for AU565 cells.

Our *in vitro* results, suggest that proapoptotic BikDD gene or doxorubicin drug loaded P18 labeled nanocarrier formulations may be promising drug carriers. Therefore, BikDD or doxorubicin loaded peptide 18 labeled nanocarrier formulations were tested further in preclinical studies. The significant decrease of tumor volume of P18-PEtOx-DOPE-DOX, P18-PEtOx-*b*-PLA-DOX, and P18-PEtOx-PEI_{30%}-PCL-DOX compared to control cohorts suggests doxorubicin delivered by these nanocarrier formulations showed strong antitumor response. Delivery of doxorubicin by these nanocarrier was effective and safe enough drug formulations to be used for the orthotopic AU565 cancer tumor models. However, decrease of tumor volume of P18-PEtOx-DOPE-BikDD, P18-PEtOx-*b*-PLA-BikDD, and P18-PEtOx-PEI-PCL-BikDD was insignificant compared to control cohorts. In conclusion, the findings presented in this thesis suggested that doxorubicin loaded to peptide 18-nanocarriers showed effective therapy to AU565 cells in *in vitro* and *in vivo* studies. Based on preclinical studies, doxorubicin loaded to P18-labeled nanocarrier formulations showed significant decrease in tumor volume. Therefore, P18-labeled nanocarrier specifically targeting breast cancer AU565 cells show promise for breast cancer therapy.

For further studies the loading capacity and transfection efficiency of P18-labeled nanocarrier formulations could be enhanced by addition of PEI and triglyceride and by this method stronger antitumor response of BikDD gene could be obtained in breast cancer AU565 cell lines. Furthermore, the antitumor efficacy of P18- labeled nanocarrier

formulations should be studied in different types of adenocarcinomas. Keratin 1 is also overexpressed in skin cancer, as P18 targets keratin 1, the binding affinity of P18-labeled nanocarriers to melanoma could be detected using flow cytometry. Because doxorubicin is also a drug used against melanoma, *invitro* and *invivo* studies of antitumor efficacy of doxorubicin loaded P18- labeled nanocarrier formulations could be further studied.



REFERENCES

1. Siegel RL, Miller KD, Jemal A. Cancer statistics, 2019. *CA: A Cancer Journal for Clinicians*. 2019;69(1):7-34.
2. Hanahan D, Weinberg Robert A. Hallmarks of Cancer: The Next Generation. *Cell*. 2011;144(5):646-74.
3. Hanahan D, Weinberg RA. The hallmarks of cancer. *Cell*. 2000;100(1):57-70.
4. Cheng N, Chytil A, Shyr Y, Joly A, Moses HL. Transforming growth factor- β signaling-deficient fibroblasts enhance hepatocyte growth factor signaling in mammary carcinoma cells to promote scattering and invasion. *Molecular Cancer Research*. 2008;6(10):1521-33.
5. Bhowmick NA, Neilson EG, Moses HL. Stromal fibroblasts in cancer initiation and progression. *Nature*. 2004;432(7015):332-337.
6. Davies MA, Samuels Y. Analysis of the genome to personalize therapy for melanoma. *Oncogene*. 2010;29(41):5545-5555.
7. Jiang BH, Liu LZ. Chapter 2 PI3K/PTEN Signaling in angiogenesis and tumorigenesis. *Advances in Cancer Research*. 102: Academic Press; 2009. p. 19-65.
8. Collado M, Serrano M. Senescence in tumours: evidence from mice and humans. *Nature Reviews Cancer*. 2010;10(1):51-57.
9. Evan GI, d'Adda di Fagagna F. Cellular senescence: hot or what? *Current Opinion in Genetics & Development*. 2009;19(1):25-31.
10. Adams JM, Cory S. The Bcl-2 apoptotic switch in cancer development and therapy. *Oncogene*. 2007;26(9):1324-1337.
11. Levine B, Kroemer G. Autophagy in the pathogenesis of disease. *Cell*. 2008;132(1):27-42.
12. Galluzzi L, Kroemer G. Necroptosis: A specialized pathway of programmed necrosis. *Cell*. 2008;135(7):1161-3.
13. Blasco MA. Telomeres and human disease: ageing, cancer and beyond. *Nature Reviews Genetics*. 2005;6(8):611-623.
14. Hansel DE, Meeker AK, Hicks J, De Marzo AM, Lillemoe KD, Schulick R, et al. Telomere length variation in biliary tract metaplasia, dysplasia, and carcinoma. *Modern Pathology*. 2006;19(6):772-779.

15. Polyak K, Weinberg RA. Transitions between epithelial and mesenchymal states: acquisition of malignant and stem cell traits. *Nature Reviews Cancer*. 2009;9(4):265-273.
16. Klymkowsky MW, Savagner P. Epithelial-mesenchymal transition: A cancer researcher's conceptual friend and foe. *The American Journal of Pathology*. 2009;174(5):1588-93.
17. Folkman J. Role of angiogenesis in tumor growth and metastasis. *Seminars in Oncology*. 2002;29(6):15-8.
18. Grivennikov SI, Greten FR, Karin M. Immunity, inflammation, and cancer. *Cell*. 2010;140(6):883-99.
19. Warburg O. On the origin of cancer cells. *Science*. 1956;123(3191):309-14.
20. DeBerardinis RJ, Lum JJ, Hatzivassiliou G, Thompson CB. The biology of cancer: metabolic reprogramming fuels cell growth and proliferation. *Cell Metabolism*. 2008;7(1):11-20.
21. Semenza GL. HIF-1: upstream and downstream of cancer metabolism. *Current Opinion in Genetics & Development*. 2010;20(1):51-6.
22. Jones RG, Thompson CB. Tumor suppressors and cell metabolism: a recipe for cancer growth. *Genes & Development*. 2009;23(5):537-48.
23. Smyth MJ, Dunn GP, Schreiber RD. Cancer immunosurveillance and immunoediting: The roles of immunity in suppressing tumor development and shaping tumor immunogenicity. *Advances in Immunology*. 90: Academic Press; 2006.1-50.
24. Strauss DC, Thomas JM. Transmission of donor melanoma by organ transplantation. *The Lancet Oncology*. 2010;11(8):790-6.
25. Yang L, Pang Y, Moses HL. TGF- β and immune cells: an important regulatory axis in the tumor microenvironment and progression. *Trends in Immunology*. 2010;31(6):220-7.
26. Schäfer M, Werner S. Cancer as an overheating wound: an old hypothesis revisited. *Nature Reviews Molecular Cell Biology*. 2008;9(8):628-638.
27. Hiom SC. Diagnosing cancer earlier: reviewing the evidence for improving cancer survival. *British Journal of Cancer*. 2015;112:S1-5.
28. Tothill IE. Biosensors for cancer markers diagnosis. *Seminars in Cell & Developmental Biology*. 2009;20(1):55-62.

29. Zhu A, Lee D, Shim H. Metabolic positron emission tomography imaging in cancer detection and therapy response. *Seminars in Oncology*. 2011;38(1):55-69.
30. Gulyás B, Halldin C. New PET radiopharmaceuticals beyond FDG for brain tumor imaging. *The Quarterly Journal of Nuclear Medicine and Molecular Imaging*. 2012;56(2):173-90.
31. Kumar R, Loving VA, Chauhan A, Zhuang H, Mitchell S, Alavi A. Potential of dual-time-point imaging to improve breast cancer diagnosis with (18)F-FDG PET. *Journal of Nuclear Medicine*. 2005;46(11):1819-24.
32. Afshar-Oromieh A, Avtzi E, Giesel FL, Holland-Letz T, Linhart HG, Eder M, et al. The diagnostic value of PET/CT imaging with the 68Ga-labelled PSMA ligand HBED-CC in the diagnosis of recurrent prostate cancer. *European Journal of Nuclear Medicine and Molecular Imaging*. 2015;42(2):197-209.
33. Schiepers C, Penninckx F, De Vadder N, Merckx E, Mortelmans L, Bormans G, et al. Contribution of PET in the diagnosis of recurrent colorectal cancer: comparison with conventional imaging. *European Journal of Surgical Oncology*. 1995;21(5):517-22.
34. Karantza V. Keratins in health and cancer: more than mere epithelial cell markers. *Oncogene*. 2010;30(2):127-138.
35. Hernandez BY, Frierson HF, Moskaluk CA, Li YJ, Clegg L, Cote TR, et al. CK20 and CK7 protein expression in colorectal cancer: demonstration of the utility of a population-based tissue microarray. *Human Pathology*. 2005;36(3):275-81.
36. Moll R, Divo M, Langbein L. The human keratins: biology and pathology. *Histochemistry and Cell Biology*. 2008;129(6):705-733.
37. Shao M-M, Chan SK, Yu AMC, Lam CCF, Tsang JYS, Lui PCW, et al. Keratin expression in breast cancers. *European Journal of Pathology*. 2012;461(3):313-22.
38. Johnson MC, Cutler ML. *Anatomy and Physiology of the Breast*. Cham: Springer International Publishing; 2016.
39. Macias H, Hinck L. Mammary gland development. *Wiley Interdisciplinary Reviews Developmental Biology*. 2012;1(4):533-57.
40. Zucca-Matthes G, Urban C, Vallejo A. Anatomy of the nipple and breast ducts. *Gland Surgery*. 2016;5(1):32-6.

41. Sriraman NK. The nuts and bolts of breastfeeding: Anatomy and physiology of lactation. *Current Problems in Pediatric and Adolescent Health Care*. 2017;47(12):305-10.
42. Ali S, Coombes RC. Endocrine-responsive breast cancer and strategies for combating resistance. *Nature Review Cancer*. 2002;2(2):101-12.
43. Bray F, Ferlay J, Soerjomataram I, Siegel RL, Torre LA, Jemal A. Global cancer statistics 2018: GLOBOCAN estimates of incidence and mortality worldwide for 36 cancers in 185 countries. *CA: A Cancer Journal for Clinicians*. 2018;68(6):394-424.
44. Jemal A, Bray F, Center MM, Ferlay J, Ward E, Forman D. Global cancer statistics. *CA: A Cancer Journal for Clinicians*. 2011;61(2):69-90.
45. Ginsburg O, Bray F, Coleman MP, Vanderpuye V, Eniu A, Kotha SR, et al. The global burden of women's cancers: a grand challenge in global health. *Lancet*. 2017;389(10071):847-60.
46. Smith RA, Andrews KS, Brooks D, Fedewa SA, Manassaram-Baptiste D, Saslow D, et al. Cancer screening in the United States, 2018: A review of current American Cancer Society guidelines and current issues in cancer screening. *CA: A Cancer Journal for Clinicians*. 2018;68(4):297-316.
47. Secginli S, Nahcivan NO, Gunes G, Fernandez R. Interventions promoting breast cancer screening among turkish women with global implications: A systematic review. *Worldviews on Evidence-Based Nursing*. 2017;14(4):316-23.
48. Yılmaz HH, Yazıhan N, Tunca D, Sevinç A, Olcayto EÖ, Özgül N, et al. Cancer trends and incidence and mortality patterns in Turkey. *Japanese Journal of Clinical Oncology*. 2011;41(1):10-6.
49. Youlden DR, Cramb SM, Dunn NA, Muller JM, Pyke CM, Baade PD. The descriptive epidemiology of female breast cancer: an international comparison of screening, incidence, survival and mortality. *Cancer Epidemiology*. 2012;36(3):237-48.
50. Ferlay J, Shin HR, Bray F, Forman D, Mathers C, Parkin DM. Estimates of worldwide burden of cancer in 2008: GLOBOCAN 2008. *International Journal of Cancer*. 2010;127(12):2893-917.
51. Viale G. The current state of breast cancer classification. *Annals of Oncology*. 2012;23(10):207-10.

52. Singletary SE. Rating the risk factors for breast cancer. *Annals of Surgery*. 2003;237(4):474-82.
53. Trentham-Dietz A, McElroy JA, Hampton JM, Shafer MM, Newcomb PA. Cadmium exposure and breast cancer risk. *JNCI: Journal of the National Cancer Institute*. 2006;98(12):869-73.
54. McPherson K, Steel CM, Dixon JM. ABC of breast diseases. Breast cancer-epidemiology, risk factors, and genetics. *British Medical Journal*. 2000;321(7261):624-8.
55. Hulka BS, Moorman PG. Breast cancer: Hormones and other risk factors. *Maturitas*. 2001;38(1):103-13.
56. Richie RC, Swanson JO. Breast cancer: A review of the literature. *Journal of Insurance Medicine*. 2003;35(2):85-101.
57. Mallepell S, Krust A, Chambon P, Briskin C. Paracrine signaling through the epithelial estrogen receptor alpha is required for proliferation and morphogenesis in the mammary gland. *Proceedings of the National Academy of Sciences of the United States of America*. 2006;103(7):2196-201.
58. Viale G. The current state of breast cancer classification. *Annals of Oncology*. 2012;23(S10):207-10.
59. Ossovskaya V, Wang Y, Budoff A, Xu Q, Lituev A, Potapova O, et al. Exploring molecular pathways of triple-negative breast cancer. *Genes and cancer*. 2011;2(9):870-9.
60. Blumen H, Fitch K, Polkus V. Comparison of treatment costs for breast cancer, by tumor stage and type of service. *American Health and Drug Benefits*. 2016;9(1):23-32.
61. Ahmad A. Pathways to breast cancer recurrence. *ISRN Oncology*. 2013;2013:16.
62. Silverstein MJ, Poller DN, Waisman JR, Colburn WJ, Barth A, Gierson ED, et al. Prognostic classification of breast ductal carcinoma-in-situ. *Lancet*. 1995;345(8958):1154-7.
63. Sotiriou C, Wirapati P, Loi S, Harris A, Fox S, Smeds J, et al. Gene expression profiling in breast cancer: Understanding the molecular basis of histologic grade to improve prognosis. *Journal of the National Cancer Institute*. 2006;98(4):262-72.

64. Ogston KN, Miller ID, Payne S, Hutcheon AW, Sarkar TK, Smith I, et al. A new histological grading system to assess response of breast cancers to primary chemotherapy: prognostic significance and survival. *Breast*. 2003;12(5):320-7.
65. Perou CM, Sorlie T, Eisen MB, van de Rijn M, Jeffrey SS, Rees CA, et al. Molecular portraits of human breast tumours. *Nature*. 2000;406(6797):747-52.
66. Holliday DL, Speirs V. Choosing the right cell line for breast cancer research. *Breast Cancer Research*. 2011;13(4):215-221.
67. Rahman M, Pumphrey JG, Lipkowitz S. The TRAIL to targeted therapy of breast cancer. *Advances in Cancer Research*. 2009;103:43-73.
68. Shah D, Osipo C. Cancer stem cells and HER2 positive breast cancer: The story so far. *Genes and Diseases*. 2016;3(2):114-23.
69. Carey LA, Perou CM, Livasy CA, Dressler LG, Cowan D, Conway K, et al. Race, breast cancer subtypes, and survival in the Carolina Breast Cancer Study. *The Journal of the American Medical Association*. 2006;295(21):2492-2502.
70. Rakha EA, El-Sayed ME, Green AR, Lee AHS, Robertson JF, Ellis IO. Prognostic markers in triple-negative breast cancer. *Cancer*. 2007;109(1):25-32.
71. Foulkes WD, Smith IE, Reis-Filho JS. Triple-Negative Breast Cancer. *New England Journal of Medicine*. 2010;363(20):1938-48.
72. Reis-Filho JS, Tutt ANJ. Triple negative tumours: a critical review. *Histopathology*. 2008;52(1):108-18.
73. Fang C, Zhao Y, Guo B. MiR-199b-5p targets HER2 in breast cancer cells. *Journal of Cellular Biochemistry*. 2013;114(7):1457-63.
74. Valabrega G, Montemurro F, Aglietta M. Trastuzumab: mechanism of action, resistance and future perspectives in HER2-overexpressing breast cancer. *Annals of Oncology*. 2007;18(6):977-84.
75. Casalini P, Iorio MV, Galmozzi E, Ménard S. Role of HER receptors family in development and differentiation. *Journal of Cellular Physiology*. 2004;200(3):343-50.
76. Labuschagne CF, Zani F, Vousden KH. Control of metabolism by p53 - cancer and beyond. *Biochimica et Biophysica Acta Reviews on Cancer*. 2018;1870(1):32-42.
77. Gasco M, Shami S, Crook T. The p53 pathway in breast cancer. *Breast Cancer Research*. 2002;4(2):70-6.

78. Berger C, Qian Y, Chen X. The p53-estrogen receptor loop in cancer. *Current Molecular Medicine*. 2013;13(8):1229-40.
79. Gasco M, Shami S, Crook T. The p53 pathway in breast cancer. *Breast cancer research*. 2002;4(2):70-6.
80. Butti R, Das S, Gunasekaran VP, Yadav AS, Kumar D, Kundu GC. Receptor tyrosine kinases (RTKs) in breast cancer: signaling, therapeutic implications and challenges. *Molecular Cancer*. 2018;17(1):34-51.
81. Lin NU, Winer EP. New targets for therapy in breast cancer: small molecule tyrosine kinase inhibitors. *Breast Cancer Research*. 2004;6(5):204-10.
82. Xia W, Lau Y-K, Zhang H-Z, Xiao F-Y, Johnston DA, Liu A-R, et al. Combination of EGFR, HER-2/neu, and HER-3 is a stronger predictor for the outcome of oral squamous cell carcinoma than any individual family members. *Clinical Cancer Research*. 1999;5(12):4164-4174.
83. Baselga J. Why the epidermal growth factor receptor? The rationale for cancer therapy. *The Oncologist*. 2002;7(S4):2-8.
84. Luo J, Manning BD, Cantley LC. Targeting the PI3K-Akt pathway in human cancer: Rationale and promise. *Cancer Cell*. 2003;4(4):257-62.
85. Zhang W, Liu HT. MAPK signal pathways in the regulation of cell proliferation in mammalian cells. *Cell Research*. 2002;12(1):9-18.
86. Henjes F, Bender C, von der Heyde S, Braun L, Mannsperger HA, Schmidt C, et al. Strong EGFR signaling in cell line models of ERBB2-amplified breast cancer attenuates response towards ERBB2-targeting drugs. *Oncogenesis*. 2012;1(7):16-9.
87. Normanno N, De Luca A, Bianco C, Strizzi L, Mancino M, Maiello MR, et al. Epidermal growth factor receptor (EGFR) signaling in cancer. *Gene*. 2006;366(1):2-16.
88. Grünwald V, Hidalgo M. Developing Inhibitors of the epidermal growth factor receptor for cancer treatment. *Journal of the National Cancer Institute*. 2003;95(12):851-67.
89. Masuda H, Zhang D, Bartholomeusz C, Doihara H, Hortobagyi GN, Ueno NT. Role of epidermal growth factor receptor in breast cancer. *Breast Cancer Research and Treatment*. 2012;136(2):331-45.

90. Myers E, Hill ADK, Kelly G, McDermott EW, O'Higgins NJ, Young LS. A positive role for PEA3 in HER2-mediated breast tumour progression. *British Journal of Cancer*. 2006;95(10):1404-9.
91. Lowery AJ, Kell MR, Glynn RW, Kerin MJ, Sweeney KJ. Locoregional recurrence after breast cancer surgery: a systematic review by receptor phenotype. *Breast Cancer Research and Treatment*. 2012;133(3):831-41.
92. Mitri Z, Constantine T, O'Regan R. The HER2 receptor in breast cancer: pathophysiology, clinical use, and new advances in therapy. *Chemotherapy Research and Practice*. 2012;2012:743193-7.
93. Subik K, Lee JF, Baxter L, Strzepak T, Costello D, Crowley P, et al. The expression patterns of ER, PR, HER2, CK5/6, EGFR, Ki-67 and AR by immunohistochemical analysis in breast cancer cell lines. *Breast Cancer : Basic and Clinical Research*. 2010;4:35-41.
94. Rahman M, Mohammed S. Breast cancer metastasis and the lymphatic system. *Oncology Letters*. 2015;10(3):1233-9.
95. Morimoto T, Komaki K, Inui K, Umemoto A, Yamamoto H, Harada K, et al. Involvement of nipple and areola in early breast cancer. *Cancer*. 1985;55(10):2459-63.
96. Donegan WL. The influence of untreated internal mammary metastases upon the course of mammary cancer. *Cancer*. 1977;39(2):533-8.
97. Veronesi U, Cascinelli N, Bufalino R, Morabito A, Greco M, Galluzzo D, et al. Risk of internal mammary lymph node metastases and its relevance on prognosis of breast cancer patients. *Annals of Surgery*. 1983;198(6):681-4.
98. Guan X. Cancer metastases: challenges and opportunities. *Acta Pharmaceutica Sinica B*. 2015;5(5):402-18.
99. Giuliano M, Giordano A, Jackson S, De Giorgi U, Mego M, Cohen EN, et al. Circulating tumor cells as early predictors of metastatic spread in breast cancer patients with limited metastatic dissemination. *Breast Cancer Research*. 2014;16(5):1-9.
100. Gloyeske NC, Goreal W, O'Neil M, Connor C, Tawfik OW, Fan F. Outcomes of breast cancer patients with micrometastases and isolated tumor cells in sentinel lymph nodes. *In vivo*. 2011;25(6):997-1001.

101. Roy PG, Chan SM, Ng V, Smith BM, Umeh H, Courtney SP. Risk stratification of patients with early breast cancer. *Clinical Breast Cancer*. 2014;14(1):68-73.
102. Scully OJ, Bay BH, Yip G, Yu Y. Breast cancer metastasis. *Cancer Genomics and Proteomics*. 2012;9(5):311-20.
103. Martins CP, Brown-Swigart L, Evan GI. Modeling the therapeutic efficacy of p53 restoration in tumors. *Cell*. 2006;127(7):1323-34.
104. The Cancer Genome Atlas N, Koboldt DC, Fulton RS, McLellan MD, Schmidt H, Kalicki-Veizer J, et al. Comprehensive molecular portraits of human breast tumours. *Nature*. 2012;490(7418):61-70.
105. Rivera E, Gomez H. Chemotherapy resistance in metastatic breast cancer: the evolving role of ixabepilone. *Breast Cancer Research*. 2010;12(2):1-12.
106. Blanco E, Ferrari M. Emerging nanotherapeutic strategies in breast cancer. *Breast*. 2014;23(1):10-8.
107. Martin HL, Smith L, Tomlinson DC. Multidrug-resistant breast cancer: current perspectives. *Breast Cancer*. 2014;6:1-13.
108. Jordan VC. The development of tamoxifen for breast cancer therapy: a tribute to the late Arthur L. Walpole. *Breast Cancer Research and Treatment*. 1988;11(3):197-209.
109. Leyland-Jones B. Trastuzumab: hopes and realities. *The Lancet Oncology*. 2002;3(3):137-44.
110. Gajria D, Chandarlapaty S. HER2-amplified breast cancer: mechanisms of trastuzumab resistance and novel targeted therapies. *Expert Review of Anticancer therapy*. 2011;11(2):263-75.
111. Loibl S, Gianni L. HER2-positive breast cancer. *Lancet*. 2017;389(10087):2415-29.
112. Medina PJ, Goodin S. Lapatinib: a dual inhibitor of human epidermal growth factor receptor tyrosine kinases. *Clinical Therapeutics*. 2008;30(8):1426-47.
113. Blackwell KL, Burstein HJ, Storniolo AM, Rugo HS, Sledge G, Aktan G, et al. Overall survival benefit with lapatinib in combination with trastuzumab for patients with human epidermal growth factor receptor 2-positive metastatic breast cancer: final results from the EGF104900 Study. *Journal of Clinical Oncology*. 2012;30(21):2585-92.
114. Awada A, Colomer R, Inoue K, et al. Neratinib plus paclitaxel vs trastuzumab plus paclitaxel in previously untreated metastatic ERBB2-positive breast cancer: The

- NEfERT-T randomized clinical trial. *The Journal of the American Medical Association Oncology*. 2016;2(12):1557-64.
115. Corkery B, Crown J, Clynes M, O'Donovan N. Epidermal growth factor receptor as a potential therapeutic target in triple-negative breast cancer. *Annals of Oncology*. 2009;20(5):862-7.
116. Jernstrom S, Hongisto V, Leivonen SK, Due EU, Tadele DS, Edgren H, et al. Drug-screening and genomic analyses of HER2-positive breast cancer cell lines reveal predictors for treatment response. *Breast Cancer*. 2017;9:185-98.
117. Thorn CF, Oshiro C, Marsh S, Hernandez-Boussard T, McLeod H, Klein TE, et al. Doxorubicin pathways: pharmacodynamics and adverse effects. *Pharmacogenetics and Genomics*. 2011;21(7):440-6.
118. Mobaraki M, Zare M, Dolati P, Ataei M, Dehghan Manshadi HR. Molecular mechanisms of cardiotoxicity: A review on the major side-effect of doxorubicin. *Indian Journal of Pharmaceutical Sciences*. 2017;79(3):335-44.
119. Jain S, Patil SR, Swarnakar NK, Agrawal AK. Oral delivery of doxorubicin using novel polyelectrolyte-stabilized liposomes (layersomes). *Molecular Pharmaceutics*. 2012;9(9):2626-35.
120. Tacar O, Sriamornsak P, Dass CR. Doxorubicin: an update on anticancer molecular action, toxicity and novel drug delivery systems. *The Journal of Pharmacy and Pharmacology*. 2013;65(2):157-70.
121. Lao J, Madani J, Puertolas T, et al. Liposomal doxorubicin in the treatment of breast cancer patients: A Review. *Journal of Drug Delivery*. 2013;2013:456409-12.
122. DiGiulio S. FDA approves generic version of doxil; expected to help resolve shortage. *Oncology Times*. 2013;35(6):25.
123. Duggan ST, Keating GM. Pegylated liposomal doxorubicin: a review of its use in metastatic breast cancer, ovarian cancer, multiple myeloma and AIDS-related Kaposi's sarcoma. *Drugs*. 2011;71(18):2531-58.
124. Corti A, Curnis F. Tumor vasculature targeting through NGR peptide-based drug delivery systems. *Current Pharmaceutical Biotechnology*. 2011;12(8):1128-34.
125. Burade V, Bhowmick S, Maiti K, Zalawadia R, Ruan H, Thennati R. Lipodox® (generic doxorubicin hydrochloride liposome injection): in vivo efficacy and bioequivalence versus Caelyx® (doxorubicin hydrochloride liposome injection) in

- human mammary carcinoma (MX-1) xenograft and syngeneic fibrosarcoma (WEHI 164) mouse models. *BioMed Central Cancer*. 2017;17(1):405-12.
126. Brucker J, Mayer C, Gebauer G, Mallmann P, Belau AK, Schneeweiss A, et al. Non-pegylated liposomal doxorubicin for patients with recurrent ovarian cancer: A multicentric phase II trial. *Oncology Letters*. 2016;12(2):1211-5.
127. Bernardi D, Errante D, Stefani M, Salvagno L. Non-pegylated liposomal doxorubicin in metastatic breast cancer patients: a valuable therapeutic option requiring caution. *Breast*. 2010;19(6):549-50.
128. McCrudden CM, McCarthy HO. Current status of gene therapy for breast cancer: progress and challenges. *The Application of Clinical Genetics*. 2014;7:209-20.
129. Yoo GH, Hung MC, Lopez-Berestein G, LaFollette S, Ensley JF, Carey M, et al. Phase I trial of intratumoral liposome E1A gene therapy in patients with recurrent breast and head and neck cancer. *Clinical Cancer Research*. 2001;7(5):1237-45.
130. Gribben JG, Ryan DP, Boyajian R, Urban RG, Hedley ML, Beach K, et al. Unexpected association between induction of immunity to the universal tumor antigen CYP1B1 and response to next therapy. *Clinical Cancer Research*. 2005;11(12):4430-6.
131. Amidi M, Mastrobattista E, Jiskoot W, Hennink WE. Chitosan-based delivery systems for protein therapeutics and antigens. *Advanced Drug Delivery Review*. 2010;62(1):59-82.
132. Kim SK, Foote MB, Huang L. The targeted intracellular delivery of cytochrome C protein to tumors using lipid-apolipoprotein nanoparticles. *Biomaterials*. 2012;33(15):3959-66.
133. Li X, Yang W, Zou Y, Meng F, Deng C, Zhong Z. Efficacious delivery of protein drugs to prostate cancer cells by PSMA-targeted pH-responsive chimaeric polymersomes. *Journal of Controlled Release*. 2015;220(Pt B):704-714.
134. Ulukaya E, Acilan C, Yilmaz Y. Apoptosis: why and how does it occur in biology? *Cell Biochemistry and Function*. 2011;29(6):468-80.
135. Kang MH, Reynolds CP. Bcl-2 inhibitors: targeting mitochondrial apoptotic pathways in cancer therapy. *Clinical Cancer Research*. 2009;15(4):1126-32.
136. Shamas-Din A, Brahmabhatt H, Leber B, Andrews DW. BH3-only proteins: Orchestrators of apoptosis. *Biochimica et Biophysica Acta*. 2011;1813(4):508-20.

137. Koff JL, Ramachandiran S, Bernal-Mizrachi L. A time to kill: targeting apoptosis in cancer. *International Journal of Molecular Sciences*. 2015;16(2):2942-55.
138. Jiao S, Wu M, Ye F, Tang H, Xie X, Xie X. BikDDA, a mutant of Bik with longer half-life expression protein, can be a novel therapeutic gene for triple-negative breast cancer. *PloS One*. 2014;9(3):92172-9.
139. Yip KW, Reed JC. Bcl-2 family proteins and cancer. *Oncogene*. 2008;27(50):6398-406.
140. Bratton SB, Salvesen GS. Regulation of the Apaf-1-caspase-9 apoptosome. *Journal of Cell Science*. 2010;123(Pt 19):3209-14.
141. Cory S, Adams JM. The Bcl2 family: regulators of the cellular life-or-death switch. *Nature Reviews Cancer*. 2002;2(9):647-56.
142. Li YM, Wen Y, Zhou BP, Kuo H-P, Ding Q, Hung M-C. Enhancement of antitumor effect by Bik mutants. *Cancer Research*. 2003;63(22):7630-7633.
143. Lang J-Y, Hsu JL, Meric-Bernstam F, Chang C-J, Wang Q, Bao Y, et al. BikDD eliminates breast cancer initiating cells and synergizes with lapatinib for breast cancer treatment. *Cancer Cell*. 2011;20(3):341-56.
144. Gaspar VM, Gonçalves C, de Melo-Diogo D, Costa EC, Queiroz JA, Pichon C, et al. Poly(2-ethyl-2-oxazoline)-PLA-g-PEI amphiphilic triblock micelles for co-delivery of minicircle DNA and chemotherapeutics. *Journal of Controlled Release*. 2014;189:90-104.
145. Tiwari G, Tiwari R, Sriwastawa B, Bhati L, Pandey S, Pandey P, et al. Drug delivery systems: An updated review. *International Journal of Pharmaceutical Investigation*. 2012;2(1):2-11.
146. Schmaljohann D. Thermo- and pH-responsive polymers in drug delivery. *Advanced Drug Delivery Reviews*. 2006;58(15):1655-70.
147. Agarwal S, Curtin J, Duffy B, Jaiswal S. Biodegradable magnesium alloys for orthopaedic applications: A review on corrosion, biocompatibility and surface modifications. *Materials Science and Engineering: C*. 2016;68:948-63.
148. Coelho JF, Ferreira PC, Alves P, Cordeiro R, Fonseca AC, Góis JR, et al. Drug delivery systems: Advanced technologies potentially applicable in personalized treatments. *The EPMA Journal*. 2010;1(1):164-209.

149. Yezhelyev MV, Gao X, Xing Y, Al-Hajj A, Nie S, O'Regan RM. Emerging use of nanoparticles in diagnosis and treatment of breast cancer. *The Lancet Oncology*. 2006;7(8):657-67.
150. Alvarez-Lorenzo C, Concheiro A. Smart drug delivery systems: from fundamentals to the clinic. *Chemical Communications*. 2014;50(58):7743-7765.
151. Singh SK, Singh S, Lillard JW, Jr., Singh R. Drug delivery approaches for breast cancer. *International Journal of Nanomedicine*. 2017;12:6205-6218.
152. Din FU, Aman W, Ullah I, Qureshi OS, Mustapha O, Shafique S, et al. Effective use of nanocarriers as drug delivery systems for the treatment of selected tumors. *International Journal of Nanomedicine*. 2017;12:7291-309.
153. Sun T, Zhang YS, Pang B, Hyun DC, Yang M, Xia Y. Engineered nanoparticles for drug delivery in cancer therapy. *Angewandte Chemie International Edition*. 2014;53(46):12320-64.
154. Singh R, Lillard JW, Jr. Nanoparticle-based targeted drug delivery. *Experimental and Molecular Pathology*. 2009;86(3):215-23.
155. Friedman AD, Claypool SE, Liu R. The smart targeting of nanoparticles. *Current Pharmaceutical Design*. 2013;19(35):6315-29.
156. Panyam J, Labhasetwar V. Biodegradable nanoparticles for drug and gene delivery to cells and tissue. *Advanced Drug Delivery Reviews*. 2003;55(3):329-47.
157. Liechty WB, Kryscio DR, Slaughter BV, Peppas NA. Polymers for drug delivery systems. *Annual Review of Chemical and Biomolecular Engineering*. 2010;1:149-73.
158. Taubmann C, Luxenhofer R, Cesana S, Jordan R. First aldehyde-functionalized poly(2-oxazoline)s for chemoselective ligation. *Macromolecular Bioscience*. 2005;5(7):603-612.
159. Obeid R, Scholz C. Synthesis and self-Assembly of well-defined poly(amino acid) end-Capped poly(ethylene glycol) and poly(2-methyl-2-oxazoline). *Biomacromolecules*. 2011;12(10):3797-3804.
160. Adams N, Schubert US. Poly(2-oxazolines) in biological and biomedical application contexts. *Advanced Drug Delivery Reviews*. 2007;59(15):1504-20.
161. Zhang M, Xue Y-N, Liu M, Zhuo R-X, Huang S-W. Biocleavable polycationic micelles as highly efficient gene delivery vectors. *Nanoscale Research Letters*. 2010;5(11):1804-11.

162. Neu M, Fischer D, Kissel T. Recent advances in rational gene transfer vector design based on poly(ethylene imine) and its derivatives. *The Journal of Gene Medicine*. 2005;7(8):992-1009.
163. Liu C, Liu F, Feng L, Li M, Zhang J, Zhang N. The targeted co-delivery of DNA and doxorubicin to tumor cells via multifunctional PEI-PEG based nanoparticles. *Biomaterials*. 2013;34(10):2547-64.
164. Hildebrandt IJ, Iyer M, Wagner E, Gambhir SS. Optical imaging of transferrin targeted PEI/DNA complexes in living subjects. *Gene Therapy*. 2003;10(9):758-764.
165. Mochizuki S, Kanegae N, Nishina K, Kamikawa Y, Koiwai K, Masunaga H, et al. The role of the helper lipid dioleoylphosphatidylethanolamine (DOPE) for DNA transfection cooperating with a cationic lipid bearing ethylenediamine. *Biochimica et Biophysica Acta*. 2013;1828(2):412-8.
166. Cheng X, Lee RJ. The role of helper lipids in lipid nanoparticles (LNPs) designed for oligonucleotide delivery. *Advanced Drug Delivery Reviews*. 2016;99:129-37.
167. Du Z, Munye MM, Tagalakis AD, Manunta MDI, Hart SL. The role of the helper lipid on the DNA transfection efficiency of lipopolyplex formulations. *Scientific Reports*. 2014;4:7107-6.
168. Popova P, Notabi MK, Code C, Arnspang EC, Andersen MØ. Co-delivery of siRNA and etoposide to cancer cells using an MDEA esterquat based drug delivery system. *European Journal of Pharmaceutical Sciences*. 2019;127:142-50.
169. Park JH, Lee BK, Park SH, Kim MG, Lee JW, Lee HY, et al. Preparation of biodegradable and elastic poly(ϵ -caprolactone-co-lactide) copolymers and evaluation as a localized and sustained drug delivery carrier. *International Journal of Molecular Sciences*. 2017;18(3):671.
170. Xiao RZ, Zeng ZW, Zhou GL, Wang JJ, Li FZ, Wang AM. Recent advances in PEG-PLA block copolymer nanoparticles. *International Journal of Nanomedicine*. 2010;5:1057-65.
171. Saini P, Arora M, Kumar MNVR. Poly(lactic acid) blends in biomedical applications. *Advanced Drug Delivery Reviews*. 2016;107:47-59.
172. Liu MM, Tuo J, Chan CC. Gene therapy for ocular diseases. *The British Journal of Ophthalmology*. 2011;95(5):604-12.

173. Nair LS, Laurencin CT. Polymers as biomaterials for tissue engineering and controlled drug delivery. *Advances in Biochemical Engineering/Biotechnology*. 2006;102:47-90.
174. Mofokeng JP, Luyt AS. Morphology and thermal degradation studies of melt-mixed poly(lactic acid) (PLA)/poly(ϵ -caprolactone) (PCL) biodegradable polymer blend nanocomposites with TiO₂ as filler. *Polymer Testing*. 2015;45:93-100.
175. Kim Y-J, Park MR, Kim MS, Kwon OH. Polyphenol-loaded polycaprolactone nanofibers for effective growth inhibition of human cancer cells. *Materials Chemistry and Physics*. 2012;133(2):674-80.
176. Ali R, Farah A, Binkhathlan Z. Development and characterization of methoxy poly(ethylene oxide)-block-poly(ϵ -caprolactone) (PEO-b-PCL) micelles as vehicles for the solubilization and delivery of tacrolimus. *Saudi Pharmaceutical Journal*. 2017;25(2):258-65.
177. Gregoriadis G. Liposomes in drug delivery: How it all happened. *Pharmaceutics*. 2016;8(2):19-5.
178. Akbarzadeh A, Rezaei-Sadabady R, Davaran S, Joo SW, Zarghami N, Hanifehpour Y, et al. Liposome: classification, preparation, and applications. *Nanoscale Research Letters*. 2013;8(1):102-11.
179. Johnston MJW, Semple SC, Klimuk SK, Ansell S, Maurer N, Cullis PR. Characterization of the drug retention and pharmacokinetic properties of liposomal nanoparticles containing dihydrosphingomyelin. *Biochimica et Biophysica Acta (BBA) - Biomembranes*. 2007;1768(5):1121-7.
180. Shehata T, Ogawara K-i, Higaki K, Kimura T. Prolongation of residence time of liposome by surface-modification with mixture of hydrophilic polymers. *International Journal of Pharmaceutics*. 2008;359(1):272-9.
181. Han HD, Jeon YW, Kwon HJ, Jeon HN, Byeon Y, Lee CO, et al. Therapeutic efficacy of doxorubicin delivery by a CO₂ generating liposomal platform in breast carcinoma. *Acta Biomaterialia*. 2015;24:279-285.
182. Hong SS, Kim SH, Lim SJ. Effects of triglycerides on the hydrophobic drug loading capacity of saturated phosphatidylcholine-based liposomes. *International Journal of Pharmaceutics*. 2015;483(1-2):142-50.

183. Godbey WT, Wu KK, Hirasaki GJ, Mikos AG. Improved packing of poly(ethylenimine)/DNA complexes increases transfection efficiency. *Gene Therapy*. 1999;6(8):1380-1388.
184. Park JH, Cho HJ, Yoon HY, Yoon IS, Ko SH, Shim JS, et al. Hyaluronic acid derivative-coated nanohybrid liposomes for cancer imaging and drug delivery. *Journal of Controlled Release*. 2014;174(1):98-108.
185. Bozzuto G, Molinari A. Liposomes as nanomedical devices. *International Journal of Nanomedicine*. 2015;10:975-99.
186. Zhang Y, Huang Y, Li S. Polymeric micelles: nanocarriers for cancer-targeted drug delivery. *AAPS PharmSciTech*. 2014;15(4):862-71.
187. Sadat SM, Saeidnia S, Nazarali AJ, Haddadi A. Nano-pharmaceutical formulations for targeted drug delivery against HER2 in breast cancer. *Current Cancer Drug Targets*. 2015;15(1):71-86.
188. Lee AL, Wang Y, Cheng HY, Pervaiz S, Yang YY. The co-delivery of paclitaxel and Herceptin using cationic micellar nanoparticles. *Biomaterials*. 2009;30(5):919-27.
189. Lee KS, Chung HC, Im SA, Park YH, Kim CS, Kim SB, et al. Multicenter phase II trial of Genexol-PM, a Cremophor-free, polymeric micelle formulation of paclitaxel, in patients with metastatic breast cancer. *Breast Cancer Research and Treatment*. 2008;108(2):241-50.
190. Alakhova DY, Zhao Y, Li S, Kabanov AV. Effect of doxorubicin/pluronic SP1049C on tumorigenicity, aggressiveness, DNA methylation and stem cell markers in murine leukemia. *PloS One*. 2013;8(8):e72238- e72238.
191. Simon-Gracia L, Hunt H, Scodeller P, Gaitzsch J, Kotamraju VR, Sugahara KN, et al. iRGD peptide conjugation potentiates intraperitoneal tumor delivery of paclitaxel with polymersomes. *Biomaterials*. 2016;104:247-57.
192. Shenoy DB, Amiji MM. Poly(ethylene oxide)-modified poly(epsilon-caprolactone) nanoparticles for targeted delivery of tamoxifen in breast cancer. *International Journal of Pharmaceutics*. 2005;293(1-2):261-70.
193. Li Y, Xu B, Bai T, Liu W. Co-delivery of doxorubicin and tumor-suppressing p53 gene using a POSS-based star-shaped polymer for cancer therapy. *Biomaterials*. 2015;55:12-23.

194. Soudy R, Etayash H, Bahadorani K, Lavasanifar A, Kaur K. Breast cancer targeting peptide binds keratin 1: A new molecular marker for targeted drug delivery to breast cancer. *Molecular Pharmaceutics*. 2017;14(3):593-604.
195. Peer D, Karp JM, Hong S, Farokhzad OC, Margalit R, Langer R. Nanocarriers as an emerging platform for cancer therapy. *Nature Nanotechnology*. 2007;2(12):751-60.
196. Muro S. Challenges in design and characterization of ligand-targeted drug delivery systems. *Journal of Controlled Release*. 2012;164(2):125-37.
197. Skwarczynski M, Toth I. Peptide-based synthetic vaccines. *Chemical Science*. 2016;7(2):842-54.
198. Wu C-H, Liu IJ, Lu R-M, Wu H-C. Advancement and applications of peptide phage display technology in biomedical science. *Journal of Biomedical Science*. 2016;23(1):1-14.
199. Ahmed S, Mathews AS, Byeon N, Lavasanifar A, Kaur K. Peptide arrays for screening cancer specific peptides. *Analytical Chemistry*. 2010;82(18):7533-41.
200. Mathews AS, Ahmed S, Shahin M, Lavasanifar A, Kaur K. Peptide modified polymeric micelles specific for breast cancer cells. *Bioconjugate Chemistry*. 2013;24(4):560-70.
201. Liu Z, Wang F, Chen X. Integrin $\alpha(v)\beta(3)$ -targeted cancer therapy. *Drug Development Research*. 2008;69(6):329-39.
202. Huang H, Yu H, Tang G, Wang Q, Li J. Low molecular weight polyethylenimine cross-linked by 2-hydroxypropyl-gamma-cyclodextrin coupled to peptide targeting HER2 as a gene delivery vector. *Biomaterials*. 2010;31(7):1830-8.
203. Shahin M, Soudy R, Aliabadi HM, Kneteman N, Kaur K, Lavasanifar A. Engineered breast tumor targeting peptide ligand modified liposomal doxorubicin and the effect of peptide density on anticancer activity. *Biomaterials*. 2013;34(16):4089-97.
204. Kagawa S, He C, Gu J, Koch P, Rha SJ, Roth JA, et al. Antitumor activity and bystander effects of the tumor necrosis factor-related apoptosis-inducing ligand (TRAIL) gene. *Cancer Research*. 2001;61(8):3330-8.
205. Origene, BIK (NM_001197) Human Tagged ORF Clone Lentiviral Particle. 2014 [cited 2014 October 21] Available from: <https://www.origene.com/catalog/cdna->

- clones/lentiviral-particles/rc20054613v/bik-nm_001197-human-tagged-orf-clone-lentiviral-particle.
206. Matsuda T, Cepko CL. Controlled expression of transgenes introduced by in vivo electroporation. *Proceedings of the National Academy of Sciences*. 2007; 104(3):1027-32.
 207. Faustino-Rocha A, Oliveira PA, Pinho-Oliveira J, Teixeira-Guedes C, Soares-Maia R, da Costa RG, et al. Estimation of rat mammary tumor volume using caliper and ultrasonography measurements. *Lab Animal*. 2013;42(6):217-24.
 208. Huang C, Chen YJ, Chen W-J, Lin C-L, Wei YX, Huang HC. Combined treatment with chrysin and 1,2,3,4,6-penta-O-galloyl- β -D-glucose synergistically inhibits LRP6 and Skp2 activation in triple-negative breast cancer and xenografts. *Molecular Carcinogenesis*. 2015;54(12):1613-25.
 209. Li YM, Wen Y, Zhou BP, Kuo H-P, Ding Q, Hung M-C. Enhancement of antitumor effect by mutants. *Cancer Research*. 2003;63(22):7630-7633.
 210. Day C-P, Merlino G, Van Dyke T. Preclinical mouse cancer models: A maze of opportunities and challenges. *Cell*. 2015;163(1):39-53.
 211. Morton CL, Houghton PJ. Establishment of human tumor xenografts in immunodeficient mice. *Nature Protocols*. 2007;2(2):247-251.
 212. Clarke R. Human breast cancer cell line xenografts as models of breast cancer. The immunobiologies of recipient mice and the characteristics of several tumorigenic cell lines. *Breast Cancer Research and Treatment*. 1996;39(1):69-86.
 213. Carreno BM, Garbow JR, Kolar GR, Jackson EN, Engelbach JA, Becker-Hapak M, et al. Immunodeficient mouse strains display marked variability in growth of human melanoma lung metastases. *Clinical Cancer Research*. 2009;15(10):3277-86.
 214. Puchalapalli M, Zeng X, Mu L, Anderson A, Hix Glickman L, Zhang M, et al. NSG mice provide a better spontaneous model of breast cancer metastasis than athymic (nude) mice. *PloS One*. 2016;11(9):e0163521-e0163521.
 215. Szadvari I, Krizanova O, Babula P. Athymic nude mice as an experimental model for cancer treatment. *Physiological Research*. 2016;65(S4):441-53.
 216. Romano R, Palamaro L, Fusco A, Iannace L, Maio S, Vigliano I, et al. From murine to human nude/SCID: the thymus, T-cell development and the missing link. *Clinical and Developmental Immunology*. 2012;2012:467101-467101.

217. Xu W, Qian J, Hou G, Wang Y, Wang J, Sun T, et al. A dual-targeted hyaluronic acid-gold nanorod platform with triple-stimuli responsiveness for photodynamic/photothermal therapy of breast cancer. *Acta Biomaterialia*. 2019;83:400-13.
218. Wang K, Yao H, Meng Y, Wang Y, Yan X, Huang R. Specific aptamer-conjugated mesoporous silica-carbon nanoparticles for HER2-targeted chemo-photothermal combined therapy. *Acta Biomaterialia*. 2015;16:196-205.
219. Haddad TC, Goetz MP. Landscape of Neoadjuvant Therapy for Breast Cancer. *Annals of Surgical Oncology*. 2015;22(5):1408-15.
220. Kulhari H, Pooja D, Rompicharla SVK, Sistla R, Adams DJ. Biomedical Applications of Trastuzumab: As a therapeutic agent and a targeting ligand. *Medicinal Research Reviews*. 2015;35(4):849-76.
221. Kang X, Guo X, Niu X, An W, Li S, Liu Z, et al. Photothermal therapeutic application of gold nanorods-porphyrin-trastuzumab complexes in HER2-positive breast cancer. *Scientific Reports*. 2017;7:42069-72.
222. Liu Q, Li R, Zhu Z, Qian X, Guan W, Yu L, et al. Enhanced antitumor efficacy, biodistribution and penetration of docetaxel-loaded biodegradable nanoparticles. *International Journal of Pharmaceutics*. 2012;430(1-2):350-8.
223. Jadia R, Scandore C, Rai P. Nanoparticles for effective combination therapy of cancer. *International Journal of Nanotechnology and Nanomedicine*. 2016;1(1):1-27.
224. Strebhardt K, Ullrich A. Paul Ehrlich's magic bullet concept: 100 years of progress. *Nature Reviews Cancer*. 2008;8(6):473-80.
225. Scott AM, Allison JP, Wolchok JD. Monoclonal antibodies in cancer therapy. *Cancer Immunity*. 2012;12(1):14-21.
226. Chames P, Van Regenmortel M, Weiss E, Baty D. Therapeutic antibodies: successes, limitations and hopes for the future. *British Journal of Pharmacology*. 2009;157(2):220-33.
227. Hamamoto K, Kida Y, Zhang Y, Shimizu T, Kuwano K. Antimicrobial activity and stability to proteolysis of small linear cationic peptides with D-amino acid substitutions. *Microbiology and Immunology*. 2002;46(11):741-9.
228. Thundimadathil J. Cancer treatment using peptides: current therapies and future prospects. *Journal of Amino Acids*. 2012;2012:967347-59.

229. Yavari B, Mahjub R, Saidijam M, Raigani M, Soleimani M. The potential use of peptides in cancer treatment. *Current Protein and Peptide Science*. 2018;19(8):759-70.
230. Sercombe L, Veerati T, Moheimani F, Wu SY, Sood AK, Hua S. Advances and challenges of liposome assisted drug delivery. *Frontiers in Pharmacology*. 2015;6:1-13.
231. Hua S, Wu SY. The use of lipid-based nanocarriers for targeted pain therapies. *Frontiers in Pharmacology*. 2013;4:143-9.
232. Gutiérrez-Praena D, Pichardo S, Sánchez E, Grilo A, Cameán AM, Jos A. Influence of carboxylic acid functionalization on the cytotoxic effects induced by single wall carbon nanotubes on human endothelial cells (HUVEC). *Toxicology In Vitro*. 2011;25(8):1883-8.
233. Garg A, Tisdale AW, Haidari E, Kokkoli E. Targeting colon cancer cells using PEGylated liposomes modified with a fibronectin-mimetic peptide. *International Journal of Pharmaceutics*. 2009;366(1):201-10.
234. Monteiro-Riviere NA, Inman AO. Challenges for assessing carbon nanomaterial toxicity to the skin. *Carbon*. 2006;44(6):1070-8.
235. You J-O, Auguste DT. The effect of swelling and cationic character on gene transfection by pH-sensitive nanocarriers. *Biomaterials*. 2010;31(26):6859-66.
236. Corsi K, Chellat F, Yahia LH, Fernandes JC. Mesenchymal stem cells, MG63 and HEK293 transfection using chitosan-DNA nanoparticles. *Biomaterials*. 2003;24(7):1255-64.
237. Chung T-H, Wu S-H, Yao M, Lu C-W, Lin Y-S, Hung Y, et al. The effect of surface charge on the uptake and biological function of mesoporous silica nanoparticles in 3T3-L1 cells and human mesenchymal stem cells. *Biomaterials*. 2007;28(19):2959-66.
238. Scherzed A, Hackenberg S, Radeloff A, Froelich K, Rak K, Hagen R, et al. Human mesenchymal stem cells promote cancer motility and cytokine secretion in vitro. *Cells, Tissues, Organs*. 2013;198(5):327-37.
239. Gulyuz SO, U. U.; Kocak, P.; Telci, D.; Yilmaz, O.; Tasdelen, M. A. In-vitro cytotoxic activities of poly(2-ethyl-2-oxazoline)-based amphiphilic block copolymers prepared by CuAAC click chemistry. *Express Polymer Letters*. 2018;12(2):146-58.

240. Wang X, Li X, Li Y, Zhou Y, Fan C, Li W, et al. Synthesis, characterization and biocompatibility of poly(2-ethyl-2-oxazoline)-poly(D,L-lactide)-poly(2-ethyl-2-oxazoline) hydrogels. *Acta Biomaterialia*. 2011;7(12):4149-59.
241. Wang J, Mongayt D, Torchilin VP. Polymeric micelles for delivery of poorly soluble drugs: preparation and anticancer activity in vitro of paclitaxel incorporated into mixed micelles based on poly(ethylene glycol)-lipid conjugate and positively charged lipids. *Journal of Drug Targeting*. 2005;13(1):73-80.
242. Hanafy NAN, El-Kemary M, Leporatti S. Micelles structure development as a strategy to improve smart cancer therapy. *Cancers*. 2018;10(7):238.
243. Godbey WT, Wu KK, Mikos AG. Poly(ethylenimine)-mediated gene delivery affects endothelial cell function and viability. *Biomaterials*. 2001;22(5):471-80.
244. Lv H, Zhang S, Wang B, Cui S, Yan J. Toxicity of cationic lipids and cationic polymers in gene delivery. *Journal of Controlled Release*. 2006;114(1):100-9.
245. Godbey WT, Wu KK, Mikos AG. Poly(ethylenimine)-mediated gene delivery affects endothelial cell function and viability. *Biomaterials*. 2001;22(5):471-80.
246. Navarro G, Sawant RR, Biswas S, Essex S, Tros de Ilarduya C, Torchilin VP. P-glycoprotein silencing with siRNA delivered by DOPE-modified PEI overcomes doxorubicin resistance in breast cancer cells. *Nanomedicine*. 2012;7(1):65-78.
247. Nair K L, Jagadeeshan S, Nair S A, Kumar GSV. Folic acid conjugated δ -valerolactone-poly(ethylene glycol) based triblock copolymer as a promising carrier for targeted doxorubicin delivery. *PloS One*. 2013;8(8):e70697-e70697.
248. Xie X, Li L, Xiao X, Guo J, Kong Y, Wu M, et al. Targeted expression of BikDD eliminates breast cancer with virtually no toxicity in noninvasive imaging models. *Molecular Cancer Therapeutics*. 2012;11(9):1915-24.
249. Xie X, Kong Y, Tang H, Yang L, Hsu JL, Hung M-C. Targeted BikDD expression kills androgen-dependent and castration-resistant prostate cancer cells. *Molecular Cancer Therapeutics*. 2014;13(7):1813-25.
250. Xie X, Xia W, Li Z, Kuo H-P, Liu Y, Li Z, et al. Targeted expression of BikDD eradicates pancreatic tumors in noninvasive imaging models. *Cancer Cell*. 2007;12(1):52-65.
251. Sher Y-P, Liu S-J, Chang C-M, Lien S-P, Chen C-H, Han Z, et al. Cancer-targeted BikDD gene therapy elicits protective antitumor immunity against lung cancer. *Molecular Cancer Therapeutics*. 2011;10(4):637-47.

252. Hafez IM, Maurer N, Cullis PR. On the mechanism whereby cationic lipids promote intracellular delivery of polynucleic acids. *Gene Therapy*. 2001;8:1188.
253. Douglas KL, Piccirillo CA, Tabrizian M. Cell line-dependent internalization pathways and intracellular trafficking determine transfection efficiency of nanoparticle vectors. *European Journal of Pharmaceutics and Biopharmaceutics*. 2008;68(3):676-87.
254. Izumisawa T, Hattori Y, Date M, Toma K, Maitani Y. Cell line-dependent internalization pathways determine DNA transfection efficiency of decaarginine-PEG-lipid. *International Journal of Pharmaceutics*. 2011;404(1):264-70.
255. Day CP, Rau KM, Qiu L, Liu CW, Kuo HP, Xie X, et al. Mutant Bik expression mediated by the enhanced minimal topoisomerase II α promoter selectively suppressed breast tumors in an animal model. *Cancer Gene Therapy*. 2006;13:706.
256. Li LY, Dai HY, Yeh FL, Kan SF, Lang J, Hsu JL, et al. Targeted hepatocellular carcinoma proapoptotic BikDD gene therapy. *Oncogene*. 2010;30(15):1773-83.
257. Hsiue G-H, Chiang H-Z, Wang C-H, Juang T-M. Nonviral gene carriers based on diblock copolymers of Poly(2-ethyl-2-oxazoline) and linear polyethylenimine. *Bioconjugate Chemistry*. 2006;17(3):781-6.
258. Wang W, Balk M, Deng Z, Wischke C, Gossen M, Behl M, et al. Engineering biodegradable micelles of polyethylenimine-based amphiphilic block copolymers for efficient DNA and siRNA delivery. *Journal of Controlled Release*. 2016;242:71-79.
259. Ganesh S, Iyer AK, Gattacceca F, Morrissey DV, Amiji MM. In vivo biodistribution of siRNA and cisplatin administered using CD44-targeted hyaluronic acid nanoparticles. *Journal of Controlled Release*. 2013;172(3):699-706.
260. Lovitt CJ, Shelper TB, Avery VM. Doxorubicin resistance in breast cancer cells is mediated by extracellular matrix proteins. *BioMed Central Cancer*. 2018;18(1):41-51.
261. Zhao L, Zhang B. Doxorubicin induces cardiotoxicity through upregulation of death receptors mediated apoptosis in cardiomyocytes. *Scientific Reports*. 2017;7:44735-45.

262. Lao J, Madani J, Puértolas T, Alvarez M, Hernández A, Pazo-Cid R, et al. Liposomal doxorubicin in the treatment of breast cancer patients: a review. *Journal of Drug Delivery*. 2013;2013:1-12.
263. Gabizon AA, Patil Y, La-Beck NM. New insights and evolving role of pegylated liposomal doxorubicin in cancer therapy. *Drug Resistance Updates*. 2016;29:90-106.
264. Barenholz Y. Doxil(R)--the first FDA-approved nano-drug: lessons learned. *Journal of Controlled Release*. 2012;160(2):117-34.
265. Munster P, Krop IE, LoRusso P, Ma C, Siegel BA, Shields AF, et al. Safety and pharmacokinetics of MM-302, a HER2-targeted antibody-liposomal doxorubicin conjugate, in patients with advanced HER2-positive breast cancer: a phase 1 dose-escalation study. *British Journal of Cancer*. 2018;119(9):1086-93.
266. Reynolds JG, Geretti E, Hendriks BS, Lee H, Leonard SC, Klinz SG, et al. HER2-targeted liposomal doxorubicin displays enhanced anti-tumorigenic effects without associated cardiotoxicity. *Toxicology and Applied Pharmacology*. 2012;262(1):1-10.
267. Soudy R, Chen C, Kaur K. Novel peptide-doxorubicin conjugates for targeting breast cancer cells including the multidrug resistant cells. *Journal of Medicinal Chemistry*. 2013;56(19):7564-73.
268. She W, Luo K, Zhang C, Wang G, Geng Y, Li L, et al. The potential of self-assembled, pH-responsive nanoparticles of mPEGylated peptide dendron-doxorubicin conjugates for cancer therapy. *Biomaterials*. 2013;34(5):1613-23.
269. Duan X, Xiao J, Yin Q, Zhang Z, Yu H, Mao S, et al. Smart pH-sensitive and temporal-controlled polymeric micelles for effective combination therapy of doxorubicin and disulfiram. *ACS Nano*. 2013;7(7):5858-69.
270. Rashid OM, Takabe K. Animal models for exploring the pharmacokinetics of breast cancer therapies. *Expert Opinion On Drug Metabolism and Toxicology*. 2015;11(2):221-30.
271. Aston WJ, Hope DE, Nowak AK, Robinson BW, Lake RA, Lesterhuis WJ. A systematic investigation of the maximum tolerated dose of cytotoxic chemotherapy with and without supportive care in mice. *BMC Cancer*. 2017;17(1):684.
272. Davis ME, Chen ZG, Shin DM. Nanoparticle therapeutics: an emerging treatment modality for cancer. *Nature Reviews Drug Discovery*. 2008;7(9):771-82.

273. Torchilin VP. Micellar nanocarriers: Pharmaceutical perspectives. *Pharmaceutical Research*. 2006;24(1):1-16.



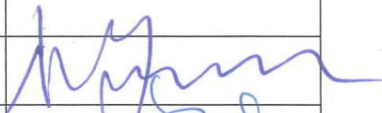

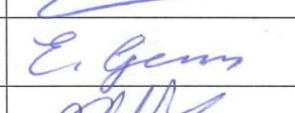





APPENDIX A: ETHICAL APPROVAL FORM



T.C. YEDİTEPE ÜNİVERSİTESİ, DENEY HAYVANLARI ETİK KURULU
(YÜDHEK)
ETİK KURUL KARARI

Toplantı Tarihi	Karar No	İlgi	Proje Yürütücüsü
22.02.2018	644	08.02.2018	Doç.Dr.Dilek TELCİ

‘Prostat ve meme kanseri teşhis ve tedavisinde kullanılacak poli(2-etil-2-oksazolin) (PEtOx) esaslı çok işlevsel taşıyıcı sistemlerin geliştirilmesi’ adlı bilimsel çalışma etik kurulumuzda görüşülmüş olup, çalışmanın etik kurallara uygun olduğuna oy birliğiyle karar verilmiştir.		
Etik Onay Geçerlilik Süresi: 3 Yıl	Hayvan Türü ve cinsiyeti: Fare ♂♀	Hayvan Sayısı: 96

GÖREVİ	ADI SOYADI	
Başkan	Prof. Dr. Bayram YILMAZ	
Başkan Yardımcısı	Prof. Dr. Erdem YEŞİLADA	
Raportör	Vet. Hekim Engin SÜMER	
Üye	Prof. Dr. M. Ece GENÇ	
Üye	Prof. Dr. Rukset ATTAR	
Üye	Doç. Dr. Soner DOĞAN	
Üye	Doç. Dr. Ediz DENİZ	KATILMADI
Üye	Prof. Dr. Gamze TORUN KÖSE	KATILMADI
Üye	Doç. Dr. Aylin YABA UÇAR	
Üye	Hakan GÖKSEL	
Üye	Ahmet ŞENKARDEŞLER	